NUREG/CR-4356
EGG-2626
Vol. 1

TRAC-BF1/MOD1: An Advanced Best-Estimate Computer Program for BWR Accident Analysis

Model Description

Edited by
J. A. Porkowski, N. L. Wade

Idaho National Engineering Laboratory
EG&G Idaho, Inc.

Prepared for
U.S. Nuclear Regulatory Commission

NUREG/CR-4356
EGG-2626
Vol. 1
R4

TRAC-BF1/MOD1: An Advanced Best-Estimate Computer Program for BWR Accident Analysis

Model Description

Manuscript Completed: July 1992
Date Published: August 1992

Edited by
J. A. Borkowski, N. L. Wade

Contributing Authors
M. M. Giles, S. Z. Rouhani, R. W. Shumway,
G. L. Singer, D. D. Taylor, W. L. Weaver

Idaho National Engineering Laboratory
Managed by the U.S. Department of Energy

EG&G Idaho, Inc.
Idaho Falls, ID 83415

Prepared for
Division of Systems Research
Office of Nuclear Regulatory Research
U.S. Nuclear Regulatory Commission
Washington, DC 20555
NRC FIN L2031
Under DOE Contract No. DE-AC07-76ID01570

AVAILABILITY NOTICE

Availability of Reference Materials Cited in NRC Publications

Most documents cited in NRC publications will be available from one of the following sources:

1. The NRC Public Document Room, 2120 L Street, NW., Lower Level, Washington, DC 20555

2. The Superintendent of Documents, U.S. Government Printing Office, P.O. Box 37082, Washington, DC 20013-7082

3. The National Technical Information Service, Springfield, VA 22161

Although the listing that follows represents the majority of documents cited in NRC publications, it is not intended to be exhaustive.

Referenced documents available for inspection and copying for a fee from the NRC Public Document Room include NRC correspondence and internal NRC memoranda; NRC bulletins, circulars, information notices, inspection and investigation notices; licensee event reports; vendor reports and correspondence; Commission papers; and applicant and licensee documents and correspondence.

The following documents in the NUREG series are available for purchase from the GPO Sales Program: formal NRC staff and contractor reports, NRC-sponsored conference proceedings, international agreement reports, grant publications, and NRC booklets and brochures. Also available are regulatory guides, NRC regulations in the *Code of Federal Regulations*, and *Nuclear Regulatory Commission Issuances*.

Documents available from the National Technical Information Service include NUREG-series reports and technical reports prepared by other Federal agencies and reports prepared by the Atomic Energy Commission, forerunner agency to the Nuclear Regulatory Commission.

Documents available from public and special technical libraries include all open literature items, such as books, journal articles, and transactions. *Federal Register* notices, Federal and State legislation, and congressional reports can usually be obtained from these libraries.

Documents such as theses, dissertations, foreign reports and translations, and non-NRC conference proceedings are available for purchase from the organization sponsoring the publication cited.

Single copies of NRC draft reports are available free, to the extent of supply, upon written request to the Office of Administration, Distribution and Mail Services Section, U.S. Nuclear Regulatory Commission, Washington, DC 20555.

Copies of industry codes and standards used in a substantive manner in the NRC regulatory process are maintained at the NRC Library, 7920 Norfolk Avenue, Bethesda, Maryland, for use by the public. Codes and standards are usually copyrighted and may be purchased from the originating organization or, if they are American National Standards, from the American National Standards Institute, 1430 Broadway, New York, NY 10018.

DISCLAIMER NOTICE

This report was prepared as an account of work sponsored by an agency of the United States Government. Neither the United States Government nor any agency thereof, or any of their employees, makes any warranty, expressed or implied, or assumes any legal liability of responsibility for any third party's use, or the results of such use, of any information, apparatus, product or process disclosed in this report, or represents that its use by such third party would not infringe privately owned rights.

ABSTRACT

The TRAC-BWR code development program at the Idaho National Engineering Laboratory has developed versions of the Transient Reactor Analysis Code (TRAC) for the U.S. Nuclear Regulatory Commission and the public. The TRAC-BF1/MOD1 version of the computer code provides a best-estimate analysis capability for analyzing the full range of postulated accidents in boiling water reactor (BWR) systems and related facilities. This version provides a consistent and unified analysis capability for analyzing all areas of a large- or small-break loss-of-coolant accident (LOCA), beginning with the blowdown phase and continuing through heatup, reflood with quenching, and, finally, the refill phase of the accident. Also provided is a basic capability for the analysis of operational transients up to and including anticipated transients without scram (ATWS). The TRAC-BF1/MOD1 version produces results consistent with previous versions. Assessment calculations using the two TRAC-BF1 versions show overall improvements in agreement with data and computation times as compared to earlier versions of the TRAC-BWR series of computer codes.

FIN No. L2031--Documentation and Maintenance of TRAC-BF1/MOD1

CONTENTS

FIGURES

TABLES

SUMMARY

The TRAC-BWR Code Development Program at the Idaho National Engineering Laboratory (INEL) is developing versions of TRAC (Transient Reactor Analysis Code) to provide the U.S. Nuclear Regulatory Commission (NRC), and the public, a best-estimate capability for the analysis of postulated accidents and transients in boiling water reactor (BWR) systems and related experimental facilities. The first publicly released version of the code, TRAC-BD1, provided a basic capability for the analysis of design basis loss-of-coolant accidents (DBLOCAs). The second publicly released version of the code, TRAC-BD1/MOD1, was developed to provide an analysis capability for operational transients, including anticipated transients without scram (ATWS), as well as to provide an improved analysis capability for both large- and small-break LOCAs. The third release, TRAC-BF1, is a further improvement, particularly in the areas of computational speed and space-dependent (one-dimensional) neutron kinetics modeling capability. The fourth release, TRAC-BF1/MOD1, again improves the calculational speed, provides an improved steam separator-dryer model, and corrects many errors or omissions.

The code provides a consistent and unified analysis capability for an entire accident sequence. For a large break LOCA, this includes the blowdown phase, heatup, reflood with quenching, and, finally, the refill phase of the LOCA accident sequence. For an ATWS event initiated by the closure of the main steam isolation valve, the sequence includes the initiating event, the reactor power excursion caused by void collapse and terminated by reactivity feedback, periodic power excursion caused by cycling of the safety relief valves, and ultimate reactor shutdown though the injection of soluble boron poison.

Unique features of the code include (a) a full nonhomogeneous, nonequilibrium, two-fluid, thermal-hydraulic model of two-phase flow in all portions of a BWR system, including a three-dimensional thermal-hydraulic treatment of a BWR vessel; (b) detailed modeling of a BWR fuel bundle, including a thermal radiation heat transfer model for radiative heat transfer between multiple fuel rod groups, liquid and vapor phases, and the fuel channel wall, with quench front tracking on all fuel rod surfaces and inside and outside of the fuel channel wall for both bottom flooding and falling film quench fronts; (c) detailed models of BWR hardware, such as jet pumps and separator-dryers; and (d) a countercurrent flow limiting model for BWR-like geometries.

Other features of the code include a nonhomogeneous, thermal equilibrium critical flow model and flow-regime-dependent constitutive relations for the interchanges of mass, energy, and momentum between the fluid phases and between the phases and structure.

TRAC-BD1/MOD1 contained several upgrades and component enhancements.

These include:

- Balance of plant component models, such as turbines, feedwater heaters, and steam condensers
- A simple lumped parameter containment model
- A comprehensive control system model
- Reactivity feedback model, including the effect of soluble boron
- Boron transport model
- Noncondensable gas transport model, including the effects of noncondensable gas on heat transfer
- Mechanistic separator-dryer model
- Two-phase level tracking model
- Generalized component-to-component heat and mass transfer models
- Moving mesh quench front tracking model for fuel rods and both inside and outside surfaces of fuel channel wall
- Improved constitutive relations for heat, mass, and momentum transfer between the fluid phases and between the fluid phases and structure
- A free-format input processor with extensive error checking.

New features of TRAC-BF1/MOD1 not available in the previously released version of the code include:

- Courant-limit-violating (fast-running) numerical solution for all one-dimensional hydraulic components
- Implicit steam separator/dryer model
- Implicit turbine model
- Improved interfacial package
- Condensation model for stratified vertical flow for realistic prediction of condensation in such cases
- One-dimensional neutron kinetic model (for space-dependent variations of power in ATWS-type transients)

- Improved control system solution logic
- Preload processor
- Conversion to ANSI standard FORTRAN 77.

From the very beginning of the TRAC-BF1/MOD1 development, adherence to a strict quality control program ensured that a well-documented, working version of the code would be available at all times. All changes to the code, however small, are given a program change label that appears on the modified FORTRAN statements and on all documentation that accompanies the changes. This ensures that all changes are traceable to documents that describe the basis for the change and the model developer making the change. A set of test cases was developed and executed after each successive working version of the code was assembled to ensure that recent changes did not affect changes or models inserted into previous versions of the code.

After the final working version of TRAC-BF1/MOD1 was assembled, a series of developmental assessment test cases was executed. These test cases provided insight into the code simulation capabilities for various separate effects hydrodynamic tests, separate effects heat transfer tests, and integral system effects tests. On the whole, agreement between the TRAC-BF1/MOD1 simulation of the various problems and measured test data is excellent.

The TRAC-BF1/MOD1 code is described by three documents: *TRAC-BF1/MOD1: An Advanced Best-Estimate Computer Program for Boiling Water Reactor Accident Analysis, Volumes 1 and 2, and TRAC-BF1/MOD1 Models and Correlations. Volume 1: Model Description* describes the thermal-hydraulic models, numerical methods, and component models available. *Volume 2: User's Guide* describes the input and output of the TRAC-BF1/MOD1 code and provides guidelines for use of the code modeling of BWR systems. *TRAC-BF1/MOD1 Models and Correlations* is designed for those users wishing a detailed mathematical description of each of the models and correlations available in TRAC-BF1/MOD1. This document reflects the as-coded configuration of the descriptive information provided in Volume 1.

ACKNOWLEDGMENTS

Contributors to TRAC-BF1 Development
(In Alphabetical Order)

Monte M. Giles	Thermal-Hydraulic and Control System Models
Gerald A. Jayne	Programming Assistance
S. Zia Rouhani	Program Management
Rex W. Shumway	Principal Investigator for Heat Transfer
Gilbert L. Singer	Code Architecture and Quality Control
Dean D. Taylor	Thermal-Hydraulic Model Development
Walter L. Weaver III	Principal Investigator for Thermal-Hydraulics

TRAC-BD1/MOD1 and TRAC-BF1/MOD1 are the results of technical collaboration between General Electric Company (GE), and EG&G Idaho, Inc., at the Idaho National Engineering Laboratory (INEL). Substantial contributions to the models in TRAC-BD1/MOD1 and TRAC-BF1 have been made by Messrs. Mohammed Alamgir, Jens G. M. Andersen, Chester Cheung, Kee H. Chu, James C. Shaug, and Bharat S. Shiralkar of GE. In addition, the contributions of Messrs. Felix Aguilar, Douglas W. Croucher, Stewart R. Fisher, Scott T. Free, James M. Milton, Charles M. Mohr, Jr., David Nigg, Andrew C. Peterson, Jr., Robert E. Phillips, Jay W. Spore, Mildred A. Stone, John E. Tolli, and Cheng-chii Tsai of the INEL in various stages of this development are greatly appreciated. Also, the work of Messrs. Everett G. Gruen, Douglas G. Hall, Kenneth C. Wagner, Phillip D. Wheatley, and Briant L. Charboneau on the developmental assessment of TRAC-BD1/MOD1 and TRAC-BF1 is sincerely acknowledged.

Like the earlier versions of this code, TRAC-BD1/MOD1 and TRAC-BF1 have many inherited features of TRAC-PD2 developed at the Los Alamos National Laboratory (LANL). The contribution of these features, as well as the useful consultations obtained from the members of the Safety Code Development Group at LANL, is gratefully appreciated. Finally, the sponsorship of the U.S. Nuclear Regulatory Commission (NRC), as well as technical discussions and project support provided in the course of this development by Dr. Fuat Odar, Dr. Richard Lee, Dr. Yi-Shung Chen, and Mr. Harold Scott of the NRC and Drs. Debu Majumdar and Walter H. Rettig, of the Department of Energy, Idaho Field Office, is sincerely appreciated.

NOMENCLATURE

Most of the symbols used in equations are described within the text where they first appear. Since different sets of symbols are used in describing some models in TRAC-BF1/MOD1, this nomenclature is divided into different sections corresponding to different models in the text. The first section is a general set that applies to all the original TRAC-BD1/MOD1 models, as well as to the Courant limit violating numerics, interfacial heat transfer, and interfacial friction discussions.

PART I: GENERAL NOMENCLATURE

A	area
a	absorptivity
a_{HE}	homogeneous equilibrium sound speed
B	radiosity
C	shear coefficient or reactivity coefficient
C_I	coefficient of modified relative velocity in interfacial shear term
C_p	heat capacity at constant pressure
C_v	heat capacity at constant volume
CNB	number of bubbles per unit volume
C_o	distribution parameter in drift-flux model or liquid velocity coefficient in interfacial shear term
C_1	vapor velocity coefficient in interfacial shear term
c	specific heat or nozzle efficiency constant
C_B	boron mass per unit mass of liquid
D	diameter or diffusion coefficient
DZ	hydrodynamic cell height
DZL	height of two-phase level above bottom of cell
D_B	baffle separation distance

D_H	hydraulic diameter
dV	incremental volume
D_t	tube diameter
d_H	bubble or droplet hydraulic diameter
e	specific internal energy
E	entrainment fraction
F	friction factor (Darcy)
Fr	Froude number
f	friction factor (Fanning)
f_i	interfacial friction force per unit volume
G	mass flux
Gr	Grashof number
g	acceleration of gravity
H	incident radiation heat flux
H	enthalpy flow rate
h	heat transfer coefficient or mixture specific enthalpy
h_{fg}	latent heat of vaporization
J	volumetric flux
j	volumetric flux
K	absorption coefficient, number of subintervals for integration of point kinetics equations, or degrees Kelvin
k	thermal conductivity, form loss coefficient, or neutron multiplication factor
k_B	Boltzman's constant
k_{vm}	virtual mass coefficient
L	length along flow path
M	mass flow rate
m	mass

N	number density
Nu	Nusselt number
P	pressure or reactor power
Pe	Peclet number
P_h	heated perimeter
Pr	Prandtl number
P_w	wetted perimeter
Q	volumetric heat transfer rate or volume flow rate
q	heat flux
q'''	volumetric heat generation rate
q_{mw}'''	volumetric heat source due to metal-water reaction
R	reactivity
Re	Reynolds number
R_f	radial power peaking factor
r	radial position
S	entropy
s	slip factor (V_g/V_ℓ)
T	temperature or torque
TM	thermal margin
T_{min}	minimum film boiling temperature
T_c	critical temperature
T_r	reduced temperature (T/T_c)
t	time
Δt_{max}	maximum time step for integration of point kinetics equations
Δt_p	problem time step
Δt_{rk}	integration time step for point kinetics equations
U	energy flow rate

U	energy flow rate
u′	turbulent velocity variation
V	velocity (mean)
Vol	volume
v_{gj}	drift velocity in drift flux model
V_c	velocity of continuous phase
V_D	velocity of dispersed phase
V_{LEV}	two-phase level velocity
v_m	mixture mean velocity
V_R	relative velocity (Vg - Vℓ)
v	specific volume
We	Weber number
W_f	weighting factor
'	wave number
X	quality or mass fraction
X_f	flow quality or fraction of node that transfers heat to the lower outer cell, which it overlaps
x	axial distance
Y	vector of mass and energy inventories inside containment components
ZQF	quench front axial location
z	axial coordinate in reactor vessel or core
α	volume fraction
β	volume coefficient of expansion; $\sqrt{\frac{(k\rho C_p)_\ell}{(k\rho c)_w}}$ (Section 2.2)
Γ	interfacial mass transfer rate or mass generation rate
Γ_B	boron mass source

Γ_{NC}	noncondensable (air) mass source
ρ	density
e	emissivity or fast fission factor
ζ	surface roughness divided by hydraulic radius
ϕ	neutron flux
ϕ^2	two-phase friction multiplier
Ω	turbine rotor angular velocity
σ	surface tension
υ	average number of neutrons emitted per fission viscosity, or anisotropic reflection factor
Σ	neutron cross section
σ_{SB}	Stefan-Boltzman constant
τ	transmissivity
χ	fission neutron spectrum
χ_{TT}	Lockhart-Martinelli factor
ψ	importance or adjoint function

Subscripts

a	air property
B	boron
b	bubble property or bearing windage
C	continuous phase property
CHF	critical heat flux
c	critical state of water
d	droplet property
e	energy source
eff	effective

F	fuel
f	liquid or film property fission, or friction
g	vapor property
HE	homogeneous equilibrium
i	interfacial property, or node index
ig	interface to gas
iℓ	interface to liquid
j	cell or node index
L	liquid property
ℓ	liquid property or lower node property
M	moderator
m	mixture property or mass source
N	outer slab surface node
NC	noncondensable gas
n	old-time property
n+1	new-time property
NF	outer fuel conduction node
NF+1	inner cladding conduction node
q	core property
R	relative velocity between gas and liquid ($V_R = V_g - V_\ell$), or rated value
r	radiation heat transfer property
S	source term
s	saturated property
sat	saturation property
sg	saturated vapor property
sl	saturated liquid property

st	steam property
[illegible]	fuel temperature
TM	moderator temperature
tp	two-phase
turb	turbine
u	upper node property
v	vapor property
VD	void
v	vapor property
w	wall property
wg	wall to gas
Wℓ	wall to liquid
Zr	zirconium property
1ϕ	single-phase
1	fast neutron group
1-2	fast thermal neutron group
2	thermal neutron group

Superscripts

+	property in cell above a two-phase level
-	property in cell below a two-phase level

Other

$\bar{A}$	a bar above a symbol indicates a vector quantity or a mean value

PART II: NOMENCLATURE FOR ONE-DIMENSIONAL NEUTRON KINETICS

a	expansion coefficient
A	option dependent parameter
b	boron concentration (ppm)
B	boron mass density (kg/m^3)
Cf	control fraction (-)
D	diffusion coefficient (1/cm)
f	relative insertion of control rod
p	power density (w/cm^3)
R	weight factor
T	temperature (K)
u	user-input value
V,Vol	volume (m^3)
W_r	vessel relative weight factor
X	neutron cross section (1/cm)
ρ	fluid density
ν	number of neutrons emitted during fission macroscopic neutron cross section

Subscripts

1	fast neutron group
2	thermal neutron group
a	absorption
i	CHANNEL cell index
j	VESSEL level index
jei	VESSEL level relevant to cell i
l	liquid
r	removal

f fission

Part III: Nomenclature for Implicit Turbine

C friction coefficient

DISS frictional energy dissipation

DX spatial increment corresponding to computational grid

E integrated internal energy flux

$$= \int_t^{t+\Delta t} dt \int_{surface} [\alpha \rho e \bar{V} \overline{d(FA)}], j$$

f form or friction loss coefficient

FA flow area (m^2)

k virtual mass coefficient

m integrated mass flux

$$= \int_t^{t+\Delta t} dt \int_{surface} [\alpha \rho \bar{V} \overline{d(FA)} \ (kg)$$

NSTAGE total number of turbine stages

Q heating rate per unit volume (j/m^3-s)

r individual turbine stage pressure ratio = $\left(\frac{P_2}{P_1}\right)^{\frac{1}{NSTAGE}}$

X spatial coordinate (m)

w mechanical energy extraction per unit mass of working fluid (J/kg)

W power input to turbine rotor (W)

WFL wall friction coefficient on liquid computed in TRAC

WFV wall friction coefficient on vapor computed in TRAC

α_ρ volume fraction of phase ρ

∇ divergence operator

Δ	incremental value
γ	specific heat ratio = C_p/C_v
Γ	volumetric mass source due to interphase transfer (kg/m^3-s)
η	turbine stage efficiency
ρp	mass density of phase p (kg/m^3)
$\bar{V}\&Z$	$(\bar{V} \cdot \Delta) Z$

Subscripts

a	property associated with junction a (Figure 3.11-2)
b	property associated with junction b (Figure 3.11-2)
b_1	property at entrance to turbine membrane (Junction b, Figure 3.11-2)
b_2	property at exit to turbine membrane (Junction b, Figure 3.11-2)
c	property associated with junction c (Figure 3.11-2)
crit	critical (choked) flow
C	continuous phase
d	property associated with junction d (Figure 3.11-2)
D	dispersed phase
DC	donor cell value
g	vapor property
i	vapor-liquid interfacial property
ig	transport property between saturated interface and vapor
k	value at center of kth spatial node
k+1/2	value at junction between kth and (k+1)st spatial nodes
ℓ	liquid property
m	homogeneous mixture property
p	phase indicator ("g" for vapor phase, "ℓ" for liquid phase)

NOZ	property at first turbine nozzle exit
turb	property associated with turbine internals (nozzles, blades, etc.)
vm	virtual mass
wg	wall property for vapor phase
wℓ	wall property for liquid phase

Superscripts

n	value at nth computational time step

Overbars

$\bar{V}$	vector quantity
$\tilde{V}$	explicit estimate for value of V at end of current time step

TRAC-BF1/MOD1: AN ADVANCED BEST-ESTIMATE COMPUTER PROGRAM FOR BOILING WATER REACTOR ACCIDENT ANALYSIS VOLUME 1: MODEL DESCRIPTION

1. INTRODUCTION

The TRAC-BWR Code Development Program at the Idaho National Engineering Laboratory (INEL) is a program developing versions of the Transient Reactor Analysis Code (TRAC) to provide the U. S. Nuclear Regulatory Commission (NRC) and the public with a best-estimate capability for the analysis of accidents and transients in boiling water reactor (BWR) systems and related experimental facilities. This effort began in October 1979 and resulted in the first publicly released version of the code, TRAC-BD1,[1-1] which was sent to the National Energy Software Center in February 1981. The mission of this first version of the code was to provide a best-estimate capability for the analysis of design basis loss-of-coolant accidents (LOCAs) in BWRs. The code provided a unified and consistent treatment of the design basis LOCAs sequence beginning with the blowdown phase, through heatup, then reflood with quenching, and finally ending with the refill phase of the LOCAs scenario. New models developed for TRAC-BD1 in order to accomplish its mission included (a) a full two-fluid nonequilibrium, nonhomogeneous thermal-hydraulic model of two-phase flow in all parts of the BWR system, including a three-dimensional treatment of the BWR pressure vessel; (b) a detailed model of a BWR fuel bundle, which includes the following models: a radiation heat transfer model for thermal radiation between multiple fuel rod groups, the inner surface of the channel wall, and the liquid and steam phases in the channel; a leakage path model; and a quench front tracking capability for both falling films and bottom flooding quench fronts on all rod groups and the inner surface of the channel wall; (c) simplified models of BWR hardware components, such as the jet pump and separator-dryer; (d) a countercurrent flow limiting model for BWR geometries; (e) a nonhomogeneous critical flow model; and (f) flow regime-dependent constitutive relations for the transfer of mass, energy, and momentum between the liquid and steam phases in two-phase flow and between each phase and structure.

The mission of the second publicly released version of the code, TRAC-BD1/MOD1,[1-2,3,4,5] was expanded to include not only large- and small-break LOCAs but also operational transients and anticipated transients without scram (ATWS) for which point reactor kinetics is applicable. Models developed to support the broadening of the scope of the mission of the TRAC-BWR codes included:

- Balance of plant models, such as turbine, feedwater heaters, and condenser

- A simple lumped parameter containment model
- Reactivity feedback model for use in the point reactor kinetics model
- Soluble boron transport model
- Noncondensable gas transport model
- Two-phase level tracking model
- Control systems model
- Generalized component-to-component heat and mass transfer models
- Improved constitutiv models for the transfer of mass, energy, and momentum between t' two phases and between the phases and structure.

User convenience features, such as free-format input and extensive error checking of the input data, were also included in TRAC-BD1/MOD1.

The mission of TRAC-BF1/MOD1 is the same as for TRAC-BD1/MOD1, but the new capabilities built into this code make it more suitable for that mission. The new models and capabilities in TRAC-BF1/MOD1 include:

- Material Courant-limit-violating numerical solution for all one-dimensional hydraulic components
- Implicit steam separator/dryer model
- Implicit turbine model
- Improved interfacial heat transfer
- Improved interfacial shear model
- A condensation model for stratified vertical flow
- One-dimensional neutron kinetics model
- Improved control system logic and solution method

In addition to these code improvements, a preload processor has been written for TRAC-BF1, its graphic routines have been improved for adaptation to the Nuclear Plant Analyzer (NPA) at the INEL, and more than 95% of the coding has been converted to ANSI Standard FORTRAN 77.

TRAC-BF1/MOD1 can be applied to any BWR accident analysis or thermal-hydraulic test facility, including those requiring reactivity feedback effects, control system simulation, and/or a balance-of-plant model.

TRAC-BF1/MOD1 has been applied to experimental facilities ranging from simple pipe blowdowns, such as the Edwards pipe tests, to integral LOCA tests, such as the two-loop test apparatus (TLTA) facility, and even to multidimensional test facilities such as the slab core test facility (SCTF). BWR small-break LOCAs have also been simulated with TRAC-BD1. The BWR fuel bundle model is quite versatile and has been used to simulate not only BWR fuel bundles within a BWR reactor vessel but also stand-alone, single-bundle experiments in which advanced bundle hydraulics and heat transfer models are required.

1.1 BACKGROUND

The Reactor Safety Code Development Group at the Los Alamos National Laboratory (LANL) has been working toward development of the TRAC code to provide a modeling technique for analysis of loss-of-coolant transients in pressurized water reactors (PWRs). Several PWR versions of TRAC have been released, including TRAC-P1, TRAC-P1A, TRAC-PD2, and TRAC-PF1/MOD1 and MOD2. These codes employ a full two-fluid thermal-hydraulic model in the three-dimensional vessel component model and a five-equation drift flux model in the one-dimensional components. The base code from which TRAC-BWR codes have been developed was an interim version of TRAC-PF1. The base version contains a full two-fluid thermal-hydraulic model in both one- and three-dimensional component models.

The TRAC-PWR code versions present the user with several problems when trying to analyze transients in BWRs. The main difficulty is accurately simulating the BWR core during system transients. The reactor core of a PWR is contained in an open lattice of fuel elements, while the fuel elements in a BWR are contained within individual channel boxes. The presence of the channel wall introduces many thermal-hydraulic phenomena that must be considered for analysis of BWR transients that are either not present or not important for analysis of LOCAs in PWRs.

The first major phenomenon introduced by the presence of the channel wall is radiation heat transfer. Small water gaps exist between the fuel channel boxes that fill with emergency core cooling system (ECCS) liquid during reflood and cool the channel walls. The colder channel wall provides a heat sink for thermal radiation. Radiation heat transfer is also present in PWRs, but the magnitude of the radiation heat flux is small, since there is no cold structure within the PWR core. Another important effect of the channel wall is to divide the fluid in the core regions into two separate fluid streams [the two-phase fluid within the fuel channels, which is heated by contact with the hot fuel rods, and the fluid in the bypass (or gap) region between fuel bundles, which is heated by heat conduction through the channel walls.] The PWR versions of TRAC cannot easily address these geometry and heat transfer aspects of a BWR core.

Another important phenomenon that results from the geometric arrangement of the BWR reactor core is countercurrent flow limiting or flooding. ECCS liquid is injected directly into the upper plenum of a BWR and drains down

into the bypass region through the upper core support plate and into the fuel bundles through the upper tie plates. Countercurrent flow limiting can also occur at the side entry orifice at the bottom of the fuel bundle. This phenomenon is very dependent on flow geometry and can only be modeled at this time by experimentally derived empirical correlations. Such correlations and the methodology for their application are not available in any BWR versions of the TRAC code.

Fluid in a BWR is circulated through the reactor core by use of jet pumps. Jet pumps could only be modeled by nonphysical (negative) form loss coefficients due to the nonconservative form of the momentum equations used in the PWR versions of TRAC.

1.2 TRAC-BD1/MOD1 AND TRAC-BF1/MOD1 MODELS AND CAPABILITIES

One set of changes to the LANL code was implemented in TRAC-BD1/MOD1. Most changes and additions to the base code obtained from LANL were made by the Thermal-Hydraulic Code Development Branch at the INEL. The major modeling change was development of the BWR fuel bundle model, using the CHAN component. This component is a one-dimensional flow component developed from the PIPE component by the addition of fuel rod convective heat transfer and a thermal radiation heat transfer model. Multiple fuel rod groups are used within each CHAN to model the local fuel rod temperature variation due to power peaking within the fuel bundle. The thermal radiation model includes radiation between fuel rod groups, the channel wall, and any liquid and vapor in the fuel bundle. A leakage path model for leakage flow between the fuel bundle and the core bypass region is also included. A moving mesh quench front tracking capability for both falling films and bottom flooding quench fronts on all rod groups and the inner and outer surfaces of the channel wall has also been developed. Figure 1-1 shows a typical nodalization of a BWR system and how the CHAN component addresses the modeling concerns discussed in the previous section. The TRAC vessel is divided into three radial rings, representing the hot, average, and low power regions of the BWR core, while the outer radial ring represents the vessel downcomer. CHAN components are connected axially across the core region in each of the radial rings. Each CHAN may contain multiple fuel rods for modeling local (within fuel bundle) radial temperature distributions, while the various power regions of the core are represented by several radial rings. Fluid flow in the bypass is computed using the normal three-dimensional solution algorithm, and fluid conditions within each CHAN are computed using the one-dimensional solution algorithm. Heat conduction through the channel wall provides a heat transfer path from the interior of the CHAN to the bypass fluid. The CHAN component allows the nodalization in the VESSEL to be relatively coarse (three radial, two azimuthal, and two axial subdivisions, or a total of 12 mesh cells) in the core bypass region, while any reasonable number of axial cells may be used within each CHAN component to resolve the axial profiles of power, temperature, and void fraction.

A nonhomogeneous, thermal equilibrium critical flow model was developed

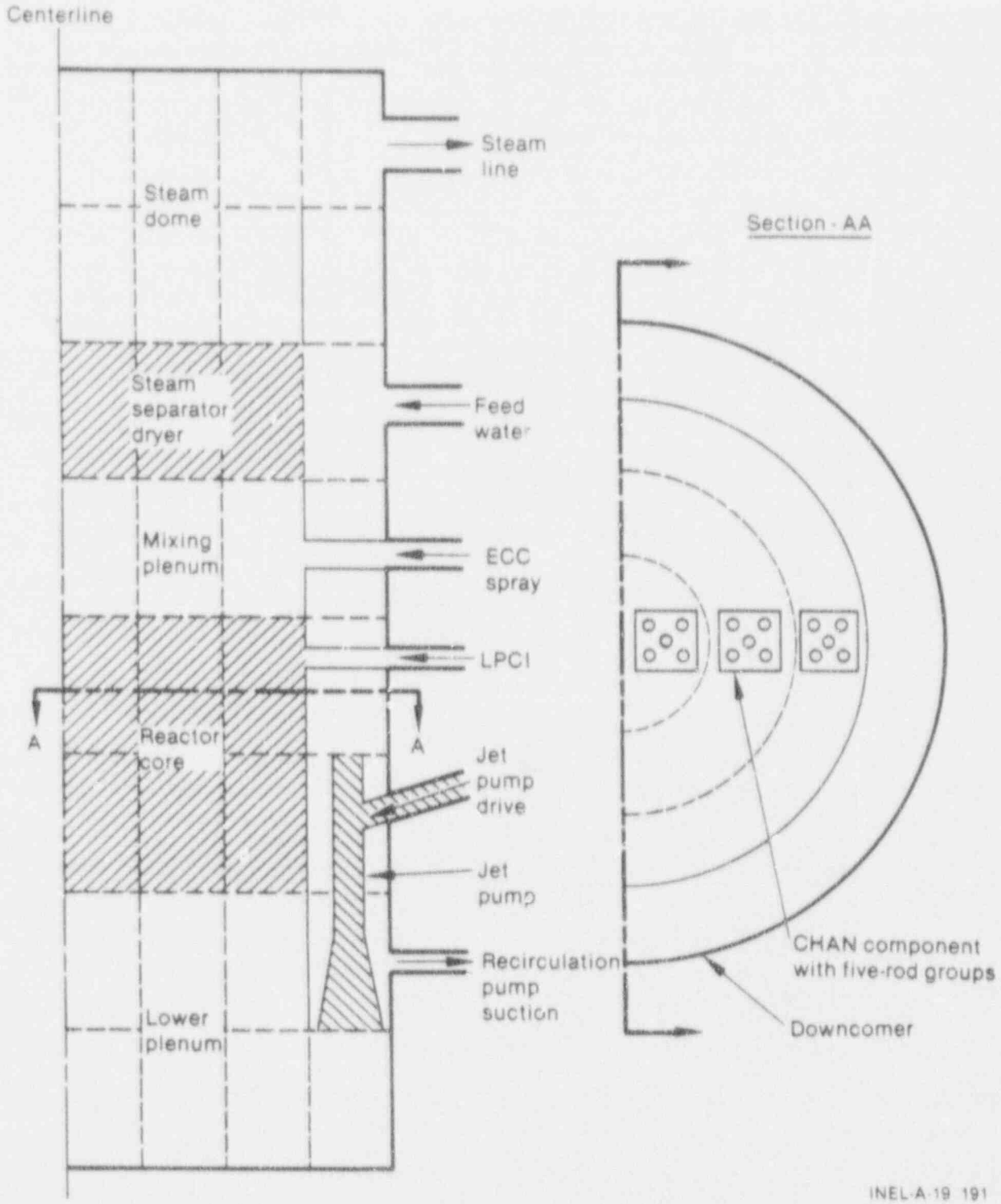

Figure 1-1. TRAC boiling water reactor nodalization (vessel half-section).

and implemented into the momentum solution of TRAC-BD1/MOD1. This critical flow model allows longer mesh cells to be used near a break; thus, large time steps can be used, reducing computational costs of BWR blowdown computations.

A methodology for use of countercurrent flow limiting correlations in the numerical solution of the momentum equations is also included in TRAC-BD1/MOD1. Several correlations have been included in the code for simulation of countercurrent flow limiting at BWR fuel bundle upper tie plates and side entry orifices.

TRAC-BD1/MOD1 incorporates a user-convenient jet pump component, JETP, for simulation of jet pumps in a BWR system (see Figure 1-1). This model provides corrections to the nonconservative momentum equations for accurate calculation of mixing losses in the throat of the jet pump. Data requirements of this component have been reduced substantially for user convenience.

A boiling transition model appropriate for high-quality CHF applications typical of BWR conditions has been implemented. This model is necessary to predict the time to CHF for BWR conditions.

A multiple pipe-to-vessel connection capability has been developed that allows the user to connect more than one one-dimensional component to the same three-dimensional VESSEL cell. Previous versions of TRAC only allowed for a single connection between one-dimensional components and vessel cells. This multiple connection capability allows coarser noding in the VESSEL component, reducing the computational cost of BWR analysis.

Many other changes in the areas of user-convenience or improved modeling capabilities have also been made. Some of these improvements are discussed below. The latest ANS decay heat standard has been incorporated into the code to improve the accuracy of the decay heat calculations.

An improved VALVE model has been developed for accurate simulation of the automatic depressurization system (ADS) and main steam isolation valves (MSIV) in the BWR system.

Generalized heat slab and pipe wall heat transfer models have been developed that allow accurate computation of stored energy and energy release rates from the BWR pressure vessel and its internal structures.

Finally, many user-convenience features were implemented into the TRAC-BD1 code to make it easier for the user to set up, run, and examine the computed results of a TRAC simulation. Some of these features include free-format input, extensive error and range checking of the input stream, more readable printed output, improved graphics, and improved traceback capabilities to assist with diagnosing a code abort.

Additional improvements have been implemented in the TRAC-BF1/MOD1 release of the code. The Courant-limit-violating numerical solution, which is based on the Two-Step method (fast numerics) developed by Mahaffy[1-6] at LANL, allows the code users to run slow transients with large time steps. This cuts

the computation time and cost considerably. The inclusion of implicit steam separator/dryer and implicit turbine models was a necessary step in making the fast numerics applicable to all one-dimensional components.

The one-dimensional neutron kinetics model is a more realistic way of representing axial power variations during a BWR transient. This is considered particularly important in ATWS calculations, where the use of a point kinetic model is considered inadequate.

Tne new condensation model for stratified vertical flow is particularly useful in realistic prediction of interfacial heat exchange in a volume with stagnant or moving stratified liquid level. The old general interfacial heat transfer model would grossly overpredict the rate of condensation in such situations.

The improved control system logic relieves the code user from the burden of carefully numbering all the control blocks according to the flow of signals. The user may now number the control blocks in any arbitrary order in the inputs, and the code automatically establishes the correct order to treating them according to their function and the paths of signals. Furthermore, in order to avoid inaccuracies due to large time steps allowed in the hydraulics solution, the new control logic selects its own time step and solves interconnected control blocks implicitly.

The preload processor checks TRAC-BF1/MOD1 inputs and loads only the subroutines needed for solving that problem, thereby adjusting the computer memory requirement to the size and nature of the problem. This has been shown to improve turnaround time on a time-shared computer and has given savings in computation cost.

Conversion to ANSI Standard FORTRAN provides increased portability and is particularly useful in implementation of TRAC-BF1/MOD1 on a Cray[a] or on an IBM system.

1.3 Quality Assurance Program

From the beginning, development of the TRAC-BWR code has proceeded toward a unique quality control program that ensures a well-documented working version of the code is available at all times. Any change to the code, however small, is given a unique program change label that appears on each FORTRAN change statement and is used for all documentation associated with that change to the code. Testing of all changes is performed by execution of test cases designed by the code developers during model development and

---

a. Mention of specific products and/or manufacturers in this document implies neither endorsement or preference nor disapproval by the U.S. Government, any of its agencies, or EG&G Idaho, Inc., of the use of a specific product for any purpose.

execution of the same test cases by the code architect after insertion of the changes into an official code version. The results of the test cases are described in model design reports and acceptance reports, respectively, which are referenced by the program change label assigned to the change. This procedure provides traceability of all code changes to documents that describe the basis of the change, the person making the change, a complete list of routines changed, changes to input and output of the code, and the results of execution of test cases.

When source code FORTRAN is modified, the modifications are implemented using an automated editing routine. This routine contains job control that identifies each line in the source code with a unique designation. Subsequent changes are implemented based on the relative position within the source. UPDATE is the editing routine used for UNICOS-based versions of the code. The editing and modifications done on an individual user's local system will depend on the software available at that site.

1.4 REFERENCES

1-1. J. Spore et al., *TRAC-BD1: An Advanced Best Estimate Computer Program for Boiling Water Reactor Loss-of-Coolant Analysis*, NUREG/CR-2178, October 1981.

1-2. D. D. Taylor et al., *TRAC-BD1/MOD1: An Advanced Best Estimate Computer Program for Boiling Water Reactor Transient Analysis, Volume 1: Model Description*, NUREG/CR-3633, EGG-2294, April 1984.

1-3. R. W. Shumway et al., *TRAC-BD1/MOD1: An Advanced Best Estimate Computer Program for Boiling Water Reactor Transient Analysis, Volume 2: Users Guide*, NUREG/CR-3633, EGG-2294, April 1984.

1-4. G. L. Singer et al., *TRAC-BD1/MOD1: An Advanced Best Estimate Computer Program for Boiling Water Reactor Transient Analysis, Volume 3: Code Structure and Programming Information*, NUREG/CR-3633, EGG-2294, April 1984.

1-5. R. W. Shumway et al., *TRAC-BD1/MOD1: An Advanced Best Estimate Computer Program for Boiling Water Reactor Transient Analysis, Volume 4: Developmental Assessment*, NUREG/CR-3633, EGG-2294, August 1984.

1-6. J. H. Mahaffy, *A Stability-Enhancing Two-Step Method for One-Dimensional Two-Phase Flow*, NUREG/CR-0971, LA-07951, 1979.

2. PHYSICAL AND MATHEMATICAL MODELS

The governing conservation equations solved in TRAC-BF1/MOD1 and the numerical methods employed are described in the following sections. The hydrodynamics, heat transfer, and numerical and reactor kinetics model are described.

2.1 HYDRODYNAMICS MODEL

The hydrodynamics model employed in both the one- and three-dimensional flow components is a two-fluid formulation for two-phase flow. Conservation equations for mass, energy, and momentum are formulated for both phases. Six inuependent conservation equations can be formulated for single-component one-dimensional two-phase flow. For single-component three-dimensional two-phase flow, there are ten such equations.

TRAC-BF1/MOD1 also incorporates the capability to model two-component flows in which the second component is assumed to be noncondensable gas (air). The noncondensable gas is assumed to be perfectly mixed with the vapor phase of the principal component (water), and the two gases are assumed to constitute a Gibbs-Dalton mixture. In this case, an additional conservation equation for noncondensable gas mass is added to the above-mentioned conservation equations for mass, energy, and momentum of the principal component. The transport of soluble boron is treated similarly.

The hydrodynamic equations are described in Subsection 2.1.1. To achieve closure of the equations, a large number of constitutive relations must be used. For example, the interfacial shear force must be formulated in terms of the independent hydrodynamic variables. The constitutive relations are described in Subsection 2.1.2.

The conservation equations presented here are included for mathematical completeness. These equations are repeated in Section 2.1 of the models and correlations document associated with this code manual.[2.1-1] The equations in Reference 1 are mathematically identical to these but contain minor notation differences, which represent the as-coded formulation.

2.1.1 Fluid Flow Equations

The differential field equations[2-2,3,4] for the two-fluid hydrodynamic flow model are

Mixture Mass Equation

$$\frac{\partial \rho_m}{\partial t} + \nabla \cdot (\alpha_g \rho_g \bar{V}_g + \alpha_\ell \rho_\ell \bar{V}_\ell) = 0 . \qquad (2.1\text{-}1)$$

Vapor Mass Equation

$$\frac{\partial (\alpha_g \rho_g)}{\partial t} + \nabla \cdot (\alpha_g \rho_g \bar{V}_g) = \Gamma_g . \qquad (2.1\text{-}2)$$

Noncondensable (Air) Mass Equation

$$\frac{\partial (\alpha \rho)_{NC}}{\partial t} + \nabla \cdot (\alpha \rho_{NC} \bar{V}_g) = \Gamma_{NC} . \qquad (2.1\text{-}3)$$

Boron Mass Equation

$$\frac{\partial (\alpha_\ell \rho_\ell C_B)}{\partial t} + \nabla \cdot (\alpha_\ell \bar{V}_\ell C_B) = \Gamma_B . \qquad (2.2\text{-}4)$$

Vapor Equation of Motion

$$\frac{\partial \bar{V}_g}{\partial t} + k_{vm} \left(\frac{\rho_C}{\alpha_g \rho_g} \right) \frac{\partial}{\partial t} (\bar{V}_g - \bar{V}_\ell) + \bar{V}_g \cdot \nabla \bar{V}_g$$

$$= - \frac{f_i}{\alpha_g \rho_g} - \frac{1}{\rho_g} \nabla P - \frac{C_{wg}}{\alpha_g \rho_g} \bar{V}_g |\bar{V}_g| + \bar{g} - k_{vm} \frac{\rho_C}{\alpha_g \rho_g} \bar{V}_D \cdot \nabla (\bar{V}_g - \bar{V}_\ell) . \qquad (2.2\text{-}5)$$

Liquid Equation of Motion

$$\frac{\partial \bar{V}_\ell}{\partial t} + k_{vm} \left(\frac{\rho_C}{\alpha_\ell \rho_\ell} \right) \frac{\partial}{\partial t} (\bar{V}_\ell - \bar{V}_g) + \bar{V}_\ell \cdot \nabla \bar{V}_\ell$$

$$= \frac{f_i}{\alpha_\ell \rho_\ell} - \frac{1}{\rho_\ell} \nabla P - \frac{C_{w\ell}}{\alpha_\ell \rho_\ell} \bar{V}_\ell |\bar{V}_\ell| + \bar{g} - k_{vm} \frac{\rho_C}{\alpha_\ell \rho_\ell} \bar{V}_D \cdot \nabla (\bar{V}_\ell - \bar{V}_g) . \qquad (2.2\text{-}6)$$

Mixture Energy Equation

$$\frac{\partial(\alpha_\ell \rho_\ell e_\ell + \alpha_g \rho_g e_g)}{\partial t} + \nabla \cdot (\alpha_\ell \rho_\ell e_\ell \bar{V}_\ell + \alpha_g \rho_g e_g \bar{V}_g)$$

$$= -P\nabla \cdot (\alpha_\ell \bar{V}_\ell + \alpha_g \bar{V}_g) + Q_{wg} + Q_{w\ell} + Q_{dg} + Q_{d\ell} \quad . \tag{2.1-7}$$

Vapor Energy Equation

$$\frac{\partial(\alpha_g \rho_g e_g)}{\partial t} + \nabla \cdot (\alpha_g \rho_g e_g \bar{V}_g) = -P\frac{\partial \alpha}{\partial t} - P\nabla \cdot \alpha \bar{V}_g + Q_{wg} + Q_{ig} + \Gamma_g h_{sg} + Q_{dg} \quad . \tag{2.1-8}$$

In the above equations, k_{vm} is the virtual mass coefficient, and the subscripts C and D refer to the continuous and dispersed phases, respectively.

An equivalent second set of equations may be obtained by substitution of liquid mass and energy equations for the mixture equations above. For one-dimensional flow, the first set of differential equations is solved for void fractions at or near the single-phase limits (0.0 and 1.0), while the second set is solved for void fractions in the strict two-phase region ($0.001 < \alpha < 0.999$). In this case, the velocity vector reduces to a single component so the conservation equations are six in number.

For three-dimensional flow, the velocity vector is characterized by three components, V_r, V_θ, and V_z, implying that a set of ten scalar equations will be solved. In the three-dimensional case, the mixture equations for mass and energy conservation are always solved, regardless of void fraction.

Closure of this system of equations requires specification of the thermodynamic equations of state for each phase (see Appendix A), the interfacial shear coefficient (C_i), the interfacial heat transfer rates (Q_{ig} and $Q_{i\ell}$), the interfacial mass transfer rates (Γ_g and Γ_ℓ), and the wall shear coefficients (C_{wg} and $C_{w\ell}$). Constitutive relations to obtain closure are described in Subsection 2.1.2. Jump conditions at the interface are also used to reduce the number of unknowns. These conditions are summarized below.

Interfacial Mass Continuity

$$\Gamma_g = -\Gamma_\ell \quad . \tag{2.1-9}$$

Interfacial Energy Continuity

$$\Gamma_g = \frac{-Q_{ig} - Q_{i\ell}}{h_{sg} - h_{s\ell}} \quad . \tag{2.1-10}$$

where

$$Q_{ig} = \frac{h_{ig}A_i(T_s - T_g)}{Vol} \qquad (2.1\text{-}11)$$

and

$$Q_{i\ell} = \frac{h_{i\ell}A_i(T_s - T_\ell)}{Vol} \; . \qquad (2.1\text{-}12)$$

2.1.2 Constitutive Relations

The field equations require certain auxiliary or constitutive equations to effect closure. It has been mentioned that thermodynamic equations of state for each phase are required. These are discussed in Appendix A. In addition, the liquid and vapor wall shear, interfacial shear, wall heat transfer, interfacial heat transfer, and net vaporization rate are necessary.

The wall heat transfers, Q_{wg} and $Q_{w\ell}$, are accounted for in the standard way. The surface areas represent an actual estimate of the total wall surface area wetted by each phase, whereas $h_{w\ell}$ and h_{wg} are based on heat-transfer correlations from the literature. In many two-phase flow situations, the walls are totally wetted by the liquid phase, in which case wall heat transfer to the vapor is zero.

The flashing rate Γ is determined from a simplified thermal energy jump condition [see Equation (2.1-10)]. In both the vapor-continuity equation and the vapor-thermal energy equation, the potentials $(T_s - T_g)$ and $(T_s - T_\ell)$ are evaluated at the new time level, whereas $h_{ig}A_i$ and $h_{i\ell}A_i$ are evaluated at the old time (see Subsection 2.3.7).

2.1.2.1 Wall Shear and Additive Form Loss. The wall shear coefficients, C_{wg} and $C_{w\ell}$ in Equations (2.1-5) and (2.1-6), are defined as

$$C_{wg} = \frac{\left.\frac{\partial P}{\partial x}\right|_w}{\rho_g (V_g)^2} \qquad (2.1\text{-}13)$$

$$C_{w\ell} = \frac{\left.\frac{\partial P}{\partial x}\right|_w}{\rho_\ell (V_\ell)^2} \qquad (2.1\text{-}14)$$

where $\partial P/\partial x|_w$ is the static pressure gradient due to wall friction alone. This term is calculated by using the Hancox two-phase wall shear multiplier[2.1-5] (ϕ_{HAN}) as a multiplier on the single-phase liquid wall friction factor (f_{Pfann}) obtained from the Pfann[2.1-6] correlation. The resulting wall friction term is

$$\left.\frac{\partial P}{\partial x}\right|_w = 2\rho_f V_f^2 \left(\frac{f_{Pfann}}{D_H}\right) \phi_{HAN}^2 . \qquad (2.1\text{-}15)$$

The Hancox multiplier is given by

$$\phi_{HAN}^2 = \left[1 + RX_f^{0.5}(1 - X_f)^{0.25}\right]\left\{1 + \left[\left(\frac{\rho_\ell}{\rho_v}\right)\left(\frac{\mu_v}{\mu_\ell}\right)^{0.2} - 1\right]X_f\right\} \qquad (2.1\text{-}16)$$

where

$$R = 3.1\left(1 - \frac{P}{P_c}\right)\exp^{-0.205650} , \qquad (2.1\text{-}17)$$

It should be noted that the constant in the exponent of Equation (2.1-15) differs from the value given in Reference 2.1-5. A units conversion error was discovered in the value given in Reference 2.1-5, and the value presented in Equation (2.1-15) is correct for S.I. units.

The Pfann correlation used in TRAC covers both the laminar and turbulent flow regimes and includes the effect of surface roughness e. Since this correlation is a single-valued function, it does not require an iterative solution. The correlation is

$$f_{1\phi} = \begin{cases} \dfrac{64}{Re} \text{ for } Re \le 2300 \\ \left(\dfrac{0.28}{\log Re - 0.82}\right)^2 \text{ for } 2300 < Re \le \dfrac{60}{\xi^{1.111}} \\ \left[\dfrac{0.25}{(3.393 - 0.805g_1)g_1 - 2.477 - \log\xi}\right]^2 \text{ for } \dfrac{60}{\xi^{1.111}} < Re < 424\,\dfrac{0.87 - \log\xi}{\xi} \\ \left(\dfrac{0.25}{0.87 - \log\xi}\right)^2 \text{ for } 424\,\dfrac{0.87 - \log\xi}{\xi} \le Re \end{cases} \qquad (2.1\text{-}18)$$

where

$$Re = \frac{\rho_m V_m D_H}{\mu} \tag{2.1-19}$$

$$g_1 = \log\left[\frac{Re\ \xi}{0.87 - \log\ \xi}\right] . \tag{2.1-20}$$

The basic finite-difference scheme properly calculates classical Bourda losses at an expansion but overpredicts the losses at a contraction. The user can specify an additional constant hydraulic loss coefficient in any of the coordinate directions. The user-supplied form loss coefficients (k) are defined in accordance with conventional usage or, for single-phase flow,

$$\Delta P_k = \frac{1}{2} k \rho V^2 \tag{2.1-21}$$

where ΔP_k is the form loss pressure drop between two adjoining cells.

Forward and reverse form loss coefficients k_F and k_R are input for each cell boundary in one-dimensional components. In the vessel component, separate values of k_F and k_R are input for the r, z, and θ faces of each cell. In Subroutine **FRCW**, each additive loss coefficient is converted to a friction factor and added to the wall friction factor calculated internally, using the Pfann correlation. The Fanning definition of friction factor (f) is used for this conversion, shown as

$$\Delta P_f = 2f\ \frac{L}{D_H}\ \rho V^2 . \tag{2.1-22}$$

Combining Equations (2.1-21) and (2.1-22) yields

$$f_{ADD} = 0.25\ k\ \frac{D_H}{L} \tag{2.1-23}$$

where f_{ADD} is the additive friction factor.

The value of k to be used in Equation (2.1-23) is determined by the direction of the mixture mass flux G_m, or

$$k = \begin{cases} k_f \text{ if } G_m \geq 0 \\ k_R \text{ if } G_m < 0 \end{cases} \quad (2.1\text{-}24)$$

The homogeneous two-phase friction multiplier is used as a multiplier on the additive form loss friction. This multiplier is given by

$$\phi^2_{HOM} = \frac{\rho_\ell}{\rho_m} , \quad (2.1\text{-}25)$$

where ρ_ℓ and ρ_m are liquid and homogeneous mixture density, respectively. Using the two-phase multipliers defined above, the total two-phase Fanning friction factor is given by

$$f_{TOT} = \phi^2_{HAN} f_{Pfann} + \phi^2_{HOM} f_{ADD} \quad (2.1\text{-}26)$$

where f_{Pfann} is the single-phase liquid friction factor obtained from the Pfann correlation.

The as-coded formulations for wall shear and additive losses are given in Reference 1, Section 6.2.

2.1.2.2 Interfacial Shear Model. The interfacial shear models in TRAC-BF1/MOD1 are based upon the drift flux correlations by Ishii, Anderson, and Chu.[2.1-7,8,9] These correlations assume that the drift flux parameters adequately approximate the two-fluid system under transient conditions, although the data bases have been collected under steady-state, adiabatic conditions.

The interfacial shear model is capable of distinguishing between three flow regimes: bubbly/churn flow, annular/dispersed flow, and dispersed droplet flow. Countercurrent as well as cocurrent flow is possible in each of the flow regimes. The flow regime transitions are determined by the value of the average void fraction, which is calculated from an empirically derived function of phase-dependent density, geometry, and mass flux. The as-coded mathematical description is provided in Reference 1, Section 6.1.5. In all regimes, two parameters are determined: the interfacial drag coefficient, which correlates the shear between the phases, and the interfacial area, which correlates the surface area on which the shear acts.

2.1.2.2.1 Bubbly/Churn Flow--The interfacial shear coefficients and interfacial area in bubbly/churn flow are correlated with the phase-dependent velocities and densities, void fraction, and the Weber Number. The Weber Number defines a critical value of velocity, which determines whether or not the bubble deforms for a given surface tension. The as-coded mathematical description is provided in Reference 1, Section 6.1.7.

2.1.2.2.2 **Annular/Dispersed Flow**--In annular flow, the flow is modelled as a vapor core surrounded by a smooth liquid region along the walls. Therefore, interfacial area is correlated with only the channel geometry and the void fraction. The interfacial shear coefficients are correlated with the phase-dependent velocities and densities and void fraction. Additionally, entrainment is possible in annular/dispersed flow. The as-coded mathematical description is provided in Reference 1, Section 6.1.7.

2.1.2.2.3 **Dispersed Droplet Flow**--Dispersed droplet flow is very similar to bubbly/churn flow except that in dispersed flow there are bubbles of liquid in the vapor phase. As in bubbly flow, the interfacial shear coefficients and interfacial area in dispersed droplet flow are correlated with the phase-dependent velocities and densities, void fraction, and the Weber Number. However, entrainment is possible in dispersed droplet flow. The as-coded mathematical description is provided in Reference 1, Section 6.1.7.

2.1.2.2.4 **Entrainment**--Direct entrainment of liquid droplets into the vapor stream is possible in both the annular/dispersed and dispersed droplet flow regimes. Entrainment is correlated (by Ishii[2.1-7]) with the vapor volumetric flux density, channel geometry, and the liquid Reynolds number. The entrainment correlation in TRAC-BF1/MOD1 is modified compared to the original formulation of Ishii. These modifications account for the presence of both wet and dry walls in the same hydrodynamic section of the model. The as-coded mathematical description is provided in Reference 1, Section 6.1.9.2.

2.1.2.2.5 **Counter-Current Flow Limiting**--The counter-current flow limit (CCFL) calculation is performed in hydrodynamic junctions that are flagged by the user. The CCFL model is of the Kutateladze type and based upon BWR geometric data taken by Sun.[2.1-10] More information is given in Volume 1, Section 2.1.3.2. The as-coded mathematical description is provided in Reference 1, Section 7.3.

2.1.2.3 **Interfacial Heat Transfer.** HEATIF is the subroutine that calculates the interfacial heat transfer. The purpose of the subroutine is to obtain the variables $(hA)_{i\ell}$ and $(hA)_{ig}$, i.e., for the liquid and vapor heat transfer coefficient times interfacial area, respectively. The model assumes that there is an interface that is always at the local saturation temperature and that steam and water are exchanging energy with the interface at a total rate of

$$q_i = (hA)_{i\ell}(T_\ell - T_s) + (hA)_{ig}(T_g - T_s) \quad . \tag{2.1-27}$$

The net mass transfer rate is then

$$\Gamma = \frac{q_i}{h_{sg} - h_{s\ell}} + \Gamma_{wall} \tag{2.1-28}$$

where the wall term comes from nucleate boiling, as explained later.

A simple flow-regime map[2.1-11] helps to define which correlation for h, A, or hA to use. This flow-regime map, developed for vertical pipe flow, is the simplest prescription that provides a rational means for defining the constitutive equations. Figure 2.1-1 shows the flow-regime map used in TRAC-BF1/MOD1. The flow regimes are classified according to void fraction and mass flow. The map is used to determine the flow regime that exists in a given computational cell independent of the fluid cell orientation. Once the flow regime in a cell is determined, the constitutive relations for that flow regime are used to determine the interfacial area and interfacial heat transfer coefficients for the cell. Figure 2.1-2 shows the logic flow paths for the calculation. The as-coded mathematical description is provided in Reference 1, Section 4.1.

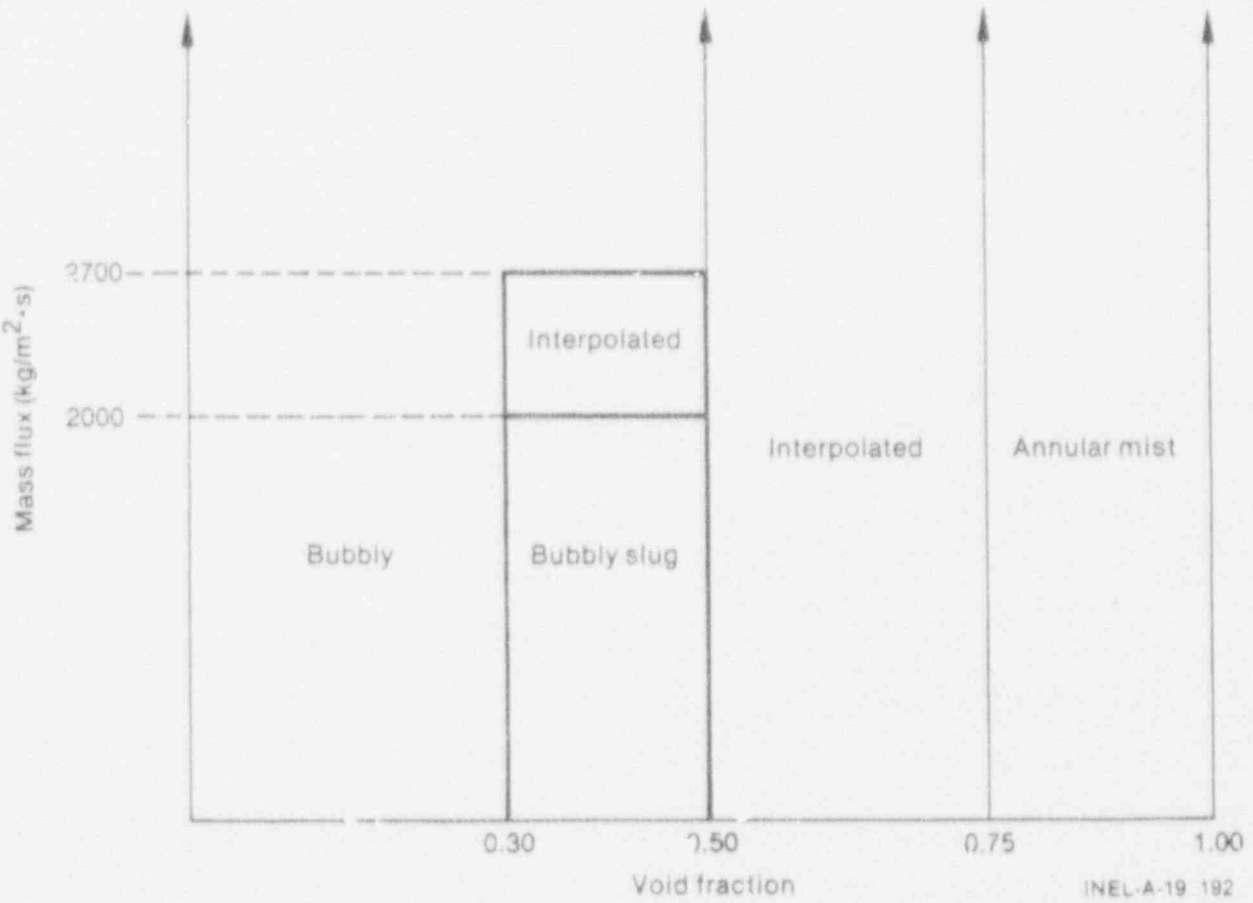

Figure 2.1-1. Flow regime map.

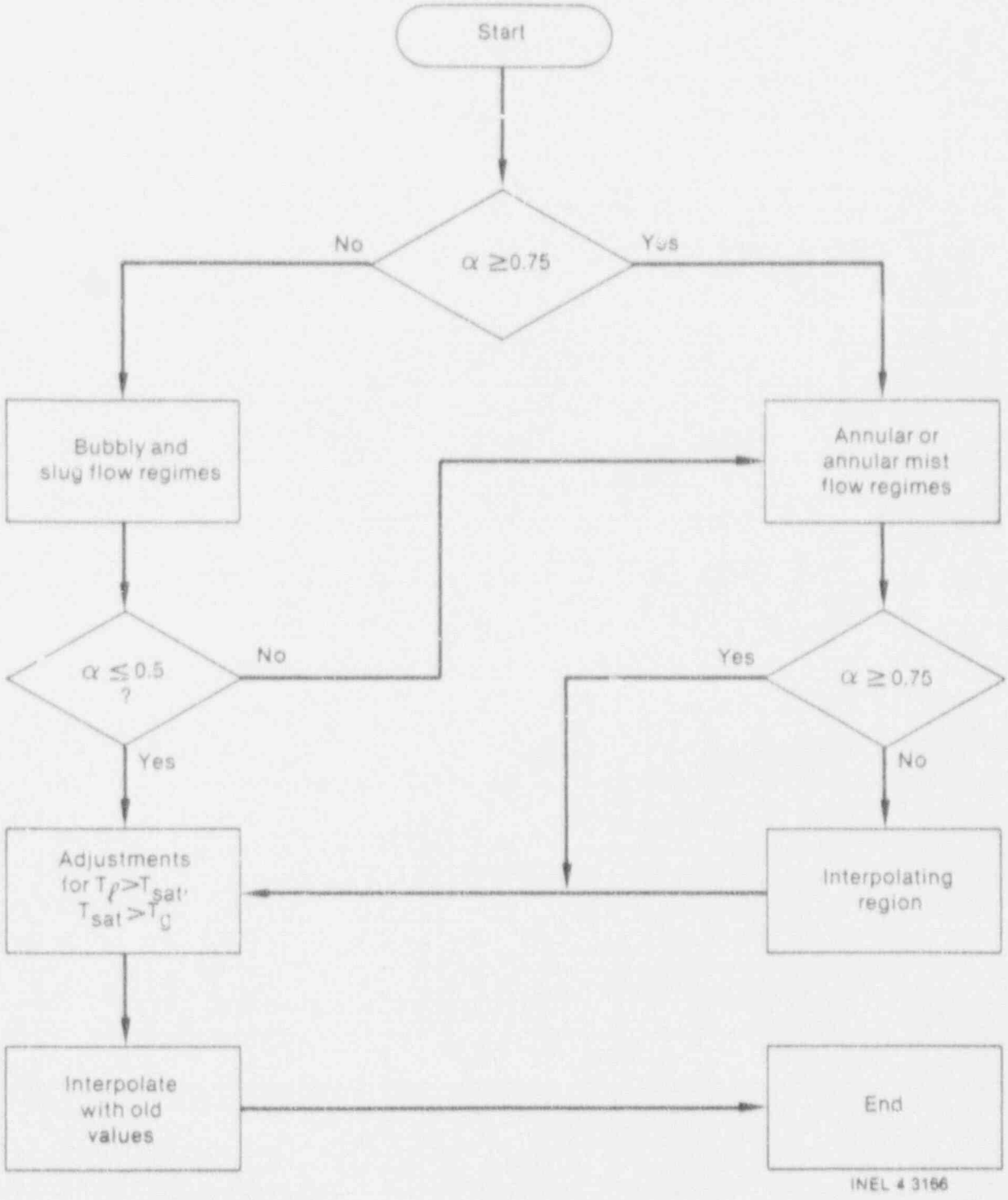

Figure 2.1-2. Flow chart for interfacial HTC.

2.1.2.3.1 Bubbly or Bubbly-Slug Flow Regime--If the void fraction is ≤ 0.75, bubbly or bubbly-slug flow interfacial correlations are evaluated. The interfacial surface area in bubbly flow is calculated in conjunction with a critical bubble Weber number, We_b. A value of $We_b = 7.5$ is used in the present code version. This value was chosen based on comparisons between TRAC predictions and experimental results for low subcooling (shear-dominated) downcomer tests performed by Creare Inc.[2.1-12] The expressions relating interfacial surface area to We_b are

$$We_b = \rho_\ell V_R^2 \frac{D_B}{\sigma} \tag{2.1-29}$$

$$D_B = We_b \frac{\sigma}{\rho_\ell V_R^2} \tag{2.1-30}$$

where D_b is the bubble diameter. The code minimum for V_R is 1.0, and the value of the bubble diameter obtained from Equation (2.1-30) is limited to be less than the hydraulic diameter of the mesh cell and >0.001 m. For this diameter, assuming a uniform bubble distribution within the mesh-cell volume, the bubble density is

$$CNB = \frac{6\alpha_b}{\pi D_b^3} \tag{2.1-31}$$

and the interfacial area in fluid volume Vol is

$$A_b = CNB\pi D_B^2 Vol = \frac{6\alpha_b Vol \rho_\ell V_R^2}{\sigma We_b} . \tag{2.1-32}$$

If the relative velocity is small, the interfacial area can become small enough to allow significant disequilibrium to occur. In this case, another surface area based on a minimum number density (CNB =- 10^{10} bubbles/m^3) is computed from Equations (2.1-31) and (2.1-32). The result is

$$A_b = 4.836\alpha_b^{2/3} 10^{10/3} Vol . \tag{2.1-33}$$

The maximum area from Equations (2.1-32) and (2.1-33) is used for the interfacial heat transfer area.

The void fraction α_b in the above equations may differ from the cell void fraction when the latter is >0.3. If the cell-average mass flux is <2000 kg/m^2-s and the void fraction is between 0.3 and 0.5, the flow enters the bubbly-slug regime. In this flow regime, the vapor is divided between vapor

slugs and small bubbles dispersed in the liquid. The void fraction in the vapor slugs (α_s) increases linearly from 0.0 at an overall void fraction of 0.3 to a value of 0.3 at an overall void fraction of 0.5. The void fraction in the bubbles is the difference between the overall void fraction and α_s. If the mass flux >2700 kg/m^2-s, all vapor is assumed to exist in bubble form. Linear interpolation in mass flux is used in the range 2000 to 2700 kg/m^2-s, as indicated in Figure 2.1-3. For mass flux <2000 kg/m^2-s, the amount of void in the bubbly region is reduced, and the amount in the slug region is increased as the overall void fraction increases from 0.3 to 0.5. At a void fraction of 0.5, 60% of the vapor is in the slugs and 40% in the bubbles.

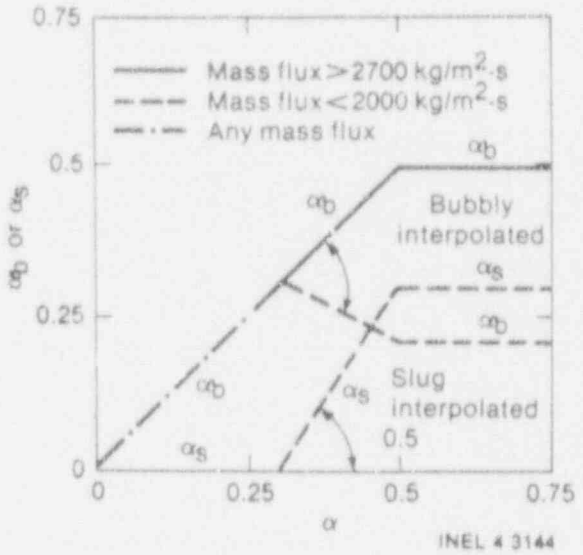

Figure 2.1-3. Bubbly slug void fraction versus cell average void fraction.

The bubbly flow liquid side interfacial Nusselt number is the larger of the value given by an approximate formulation of the Plesset Zwick bubble growth model,[2.1-13,14]

$$Nu_\ell = \frac{12}{\pi}(DTL)\rho_\ell \frac{C_{p\ell}}{[\rho_g(h_{sg} - h_{s\ell}]} \qquad (2.1\text{-}34)$$

and a sphere convection coefficient[2.1-15]

$$Nu_\ell = 2.0 + 0.74\, Re_b^{0.5} \qquad (2.1\text{-}35)$$

where

$$Re_b = \rho_\ell V_R \frac{D_b}{\mu_\ell} \quad (2.1\text{-}36)$$

$$DTL = Max[(T_\ell - T_s), 1.0] . \quad (2.1\text{-}37)$$

In the bubbly-slug flow regime, the interfacial area and interfacial heat transfer coefficients are the sum of the contributions from the vapor slugs and the small bubbles. The contribution for the small bubbles is computed using the formula for the bubbly flow regime [Equations (2.1-29) through (2.1-33)]. The contribution from the vapor slug portion of bubbly-slug flow is computed using the formula

$$A_s = \alpha_s \frac{Vol}{D_H} \quad (2.1\text{-}38)$$

to approximate the interfacial area of the slugs and

$$Nu_\ell = 0.02\ Re_\ell\ Pr_\ell \quad (2.1\text{-}39)$$

to compute the slug portion liquid-to-interface heat transfer coefficient. The vapor slug heat transfer coefficient is set to a value of 1.0×10^4. The total heat flow to the vapor from the interface per degree of temperature difference ($T_{sat} - T_v$) is chosen to be the greater of $h_{ig}(A_s + A_b)$ and 1.0×10^7 (W/K-m^3) x Vol, where Vol is the cell volume. The reason for the large lower bound is to ensure that the vapor temperature stays close to the saturation value.

The as-coded mathematical description for interfacial area in bubbly/churn flow is provided in Reference 1, Section 4.1.7.1. The as-coded mathematical description for interfacial heat transfer coefficients in bubbly/churn flow is provided in Reference 1, Section 4.1.8.1.

2.1.2.3.2 Drop or Annular Mist Flow Regime--The void fraction, α_d, used in the drop regime is constrained to lie between 0.999999 and 0.75. Since the liquid in a cell can be both in entrained drops and in a liquid wall film, a modified Ishii[2.1-16] entrainment correlation is used to partition the liquid and is expressed as

$$E = \frac{n}{\left[1 + (0.1 + n)^2\right]^{1/2}} \quad (2.1\text{-}40)$$

where

$$n = 1 \times 10^{-6} \left(U_g^{*10} D^{*5} Re_L\right)^{1/4} \quad (2.1\text{-}41)$$

$$U_g^* = \frac{\alpha V_g}{\left[\frac{\sigma g \Delta\rho \left(\frac{\rho_g}{\Delta\rho}\right)^{2/3}}{\rho_g^2}\right]^{1/4}} \qquad (2.1\text{-}42)$$

$$Re_L = Max\left[370., \frac{(1-\alpha)\rho_\ell V_\ell D_H}{\mu_\ell}\right] \qquad (2.1\text{-}43)$$

$$D^* = L_c\left(\frac{g\Delta\rho}{\sigma}\right)^{1/2} \qquad (2.2\text{-}44)$$

The entrainment fraction is modified by the fraction of the wall that is wetted, WA_{CRT}, and shown as

$$E' = E + (1 - E)WA_{CRT} \qquad (2.1\text{-}45)$$

where

E' = modified entrainment fraction

$$WA_{CRT} = WA_f/WA_{TOT}. \qquad (2.1\text{-}46)$$

WA_{TOT} is the total of the rod and wall surface areas for the cell. WA_f is the sum of the rod and wall areas in the cell that are not in the film boiling or steam cooling mode. If WA_f is greater than zero, the minimum film thickness is calculated so that WA_f can be reduced if there is insufficient water to cover all the wetted surface. The minimum film thickness is calculated from the laminar film equation[2.1-17] as

$$\delta = \left(\frac{3\mu_\ell G_\ell}{g\rho_\ell^2}\right)^{1/3} \qquad (2.1\text{-}47)$$

where

$$G_f = Vol_{\rho\ell} V_\ell / WA_f \qquad (2.1\text{-}48)$$

$$Vol_f = (1 - \alpha)(1 - E')Vol = \text{(volume of liquid in the film)} \qquad (2.1\text{-}49)$$

Vol is the cell volume. The new wall area covered with liquid film is

$$WA_f = \min[WA_f, Vol_f/\delta] \tag{2.1-50}$$

If the entrainment fraction is >0.75, the wetted wall area is further modified as

$$WA'_f = 2WA_f(1.02 - E)(3.7) \ . \tag{2.1-51}$$

The film heat transfer coefficient between both liquid and vapor and the interface is calculated from the Nusselt number expression

$$Nu = 0.02\ Re\ Pr \tag{2.1-52}$$

if the liquid is subcooled. Equation (2.1-52) reduces to

$$(hA)_{i\ell} = 0.02(WA'_f)\rho_\ell V_R C_{p\ell} \tag{2.1-53}$$

for the liquid. If the liquid is not subcooled, a calculation of the total wall heat flux to the liquid is performed and divided by $(T_f - T_s)$ to obtain a new $(hA)_{i\ell}$ for the film. If this wall value for (hA) exceeds the previously computed interfacial value, it is used for the liquid interfacial heat transfer calculation to minimize further superheating of the liquid.

The droplet interfacial area is obtained in a manner analogous to that used to compute the bubble interfacial area in Equations (2.1-45) through (2.1-48). The result is

$$A_d = \frac{6E(1 - \alpha_d)(Vol)\rho_g V_R^2}{\sigma We_d} \tag{2.1-54}$$

where a critical Weber number equal to 4.0 for the drops is used. This value of the Weber number is appropriate for accelerating drops. For those cases where sensitivity to We_d was tested, the results were not influenced strongly by We_d in the range $2 \leq We_d \leq 12$. The liquid side heat-transfer coefficient is simply

$$h_{i\ell} = \frac{Ck_\ell}{D_d} \tag{2.1-55}$$

where C, a constant, has been chosen to force the droplets to equilibrium under a variety of flow conditions. The constant C = 11,300 implies a thermal boundary layer in the drops that is about a thousandth of the drop diameter.

The WCS[2.1-18] model is used to compute the vapor-to-droplet heat transfer

$$(ha)_{ig} = 1.32 \left(\frac{P_c}{P}\right)^{1.1} \rho_g \left(\frac{V_g \alpha}{\alpha_{HE}}\right)^2 Vol(1 - \alpha_{HE})^{2/3} \frac{k_g}{\alpha D_H} \quad (2.1\text{-}56)$$

where

$$D_H = Min\,[D_H, 0.03] \quad (2.1\text{-}57)$$

$$\alpha_{HE} = \frac{1}{1 + \frac{\rho_g(1 - X)}{\rho_\ell X}} \quad (2.1\text{-}58)$$

$$X = \frac{1}{1 + \frac{\rho_\ell(1 - \alpha)}{\rho_v s \alpha}} \quad (2.1\text{-}59)$$

The droplet and film values for hA are added together to obtain the final values for both liquid and vapor.

The as-coded mathematical description for interfacial area in droplet flow is provided in Reference 1, Section 4.1.7.2. The as-coded mathematical description for interfacial heat transfer coefficients in droplet flow is provided in Reference 1, Section 4.1.8.2.

2.1.2.3.3 Annular Film Flow--The interfacial area is determined by first determining the thickness of the annular film. The film thickness is the maximum of the actual film thickness implied by void fraction and a minimum thickness implied by a force balance on the creeping film. These data are used to calculate the interfacial area per unit volume from the channel geometry.

The vapor interfacial heat transfer coefficient is determined from the well-known Dittus-Boelter correlation in the turbulent regime. In the laminar regime, the coefficient is adapted from the classical solution where Nu = 4.364. The liquid heat transfer coefficient is determined from the Megahed correlation. The as-coded mathematical description for interfacial area in film flow is provided in Reference 1, Section 4.1.7.3. The as-coded mathematical description for interfacial heat transfer coefficients in film flow is provided in Reference 1, Section 4.1.8.3.

2.1.2.3.4 Transition Regime--If the cell void fraction is between 0.5 and 0.75, a spline interpolation between the values of hA for annular mist flow (α = 0.75) and bubbly-slug flow (α = 0.5) is used to obtain both the

liquid and vapor hA.

The as-coded mathematical description for interpolation in the transition regime is provided in Reference 1, Section 4.1.8.4.

2.1.2.3.5 Final Adjustments--If the vapor is subcooled, $(hA)_{ig}$ is increased to help remove the superheat by using

$$(ha)_{ig} = (hA)_{ig} e^{DTV} \tag{2.1-60}$$

where

$$DTV = T_s - T_g \, . \tag{2.1-61}$$

DTV is limited to be <7.0 and ≥0.0.

The liquid side hA is compared with (1000)(Vol)/ΔX, and the larger of the two values is chosen. Thus, the minimum allowed value for $(hA)_{i\ell}$ is arbitrarily set to 1000 times the cell flow area. Additional liquid side adjustments are made if the liquid is subcooled. A modified Unal[2.1-19] correlation is calculated

$$(hA)_{i\ell,b} = 3\alpha \, Vol \, c \, \phi \, \frac{h_{sg} - h_{s\ell}}{\rho^*} \tag{2.1-62}$$

where

$$c = \begin{cases} \dfrac{0.23 \times 10^{10}}{P^{1.418}} \; for \; P \geq 1.0 \; MPa \\ 61.0 - 0.0000649 \, (P - 1.7 \times 10^5) \; for \; P < 1.0 \; MPa \end{cases} \tag{2.1-63}$$

$$\phi = \left[Max \left(\frac{|V_\ell|}{0.61}, \, 1. \right) \right]^{0.47} \tag{2.1-64}$$

and

$$\rho^* = \frac{\rho_\ell - \rho_g}{\rho_\ell \rho_g} \, . \tag{2.1-65}$$

The Unal correlation value of $(hA)_{i\ell}$ is used for void fractions between 0.0 and 0.5, while the drop-annular value is used >0.75. A spline

interpolation between the Unal and drop-annular values is used in the transition range of void fractions ($0.5 \leq \alpha \leq 0.75$).

Relative velocity weighting is also performed on the liquid side hA if the liquid is subcooled. The weight factor, WVR, is the ratio of two relative velocity estimates

$$WVR = VREL/V_{gj} \tag{2.1-66}$$

where

$$V_{gj} = 2\left(\frac{\sigma g \Delta\rho}{\rho_g^2}\right)^{1/4} \tag{2.1-67}$$

$$VREL = (1 - \alpha C_o)V_g - (1 - \alpha)C_o V_\ell \ . \tag{2.1-68}$$

Below a void fraction of 0.5, C_o is assumed to be C_{ob}, where C_{ob} is computed as

$$C_{ob} = 1 + 0.2\left[\frac{\rho_\ell (g_c D_H)^{1/2}}{|G_\ell| + |G_v|}\right]^{1/2}(1 - e^{-18\alpha}) \ . \tag{2.1-69}$$

Above a void fraction of 0.75, C_o is assumed to be 1.0. Spline interpolation is used to obtain C_o in the transition range.

A reduction in the liquid side hA for subcooled liquid is also performed if noncondensable gas (air) is present. In this case, $(hA)_{i\ell}$ is multiplied by

$$C_{NDM} = 0.168\left[\frac{\alpha(\rho_g - \rho_{NC})^2}{(1 - \alpha)\rho_g \rho_\ell}\right]^{0.1} \ . \tag{2.1-70}$$

With $(hA)_{ig}$ and $(hA)_{i\ell}$ as calculated from the above considerations, Equation (2.1-28) is next multiplied by the time step size to obtain the predicted net interfacial mass transfer Δm_i. If Δm_i is positive (flashing case) and >90% of the cell liquid mass, m_ℓ, or if Δm_i is negative (condensing case) and $|\Delta m_i|$ is >90% of the cell vapor mass, m_g, both $(hA)_{ig}$ and $(hA)_{i\ell}$ are reduced by the factor

$$\frac{0.9(M_\ell \text{ or } m_g)}{|\Delta m_i|}$$

to improve stability of the numerical scheme.

Finally, the coefficients $(hA)_{if}$ and $(hA)_{ig}$ are constrained to lie within the limits (Vol) and (1.0×10^{9})(Vol).

The as-coded mathematical description for adjustments and limits imposed on the interfacial heat transfer coefficient is provided in Reference 1, Sections 4.1.9-11.

2.1.3 Flow Limit Models

A critical flow model and a countercurrent flow limitation (CCFL) model have been implemented into TRAC-BF1/MOD1 to improve the available modeling flexibility. These models are identified in TRAC as flow limit models. For the critical flow model, the limitation is on a hybrid mixture velocity and is based on a two-phase homogeneous equilibrium sound speed. For the CCFL model, the limitation is on the liquid downflow rate for a given vapor upflow rate and is based on an experimentally determined CCFL correlation. The numerics associated with implementation of these flow limit models are described in Subsection 2.3.4. The models employed in TRAC-BF1/MOD1 for the critical or choked flow velocity and CCFL are described in Subsections 2.1.3.1 and 2.1.3.2, respectively.

A critical flow model was found to be advantageous to the user, since it eliminates the need for a fine spatial noding near the choking plane where large spatial gradients can occur. For semi-implicit numerics available in TRAC, such a noding scheme would be very expensive to execute. Also, if a critical flow model is not available, the user must anticipate the choking locations before setting up the model or performing the calculation since fine noding would be required at this location. For these reasons, a special critical flow model was developed and implemented.

2.1.3.1 Critical Flow Model. In previous versions of TRAC-BF1, the criteria for choked flow were determined by a characteristic analysis of the partial differential equations governing the flow. Ideally, such an approach is correct. However, it has been found empirically[2.1-20] that a simplified, approximate criterion

$$\frac{\alpha_g \rho_f V_g + \alpha_f \rho_g V_f}{\alpha_g \rho_f + \alpha_f \rho_g} = \pm a_{HE} \qquad (2.1\text{-}71)$$

may be used in place of the detailed characteristic analysis and still obtain good code/data comparisons. Accordingly, this criterion is used in TRAC-BF1/MOD1 to determine whether the flow is choked.

The homogeneous equilibrium sound speed (a_{HE}) depends on the void fraction of the flow just upstream of the choking point. For very low void fractions ($\alpha < 0.01$), a_{HE} is the larger of (a) the liquid velocity at the point where flashing begins and (b) the two-phase value of the homogeneous equilibrium sound speed. For moderate and high void fractions ($\alpha \geq 0.01$), a_{HE} is simply

the two-phase value of the homogeneous equilibrium sound speed, (b).

The liquid velocity (a) is estimated by assuming single-phase liquid flow up to the point where flashing begins. Choking is assumed to occur as a result of initiation of liquid flashing.[2.1-20] This takes place when the fluid pressure drops sufficiently far below the saturation pressure corresponding to the liquid temperature. This saturation pressure undershoot is computed from a modified Burnell subcooled choking model[2.1-21,22]

$$\Delta P_{undershoot} = 0.284\ P_s \left(\frac{\sigma}{\sigma_{REF}} \right) \qquad (2.1\text{-}72)$$

where σ_{REF} is the surface tension at 200 psia pressure. Using the above expression for the pressure undershoot, the critical subcooled liquid velocity is computed from the Bernoulli equation. The two-phase homogeneous equilibrium sound speed (b) above is computed from

$$a_{HE} = \left(\frac{\partial P}{\partial \rho} \right)_s^{1/2} . \qquad (2.1\text{-}73)$$

The as-coded mathematical description for the critical flow model is provided in Reference 1, Section 7.2.

2.1.3.2 CCFL Model. Countercurrent flow limiting, also called flooding, determines the amount of liquid that can penetrate the flow restrictions and determines spatial distribution of the ECC liquid injected into the reactor vessel. The distribution of ECC fluid determines the cooling effectiveness of the ECC systems. If limiting occurs at the upper tie plate of a BWR fuel bundle, the amount of liquid that can penetrate into the bundle is reduced. If limiting occurs at the lower core support plate or the side entry orifices, refilling of the lower plenum will be delayed. The limiting at the side entry orifice can be particularly important because it prevents water from leaving the bottom of the bundle.

Countercurrent flow limiting is a complicated hydrodynamic phenomenon and is thought to arise as a result of the interfacial friction between the liquid and vapor phases.[2.1-23] The limiting in a BWR has been found from experiments using both air-water and steam-water and prototypic hardware to be described by a Kutateladze-type correlation of the form[2.1-10]

$$K_g^{1/2} + mK_\ell^{1/2} = K^{1/2} \qquad (2.1\text{-}74)$$

where

$$K_g = \frac{\alpha_g V_g (\rho_g)^{1/2}}{[\sigma_g(\rho_\ell - \rho_g)]^{1/4}} \quad (2.1\text{-}75)$$

$$K_\ell = \frac{\alpha_\ell V_\ell (\rho_\ell)^{1/2}}{[\sigma_g(\rho_\ell - \rho_g)]^{1/4}} \quad (2.1\text{-}76)$$

and m and K are constants that depend on tne geometry.

This correlation specifies the maximum downflow liquid velocity in countercurrent flow through flow restrictions that can be obtained for a given upward vapor velocity. Thus, countercurrent flow limiting (flooding) represents an upper limit in the liquid penetration rate in countercurrent flow that is analogous to choking, which determines the upper limit of the discharge flow rate in cocurrent flow from a source of fluid at high pressure.

The constants in the flooding correlation, Equation (2.1-76), depend on the geometry of the simulated restriction. Two sets of constants are available in TRAC to simulate the upper tie plate of a BWR 7 x 7 or 8 x 8 fuel assembly and to simulate the side entry orifice in the fuel support piece (see Reference 2.1-26). For an upper tie plate, the constants are m = 1.0 and K = 4.2. These constants were chosen on the basis of the correlations discussed in Reference 2.1-26. For a side entry orifice, the data are well represented by m = 0.59 and

$$K = [f(P_w^*)]^2 \quad (2.1\text{-}77)$$

where

$$f(P_w^*) = 2.14 - 0.008\, P_w^* \quad (2.1\text{-}78)$$

and

$$P_w^* = \frac{P_w}{\left(\frac{\sigma}{g(\rho_\ell - \rho_g)}\right)^{1/2}} . \quad (2.1\text{-}79)$$

The as-coded mathematical description for the CCFL model is provided in Reference 1, Section 7.3.

2.1.4 Level Tracking Model

In the normal TRAC solution of the fluid flow equations, the mean cell void fraction is assumed to exist uniformly throughout each hydrodynamic fluid cell. If there exists in the cell a phase boundary, or liquid level, the numerical solution to the fluid flow equations results in an artificially high diffusion of vapor in one direction and liquid in the other.

To minimize this artificial diffusion, it is necessary to accurately predict the existence of two-phase levels that may occur in vertically oriented hydrodynamic cells and to take proper account for this in the numerical solution of the flow equations. The TRAC-BF1/MOD1 two-phase level tracking model was developed for this purpose. This model provides the capability of maintaining the sharp void fraction discontinuity across a two-phase level that may occur in vertical components.

The TRAC level tracking model consists of two parts:

1. Detection of two-phase levels plus calculation of their positions, velocities, and void fractions above and below the phase boundaries

2. Appropriate modification to the equations governing the flow when a two-phase level is present.

Part 2 above is discussed in Subsection 2.3.4. Part 1 may be further divided into two sections: (a) detection of two-phase levels and (b) calculation of the parameters necessary to describe the propagation of fluid above and below the phase boundaries.

The as-coded mathematical description for the level tracking model is provided in Reference 1, Section 6.3.

2.1.4.1 Level Detection. The first step in detecting a two-phase level is the determination of the type of vertical void profile existing around a particular cell. The level detection logic required for a normal (increasing in the vertical direction) void profile is not the same as the logic required for an inverted (decreasing in the axial direction) void profile. Once the type of void profile has been established, the model must determine if the conditions in the cell indicate the existence of a two-phase level. Although different logic is used depending on the void profile, the use of cell average void fraction differences to initiate the level calculations is common to all conditions. Generally, a level is assumed to exist in cell j if

$$(\alpha_{j+1} - \alpha_j) \text{ or } (\alpha_j - \alpha_{j-1}) > ALPCUT \qquad (2.1\text{-}80)$$

provided that no level exists in cell (j+1) or cell (j-1). Here, ALPCUT is a predetermined cutoff value.

2.1.4.2 Calculation of Level Parameters. The parameters necessary to

describe a two-phase level are the position and velocity of the level and the void fractions above and below the level. Figure 2.1-4 shows a simplified diagram of a two-phase level established in a normal void profile situation.

For a normal void profile ($\alpha_{j+1} \geq \alpha_j \geq \alpha_{j-1}$), the two-phase level parameters in cell j can be obtained from the conditions in the vessel cells above and below cell j. The position of the level in cell j can be described by the equation

$$DZL_j = DZ_j \left(\frac{\alpha_j^+ - \alpha_j}{\alpha_j^+ - \alpha_j^-} \right) \tag{2.1-81}$$

where α^+ and α^- are the void fractions above and below the level. For normal void profile conditions, the void fraction below the level α_j^- is assumed to be equal to the void fraction in the cell below, i.e.,

$$\alpha_j^- = \alpha_{j-1} . \tag{2.1-82}$$

In the absence of entrainment of liquid from below the level, the void fraction above the level, α_j^+, is assumed to be equal to the void fraction in the cell above

$$\alpha_j^+ = \alpha_{j+1} . \tag{2.1-83}$$

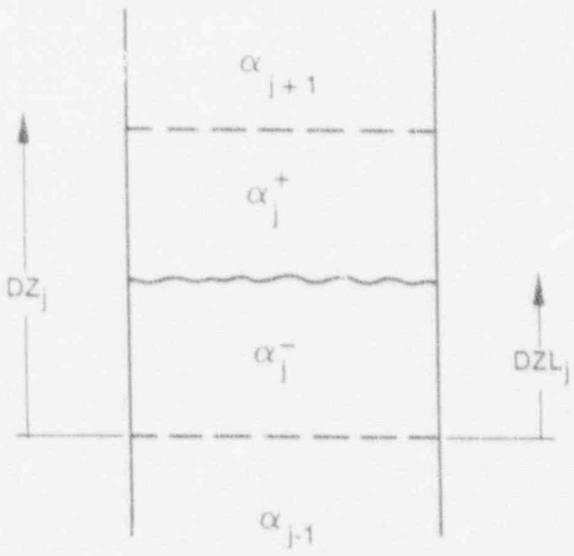

Figure 2.1-4. Two-phase level with normal void profile.

Entrainment would tend to lower the void fraction given by Equation (2.1-83). The mass flux of entrained liquid (G_{lent}) is calculated from the correlation of A. Rosen[2.1-24] as

$$G_{lent} = \left[3 \times 10^{-5}(CK^{0.5} \quad 530\ CK^{2.1}) \left(\frac{\rho_\ell - \rho_g}{\rho_g}\right)^{0.5}\right] J_g \rho_g \tag{2.1-84}$$

where

$$CK = 2\ DMAX \left[\frac{J_g}{VCRIT \left(\frac{\sigma}{g(\rho_\ell - \rho_g)}\right)^{0.5}}\right] \tag{2.1-85}$$

$$VCRIT = 2 \left(\frac{\sigma g(\rho_\ell - \rho_g)}{\rho_g^2}\right)^{0.25} \tag{2.1-86}$$

$$DMAX = 0.3375 \frac{\rho_g V_g^2}{g(\rho_\ell - \rho_g)} . \tag{2.1-87}$$

In these expressions, all fluid properties are for the cell in question, and J_g and V_g are for the upper cell boundary. For positive liquid velocity at the top of the cell, the liquid mass flux may also be represented as

$$G_{lent} = (1 - \alpha_j^*)\rho_\ell V_\ell \tag{2.1-88}$$

from which the above-level void fraction, α_j^*, is computed to be

$$\alpha_j^* = 1 - \frac{G_{lent}}{\rho_\ell V_\ell} = f(\alpha) . \tag{2.1-89}$$

For negative liquid velocity at the top of the cell, the entrainment is assumed to be zero and α_j^* is assumed equal to the void fraction in the cell above [see Equation (2.1-83)].

The level velocity, VLEVJ, is calculated as the time derivative of the level position

$$VLEV_j = \frac{DZ_j\left(\frac{\Delta\alpha_j}{\Delta t}\right) - DZL_j\left(\frac{\Delta\alpha_j^-}{\Delta t}\right) - (DZ_j - DZL_j)\left(\frac{\Delta\alpha_j^+}{\Delta t}\right)}{\alpha_j^- - \alpha_j^+} \quad (2.1\text{-}90)$$

For a normal void profile, the two-phase level can be completely described by Equations (2.1-81) to (2.1-90).

However, if the two-phase level is in a cell below a void profile inversion ($\alpha_{j+1} < \alpha_j$) or flow area reduction, Equations (2.1-83) and (2.1-89) cannot be used to determine the void fraction above the level without modification. In this situation, it is assumed that

$$J_g = 0.999\, V_g \quad (2.1\text{-}91)$$

and the two-phase level can be described by Equations (2.1-81), (2.1-82), (2.1-89), and (2.1-90). For a two-phase level occurring above a void fraction inversion ($\alpha_j < \alpha_{j-1}$) or flow area reduction, the void fraction below the level is evaluated using the drift flux model

$$\alpha_j^- = \frac{J_g^-}{C_o J^- + V_{gj}} \quad (2.1\text{-}92)$$

where C_o and V_{gj} are determined assuming bubbly/churn flow.[2.1-8]

2.1.5 References

2.1-1. J. A. Borkowski and N. L. Wade, Eds., *TRAC-BF1/MOD1 Models and Correlations*, NUREG/CR-4391, EGG-2680, August 1992.

2.1-2. G. Kocomustataogullari, "Thermo-Fluid Dynamics of Separated Two-Phase Flow," *Ph.D. Thesis, School of Mechanical Engineering*, Georgia Institute of Technology, Atlanta, Georgia, December 1971.

2.1-3. M. Ishii, *Thermo-Fluid Dynamics Theory of Two-Phase Flow*, Collection de la Direction des Etudes et Recherches D'Electricite de France, Eyrolles, Paris, 1975.

2.1-4. Los Alamos National Laboratory Safety Code Development Group, *TRAC-PD2, An Advanced Best Estimate Computer Program for Pressurized Water Reactor Loss-of-Coolant Accident Analysis*, LA-8709-MS, NUREG/CR-2054, April 1981.

2.1-5. W.T. Hancox and W. B. Nicoll, "Prediction of Time-Dependent Diabatic

Two-Phase Water Flows," *Progress in Heat and Mass Transfer*, 6, Pergamon Press, 1972, pp. 119-135.

2.1-6. J. Pfann, "A New Description of Liquid Metal Heat Transfer in Closed Conduits," *Nuclear Engineering and Design*, 41, 1977, pp. 149-163.

2.1-7. M. Ishii, *One-Dimensional Drift-Flux Model and Constitutive Equations for Relative Motion Between Phases in Various Two-Phase Flow Regimes*, ANL-77-47, October 1977.

2.1-8. J. G. M. Andersen and K. H. Chu, *BWR Refill-Reflood Program Task 4.7--Constitutive Correlations for Shear and Heat Transfer for the BWR Version of TRAC*, NUREG/CR-2134, EPRI NP-1582, 1981.

2.1-9. M. Ishii and K. Mishima, *Correlation for Liquid Entrainment in Annular Two-Phase Flow of Low Viscous Fluid*, ANL/RAS/LWR 81-2, March 1981.

2.1-10. K. H. Sun, "Flooding Correlations for BWR Bundle Upper Tie Plates and Side-Entry Orifices," *Second Multi-Phase Flow and Heat Transfer Symposium-Workshop, Miami Beach, FL, April 16-19, 1979.*

2.1-11. S. Lekach, *Development of a Computer Code for Thermal Hydraulics of Reactors (THOR)*, Brookhaven National Laboratory Quarterly Progress Report, BNL-19978, 1975.

2.1-12. C. J. Crowley, J. A. Block, and C. N. Cary, *Downcomer Effects in a 1/15 Scale PWR Geometry: Experimental Data Report*, NUREG-0281, May 1977.

2.1-13. J. G. Collier, *Convective Boiling and Condensation*, New York: McGraw-Hill Book Co. Inc., 1972.

2.1-14. W. C. Rivard and M. D. Torrey, *Numerical Calculations of Flashing from Long Pipes Using a Two-Field Model*, LA-6104-MS, 1975.

2.1-15. K. Lee and D. J. Ryley, "The Evaporation of Water Droplets in Superheated Steam," *ASME Paper 68-HT-11*, 1968.

2.1-16. J. G. M. Andersen et al., *BWR Refill-Reflood Program Task 4-7--Model Development. Basic Models for the BWR Version of TRAC*, NUREG/CR-2573, EPRI NP-2375, April 1983.

2.1-17. R. B. Bird, W. E. Stewart, and E. N. Lightfoot, *Transport Phenomena*, John Wiley & Sons, Inc., 1960.

2.1-18. S. W. Webb, J. C. Chen, and R K. Sundaram, "Vapor Generation Rate in Nonequilibrium Convective Film Boiling," *Proceedings of the 7th International Heat Transfer Conference, Munich, Germany, September 1982*, Volume 4, p. 437.

2.1-19. H. C. Unal, "Maximum Bubble Diameter, Maximum Bubble Growth Time, and

Bubble Growth Rate during the Subcooled Nucleate Flow Boiling of Water up to 17.7 MPa," *International Journal of Heat and Mass Transfer, 19*, 1976, pp. 643-649.

2.1-20. V. H. Ransom et al., *RELAP5/MOD1 Code Manual. Volume I: System Models and Numerical Methods*, NUREG/CR-1826, EGG-2070, March 1982.

2.1-21. L. S. Tong, *Boiling Heat Transfer and Two-Phase Flow*, Huntington, New York: Robert E. Krieger Publishing Company, 1975, p. 110.

2.1-22. J. G. Burnell, "Flow of Boiling Water Through Nozzles, Orifices, and Pipes," *Engineering, 164*, 1948, p. 572.

2.1-23. G. B. Wallis et al., *Countercurrent Annular Flow Regimes in Steam and Subcooled Water in a Vertical Tube*, EPRI NP-1336, January 1980.

2.1-24. A. Rosen et al., *Teploenergetikia, 11*, 1976, p. 59.

2.2 HEAT TRANSFER MODEL

Three fundamental heat-transfer mechanisms are modeled by the TRAC-BF1/MOD1 code. They include the interfacial heat transfer between the vapor and liquid phases, conduction within structural components, and heat transfer between the structures and the fluid. Interfacial heat transfer has been addressed in development of the fluid-dynamics equations. The remaining two mechanisms are discussed below.

The thermal history of the structural reactor materials is obtained from a solution of the heat-conduction equation. The energy exchange between the structures and the fluid is modeled using Newton's law of cooling. The coupling algorithm is semi-implicit. For each new time step (Figure 2.2-1), the fluid-dynamics equations are solved based on previous values for the wall heat-transfer coefficient (h) and surface wall temperatures (T_{wall}). The expression can be written as

$$q_w^{n+1} = h^n \left(T_w^n - T_f^{n+1} \right) . \qquad (2.2\text{-}1)$$

Once the fluid-dynamics equations are solved, the wall temperature distributions are deduced from the conduction equation.

2.2.1 Heat-Conduction Models

For simplicity as well as computing efficiency, the conduction models are separated according to their geometric function. They include conduction within cylindrical walls, slabs, core rods, and flat channel walls. The first model analyzes heat conduction within the pipe walls of loop components and of internal vessel components (control guide tubes and vessel wall). The second model is used to represent vessel internal structures that cannot be characterized by a cylindrical conduction model. The third model is used to represent the heat transfer in a fuel rod. The fourth model is used to represent heat conduction within the walls of the BWR fuel bundle, or channel. These walls are assumed to be flat, rather than cylindrical. Each of these four models is discussed in detail.

In addition, the TRAC-BF1/MOD1 model for the zirconium-steam oxidation reaction is discussed, together with its effect on outer fuel rod cladding radius and internal heat generation rate used in the conduction equations for the fuel rods. This section is repeated as coded in Sections 9.0 through 9.3 of the models and correlations document associated with this code manual.[2.2-1]

2.2.1.1 Cylindrical Wall Heat Conduction. The temperature distribution within the walls of a component is determined by Subroutine CYLHT. A solution is obtained from a finite difference approximation to the one-dimensional conduction equation

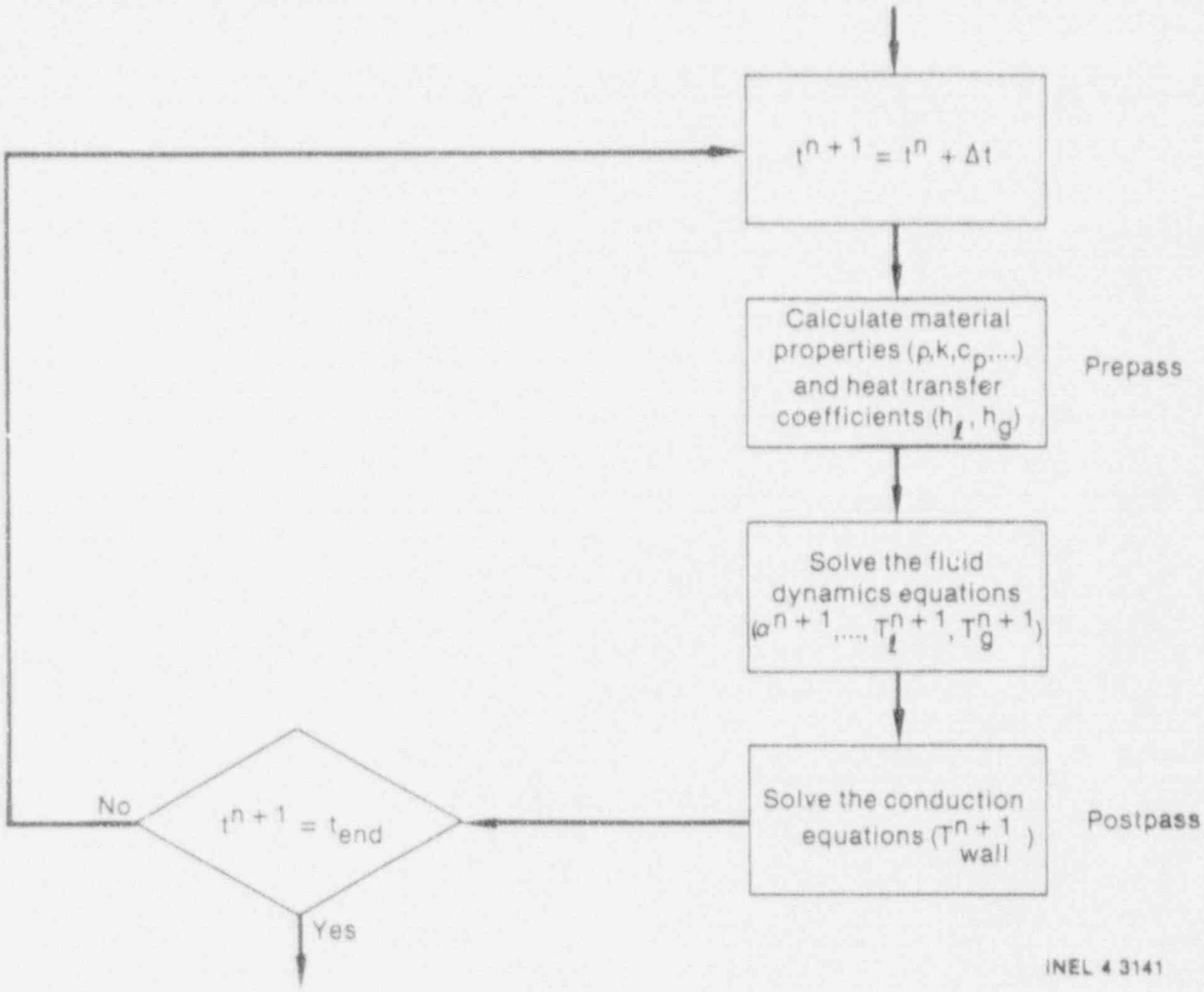

Figure 2.2-1. Semi-implicit coupling between hydrodynamics and structural heat transfer.

$$\rho c_p \frac{\partial T}{\partial t} = \frac{1}{r} \frac{\partial}{\partial r}\left(rk \frac{\partial T}{\partial r}\right) + q''' \quad . \tag{2.2-2}$$

The finite difference equations are derived by applying an integral method[2.2-2] to the elemental volumes shown in Figure 2.2-2. The general form for the ith volume ($1 < i < n$) is

$$\frac{r_{i-1/2}k_{i-1/2}}{\Delta r_{i-1}} T_{i-1}^{n+1} - \left\{ \frac{r_{i-1/2}k_{i-1/2}}{\Delta r_{i-1}} + \frac{r_{i+1/2}k_{i+1/2}}{\Delta r_i} + \frac{1}{2\Delta t}\left[\left(r_i \Delta r_{i-1} - \frac{\Delta r_{i-1}^2}{4}\right)(\rho c_p)_{i-1/2}\right.\right.$$

$$+\left(r_i\Delta r_i + \frac{\Delta r_i^2}{4}\right)(\rho c_p)_{i+1/2}\Bigg]\Bigg\} T_i^{n+1} + \frac{r_{i+1/2}k_{i+1/2}}{\Delta r_i} T_{i+1}^{n+1}$$

$$= -\frac{1}{2}\left(r_i\Delta r_i - \frac{\Delta r_{i-1}^2}{4}\right)\left[\frac{(\rho c_p)_{i+1/2}}{\Delta t} T_i^n + q'''\right] + \left(r_i\Delta r_i - \frac{\Delta r_i^2}{4}\right)\left[\frac{(\rho c_p)_{1+1/2}}{\Delta t} T_i^n + q'''\right]\Bigg\} \quad (2.2\text{-}3)$$

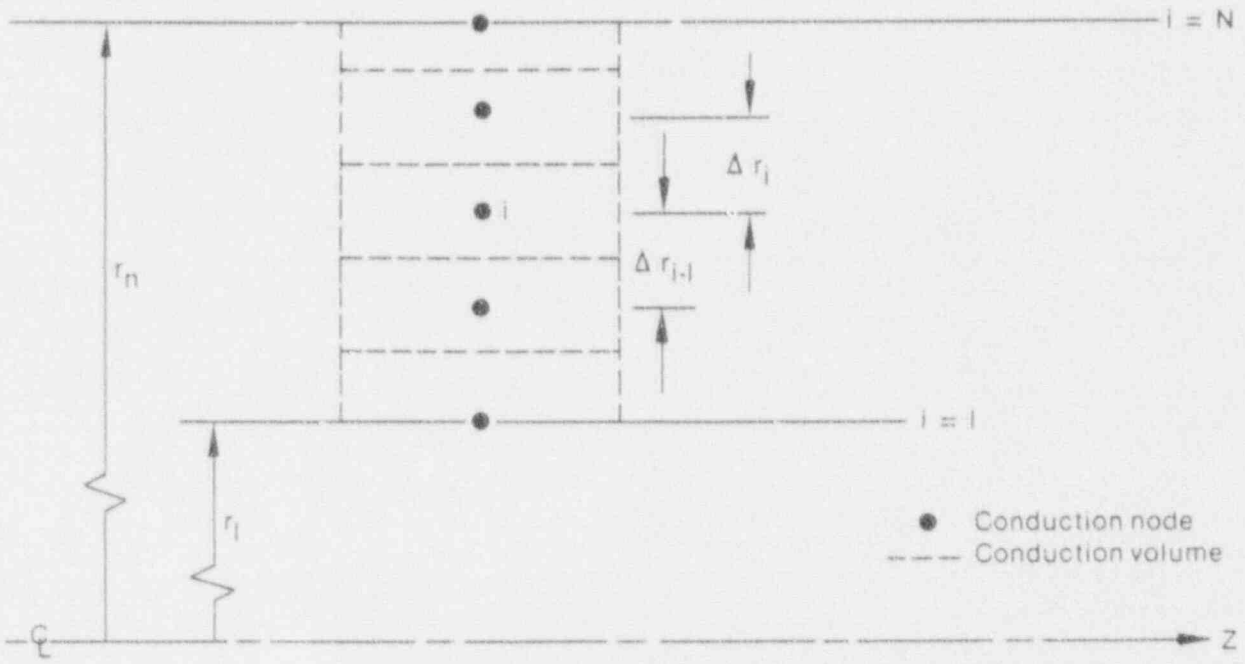

INEL-A-19 193

Figure 2.2-2. Cylindrical wall geometry.

where

$$T_i^n = T(t^N, r_i) \; . \quad (2.2\text{-}4)$$

The boundary conditions applied to the inner (i = 1) and outer (i = N) surfaces are
Applying this boundary condition to the inner surface (i = 1), the above finite difference equation becomes

$$-k\frac{\partial T}{\partial r}\bigg|_{i=1,N} = h_\ell(T_\ell - T_i) + h_g(T_g - T_i) - q_{r_i} \quad . \tag{2.2-5}$$

$$-\left[\frac{r_{3/2}k_{3/2}}{\Delta r_1} + \frac{1}{2}\left(r_1\Delta r_1 + \frac{\Delta r_1^2}{4}\right)\frac{(\rho c_p)_{3/2}}{\Delta t} + f_{ss}r_1(h_\ell + h_g)\right]T_1^{n+1} + \frac{r_{3/2}k_{3/2}}{\Delta r_1}T_2^{n+1}$$

$$= -\frac{1}{2}\left(r_i\Delta r_1 - \frac{\Delta r_1^2}{4}\right)\left[\frac{(\rho c_p)_{3/2}}{\Delta t}T_i^n + q'''\right] + r_1\left[h_\ell\left(f_t T_1^n - T_\ell^{n+1}\right) + h_g\left(f_t T_1^N - T_g^{n+1}\right)\right] + q_{r_1} \quad . \tag{2.2-6}$$

In this equation, f_{ss} and f_t are *implicitness* parameters. Because of the semi-implicit coupling with the fluid equations, f_{ss} and f_t take on the values of 0 and 1, respectively, for transient calculations. This ensures that both sets of equations use identical surface heat fluxes as boundary conditions for each time step. When a steady-state solution is required, however, large time steps are desirable. Therefore, the conduction equation is written in a fully implicit form and $f_{ss} = 1$ and $f_t = 0$.

NOTE: The above formulation conveniently positions nodal points on material interfaces. Material properties are evaluated between nodes.

The resulting linear equations are solved in a sequential fashion in the axial (z) direction. For each axial position, a solution is achieved using Gaussian elimination. A lumped parameter solution is available if the number of nodes is one (NODES = 1). For this option, the wall temperature is obtained from

$$T^{n+1} = \left\{\frac{1}{2}\left(2\Delta r + \frac{\Delta r^2}{R_i}\right)\left(\frac{\rho c_p}{\Delta t}T^n + q'''\right) + h_{\ell_i}\left(T_\ell^{n+1} - f_t T^n\right) + h_{g_i}\left(T_{g_i}^{n+1} - f_t T^n\right)\right.$$

$$\left. - \left(1 + \frac{\Delta r}{R_i}\right)\left[h_{\ell_o}\left(f_t T^n - T_{\ell_o}^{n+1}\right) + h_{g_o}\left(f_t T^n - T_{g_o}^{n+1}\right)\right]\right\} \Big/$$

$$\left\{\frac{1}{2}\left(2\Delta t + \frac{\Delta r^2}{R_i}\right)\left(\frac{\rho C_p}{\Delta t}\right) + f_{ss}\left[h_{\ell_i} + h_{g_i} + \left(1 + \frac{\Delta r}{R_i}\right)\left(h_{\ell_o} + h_{g_o}\right)\right]\right\} . \qquad (2.2\text{-}7)$$

The subscripts i and o refer to the inner and outer radii, respectively.

NOTE: The present coding does not allow for radiation heat-transfer boundary conditions when NODES = 1.

The boundary condition at the inside surface is inferred from the hydraulic conditions inside the component. The outer boundary condition is normally constant, with user-specified values for the heat transfer coefficient and fluid temperatures. Alternately, the user may utilize a generalized heat transfer capability whereby the outer surface of any one-dimensional component may be thermally coupled to the fluid inside any other component (including the vessel) in the model.

TRAC-BF1/MOD1 also be used to model the conduction heat transfer with the preceding cylindrical conduction solution within any double-sided heat slab surface within the vessel. Examples of such heat structures are the core barrel, which sees fluid conditions in both the downcomer and the core bypass, and the vessel wall, which sees ambient fluid conditions as well as downcomer fluid conditions (see Subsection 3.8).

2.2.1.2 Slab Heat Conduction. Conduction within vessel structures such as downcomer walls and support plates is modeled in Subroutine SLABHT. A lumped parameter solution is available. Through input, the user must supply the slab mass, m, surface area, A, and material properties, c_p and k, for heat slabs in each fluid-dynamic volume. The lumped parameter temperature is obtained from

$$T^{n+1} = \frac{\frac{\rho C_p}{\Delta t}\bar{x}T^n - h_\ell\left(f_t T^n - T_\ell^{n+1}\right) - h_g\left(f_t T^n - T_g^{n+1}\right)}{\frac{\rho C_p}{\Delta t}\bar{x} + f_{ss}(h_\ell + h_g)} \qquad (2.2\text{-}8)$$

where $\bar{x}$ is an effective slab thickness (m/2pA). The steady-state (f_{ss}) and transient (f_t) flags were discussed in the previous section.

2.2.1.3 Fuel Rod Conduction. Subroutine RODHT analyzes the conduction of reactor rods on a rod-by-rod basis. The formulation can model diverse rod geometries. Both nuclear and electrically heated rods can be analyzed. The effects of internal heat generation, gap conduction, metal-water reaction, and variable rod properties are included. The numerical procedures are capable of modeling the entire LOCA scenario in a consistent and mechanistic fashion. The model can also resolve large axial (z) gradients characteristic of the reflood phase.

The rod conduction solution is obtained for each rod group within each fuel bundle component specified by the user. The number of rod groups required to represent the radiation heat transfer within the bundle is optional. However, for each rod group, a conduction solution is obtained and coupling of the rod heat transfer with the hydraulics is modeled with Newton's law of cooling. Power distributions from bundle to bundle, from rod to rod, and from node to node within the rod are modeled.

The fuel rod conduction solution method is similar to that described in the cylindrical geometry section. The major differences pertain to treatment of boundary conditions, user selection of composite material structure, and provision for spatial and time-dependent internal heat generation.

The fuel rod conduction model has two significant features not found in the previous code versions. First, axial conduction is included in the finite difference equations. Second, the nodes are defined as centered at material boundaries, and the code calculates and stores special *interface* material properties that are used in the conduction solutions. Referring to Figure 2.2-3, the finite-difference equation for conduction at an interior node (i,j) is identical to that found in References 2.2-3 and 2.2-4 except that axial conduction is included and written as

$$\frac{1}{2}(\Delta z_u + \Delta z_\ell)\left[\frac{1}{4}(r + r_+)^2 - \frac{1}{4}(r + r_-)^2\right]\rho C_p \frac{T^{n+1} - T^n}{\Delta t}$$

$$= [\textit{Volumetric Source Terms}] + [\textit{Normal Radial Conduction Terms}] \qquad (2.2\text{-}9)$$

$$+\left[\frac{1}{4}(r + r_+)^2 - \frac{1}{4}(r + r_-)^2\right]\left[\frac{1}{2}(k_u + k)\frac{T_u^n - T^{n+1}}{\Delta z_u} + \frac{1}{2}(k_\ell + k)\frac{T_\ell^n - T^{n+1}}{\Delta z_\ell}\right]$$

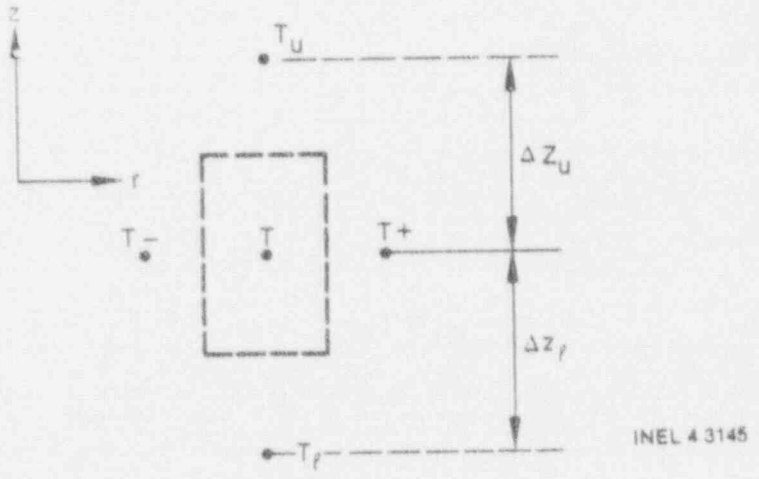

Figure 2.2-3. Nodalization for fuel rod heat conduction.

At the top and bottom of the heated length, the axial conduction terms are modified; while at the rod axis, material interfaces, and rod surface, the radial conduction terms are modified (as specified in References 2.2-3 and 2.2-4). NOTE: For each row of nodes across a rod, these finite-difference equations form a tridiagonal system of linear equations in terms of the new-time node temperatures

$$T_-^{n+1},\ T^{n+1},\ \text{and}\ T_+^{n+1}\ .$$

These linear systems are solved row by row (ascending the rod) for each rod group. Because the axial conduction terms are explicit, involving old-time temperatures

$$T_\ell^n\ \text{and}\ T_u^n$$

this row-by-row scheme may be used instead of solving for the temperature field for the whole rod at once, which would require inverting a large (although sparse) matrix (perhaps 200 x 200 or more).

The gap between the fuel and cladding of fuel rods is treated by explicit noding on fuel and cladding surfaces with a heat-transfer coefficient between these nodes. Stored energy and internal heat generation in the gap region are neglected. The finite difference equation for the outermost fuel pellet node is

$$\frac{\rho C_p}{\Delta t}\left(T^{n+1} - T^n\right) = \frac{1}{2}\,\frac{(r + r_-)\,(k + k_-)}{\left[r - \frac{1}{4}\,(r - r_-)\right](r - r_-)^2}\,(T^{n+1} - T_-^{n+1})$$

$$+\,\frac{rh_{gap}}{\frac{1}{2}\left[r - \frac{1}{4}\,(r - r_-)\right](r - r_-)}\,(T_+^{n+1} - T^{n+1})$$

$$+\,(\textit{axial conduction terms}) + (\textit{volumetric heat source})\ . \qquad (2.2\text{-}10)$$

For the innermost cladding node, the finite difference equation is

$$\frac{\rho C_p}{\Delta t}\left(T^{n+1} - T^n\right) = \frac{1}{2}\,\frac{(r_+ + r)\,(k_+ + k)}{\left[r - \frac{1}{4}\,(r_+ - r)\right](r_+ - r)^2}\,(T_+^{n+1} - T^{n+1})$$

$$+ \frac{r_- h_{gap}}{\frac{1}{2}\left[r + \frac{1}{4}(r_+ - r)\right](r_+ - r)} (T_-^{n+1} - T^{n+1})$$

+ (*axial conduction terms*) + (*volumetric heat sources*)

+ (*metal-water reaction source*) . (2.2-11)

The equation used for the outside of the cladding is similar to Equation (2.2-10) (outside surface node of the fuel region) except that the radiative heat flux and metal-water reaction are included. This equation is

$$\frac{\rho C_p}{\Delta t}(T^{n+1} - T^n) = \frac{1}{2} \frac{(r + r_-)(k + k_-)}{\left[r - \frac{1}{4}(r - r_-)\right](r - r_-)^2} (T_-^{n+1} - T^{n+1})$$

$$+ \frac{r\left[h_\ell\left(T_s - T^{n+1}\right) + h_v\left(T_v - T^{n+1}\right)\right]}{\frac{1}{2}\left[r - \frac{1}{4}(r - r_-)\right](r - r_-)}$$

+ (*axial conduction, metal-water reaction, and radiation terms*) . (2.2-12)

2.2.1.4 CHAN Wall Heat Conduction. The walls of CHAN components are modeled as flat plates rather than cylinders. In addition, axial conduction is included in the difference equations when the reflood model is activated. For the nodalization conventions used in Figure 2.2-4, the finite-difference form of the conduction equations used in TRAC-BF1/MOD1 are

1. For an inside surface node

$$\Delta z \Delta x \frac{\rho C_p}{\Delta t}(T^{n+1} - T^n) = \Delta z\left[h_{i,v}\left(T_{i,v}^{n+1} - T^{n+1}\right) + h_{i,\ell}\left(T_{i,\ell}^{n+1} - T^{n+1}\right)\right] + \Delta z k_+ \frac{T_+^{n+1} - T^{n+1}}{\Delta x_p}$$

$$+ \Delta x\left[k_u \frac{T_u^n - T^{n+1}}{\Delta z_u} + k_\ell \frac{T_\ell^n - T^{n+1}}{\Delta z_\ell}\right] + \Delta z q_{rad} + \Delta z \Delta x q''' . \quad (2.2\text{-}13)$$

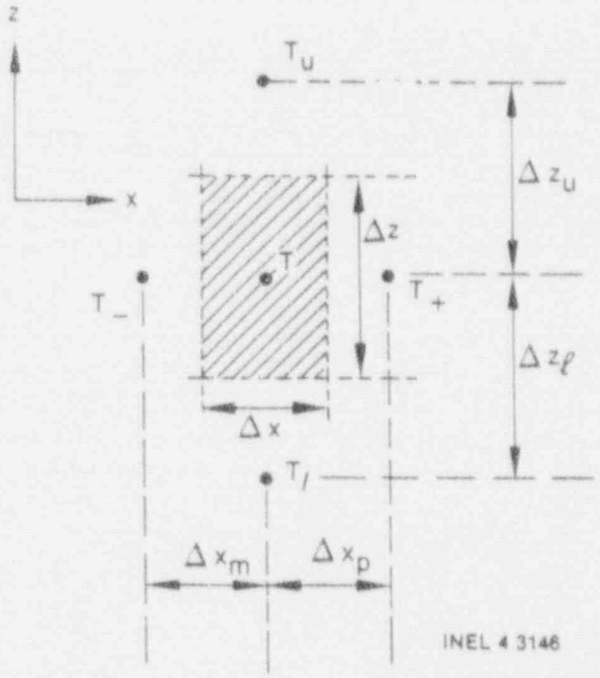

Figure 2.2-4. Nodalization for CHAN wall heat conduction.

Here, $T_{i,v}$ and $T_{i,\ell}$ refer to the vapor and liquid fluid temperatures, respectively, at the inner wall surface. $h_{i,v}$ and $h_{i,\ell}$ are the corresponding heat transfer coefficients.

2. For an outside surface node

$$\Delta z \Delta x \frac{\rho C_p}{\Delta t}\left(T^{n+1} - T^n\right) = \Delta z\left[h_{o,v}\left(T_{o,v}^{n+1} - T^{n+1}\right) + h_{o,\ell}\left(T_{i,\ell}^{n+1} - T^{n+1}\right)\right] + \Delta z k_- \frac{T_-^{n+1} - T^{n+1}}{\Delta x_m}$$

$$+ \Delta x\left[k_u \frac{T_u^n - T^{n+1}}{\Delta z_u} + k_\ell \frac{T_\ell^n - T^{n+1}}{\Delta z_\ell}\right] + \Delta z \Delta x q''' \,. \qquad (2.2\text{-}14)$$

3. For an interior node

$$\Delta z \Delta x \frac{\rho C_p}{\Delta t}\left(T^{n+1} - T^n\right) = \Delta z k_- \frac{\left(T_-^{n+1} - T^{n+1}\right)}{\Delta x_m} + \Delta z k_+ \frac{\left(T_+^{n+1} - T^{n+1}\right)}{\Delta x_p}$$

$$+ \Delta x \left[k_u \frac{T_u^n - T^{n+1}}{\Delta z_u} + k_\ell \frac{T_\ell^n - T^{n+1}}{\Delta z_\ell} \right] + \Delta z \Delta x q''' \ . \qquad (2.2\text{-}15)$$

It will be noted that the RHS of the above equations includes terms for surface convection, axial and transverse conduction, surface radiation, and internal heat generation. The four conductivities used in these equations (k_ℓ, k_u, k_+, k_-) are linear averages between the conductivity of the central node and the appropriate outer node.

The channel wall surface boundary conditions are determined from the same heat transfer correlations package as is used for other components.

2.2 1.5 **Metal-Water Reaction.** When sufficiently high temperatures are reached by zircaloy in a steam environment, an exothermic reaction may occur that will influence the peak cladding temperatures attained. The zirconium-steam reaction equation is

$$Zr + 2H_2O \rightarrow ZrO_2 + 2H_2 + Heat \ . \qquad (2.2\text{-}16)$$

In the presence of sufficient steam, the reaction rate expression of Reference 2.2-5 is written as

$$-\frac{dr}{dt} = \frac{1.126 \times 10^{-6}}{R_o - r} \exp^{-\left(\frac{18062}{T}\right)} \qquad (2.2\text{-}17)$$

where

r = reacting surface radius (m)

R_o = cladding outer radius (m)

T = cladding surface temperature

and is assumed to be valid.

The method outlined in Reference 2.2-6 is used to calculate the zirconium-oxide penetration depth and associated heat source. The mass of zirconium per unit cladding length (m_{Zr}) consumed by the reaction in one time step is

$$m_{Zr} = \pi \rho_{Zr} \left[(r^n)^2 - (r^{n+1})^2 \right] \ . \qquad (2.2\text{-}18)$$

Equation (2.2-17) is used to calculate r^{n+1}, yielding

$$r^{n+1} = R_o - \left[(r^n)^2 + 2.252 \times 10^{-6} \Delta t \exp^{-\left(\frac{18062}{T}\right)} \right]^{1/2} . \quad (2.2\text{-}19)$$

The heat source (q_{mw}) added to the conduction equations, assuming a one-region cladding, is

$$q'''_{mw} = 6.513 \times 10^6 m_{Zr} \left[\Delta t \left(R_o^2 - R_i^2 \right) \right]^{-1} \quad (2.2\text{-}20)$$

where R_i is the inner cladding radius and 6.513×10^6 J/kg corresponds to the energy release per kilogram of zirconium oxidized.

2.2.2 Wall-to-Fluid Energy Transfer

The wall-to-fluid transfer coefficients are obtained from a generalized boiling curve constructed within Subroutine HTCOR. The heat transfer coefficient (HTC) correlations in HTCOR are used by all TRAC-BF1/MOD1 primary loop components under all conditions. Figure 2.2-5 shows four regimes on the boiling curve. The single-phase vapor (Mode 5) and condensation (Mode 0) regimes are not shown in this figure. Mode 7 is a simplified representation of all six regimes. The total convective flux from a surface is

$$q = h_\ell (T_\ell - T_s) + h_v (T_v - T_s) . \quad (2.2\text{-}21)$$

The individual correlations for h_ℓ and h_v used for each heat-transfer regime, as well as the logic to decide which regime is appropriate, are discussed below.

The as-coded mathematical description for each of the wall heat transfer modes is provided in Reference 1, Section 4.2.

2.2.2.1 Wall-to-Fluid HTC Selection Logic. The HTC selection logic is outlined in the flow chart shown in Figure 2.2-6. The numbers on the left side of the figure correspond to the following steps. If the condition for a given step is not satisfied, the next step is examined.

Step 1. Initialize HTCOR by calculating absolute velocities, slip, mass flux, and equilibrium qualities. Slip is set to one for countercurrent flow and when either phase velocity is zero.

Step 2. On surfaces where the heat flux is not expected to exceed the critical heat flux (CHF) or surfaces where an accurate prediction of boiling transition is not required, users can set ICHF to 0 and use a simplified boiling curve to save computer time (Mode 7).

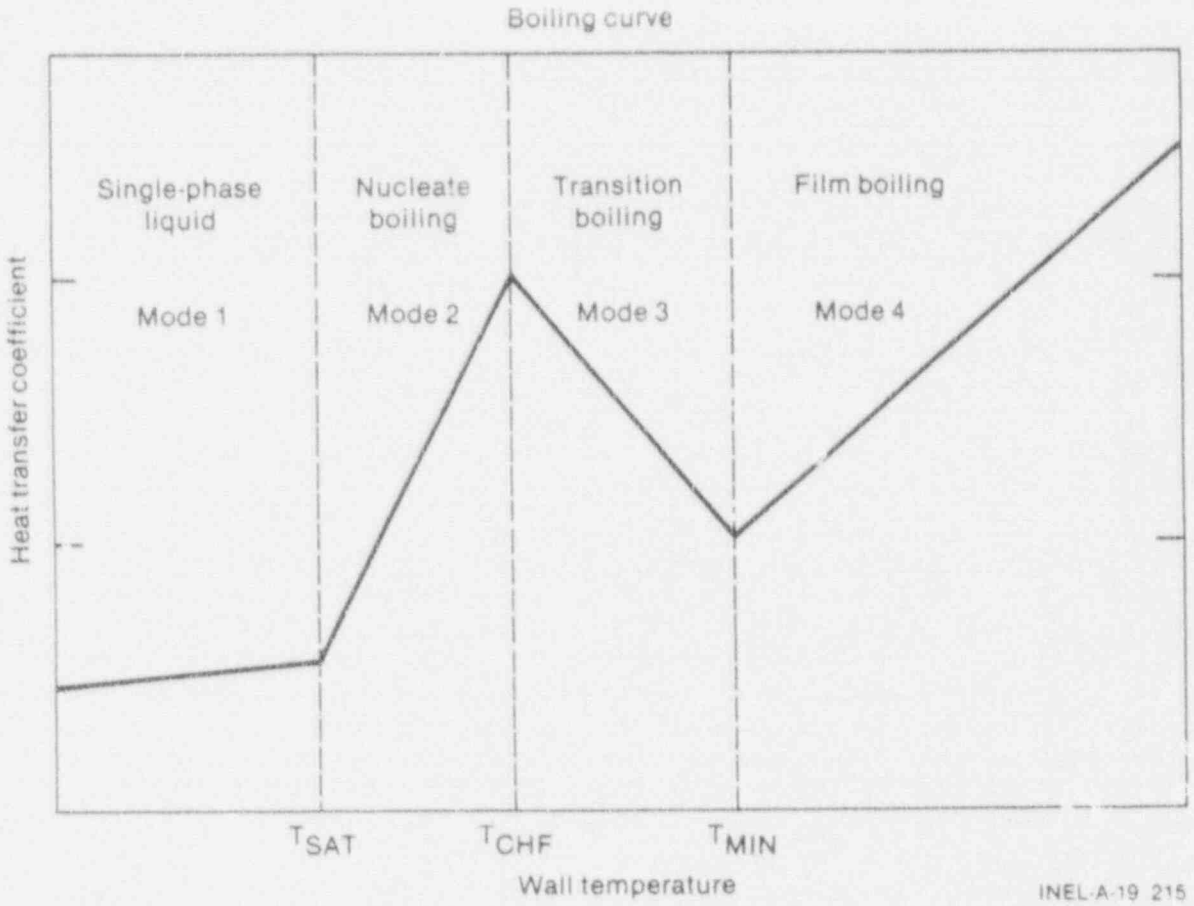

Figure 2.2-5. TRAC-BF1/MOD1 boiling curve.

Step 3. If $T_w > T_s$ and $X > 1.0$, wall condensation cannot occur. Heat transfer to single-phase vapor is assumed (Mode 5).

Step 4. T_{min} is calculated.

Step 5. If $T_w > T_{min}$, film boiling correlations are evaluated (Mode 4).

Step 6. If $T_w \leq T_s$, condensation mode (Mode 0) is assumed for $\alpha > 0.05$; convection to single-phase liquid (Mode 1) is assumed for $\alpha \leq 0.05$.

Step 7. If $T_w < T_\ell$, convection to single-phase liquid (Mode 1) is assumed.

Step 8. If $\alpha \geq 0.999$, steam cooling (Mode 5) is assumed. Nucleate boiling with negligible liquid is thereby prevented.

Step 9. Evaluate the nucleate boiling correlation.

Step 10. A negative ICHF indicates that the user does not want to calculate a boiling transition; therefore, CHF correlations need not be evaluated.

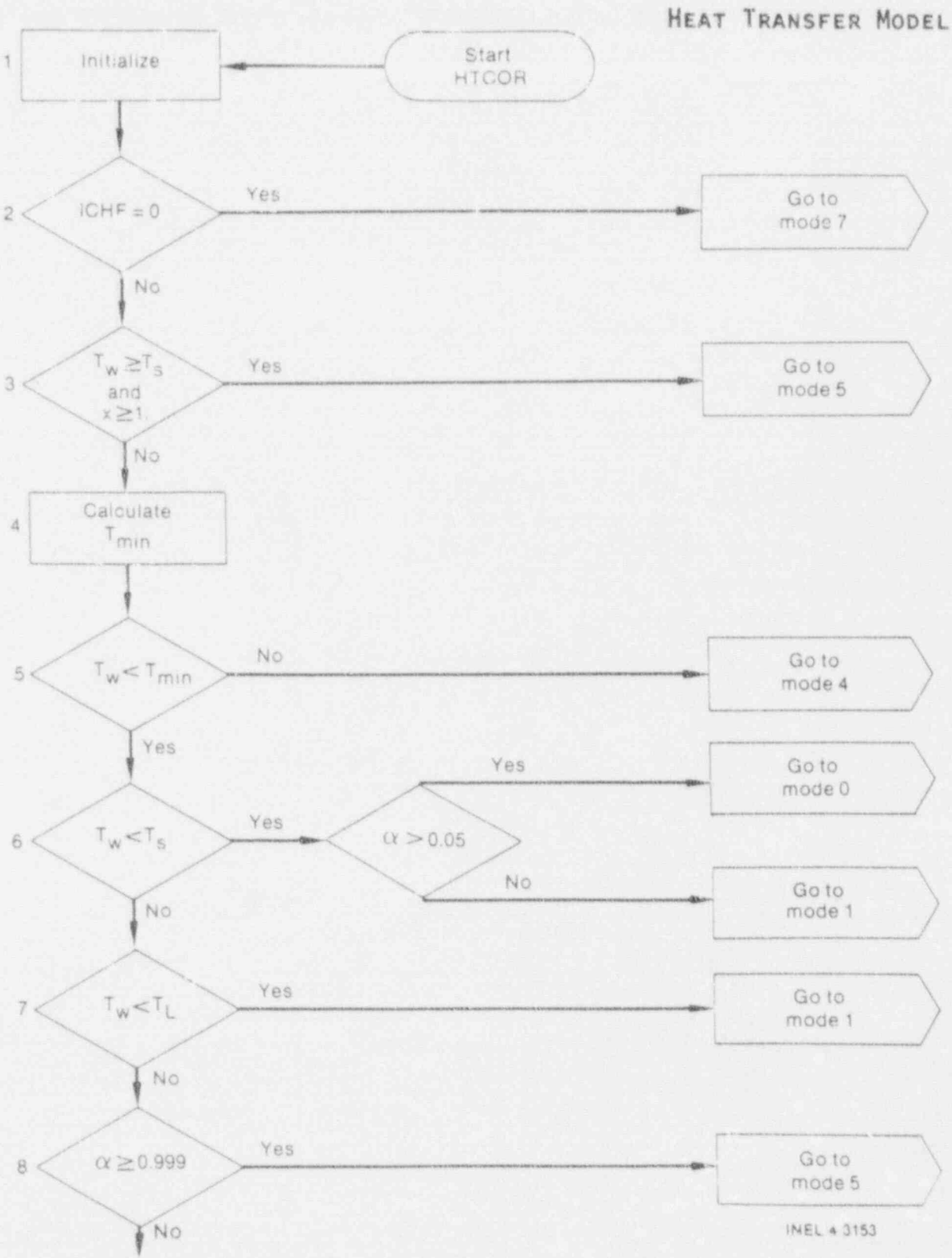

Figure 2.2-6. Heat transfer mode selection logic.

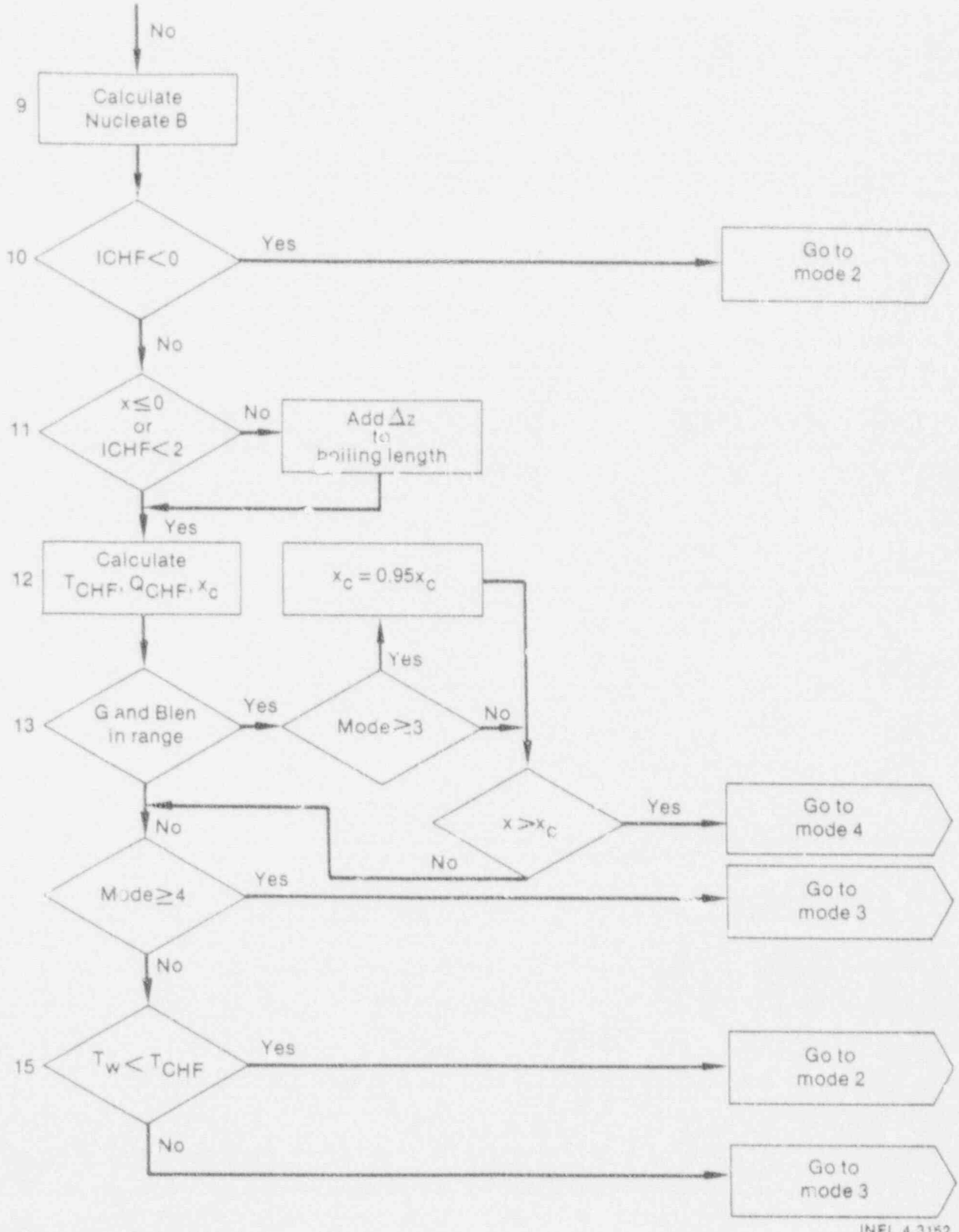

Figure 2.2-6. (continued)

Step 11. The boiling length is initialized to zero. When cell quality exceeds zero, the length of the cell is added to the boiling length if the user has chosen to use a critical quality correlation (ICHF =2 or 3).

Step 12. When a user specifies that only a local CHF condition be evaluated (ICHF = 1), critical quality is not considered. However, if the user chooses a critical quality evaluation, boiling transition can occur either when the local quality exceeds the critical value or when the wall temperature exceeds the value of T_{CHF} implied by Q_{CHF}.

Step 13. The mass flux must be >200 kg/m_2-s and the boiling length must be larger than 1 m in order to correctly apply the critical quality correlations. If departure from nucleate boiling has already occurred (i.e., Mode $\geq$ 3), the critical quality is reduced by 5% to add a hysteresis effect. When the local equilibrium quality, X, is greater than the critical quality, the logic bypasses transition boiling and assumes film boiling conditions.

Step 14. The surface in question cannot rewet without remaining in transition boiling for at least one time step.

Step 15. When the temperature is below T_{CHF}, nucleate boiling is allowed.

Step 16. Before leaving the subroutine, some smoothing of h_ℓ and h_v is performed. If the void fraction is below 0.15, h_v is linearly interpolated to zero at $\alpha = 0$. The heat flux reduction caused by the h_v decrease necessitates an h_ℓ increase.

2.2.2.2 **HTC Correlations.** In this section, the flow chart and applicable correlations for each heat transfer mode are discussed.

2.2.2.2.1 **Condensation (Mode 0)**--Figure 2.2-7 shows the flow chart for condensation. Below a quality of 0.71, use the Nusselt horizontal tube equation[2.2-7] shown as

$$h_\ell = HCOND = 0.725 \left[\frac{\rho_\ell^2 g h_{fg} K^3}{\mu_\ell D_H (T_s - T_w)} \right]^{1/4} . \qquad (2.2\text{-}22)$$

At higher qualities, the liquid film becomes thin and h_ℓ is interpolated to zero at X = 1.0. h_v is interpolated to the maximum of the Dittus-Boelter[2.2-8] forced convection equation

$$h_v = HDB = 0.023\, Re_v^{0.8} Pr_v^{1/3} \frac{K_v}{D_H} . \qquad (2.2\text{-}23)$$

NOTE: The power on the Prandtl number has been decreased from the original value of 0.4.

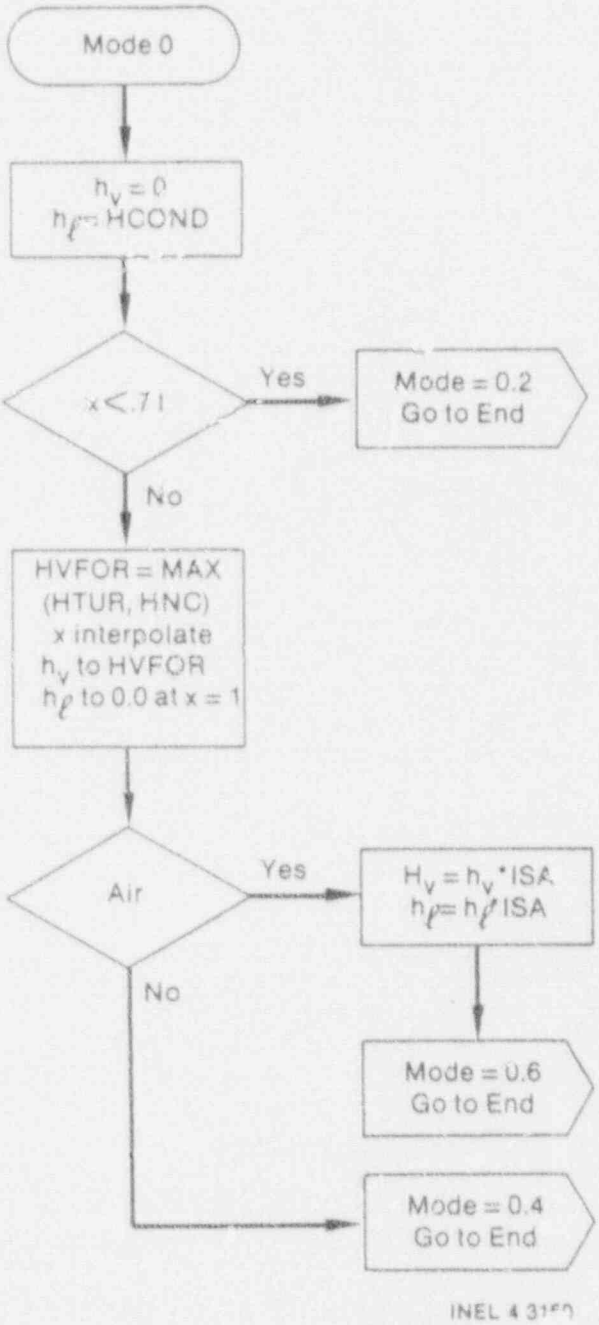

Figure 2.2-7. Film condensation flow chart.

McAdams[2.2-9] natural convection equation is

$$h_v = HNC = 0.13\ (GrPr)_v^{1/3}\ \frac{k_v}{D_H} \qquad (2.2\text{-}24)$$

where

$$Re_v = \rho_v V_v \frac{D_H}{\mu_v} \qquad (2.2\text{-}25)$$

$$Pr_v = \mu_v \frac{C_{pv}}{k_v} \qquad (2.2\text{-}26)$$

$$Gr_v = \rho_v^2 g |T_w - T_v| \frac{D_H^3}{\mu_v^2 T_v} \qquad (2.2\text{-}27)$$

where $1/T_v$ approximates the coefficient of thermal expansion.

If air is part of the gas, the heat transfer is reduced using the Russian jet data expression by Isachenko[2.2-10]

$$ISA = 0.168 \left[\frac{\alpha(\rho_v - \rho_a)^2}{(1 - \alpha)\,\rho_a \rho_\ell} \right]^{0.1} . \qquad (2.2\text{-}28)$$

2.2.2.2.2 **Single-Phase Liquid (Mode 1)**--The maximum of the Dittus-Boelter turbulent flow [Equation (2.2-22)], the McAdams natural convection [Equation (2.2-23)], and the Rohsenow and Choi[2.2-11] laminar flow

$$h_\ell = HLAM = \frac{4K_\ell}{D_H} \qquad (2.2\text{-}29)$$

is used for single-phase liquid flow. The coefficient of thermal expansion and other properties are liquid values. Figure 2.2-8 illustrates the logic flow path.

2.2.2.2.3 **Nucleate Boiling (Mode 2)**--Use the CHEN correlation.[2.2-12] The CHEN correlation is composed of two parts; a forced convection term and a nucleate boiling term that contains a suppression factor

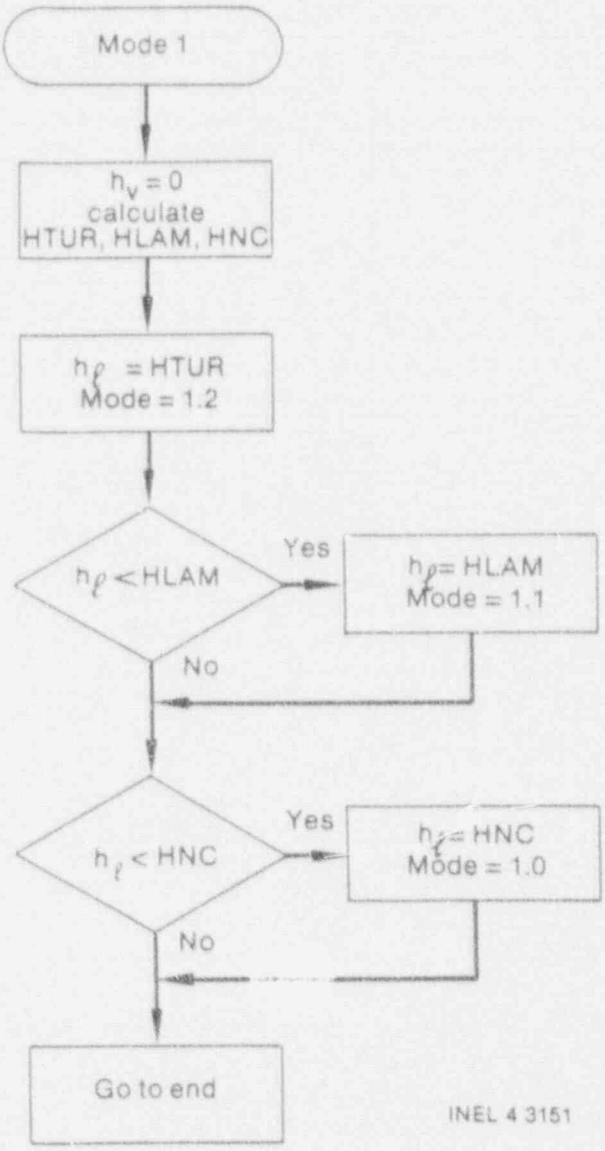

Figure 2.2-8. Single-phase liquid flow chart.

$$h_\ell = h_{forc} + Min\left[1, \left(\frac{T_w - T_s}{T_w - T_\ell}\right)\right] h_{nucb} \qquad (2.2\text{-}30)$$

where

$$h_{forc} = \text{Max [Equation (2.2-29), Dittus-Boelter correlation]} \qquad (2.2\text{-}31)$$

with liquid properties and Pr raised to the 0.4 power. In computing h_ℓ from Equation (2.2-23), the Reynolds number has been multiplied by $F^{1.25}$. F (the Reynolds number factor) can be expressed[2.2-13]

$$F = \begin{cases} 1.0, & \text{for } \chi_{TT}^{-1} \le 0.10 \\ 2.35\left(\chi_{TT}^{-1} + 0.213\right)^{0.736}, & \text{for } \chi_{TT}^{-1} > 0.10 \end{cases} \qquad (2.2\text{-}32)$$

where χ_{TT} (the Lockhart-Martinelli factor) is

$$\chi_{TT}^{-1} = \left(\frac{X}{1-X}\right)^{0.5}\left(\frac{\rho_\ell}{\rho_g}\right)^{0.5}\left(\frac{\mu_g}{\mu_\ell}\right)^{0.1} . \qquad (2.2\text{-}33)$$

The value of χ_{TT} is restricted to a value < 100.0.

The nucleate boiling term is given by

$$h_{nucb} = 0.00122\left(\frac{k_\ell^{0.79} C_{p\ell}^{0.45} \rho_\ell^{0.49}}{\sigma^{0.5} \mu_\ell^{0.29} h_{\ell g}^{0.24} \rho_g^{0.24}}\right)(T_w - T_s)^{0.24}(P_{sw} - P)^{0.75} S \qquad (2.2\text{-}34)$$

where P_{sw} is the saturation pressure corresponding to the wall temperature. The suppression factor, S,[2.2-14] can be expressed as

$$S = \begin{cases} \left[1 + 0.12(Re_{tp})^{1.14}\right]^{-1}, & \text{for } Re_{tp} < 32.5 \\ \left[1 + 0.42(Re_{tp})^{0.78}\right]^{-1}, & \text{for } 32.5 \le Re_{tp} \le 70.0 \end{cases} \qquad (2.2\text{-}35)$$

where

$$Re_{tp} = \frac{10^{-4}|V_\ell|\rho_\ell \alpha_\ell D_H F^{1.25}}{\mu_\ell} . \qquad (2.2\text{-}36)$$

The value of Re_{tp} is restricted to be <70.0.

The properties are evaluated at the liquid and vapor temperatures; X is the equilibrium quality and V_ℓ is the liquid velocity parallel to the surface. Because the nucleate boiling contribution to the CHEN correlation was developed for saturated conditions, h_{nucb} is multiplied by a temperature ratio to adjust the HTC to the actual T_ℓ. Since TRAC-BF1/MOD1 can tolerate superheated liquids, the adjustment factor is restricted to a maximum of 1.0. That is, the adjustment is made for subcooled liquid only.

The above discussion applies to the first boxed statements in the flow chart for the nucleate boiling heat transfer calculation (Figure 2.2-9). For

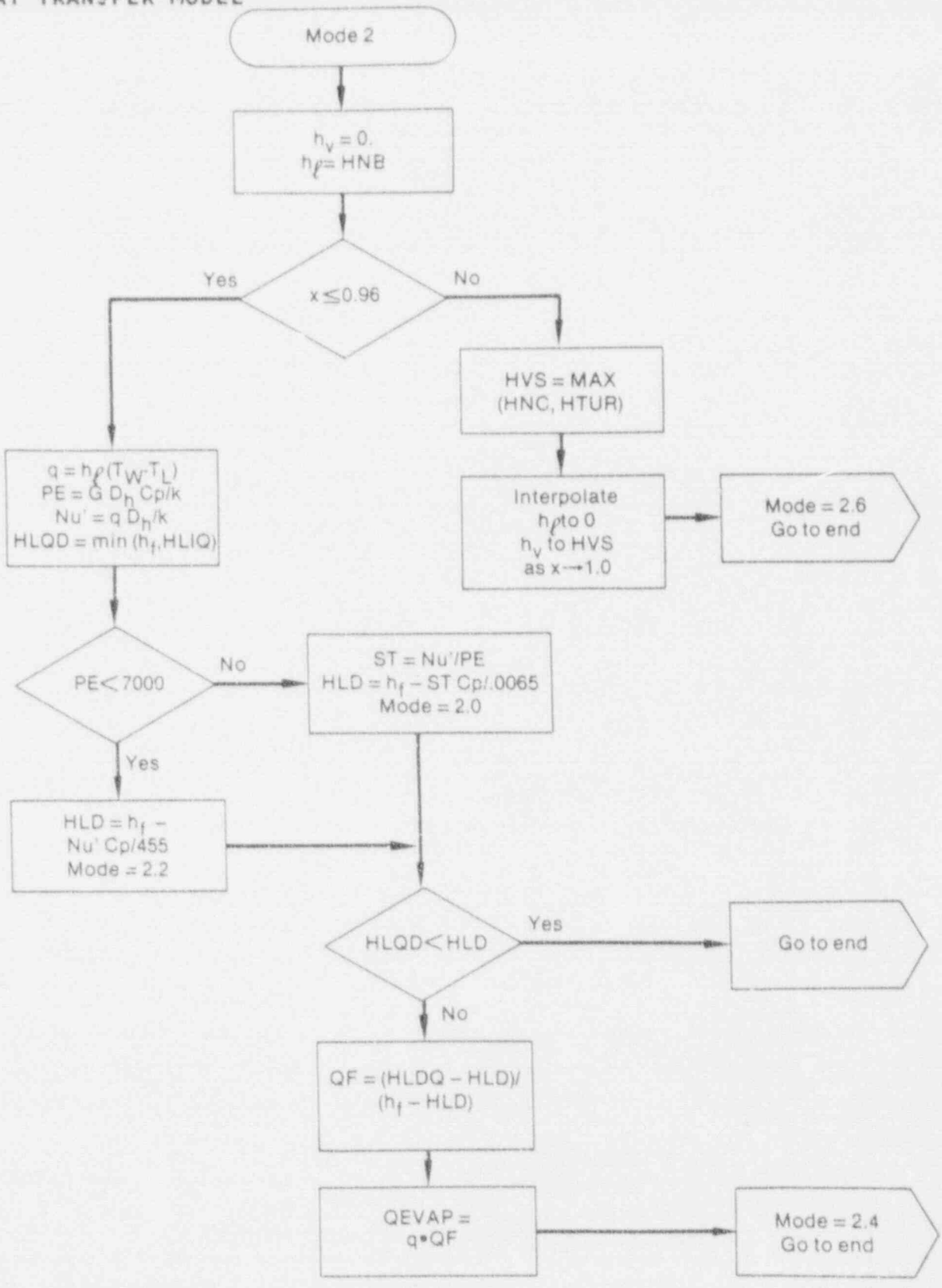

INEL 4 3149

Figure 2.2-9. Nucleate boiling flow chart.

a quality less than a cutoff value (0.96), the vapor HTC is set equal to zero. For X > 0.96, linear interpolation in X is used between the current values of h_g and h_v and the values that are calculated for single-phase vapor (Mode 5). This linear interpolation ensures that the boiling curve is smooth between heat transfer regimes.

For X < 0.96, the possibility of net vapor generation is considered even though the liquid may be subcooled. Accurate estimates of the axial core void profile are needed for reactor transients without scram because core power is very sensitive to void changes. Estimates of the bulk enthalpy needed are suggested by the *mechanistic* model proposed by Lahey.[2.2-14]

The enthalpy needed to produce net vapor[2.2-15] is expressed as

$$HLD = \begin{cases} h_f - \dfrac{St\,C_p}{0.0065}, & for\ Pe > 7000 \\ h_f - \dfrac{Nu'\,C_p}{455}, & for\ Pe \le 7000 \end{cases} \qquad (2.2\text{-}37)$$

where the Peclet, Stanton, and modified Nusselt numbers (Pe, St, and Nu', respectively) are given by

$$Pe = GD_H\frac{C_p}{k} \qquad (2.2\text{-}38)$$

$$St = \frac{Nu'}{Pe} \qquad (2.2\text{-}39)$$

$$Nu' = \frac{qD_H}{k} \ . \qquad (2.2\text{-}40)$$

The parameter HLQD is the minimum of the actual liquid enthalpy and the saturated liquid enthalpy. When the net vapor generation enthalpy, HLD, is greater than HLQD, no bubbles are generated and the generation flux, QEVAP, used in the energy equation is zero. Otherwise,

$$QEVAP = q(QF) \qquad (2.2\text{-}41)$$

where

$$QF = \frac{HDLQ - HLD}{h_f - HLD} \quad . \tag{2.2-42}$$

2.2.2.2.4 Transition Boiling (Mode 3)--Transition boiling may be considered as a combination of nucleate and film boiling. A given spot on the wall surface is wet part of the time and dry during the remainder of the time. Therefore, contributions to both the liquid and vapor HTCs exist for all conditions.

The liquid HTC contains two terms. The first is obtained using a quadratic interpolation factor (F) between the CHF and the minimum stable film boiling points[2.2-14]

$$\Gamma = \frac{(T_w - T_{min})^2}{(T_{CHF} - T_{min})^2} \tag{2.2-43}$$

where T_{CHF} is the wall temperature at CHF conditions and T_{min} is the temperature at the minimum stable film boiling point (the intersection of the transition and film boiling points). This point is found from the homogeneous nucleation or Shumway correlations, as discussed in Subsection 2.2.2.9. The second liquid term comes from the film boiling mode that uses the Bromley[2.2-16] correlation

$$HBRO = 0.62 \left[\frac{\rho_v k_v^3 (\rho_\ell - \rho_g) g_c h'_{fg}}{\mu_v (T_w - T_s) \lambda} \right]^{1/4} \tag{2.2-44}$$

where the characteristic length, λ, is

$$\lambda = 2\pi \left[\frac{\sigma}{g (\rho_\ell - \rho_v)} \right]^{0.5} \quad . \tag{2.2-45}$$

The modified latent heat of vaporization (h'_{fg}) is[2.2-17]

$$h'_{fg} = h_{fg} + 0.5 C_{p_g} (T_w - T_s) \quad . \tag{2.2-46}$$

In the final expression for h_ℓ, the Bromley correlation is void fraction weighted. Thus, the transition boiling liquid heat transfer coefficient is

$$h_\ell = (1 - \Gamma)(1 - \alpha) HBRO + \frac{\Gamma \cdot QCHF}{T_w - T_\ell} .$$

The vapor heat transfer coefficient is the maximum of the Dougall-Rohsenow[2.2-18] and the natural convection correlation given by Equation (2.2-24) times (1 - Γ). The Dougall-Rohsenow correlation is the same as the Dittus-Boelter Equation (2.2-23) except that the Reynolds number is a volumetric flow type Reynolds number written as

$$Re_v = \rho_v(\alpha|V_v| + (1 - \alpha)|V_\ell|)\frac{D_H}{\mu_v} . \qquad (2.2\text{-}48)$$

The logic flow chart given in Figure 2.2-10 shows at the end that h_ℓ goes to HBRO and h_v goes to HDR as the void fraction goes to 1. Wall void generation flux is set to F times the nucleate boiling heat flux.

2.2.2.2.5 Film Boiling (Mode 4)--The liquid and vapor heat transfer coefficients in film boiling are

$$h_\ell = (1 - \alpha) HBRO \qquad (2.2\text{-}49)$$

$$h_v = Max\ (HDR, HLAM, HNC) \qquad (2.2\text{-}50)$$

where the vapor thermal conductivity in the Dougall-Rohsenow equation has been evaluated at the film temperature in order to obtain a larger h_v. Figure 2.2-11 shows the flow chart for Mode 4.

2.2.2.2.6 Single-Phase Vapor (Mode 5)--Figure 2.2-12 shows what happens when the quality is above 1.0 and the surface temperature is above saturation. The liquid heat transfer coefficient is zero, and the vapor value is set to the maximum of the laminar turbulent or natural convection result. If the void fraction is <0.99, the Dougall-Rohsenow correlation is used in the turbulent equation; otherwise, the Dittus-Boelter correlation is used. When the void fraction is between 0.99 and 0.999, an interpolation is made between the two correlations in the turbulent regime.

2.2.2.2.7 Simple Boiling Curve (Mode 7)--The seventh heat transfer mode is specifically for nonreactor core structures or for situations where accurate values of CHF are not desired. This simplified logic allows nucleate boiling up to a wall superheat of 25 K if the quality is not greater than one and the void fraction is not >0.999. This logic is shown on the left side of Figure 2.2-13. At very dry steam conditions, h_ℓ is set to zero and h_v is the maximum of the natural convection, laminar flow, and Dittus-Boelter correlations given by Equations (2.2-24), (2.2-29), and (2.2-23), respectively. For nucleate boiling, the CHEN correlation is used; and

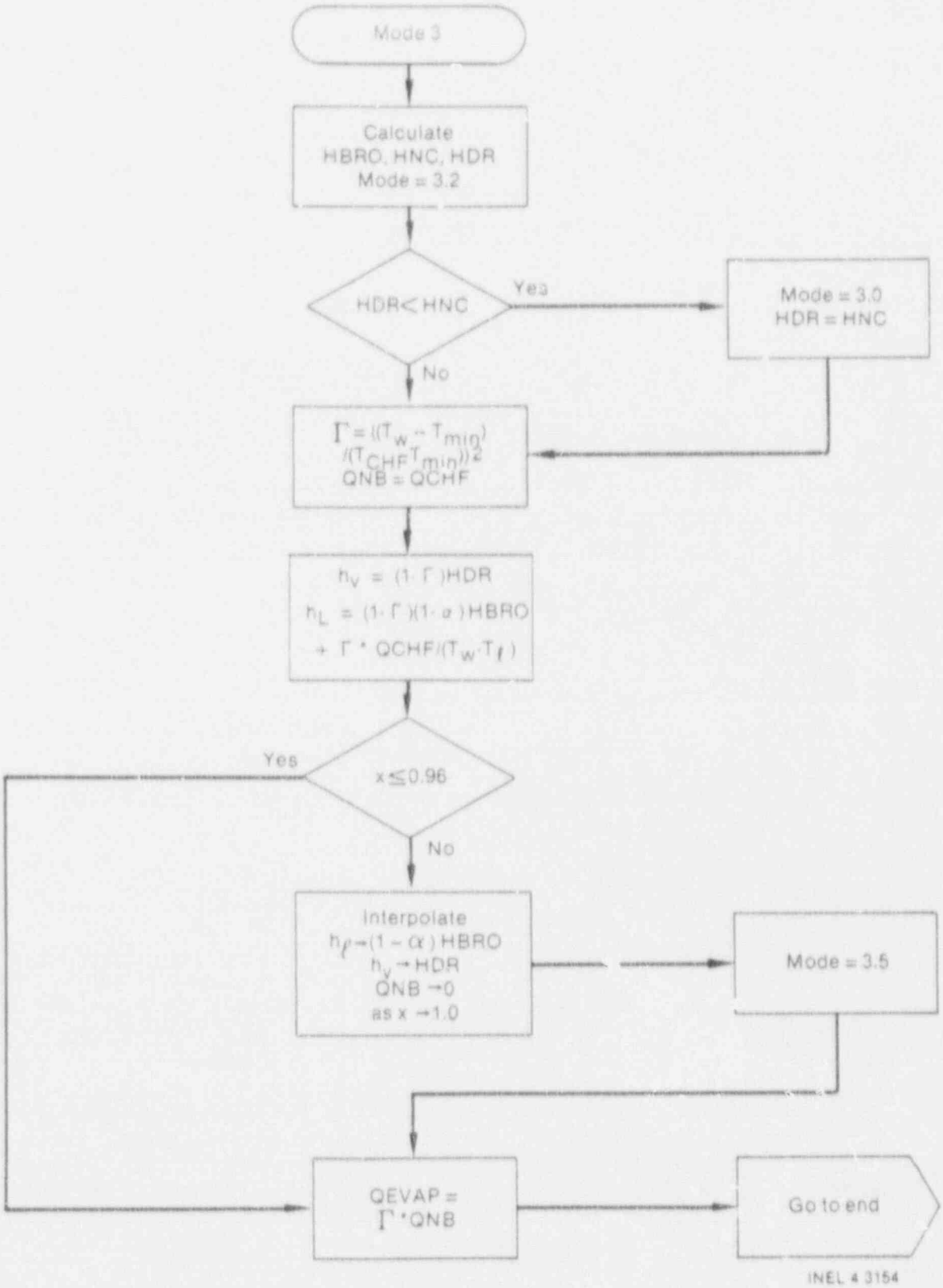

Figure 2.2-10. Transition boiling flow chart.

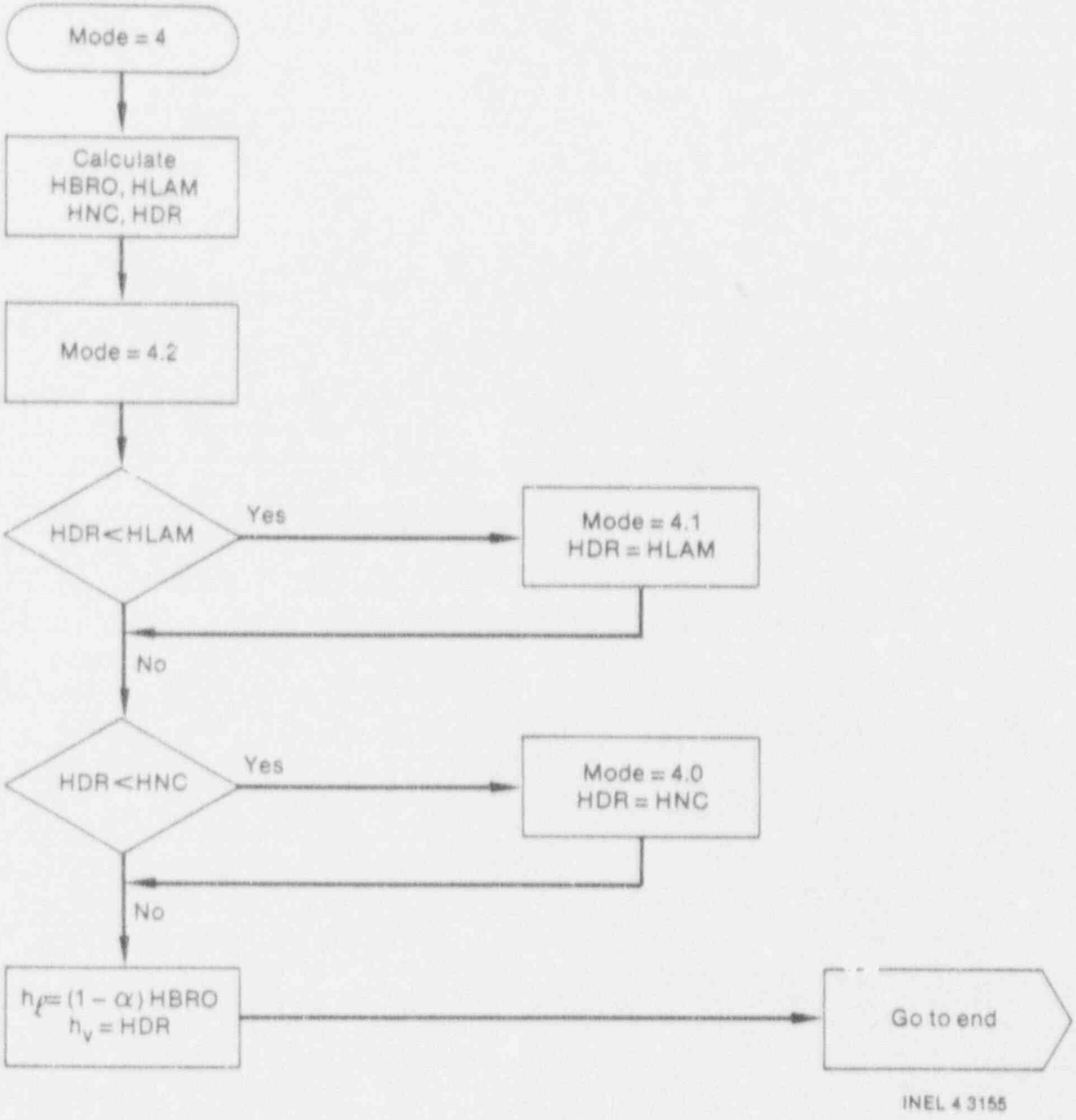

Figure 2.2-11. Film boiling flow chart.

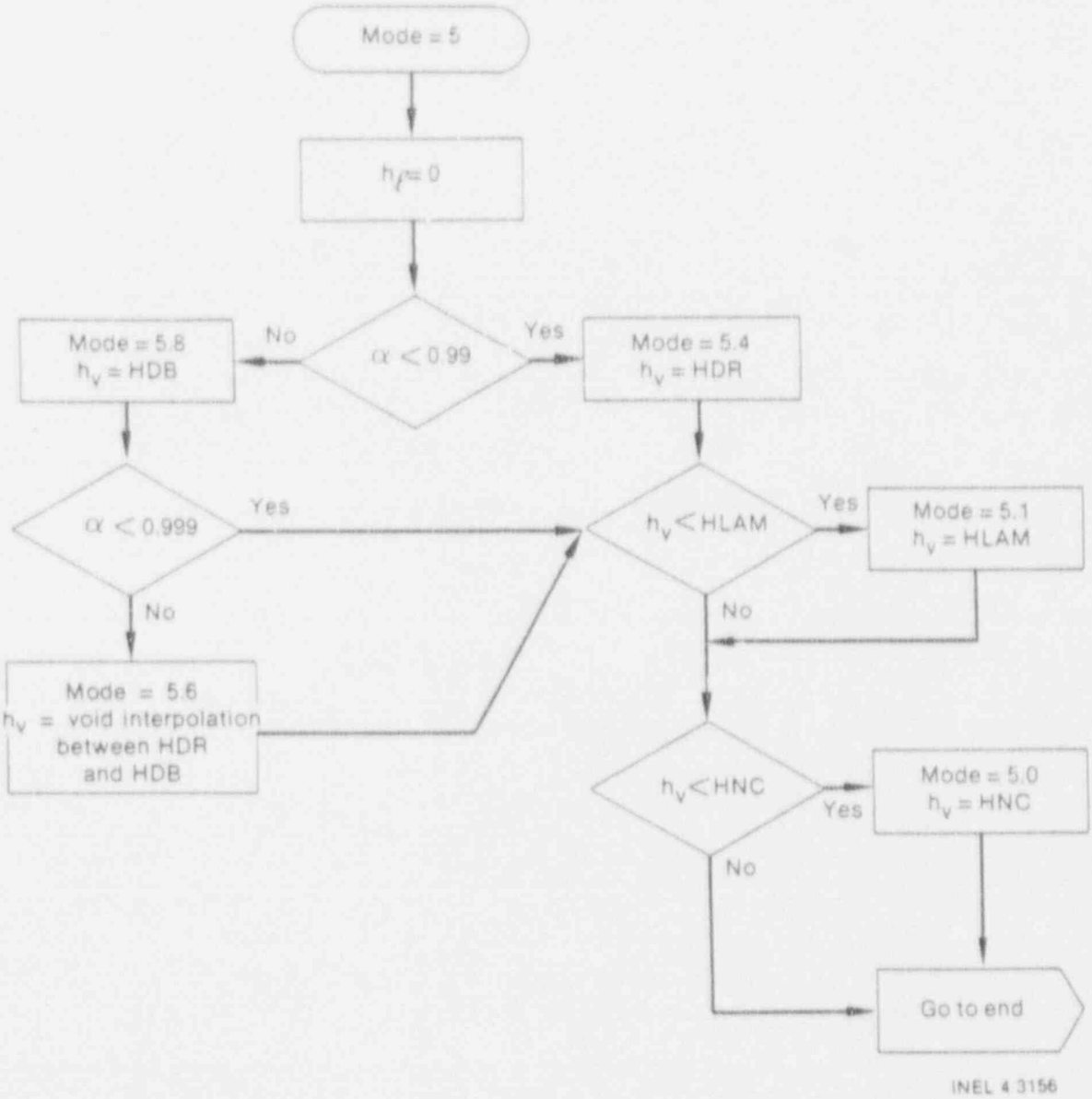

Figure 2.2-12. Single-phase vapor flow chart.

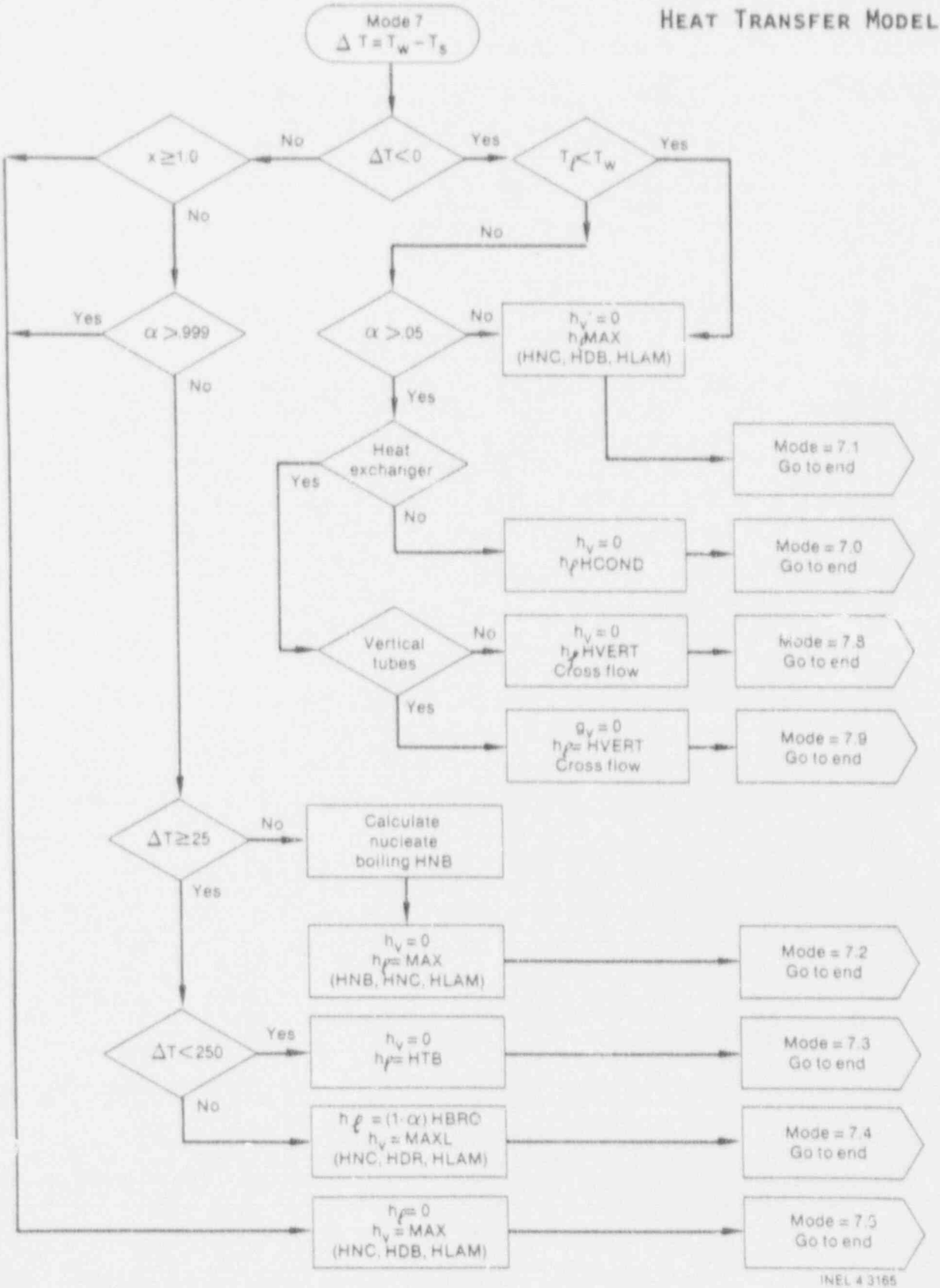

Figure 2.2-13. Simple boiling curve flow chart.

transition boiling uses the Loomis-Shumway[2.2-19] correlation

$$h_t = HTB = 2000(1 - \alpha)([62.36 + 8.804 \times 10^{-5}(P)]$$

$$- [11.3 + 1.59 \times 10^{-5}(P)\ln(\Delta T)]) \quad . \tag{2.2-51}$$

The upper right side of Figure 2.2-13 diagrams the condensation logic. Mode 7 through 7.5 follow closely Mode 0 through Mode 5; Modes 7.8 and 7.9 have been added for heat exchangers that have horizontal and vertical tubes, respectively. The equations used for horizontal and vertical tubes are related such that differences disappear as the steam flow increases. The equation is

$$Nu = FL\ Nu_1 + (1 - FL)Nu_2 \frac{T_s - T_w}{T_L - T_w} \tag{2.2-52}$$

where FL is the fraction of tube surface beneath the water pool. Nu_1 is the Nusselt number[2.2-20] below the pool surface.

$$Nu_1 = 0.36 Re_t^{0.55} Pr_t^{1/3} \quad . \tag{2.2-53}$$

Nu_2 is the Nusselt number in the steam region. For horizontal tubes[2.2-21]

$$Nu_2 = XF \left[1 + \frac{0.276}{XF^4\ Fr\ HF}\right]^{1/4} Re^{1/2} \tag{2.2-54}$$

where

$$XF = 0.9 \left[1 + \frac{1}{RF\ HF}\right]^{1/3} \tag{2.2-55}$$

$$HF = \frac{K_t(T_s - T_w)}{\mu_t h_{fg}} \tag{2.2-56}$$

$$RF = \left(\frac{\rho_t \mu_t}{\rho_v \mu_v}\right)^{1/2} \quad . \tag{2.2-57}$$

Fr is the Froude number based on the volumetric vapor velocity perpendicular to the tubes in the steam region.

Vertical tubes use Equation (2.2-22) plus the first term in Equation (2.2-54). The coefficient in Equation (2.2-22) is 0.943, as recommended by Chen[2.2-22], and the length is the distance between baffle plates instead of the hydraulic diameter. The first term of Equation (2.2-54)

$$Nu_2 = XF\ Re^{1/2} \tag{2.2-58}$$

is the only velocity-dependent term and becomes dominant at normal flow rates so that the tube orientation makes little difference.

2.2.2.2.8 Nucleate Boiling Transition--Pressurized water reactor safety codes have predicted the onset of nucleate boiling transition by using an empirical correlation to determine the local CHF. Using this transition criteria alone is inadequate for boiling water reactors since the high-quality, high-mass-flux conditions may introduce memory effects when the heat flux is nonuniform.[2.2-23]

Several methods exist for correlating CHF data for nonuniform heat fluxes. Perhaps the two most widely accepted for analyzing BWR-like phenomena are the Tong F-factor and CISE critical quality correlations.[2.2-24] Since the critical quality correlation is a simpler function to evaluate and has been used by General Electric Corporation (GE) to correlate CHF data in BWR rod bundle simulation, it has been chosen for use in TRAC-BF1. The general form of the correlation is

$$X_c = \frac{AL_B}{B + L_B} \tag{2.2-59}$$

where

X_c = critical quality

L_B = boiling length

and A and B are functions of pressure and mass flux (see Table 2.2-1).

Implemented into the code are two versions of this correlation, as shown in Table 2.2-1. The first is based upon the Biasi correlation[2.2-25] originally used in TRAC-BF1/MOD1. This correlation has been converted from a local CHF to a critical quality correlation, as described in Reference 2.2-23. The second is the CISE-GE correlation derived from data taken from experiments performed at GE. The Biasi X_c correlation gives larger values than the CISE-GE correlation.

Both correlations are included, since each has distinctive advantages. The improved Biasi correlation is based on a broad data base of CHF experiments. It is, however, subject to the assumptions used in converting to a critical quality. The CISE-GE correlation, on the other hand, is based on data from rod bundle experiments and includes effects of local peaking

Table 2.2-1. Critical quality correlation options.

Improved Biasi (ICHF = 2)	CISE-GE (ICHF = 3)
$A_1 = 1.0$	$A = 1.055 - 0.013 \left(\frac{(P - 4.137 \cdot 10^6)}{2.758 \cdot 10^6}\right)^2$
$B_1 = 1.048 \times 10^{-8} G^{1.6} D_h^{1.4} h_{fg}/H(P)$	$- 1.233(7.37 \times 10^{-4}G) + 0.907(7.37 \cdot 10^{-4}G)$
$X_{cr_1} = \frac{A_1 L_B}{B_1 + L_B} \cdot \frac{P_h}{P_w} \cdot R_f^{1/2}$	$- 1.233(7.37 \times 10^{-4}G) + 0.907(7.37 \cdot 10^{-4}G)^2$
	$- 0.285(7.37 \cdot 10^{-4}G)^3$
$A_2 = F(P)/G^{1/6}$	$B = 0.457 + 2.003(7.37 \cdot 10\ G)^{-4}$
$B_2 = G^{7/6} D_n^{1/4} h_{fg}(5.707 \cdot 10^{-8})$	$- 0.901(7.37 \cdot 10^{-4}G)^2$
$X_{cr_2} = \frac{A_2 L_B}{B_2 + L_B} \cdot \frac{P_h}{P_w} \cdot R_f^{1/2}$	If Bundle is 8 x 8, B = B/1.12
$X_c = \text{Max}(X_{cr_1}, X_{cr_2})$	$X_c = \frac{A L_B}{B + L_B} \frac{1.24}{R_f}$
$H(P) = -1.159 + 0.149(P \cdot 10^{-5}) \exp(-.019\ P) + \frac{8.99}{10 + (P \cdot 10^{-5})^2}$	
$F(P) = 0.7249 + 0.099\ (P \cdot 10^{-5}) \exp(-3.2 \cdot 10^{-7} P)$	

factors. The data base from which it is derived is limited to mass fluxes in the range 300 kg/m^2-s $\leq$ G $\leq$ 1400 kg/m^2-s.

The local CHF Biasi correlation has a data base that covers the mass flux (G) range between 100 and 6000 kg/m^2-s. The local flux Biasi correlation logic uses the maximum of

$$q_{CHF} = \frac{1.883 \times 10^7}{D_H^n G^{1/6}} \left(\frac{f_p}{G^{1/6}} - X \right) \quad (2.2\text{-}60)$$

$$q'_{CHF} = \frac{3.78 \times 10^7}{D_H^n G^{0.6}} h_p (1 - X) \quad (2.2\text{-}61)$$

where

$$n = \begin{cases} 0.4 \text{ for } D \geq 1 \text{ cm} \\ 0.6 \text{ for } D < 1 \text{ cm} \end{cases} \quad (2.2\text{-}62)$$

$$f_p = 0.7249 + (0.099)(P)[\exp^{-0.032P}] \quad (2.2\text{-}63)$$

D_H = hydraulic diameter (cm)

G = mass flux (g/cm^2-s)

$$h_p = -1.159 + (0.149)(P)[\exp] + 8.99(P)/(10. + P^2) \quad (2.2\text{-}64)$$

P = pressure (bars).

NOTE: The Biasi correlation uses cgs units, but the constants in Equations (2.2-60) and (2.2-61) have been changed so that Q_{CHF} is in W/m^2.

If Equation (2.2-60) is used, 0.02 is added to the heat transfer mode number. If Equation (2.2-61) is used, 0.01 is added to the mode number. Below a mass flux of 200 kg/m^2-s, the critical quality correlations are not used. Above 200, departure from nucleate boiling will occur if the local wall flux exceeds the Biasi CHF or the local quality exceeds either critical quality correlation specified by the user.

Between a mass flux of 200 and -700 kg/m^2-s, the local flux Biasi correlation is linearly interpolated with the Zuber[2.2-26] pool boiling correlation at a mass flux of zero and the Biasi correlation evaluated at G = 200 for positive flow and G = 700 for negative flow. The modified Zuber correlation is

$$q_{CHF} = (1 - \alpha)(0.9 \times 0.131 \, h_{fg} \rho_v \, BRAC + QSUB) \quad (2.2\text{-}65)$$

where

$$BRAC = \left[\frac{\sigma g (\rho_\ell - \rho_v)}{\rho_v^2} \right]^{1/4} \quad (2.2\text{-}66)$$

$$QSUB = \begin{cases} 0, \text{ if } T_\ell \geq T_s \\ \dfrac{2k_\ell(T_s - T_\ell)}{\left(\dfrac{\tau TAUk_\ell}{\rho_\ell c p_\ell}\right)^{1/2}}, \text{ otherwise} \end{cases} \quad (2.2\text{-}67)$$

$$TAU = 2.625 \frac{\left(\dfrac{\sigma}{g(\rho_\ell - \rho_v)}\right)^{1/2}}{BRAC} . \quad (2.2\text{-}68)$$

If the flow is countercurrent, the Zuber correlation is used; if the mass flux is less than -700 kg/m^2-s, the absolute value of the flux is used in the Biasi correlation.

Once q_{CHF} has been obtained from the Biasi correlation, the temperature corresponding to the CHF point, T_{CHF}, is calculated using a Newton-Raphson iteration[2.2-27] to determine the intersection of the heat flux found by using the nucleate boiling HTC and CHF. An iteration is required because $T_w = T_{CHF}$ must be known to evaluate the CHEN correlation; in turn, the CHEN HTC must be known to calculate the wall temperature. The expression thus becomes

$$q_{CHF} = h(T_w - T_s) . \quad (2.2\text{-}69)$$

The equation for TCHF is

$$T_{CHF}^{n+1} = T_{CHF}^{n} - \frac{T_{CHF}^{n} - T_s - \dfrac{q_{CHF}}{h}}{1 + \dfrac{q_{CHF}}{h^2}\dfrac{dh}{dT_w}} \quad (2.2\text{-}70)$$

where T_{CHF}^{n} is the CHF temperature for the nth iteration, h is the HTC evaluated using the CHEN correlation, and dh/dT_w is the derivative of the HTC with respect to the wall temperature.

Convergence occurs when $T_{CHF}^{n+1} - T_{CHF}^{n} < 1.0$. A maximum of ten iterations is allowed; if convergence does not occur, a message is printed and a fatal error results.

The CHF temperature is restricted to the range, $(T_s + 0.5) \leq T \leq (T_s +$

100). The options available to the user are

ICHF = negative, no CHF allowed

= 0, use simplified boiling curve (Mode 7)

= 1, use Biasi local CHF

= 2, use Biasi critical quality plus Biasi local CHF

= 3, use CISE-GE critical quality plus Biasi local CHF.

To assist in understanding the nature of the nucleate boiling transition for CHAN components, the output variable, FILMTRIP has been added, where

FILMTRIP = 0 implies no nucleate boiling transition

= 1 implies local CHF transition

= 2 implies critical quality transition.

2.2.2.2.9 **Minimum Stable Film Boiling Temperature, T_{min}**--The minimum stable film boiling point is the intersection point between the transition and film boiling heat-transfer regimes (Figure 2.2-5). This point is also used in the interpolation scheme for calculation of the transition boiling liquid HTC.

TRAC-BF1/MOD1 has two options for T_{min}. If the input variable ITMIN = 0, the homogeneous nucleation correlation is used; if ITMIN = 1, the correlation given by Shumway[2.2-28] is used. The homogeneous nucleation minimum stable film boiling temperature correlation is

$$T_{min} = T_{nh} + (T_{nh} - T_{\ell})R^{0.5} \qquad (2.2\text{-}71)$$

where

$$R = \frac{(k\rho C_p)_{\ell}}{(k\rho c)_w} \qquad (2.2\text{-}72)$$

and T_{nh} is the homogeneous nucleation temperature. In Equation (2.2-72), subscript ℓ indicates liquid properties and subscript w indicates wall properties. Because T_{nh} is a weak function of pressure and varies from 580 K at atmospheric pressure to the critical temperature (649.28 K) at the critical pressure, T_{nh} is set equal to the critical temperature.

The Shumway correlation depends on saturation temperature, thermodynamic state, liquid and wall transport properties, and void fraction and critical pressure

$$T_{min} = T_{SAT}$$

$$+ 3.7\left(\frac{\rho_l + \rho_g}{\Delta\rho}\right)^{-1} \frac{h_{gf}\beta}{C_{pl}Pr_l}[1 + (1 - \alpha^2)]\,(1 + 1.5E\text{-}5\ Re_l)^{0.15}\left(1 - \frac{P}{P_c}\right)^{0.1} \qquad (2.2\text{-}73)$$

The Shumway correlation has been evaluated against data in the pressure range of 0.4 to 9 MPa on tubes between 0.01 and 0.0154 m and on bundles between 0.012 and 0.0135 m.

2.2.3 Radiation Heat Transfer Model

Radiation heat transfer is neglected in all components except CHAN, where the user specifies a cutoff void fraction (ALPTST) below which radiation heat transfer is neglected. For void fractions above ALPTST, radiation heat transfer is modeled as described below. This section is repeated as coded in Reference 1, Section 4.3.

The governing equations for radiative heat transfer within an absorbing, emitting, and scattering medium are a set of integrodifferential equations for which only a few solutions for simple geometries are available.[2.2-29] Numerical solutions to these equations are also impractical in terms of cost and effort. For engineering applications, approximate methods are typically chosen. A lumped-system approximation with uniform radiosity at the surfaces has been the traditional approach.[2.2-30,31,32,33]

The lumped-system approximation of the net-radiation method has been presented in Reference 2.2-29. The governing radiation exchange equations can be obtained for the kth surface of area A_{tk} of an arbitrary enclosure of N discrete, diffuse, gray surfaces, as illustrated in Figure 2.2-14, by considering the incident and outgoing radiation components. The total radiation leaving surface k is

$$B_k A_{tk} = \varepsilon_k \sigma_{SB} T_k^4 A_{tk} + (1 - \varepsilon_k) H_k A_{tk} \qquad (2.2\text{-}74)$$

$$B_k = \varepsilon_k \sigma_{SB} T_k^4 + (1 - \varepsilon_k) H_k \ . \qquad (2.2\text{-}75)$$

As illustrated in Figure 2.2-15, the total incident radiation for surface k, assuming a transparent medium between surfaces, is

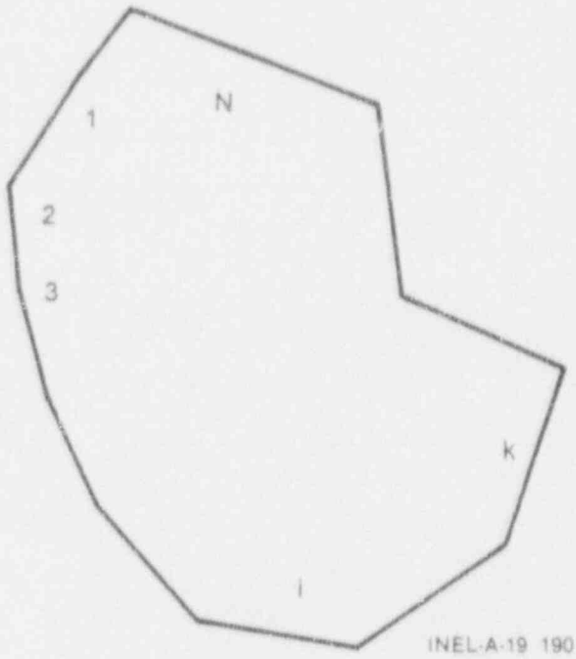

Figure 2.2-14. Enclosure of N discrete surfaces and radiation energy leaving surface k.

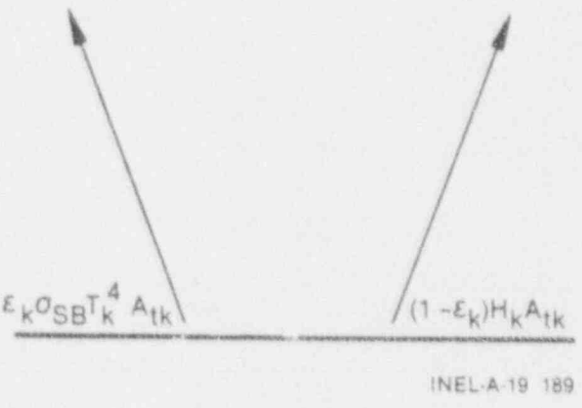

Figure 2.2-15. Radiant energy incident on surface i.

$$H_k A_{tk} = \sum_{j=1}^{N} B_j A_{tj} F_{jk} \quad . \tag{2.2-76}$$

Given the surface temperature, surface emissivities, and geometric view factors, Equations (2.2-75) and (2.2-76) can be solved for B_j and H_j. The net radiation from surface k is

$$q_k = B_k - H_k = \frac{\varepsilon_k\left(\sigma_{sB} T_k^4 - B_k\right)}{1 - \varepsilon_k} \quad . \tag{2.2-77}$$

If a two-phase mixture is present, the governing radiat.ve exchange equations would appear as

$$B_k = \varepsilon_k \sigma_{sB} T_k^4 + (1 - \varepsilon_k) H_k \tag{2.2-78}$$

$$H_k = \frac{1}{A_{tk}} \sum_{j=1}^{N} \left(B_j \tau_{jk} + \varepsilon_{gjk} \tau_{\ell jk} \sigma_{sB} T_g^4 + \varepsilon_{\ell jk} \tau_{gjk} \sigma_{sB} T_\ell^4\right) F_{jk} A_{tj} \tag{2.2-79}$$

where

$$\tau_{jk} = \tau_{gjk} \tau_{\ell jk} = (1 - a_{gjk})(1 - a_{\ell jk}) \tag{2.2-80}$$

and where the following assumptions have been made: (a) all surfaces are gray and diffused; (b) each rod is one surface at one temperature, and the channel wall is one surface at one temperature; (c) axial radiative heat transfer is negligible; (d) the droplets and vapor are gray; (e) scattering is negligible; (f) the vapor and liquid temperatures are independent of the radial dimension; and (g) the view factor of the two-phase mixture of surface j along the path k to j is given by the view factor from surface k to j (F_{kj}).

Equation (2.2-78) implies that the radiosity at surface k (B_k) is composed of two components,

1. $\varepsilon_k \sigma_{sB} T_k^4$

   --radiant heat flux emitted by surface k

2. $(1 - \varepsilon_k)H_k$

--radiation heat flux reflected from surface k due to the incident radiation heat flux on surface k (H_k).

Equation (2.2-78) gives three components to the incident radiant heat flux at surface k,

1. $\frac{1}{A_k}\sum_{j=1}^{N} B_j A_{tj} F_{jk} \tau_{jk}$

--radiation transferred from all surfaces to surface k without being absorbed by the two-phase mixture.

2. $\varepsilon_{vjk}\tau_{\ell jk}A_{tj}F_{jk}\sigma_{sB}T_v^4$

--radiation reemitted by the vapor phase along the path j to k and transferred to surface k without being reabsorbed by the liquid.

3. $\varepsilon_{\ell jk}\tau_{vjk}A_{tk}F_{jk}\sigma_{sB}T_\ell^4$

--radiation reemitted by the liquid phase along the path j to k and transferred to surface k without being absorbed in the vapor phase.

Equations (2.2-78) and (2.2-79) can be combined to yield a system of linear equations if the surface temperatures, surface emissivities, view factors, and fluid radiation properties are known and can be solved for the radiosities for each surface

$$\sum_{j=1}^{N}\left[\delta_{jk} - (1 - \varepsilon)\tau_{jk}F_{kj}\right]B_j$$

$$= \varepsilon_k\sigma_{sB}T_k^4 + (1 - \varepsilon_k)\sum_{j=1}^{N}\left(\varepsilon_{gjk}\tau_{\ell jk}\sigma_{sB}T_g^4 + \varepsilon_{\ell jk}\tau_{gjk}\sigma_{sB}T_\ell^4\right)F_{kj} \quad . \qquad (2.2\text{-}81)$$

Given the solution from Equation (2.2-81), a solution to Equation (2.2-77) can be determined to yield the net radiation heat flux from surface k. Equation (2.2-77) provides the radiation heat transfer boundary condition used for the conduction solution for surface k. However, additional calculations are required to determine the portion of radiant energy leaving surface k that is eventually absorbed into either the vapor, droplet, or film phases of the two-phase mixture.

The total radiation absorbed by the two-phase mixture is given by

$$\sum_{k=1}^{N} QABS_k = \sum_{k=1}^{N} \sum_{j=1}^{N} \left\{ A_{tk} F_{kj} \left[B_k (1 - \tau_{kj}) - \tau_{gjk} \varepsilon_{\ell kj} \sigma_{sB} T_\ell^4 - \tau_{\ell kj} \varepsilon_{gkj} \sigma_{sB} T_g^4 \right] \right\} . \quad (2.2\text{-}82)$$

It can be shown that Equations (2.2-81) and (2.2-82) form a system of radiative exchange equations that conserve radiation energy

$$\sum_{k=1}^{N} q_k A_{tk} - QABS_k = 0. \quad (2.2\text{-}83)$$

However, since TRAC-BF1/MOD1 is a nonequilibrium two-fluid code, it is necessary to determine how much of the total radiant energy absorbed by the two-mixture phase is absorbed by the vapor phase and how much by the liquid phase.

The first term on the right side of Equation (2.2-82) is the amount of radiation absorbed by the two-phase mixture along the path k to j. The second term is the amount of radiation emitted by the liquid phase along the path k to j and not reabsorbed by the vapor phase. The third term is the amount of radiant energy emitted by the vapor phase along the path k to j and not reabsorbed by the liquid phase.

One method for splitting the first term on the right side into vapor/liquid components is to consider the probability that radiation will travel a distance z along a path L from k then to j and be absorbed in the vapor phase in the next dz of path length, $P_d(z)dz$, or

$$P_d(z)\, dz = K_g e^{-(K_g + K_d)z}\, dz . \quad (2.2\text{-}84)$$

Equation (2.2-84) assumes that the radiation absorption mechanism of the two-phase mixture can be expressed as an exponential function.[2.2-34,35] If Equation (2.2-84) is integrated from 0 to L, $P_d(L)$ can be determined, which is the probability that radiation traveling along the path L will be absorbed by the vapor phase

$$P_d(L) = \frac{K_g}{K_g + K_d} \left[1 - e^{-(K_g + K_d)L} \right] . \quad (2.2\text{-}85)$$

The term of one minus the exponential can be recognized as one minus the transmissivity, since

$$\tau_{jk} = (1 - a_{gkj})(1 - a_{\ell kj}) = \left[1 - \left(1 - e^{-K_{gkj} L_{kj}} \right) \right]$$

$$\left[1 - \left(1 - e^{-K_{dkj} L_{kj}} \right) \right] = e^{-(K_{gkj} + K_{dkj}) L_{kj}} . \quad (2.2\text{-}86)$$

Equation (2.2-85) can now be written as

$$P_d(L_{kj}) = \frac{K_{gkj}}{K_{gkj} + K_{dkj}} (1 - \tau_{kj}) . \quad (2.2\text{-}87)$$

Comparing Equations (2.2-82) and (2.2-84) yields the following equation for the net radiation absorbed by the vapor phase

$$\sum_{j=1}^{N} QABSV_k = \sum_{k=1}^{N}\sum_{j=1}^{N}\left\{A_{tk}F_{kj}\left[B_k(1-\tau_{kj})\frac{K_{gkj}}{K_{gkj}+K_{dkj}}\right.\right.$$

$$\left.\left. - \varepsilon_{gkj}\tau_{\ell kj}\sigma_{sB}T_g^4 + \varepsilon_{gkj}\varepsilon_{\ell kj}\sigma_{sB}\left(T_\ell^4 - T_g^4\right)\right]\right\} . \qquad (2.2\text{-}88)$$

The last term on the right side of Equation (2.2-88) is a correction proposed by Sun et al.[2.2-34] to account for radiation heat transfer between the droplet phase and the vapor phase. The radiation absorbed by the liquid phase can be obtained in a similar manner

$$\sum_{j=1}^{N} QABSL_k = \sum_{k=1}^{N}\sum_{j=1}^{N}\left\{A_{tk}F_{kj}\left[B_k(1-\tau_{kj})\frac{K_{dkj}}{K_{dkj}+K_{gkj}}\right.\right.$$

$$\left.\left. - \varepsilon_{\ell kj}\tau_{gkj}\sigma_{sB}T_\ell^4 - \varepsilon_{gkj}\varepsilon_{\ell kj}\sigma_{sB}\left(T_\ell^4 - T_g^4\right)\right]\right\} . \qquad (2.2\text{-}89)$$

Since the sum of Equations (2.2-88) and (2.2-89) yield Equation (2.2-82), radiant energy is conserved.

Equations (2.2-88) and (2.2-89) are solved in the routine RADSLAB once B_k has been determined. The results of Equations (2.2-88) and (2.2-89) are used to determine a radiation heat transfer coefficient from the rod or channel wall surface k to the liquid phase and a radiation heat-transfer coefficient from the rod or channel wall surface k to the vapor phase

$$h_{r\ell k} = \frac{QABSL_k}{(T_{k\ell} - T_\ell)A_{tk}} \qquad (2.2\text{-}90)$$

$$h_{rgk} = \frac{QABSV_k}{(T_{kg} - T_g)A_{tk}} . \qquad (2.2\text{-}91)$$

Before Equations (2.2-77), (2.2-78), (2.2-88), and (2.2-89) can be solved by RADSLAB, the quantities, e_k, e_{vkj}, $e_{\ell kj}$, $a_{\ell kj}$, and a_{vkj} must be determined. The total emissivity for the vapor phase can be calculated as

$$\varepsilon_g = \frac{\int_0^\infty \varepsilon_g(w)B(w,T_g)\,dw}{\int_0^\infty B(w,T_g)\,dw} . \qquad (2.2\text{-}92)$$

The absorptivity for the vapor phase can be calculated as

$$a_g = \frac{\int_0^\infty a_g(w)B(w,T_g)\,dw}{\int_0^\infty B(w,T_g)\,dw} \quad . \tag{2.2-93}$$

where

T_k = surface temperature

$a_g(w)$ = $\varepsilon_g(w)$, by Kirchoff's law

w = wave number of radiation (cm^{-1}).

The absorption spectrum of water/vapor is generally considered to consist of six major absorption bands. The wave numbers and absorption coefficients associated with these bands are given in Reference 2.2-36 and Table 2.2-2. The values given in this table were obtained for the Thomson model of emissivity described in Reference 2.2-36, which is essentially the model utilized for the present calculation. The absorption coefficient values in Table 2.2-2 were obtained for a reference temperature of 300 K. These values are assumed to vary inversely with water/vapor temperature to account for various line broadening phenomena, or

$$K(w) = K_o(w)\frac{T_o}{T} \tag{2.2-94}$$

where T_o = 300 K and $K_o(W)$ is the tabular value of K_w. The values of $K(_w)$ used in the present model were assumed to be constant within each band and zero in the region between bands.

Table 2.2-2. Water vapor absorption band data.

Wave Length of Band Center (μ)	Minimum Wave Number (cm^{-1})	Maximum Wave Number (cm^{-1})	Absorption Coefficient $K_0(w)$ (Atm^{-1} cm^{-1})
20.0	195.5	804.5	0.0959
6.3	1283.0	1892.0	0.2874
2.7	3399.0	4008.0	0.2069
1.87	5043.0	5652.0	0.0166
1.38	6942.0	7551.0	0.0136
1.1	8468.0	9077.0	0.00053

Using the data in Table 2.2-2, the integrals in Equations (2.2-92) and (2.2-93) can be approximately evaluated as sums over the six bands

$$\varepsilon = \frac{\sum_{i=1}^{6} \varepsilon(\bar{w}_i)\overline{B(w_i,T)}\,\Delta w_i}{\sigma_{SB}T^4} \qquad (2.2\text{-}95)$$

$$a = \frac{\sum_{i=1}^{6} \varepsilon(\bar{w}_i)\overline{B(w_i,T_w)}\,\Delta w_i}{\sigma_{SB}T^4} \qquad (2.2\text{-}96)$$

where i is the band index and $\overline{B(w_i, T)}$ is the average value of the Planck black body function over band i. In the Thomson model, this value is obtained by integrating B(w,T) over the entire band; while in the present model, it is obtained by evaluating B(w,T) at the mean wave number w_i of the band, or

$$\overline{B(w_i,T)} = B(\bar{w}_i,T) \; . \qquad (2.2\text{-}97)$$

This model for water/vapor emissivity is incorporated into TRAC-BF1/MOD1 in Subroutine EMISS. To test the implementation of this model, EMISS was used to evaluate the emissivity of water/vapor for an applicable range of vapor temperatures and optical path lengths (PL products). The results of these calculations are compared in Figure 2.2-16 with experimental data and Thomson model results, both presented in Reference 2.2-35. Though the Thomson model gives better agreement with data than the present model, it is judged that the faster computational scheme used in the present model justifies the observed decrease in accuracy.

The droplet properties, $\varepsilon_{\ell kj}$ and $a_{\ell kj}$, are also calculated in EMISS. The model developed in Reference 2.2-34 is

$$\varepsilon_{dkj} = a_{dkj} = 1 - e^{-1.11 a_d \frac{L_{kj}}{D_d}} \qquad (2.2\text{-}98)$$

Equation (2.2-98) also gives the absorption coefficient for the droplets (K_{dkj})

$$K_{dkj} = \frac{1.11 a_d}{D_d} \; . \qquad (2.2\text{-}99)$$

The model for the steam absorptivity does not assume the form of Equation (2.2-88); therefore, K_{gkj} is calculated from

$$K_{gkj} = \frac{-\ln(1 - a_{gkj})}{L_{kj}} \; . \qquad (2.2\text{-}100)$$

The surface emissivities are input for the CHAN component and held constant over the transient. This completes information required by RADSLAB to

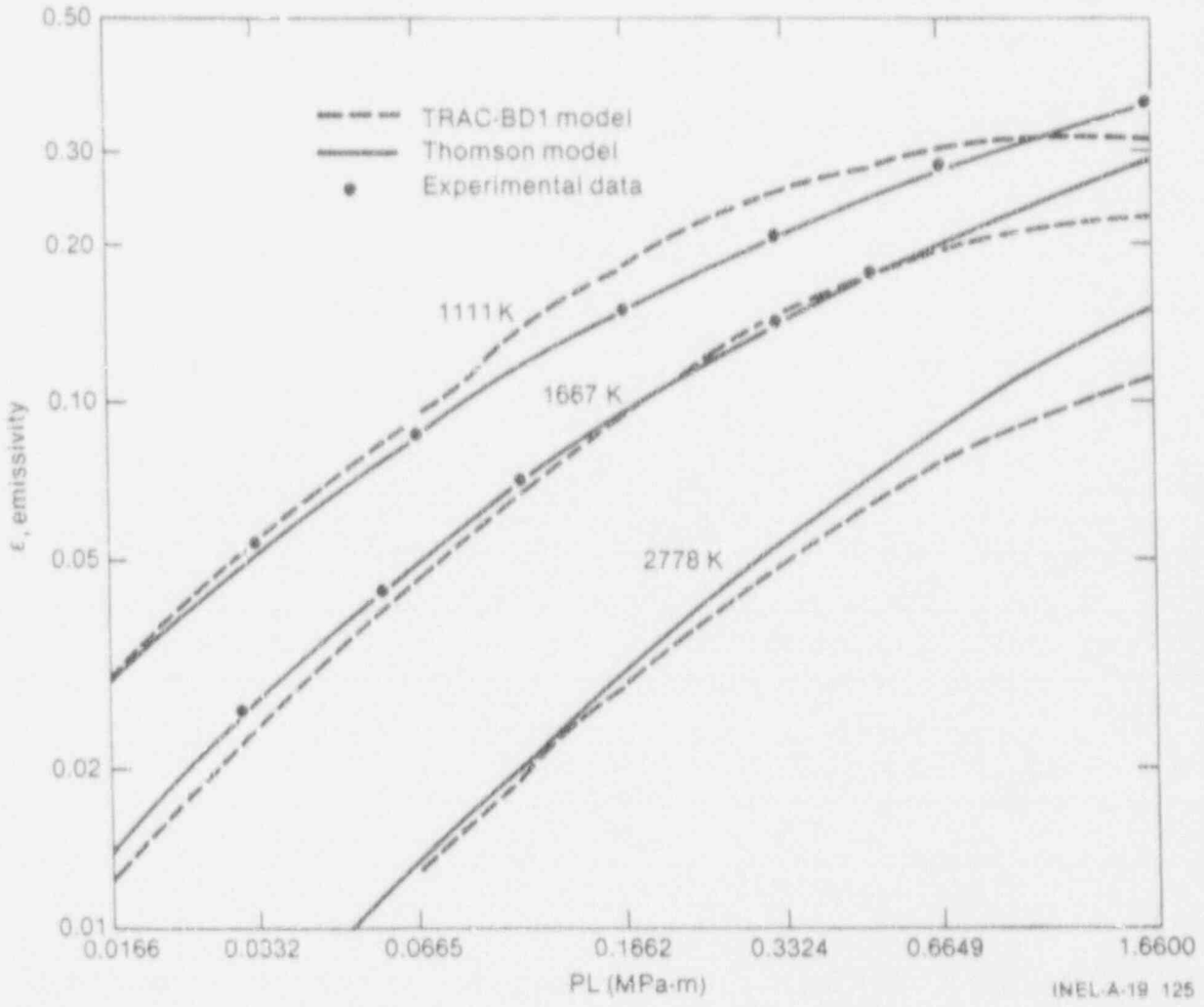

Figure 2.2-16. Water vapor emissivity.

calculate the radiation boundary condition required by TRAC-BF1/MOD1 hydrodynamics and heat transfer solution, if all involved surfaces are dry and the geometric data, F_{kj} and L_{kj}, are known.

If a surface involved in the radiation heat transfer calculation quenches, the radiation heat transfer calculation performed by RADSLAB is modified to account for the change in effective surface emissivity for the wetted or quenched surface. If a surface is quenched, the surface emissivity is set to 0.96[2.2-24] and the calculated radiation heat flux at that surface is treated as an additional energy inflow to the liquid phase, since it is the liquid film absorbing the radiant energy and not the surface.

The quenched fraction for each axial node (for each rod group) and channel wall within a given CHAN component is calculated by CHAN1 and passed

to RADSLAB. RADSLAB uses the fraction of quenched surface to linearly partition radiation at the quenching surface between the liquid phase and surface. CHAN1 also uses the fraction of quenched surface to linearly weight the dry surface emissivity with the wet surface emissivity and to linearly weight an effective wetted surface temperature with an effective dry surface temperature for the rods. Linear weighting may not be adequate. Additional work in this area may be required, depending on how the CHAN radiation model compares with data.

Calculation of the geometric quantities, F_{kj} and L_{kj}, required by the radiation model are performed in ICHAN by calls to CFIJ, GRPFIJ, and GRPLIJ. These routines were obtained from Reference 2.2-32. The methods employed to calculate view factors between individual surfaces before grouping is the crossed string method given in Reference 2.2-36. The method employed to calculate mean beam lengths between individual surfaces is the equivalent flat plate method proposed in Reference 2.2-30. The method employed in grouping of the individual view factors is the angle-factor algebra method given in Reference 2.2-35.

The CFIJ routine has been modified from that given in Reference 2.2-32. To reduce storage requirements, the channel wall is treated as one surface, rather than broken into segments and treated as 4-NROD surfaces as in Reference 2.2-32, where NROD is the number of rods on a row. For calculation of the view factor from each rod to the channel wall, conservation of radiant energy can be used. The view factor from any given rod to the channel wall is given by

$$F_{kN} = 1 - \sum_{j=1}^{N-1} F_{kj} \quad . \tag{2.2-101}$$

The reciprocity rule[2.2-35] can be used to calculate the view factor from the wall to the rod surface K

$$F_{Nk} = \frac{A_{tk} F_{kN}}{A_{tN}} \quad . \tag{2.2-102}$$

The calculation of the path length from the rod surfaces to the channel wall uses the path length from the rod surface to the nearest channel wall. This is an approximation for the path length between rod surface and the channel wall. However, it appears adequate for the outer row of rods in the bundle and is not a major factor for the inner rows of rods, since the view of the channel wall by the inner rows of rods is small. Work should be performed in the area of improving these calculations and reducing the storage requirements at the same time.

An anisotropic reflection model has been developed for TRAC-BF1/MOD1. This model modifies the view factors to account for anisotropic reflection effects from the rods and channel walls in a BWR bundle. Comparisons with experimental data indicate that this effect can be significant. The view factors are modified by the method suggested by Andersen.[2.2-37] In this method, a fraction μ_i of the radiation incident on rod i from rod j is

directly reflected back to rod j and a fraction $(1 - \mu_i)$ is reflected isotropically. This has the effect of reducing the effective view factor from rod j to rod i and increasing the effective view factor from rod j to itself, since a fraction μ_i of all radiation sent from rod j to rod i is immediately returned.

The anisotropic factor μ_i is used to modify the view factors used in Equations (2.2-76) through (2.2-88) in accordance with Equations (2.2-103) and (2.2-104):

$$F'_{ij} = F_{ij}(1 - \mu_{ij}) \text{ for } i \neq j \qquad (2.2\text{-}103)$$

$$F'_{ii} = F_{ii} + \sum_{\substack{j=1 \\ j \neq 1}}^{N} F_{ij}\mu_{ij} \; . \qquad (2.2\text{-}104)$$

These new effective view factors conserve radiant energy and satisfy the reciprocity relationship if $\mu_{ij} = \mu_{ji}$. In accordance with the recommendations of Tien et al.,[2.2-38] a value of 0.5 is used for μ_{ij} for rod-to-rod radiation and 0.15 for channel wall-to-rod radiation.

In an effort to reduce the computation time for the radiation model, the present coding only calls RADSLAB every NRADth time step where NRAD is a user-supplied input. This has the disadvantage that if wall temperatures and fluid temperatures or both are rapidly changing, the radiation heat transfer boundary conditions (q_k, h_{rvk}, h_{rfk}) calculated by RADSLAB may not be consistent with

$$\sum_{k=1}^{N} (q_k A_k - QABS_k) = 0 \; . \qquad (2.2\text{-}105)$$

Additional work should be done in this area of determining how often to call RADSLAB and what information should be calculated each time step.

2.2.4 Reflood Heat Transfer Model

The reflood fine-mesh model in TRAC-BF1/MOD1 is based on the moving-mesh reflood model developed at Los Alamos National Laboratory for the TRAC-PD2 code. An analogous model has been developed for CHAN wall reflood heat transfer. This section is repeated as coded in Reference 1, Section 9.3.A.

In the TRAC-BF1/MOD1 fuel rod model, heat transfer coarse-mesh nodes are located at the hydrodynamic cell boundaries. Figure 2.2-17 depicts a typical fuel rod and several associated hydrodynamic cells. The upper and lower elevations of each node are taken as the midpoints between the center node and the nodes above and below. In order to maintain equality between the heat transfer out of the wall nodes and the heat received by the fluid cells, average heat transfer coefficients (and associated wall or fluid temperature)

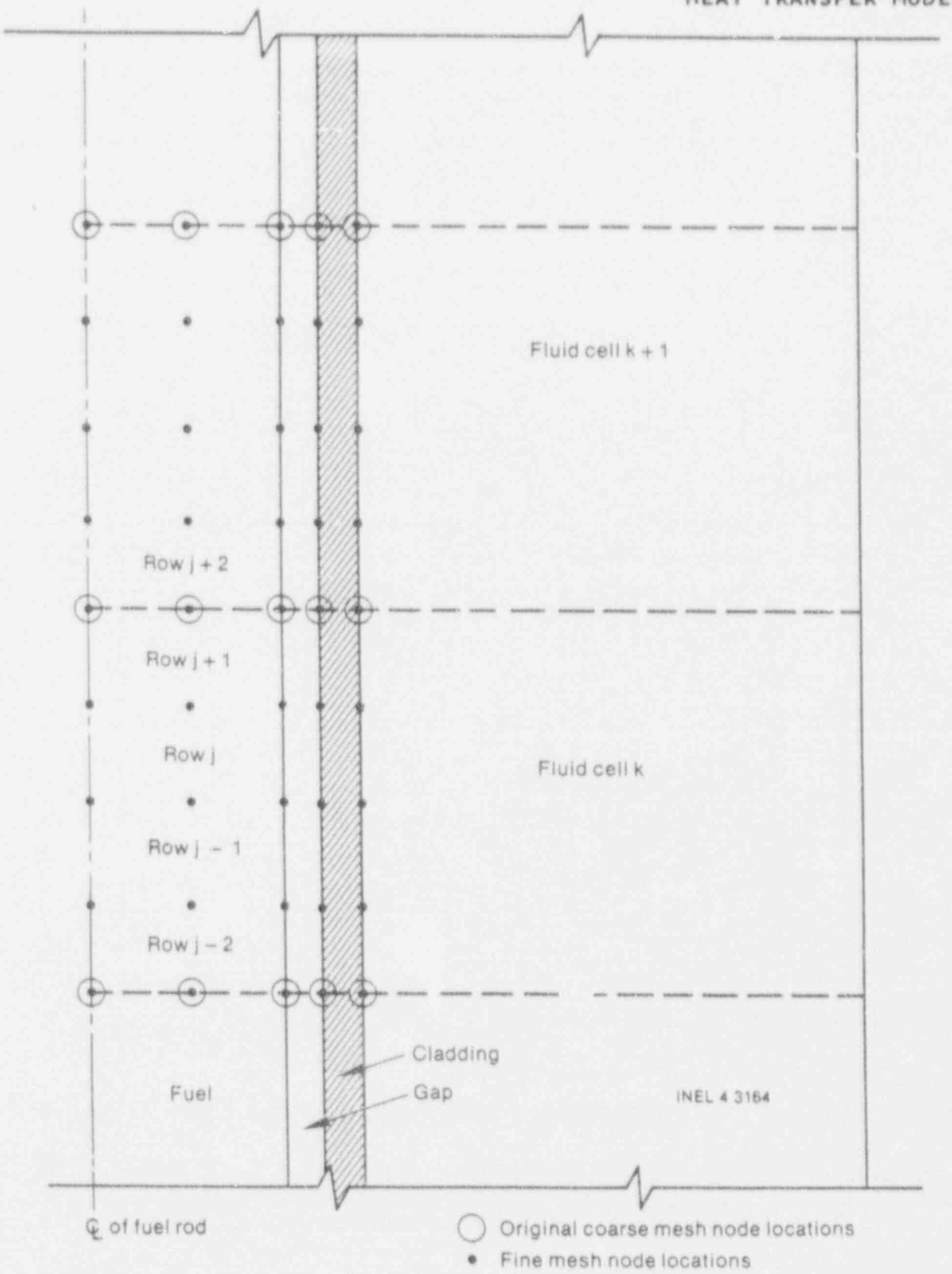

Figure 2.2-17. TRAC-BF1/MOD1 reflood model fine mesh nodalization.

must be defined for each fluid cell and each coarse mesh rod node. Figure 2.2-17 shows portions of three fluid cells and two associated coarse-mesh nodes. NOTE: Each coarse-mesh node transfers heat to two fluid cells. For the situation shown in Figure 2.2-17, the total rod-to-liquid heat transfer to liquid in fluid cell k is

$$Q_{TOT,\ell,k} = W.P. \left[z_{j+1} - \frac{1}{2}(z_{j+1} + z_j)\right] h_{\ell,j+1\to k}(T_{w,j+1} - T_{\ell,k})$$

$$+ W.P. \left[\frac{1}{2}(z_{j+1} + z_j) - z_j\right] h_{\ell,j+1\to k}(T_{w,j} - T_{\ell,k}) \qquad (2.2\text{-}106)$$

where

W.P.	=	rod wall wetted perimeter
Z_j	=	elevation of Node j
$h_{\ell j\to,k}$	=	rod-to-liquid heat transfer coefficient for Node j to fluid cell k
$T_{w,j}$, $T_{\ell,k}$	=	wall Node j and liquid cell k temperatures.

We define an appropriate average wall temperature and heat transfer coefficient as

$$T_{w,\ell,k} = \frac{\frac{1}{2}(z_{j+1} - z_j)h_{\ell,j+1}T_{w,j+1} + \frac{1}{2}(z_{j+1} - z_j)h_{\ell,j}T_{w,j}}{\frac{1}{2}(z_{j+1} - z_j)h_{\ell,j+1} + \frac{1}{2}(z_{j+1} - z_j)h_{\ell,j}} \qquad (2.2\text{-}107)$$

$$h_{\ell,w\to k} = \frac{\frac{1}{2}(z_{j+1} - z_j)h_{\ell,j+1} + \frac{1}{2}(z_{j+1} - z_j)h_{\ell,j}}{z_{j+1} - z_j} \qquad (2.2\text{-}108)$$

Analogous expressions for vapor $T_{w,v}$ and $h_{v,w\to k}$ may be derived.

Inspection shows that, for these definitions of $T_{w,\ell}$ and h_ℓ,

$$Q_{TOT,\ell,k} = h_{\ell,w\to k}(T_{w,\ell,k} - T_{\ell,k})(z_{j+1} - z_j)W.P. \; . \qquad (2.2\text{-}109)$$

A similar average must be derived for the wall nodes that are in thermal contact with two fluid cells. These averages become more complicated when fine-mesh nodes are introduced, but the general form remains similar.

Another feature unique to the reflood package is the adjustment of the void fraction used in calculating heat transfer coefficient if the quench

front is near the node. Referring to Figure 2.2-17, the void fraction α_j used at Node j is

$$\bar{\alpha}_j = \begin{cases} \alpha_\ell \text{ for } ZQF > z_{j+1} \\ \alpha_v \text{ for } ZQF < z_j \\ \frac{1}{2}[\alpha_k + X\alpha_{k+1} + (1 - X)\alpha_{k-1}] \text{ for } z_j \le ZQF \le z_{j+1} \end{cases} \quad (2.2\text{-}110)$$

where

ZQF = elevation of the quench front

$$\alpha_\ell = \frac{1}{2}(\alpha_k + \alpha_{k-1}) \quad (2.2\text{-}111)$$

$$\alpha_v = \frac{1}{2}(\alpha_{k+1} + \alpha_k) \quad (2.2\text{-}112)$$

$$X = \frac{z_{j+1} - ZQF}{z_{j+1} - z_j} . \quad (2.2\text{-}113)$$

This adjustment permits a smooth void fraction transition as the quench front moves up in the node.

The model has three distinct types of heat transfer nodes. The coarse-mesh nodes, used before reflood is specified, are centered on fluid cell boundaries, as previously illustrated. The fixed fine-mesh nodes are introduced at the beginning of reflood, and do not *move*. These are similar to the fine-mesh nodes in earlier versions of the code. The user specifies in input how many of these nodes should be introduced between each pair of adjacent coarse-mesh nodes. Finally, the third kind of nodes are the *moving* nodes. The placement of these nodes is done by the code, subject to limitations imposed by user input. These limitations are:

1. Maximum total number of heat transfer nodes per rod group (specified by the user).

2. Minimum spacing between heat transfer nodes (required for stability).

3. Minimum surface temperature difference between adjacent existing nodes. If this temperature difference is exceeded, the code will attempt to insert another row of fine mesh nodes between the two nodes that have the excessive temperature difference.

Nodes are inserted in such a manner as to minimize disruption of energy conservation. When rows are deleted, however, the temperatures of the nodes above and below are not adjusted, so that some minor energy loss (or gain) may

occur. The algorithm for calculating the temperature of an inserted node is

$$T_j = \frac{\rho_{j-1} C_{p,j-1} T_{j-1} + \rho_{j+1} C_{p,j+1} T_{j+1}}{2\rho_j C_{p,j}} \quad (2.2\text{-}114)$$

where ρ_{j-1}, $C_{p,j-1}$, ρ_{j+1}, $C_{p,j+1}$ are the density and specific heat for the nodes below and above the inserted node and

$$\rho_j = \frac{\rho_{j-1} + \rho_{j+1}}{2} \quad (2.2\text{-}115)$$

$$C_{pj} = \frac{C_{p,j-1} + C_{p,j+1}}{2} \quad (2.2\text{-}116)$$

In general, T_j should be very close to 1/2 $(T_{j+1} + T_{j-1})$, and energy conservation should not be seriously violated for deletion of rows of nodes.

Falling film and bottom flood quench fronts are tracked on each rod group. A node is considered quenched whenever the node is in any heat transfer mode except 4 or 5. The quench front positions are taken as the lowermost consecutive quenched node for the falling film and the uppermost consecutive quenched node for the bottom flood position.

The surface heat transfer on the inside of the channel wall is analogous to the rod surface heat transfer. Coarse mesh nodes are located at cell boundaries, and the same temperature and heat-transfer coefficient averaging schemes are used. Volumetric heat sources and radiation are included, and the same method for averaging void fractions near a quench front is employed.

The heat transfer situation on the outside of the channel wall is complicated by the fact that the coarse-mesh nodes may not be located at fluid boundaries. Previous versions of the reflood model handled this by assuming that all the heat transfer from a wall node went into the fluid cell that overlapped most of the node. The present model partitions the heat transfer according to the fraction of overlap with each fluid cell. The model is limited, however, since it only permits a wall node to contact 1 or 2 fluid cells. This places some burden on the user to ensure proper alignment of channel and outside-component cells in order to comply with this rule. In general, however, the restriction is reasonable, since channels are always noded much finer than the surrounding bypass region. Figure 2.2-18 shows several fluid cells (both CHAN and outside component) and associated wall heat transfer nodes (both fine and coarse mesh).

A variable X_f has been defined for each wall node that is the fraction of the node that transfers heat to the lowest outer cell which it overlaps. Referring to Figure 2.2-18, we have

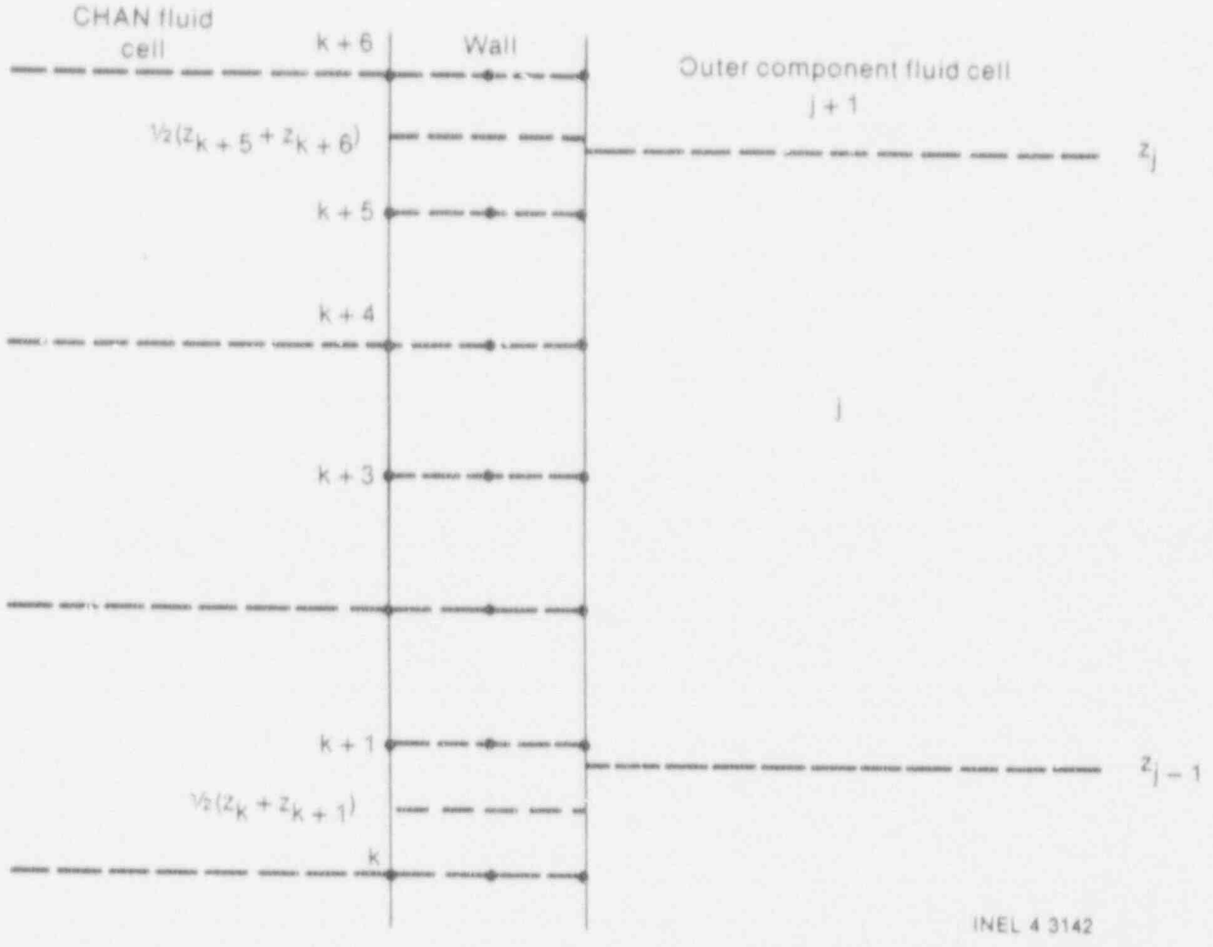

Figure 2.2-18. CHAN wall fine mesh nodalization scheme and relationship to adjacent fluid cells.

$$(Xf)_{k+1} = \frac{z_{j-1} - \frac{1}{2}(z_k + z_{k+1})}{\frac{1}{2}(z_{k+2} - z_k)} \qquad (2.2\text{-}117)$$

$$(Xf)_{k+2} = 1 \qquad (2.2\text{-}118)$$

$$(Xf)_{k+3} = 1 \qquad (2.2\text{-}119)$$

$$(Xf)_{k+4} = 1 \qquad (2.2\text{-}120)$$

$$(Xf)_{k+5} = \frac{z_j - \frac{1}{2}(z_{k+5} + z_{k+6})}{\frac{1}{2}(z_{k+6} - z_{k+4})} \qquad (2.2\text{-}121)$$

Previous code versions contained variables (KRVC and KLVC) defined on the fine-mesh nodes that stored the outer component cell number that most overlapped the wall node. These variables now store the *lowest* outer component cell that the node overlaps. Combined with X_f and the rule that only two cells may overlap a node, the fraction of each node in contact with each cell is completely defined. However, since this model can add and delete fine-mesh nodes according to the wall temperature profile, these two values need to be redefined each time node spacing is altered. A flow chart indicating the logic used for different situations when a node is added is given in Figure 2.2-19. A similar chart for the deletion of a node is given in Figure 2.2-20. The variable $\ell_{f,k}$ used in these flow charts refers to the lowest outer component cell (or level, in a vessel) in thermal contact with Node k. When a vessel (or other outer component) cell boundary is near the added or deleted node, the boundary location is determined using the previous X_f's and ℓ_f's, and this information is combined with the new H.T. node boundary elevation to calculate the new X_f's and ℓ_f's using Equations (2.2-117) through (2.2-121).

In previous versions of TRAC-BF1/MOD1, quench fronts were tracked only on the rods and inside surface of the CHAN wall using explicit quench front velocity correlations. The present model tracks quench fronts (both falling film and bottom flood) on the outside of the CHAN wall as well. The explicit quench front velocity correlations have been abandoned, and the presence of a liquid film is inferred from the code-calculated heat transfer mode. The actual quench front locations are taken to be the uppermost (or lowermost, for a falling film quench front) continuously wetted node, starting at the end of the heated section (or CHAN wall).

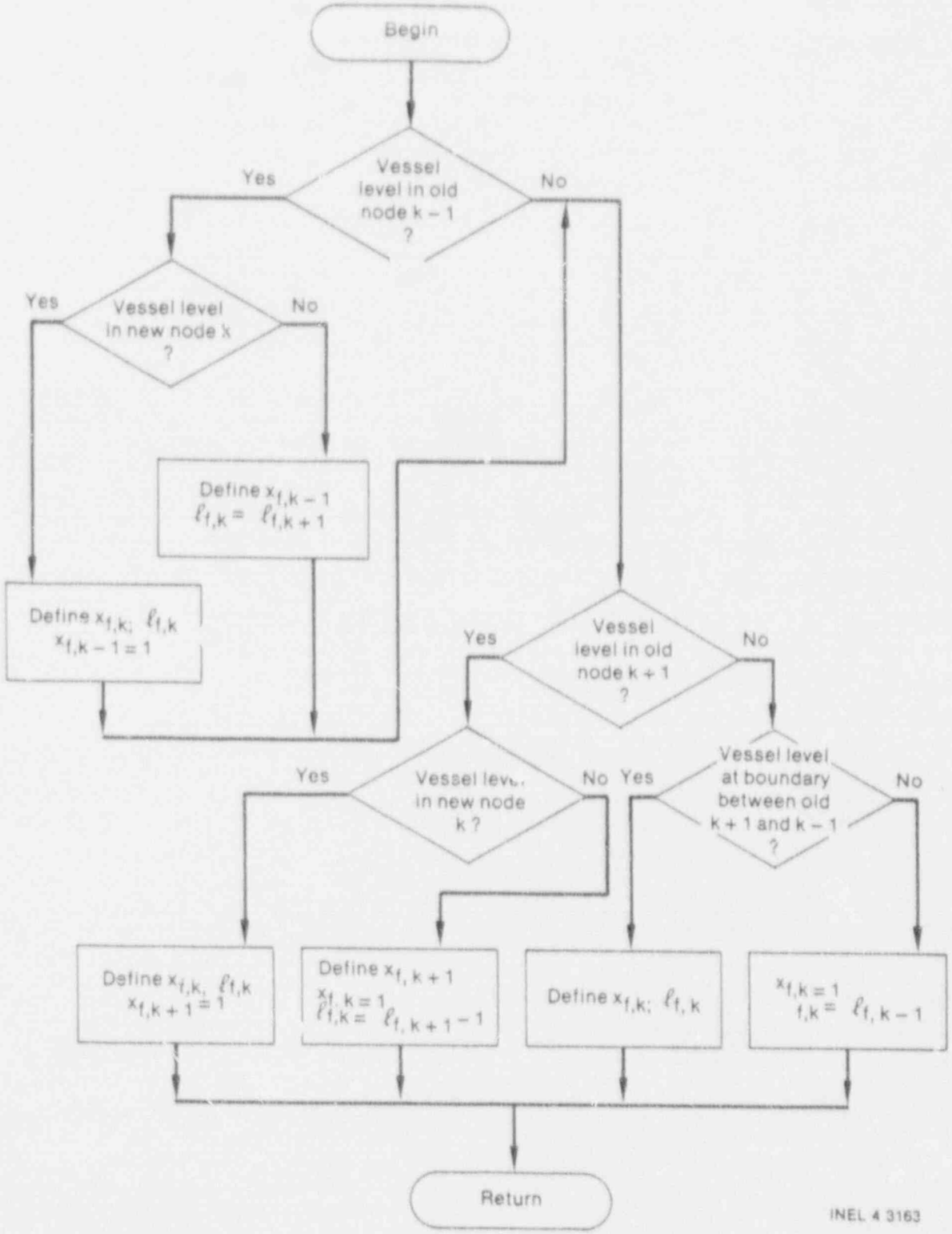

Figure 2.2-19. Logic for addition of a fine-mesh channel wall node and redefinition of node overlap parameters.

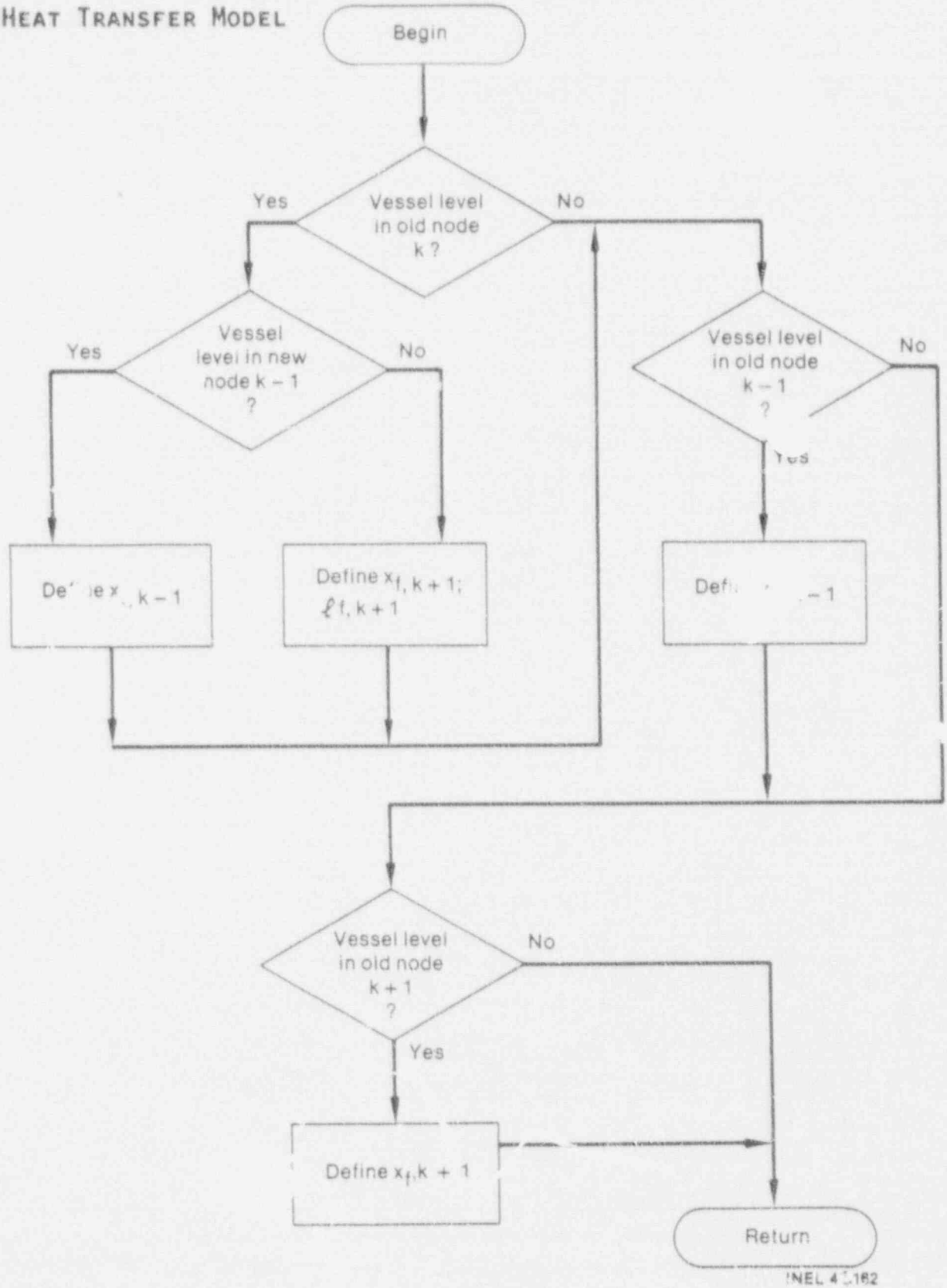

Figure 2.2-20. Logic for removal of a fine-mesh channel wall node and redefinition of node overlap parameters.

2.2.5 References

2.2-1. J. A. Borkowski and N. L. Wade, Eds., *TRAC-BF1/MOD1 Models and Correlations*, NUREG/CR-4391, EGG-2680, August 1992.

2.2-2. P. J. Roache, *Computational Fluid Dynamics*, Albuquerque: Hemosa Publishers, 1972.

2.2-3. J. Spore et al., *TRAC-BD1: An Advanced Best Estimate Computer Program for Boiling Water Reactor Loss-of-Coolant Analysis*, NUREG/CR-2178, October 1981.

2.2-4. Los Alamos National Laboratory Safety Code Development Group, *TRAC-PD2, An Advanced Best Estimate Computer Program for Pressurized Water Reactor Loss-of-Coolant Accident Analysis*, NUREG/CR-2054, LA-8709-MS, April 1981.

2.2-5. J. V. Cathcart, *Quarterly Progress Report on the Zirconium Metal-Water Oxidation Kinetics Program*, ORNL/NUREG/TM-41, August 1976.

2.2-6. *RELAP4/MOD5: A Computer Program for Transient Thermal-Hydraulic Analysis of Nuclear Reactors and Related Systems, Volume 1*, ANCR-NUREG-1335, September 1976,

2.2-7. F. Kreith, *Principles of Heat Transfer*, International Textbook Company, 1973, p. 442.

2.2-8. F. W. Dittus and L. K. Boelter, "Heat Transfer in Automobile Radiators of Tubular Type," *Publications in Engineering*, University of California, Berkeley, CA, 1930, pp. 443-461.

2.2-9. W. H. McAdams, *Heat Transmission*, Third Edition, New York: McGraw-Hill Book Company, Inc., 1954.

2.2-10. V. P. Isachenko, "Heat Transfer in Condensation in Turbulent Jets," *Teploenergetika, 2*, 1976, pp. 7-10.

2.2-11. W. M. Rohsenow and H. Y. Choi, *Heat, Mass, and Momentum Transfer*, Englewood Cliffs: Prentice-Hall, Inc., 1961.

2.2-12. J. Chen, "A Correlation for Boiling Heat Transfer of Saturated Fluids in Convective Flow," *ASME paper 63-HT-34*, 1963.

2.2-13. T. A. Bjornard and P. Griffith, "PWR Blowdown Heat Transfer," *Thermal and Hydraulic Aspects of Nuclear Reactor Safety, 1*, New York: ASMT, 1977, pp. 17-41.

2.2-14. R. T. Lahey, "A Mechanistic Subcooled Boiling Model," *Proceedings of the Sixth International Heat Transfer Conference, 1, Toronto, Canada, 1978*, pp. 293-295.

2.2-15. P. Saha and N. Zuber, "Point of Net Vapor Generation and Vapor Void Fraction in Subcooled Boiling," *Proceedings of the Fifth International Heat Transfer Conference, 4, 1974.*

2.2-16. L. A. Bromley, "Heat Trasnfer in Stable Film Boiling," *Chemical Engineering Progress, 46,* May 1950, pp. 221-227.

2.2-17. S. S. Kutateladze, "Heat Transfer During Film Boiling," *Heat Transfer in Condensation and Boiling,* AEC-TR-3770, 1952.

2.2-18. R. S. Dougall and W. M. Rohsenow, *Film Boiling on the Inside of Vertical Tubes with Upward Flow of the Fluid at Low Qualities,* Massachusetts Institute of Technology, Mechanical Engineering, 9079-26, 1963.

2.2-19. G. G. Loomis and R. W. Shumway, "Transition Boiling Heat Transfer in the Semiscale Mod-3 Core During Reflood," *Nuclear Technology, 56,* 3, March 1982, p. 426.

2.2-20. D. Q. Kern, *Process Heat Transfer,* New York: McGraw-Hill Book Company, Inc., 1950.

2.2-21. T. Fujii, H. Vehara, and C. Kurato, "Laminar Filmwise Condensation of Flowing Vapour on a Horizontal Cylinder," *International Journal of Heat and Mass Transactions, 14,* Great Britain: Pergamon Press, 1972, pp. 235-246.

2.2-22. M. M. Chen, "An Analytical Study of Laminar Film Condensation: Part 1--Flat Plates," *Transactions of the ASME,* February 1961, p. 48.

2.2-23. R. E. Phillips, R. W. Shumway, and K. H. Chu, "Improvements to the Prediction of Boiling Transition in BWR Transient Calculations," *Proceedings of the 20th ASME/AIChE National Heat Transfer Conference, Milwaukee, WI, August 2-5, 1981.*

2.2-24. R. T. Lahey, Jr., and F. Moody, *The Thermal Hydraulics of a Boiling Water Nuclear Reactor,* ANS, 1977.

2.2-25. L. Biasi et al., "Studies on Burnout: Part 3," *Energia Nucleare, 14,* 1967, pp. 530-536.

2.2-26. N. Zuber, M. Tribus, and J. W. Westwater, "The Hydrodynamic Crisis in Pool Boiling of Saturated and Subcooled Liquids, *International Developments in Heat Transfer,* 2, 1961, pp. 230-236.

2.2-27. F. B. Hildebrand, *Introduction to Numerical Analysis,* New York: McGraw-Hill Book Company, Inc., 1972.

2.2-28. R. W. Shumway, "Return to Nucleate Boiling," *Proceedings of the American Nuclear Society National Heat Transfer Conference, Denver, CO, August 1985.*

2.2-29. R. Siegel and J. R. Howell, *Thermal Radiation Heat Transfer*, New York: McGraw-Hill Book Company, Inc., 1972.

2.2-30. J. G. M. Andersen et al., *NORCOOL1, A Model for Analysis of a BWR Under LOCA Conditions*, NORHAV-D-47, August 1977.

2.2-31. M. M. Giles, "A Radiation to Steam Model for Reactor Core Thermal Analysis," *ANS Transactions, Sun Valley, ID, 1977.*

2.2-32. D. A. Mandell, *A Radiative Heat Transfer Model for the TRAC Code*, NUREG/CR-0994, LA-7965-MS, November 1979.

2.2-33. G. E. McCreery and C. E. Hendrix, "RELAP4/MOD7, Version 1 BWR Spray Cooling Calculations Compared with Data," *ANS Transactions, San Diego, CA, June 1978.*

2.2-34. K. H. Sun et al., "Calculations of Combined Radiation and Convection Heat Transfer in Rod Bundles Under Emergency Cooling Conditions," *Journal of Heat Transfer*, August 197., p. 414.

2.2-35. E. M. Sparrow and R. P. Cess, *Radiation Heat Transfer*, Monterey: Brooks/Cole Publishing Company, 1967.

2.2-36. H. C. Hottel and A. F. Sarofim, *Radiative Heat Transfer*, New York: McGraw-Hill Book Company, Inc., 1967.

2.2-37. J. G. M. Andersen and C. L. Tien, "Radiation Heat Transfer in a BWR Fuel Bundle Under LOCA Conditions," *ASME Winter Meeting, New York, New York, December 2-7, 1979*, ASME 79-WA/XX-00.

2.2-38. C. L. Tien et al., "Surface Radiation Exchange in Rod Bundles," *Transactions of the ASME, 101*, 1979, p. 378.

2.3 NUMERICAL MODEL

In TRAC-BF1/MOD1, a semi-implicit finite difference scheme is used in both the one- and three-dimensional flow components. The normal stability limit for this numerical scheme is

$$\Delta t < Min\left[\frac{Vol}{|V|A}, \frac{\Delta x}{|V|}\right] . \qquad (2.3\text{-}1)$$

However, TRAC-BF1/MOD1 employs a Courant-limit-violating numerical scheme in its one-dimensional flow components, which allows the Courant limit to be exceeded.

2.3.1 Courant-Limit-Violating Numerics in One-Dimensional Components

Two Courant-limit-violating numerical methods have been developed for TRAC-BF1/MOD1 by Los Alamos National Laboratory[2.3-1] and the General Electric Company (GE).[2.3-2] These two methods differ substantially in the way in which they satisfy the two requirements for a Courant-limit-violating numerical method. An evaluation of the two methods was performed at the INEL, and the recommendation was made to implement a hybrid Courant-limit-violating numerical method employing the best features of both of these previously developed numerical techniques. This hybrid technique employs the GE method of stabilizing the momentum equation and the LANL method of conserving mass and energy when violating the Courant limit. The hybrid numerical method will be discussed in the next sections.

The hybrid Courant-limit-violating numerical method as implemented in TRAC-BF1/MOD1 utilizes the GE method of stabilizing the momentum equation and the LANL method of conserving mass and energy. The basis of the method is to modify the momentum equation in the existing semi-implicit solution algorithm so that it is stable for time steps greater than the Courant limit. This allows larger time steps to be taken, but mass and energy are not conserved if the material Courant limit has been violated. Using the results of this step, the mass and energy equations are solved a second time to conserve mass and energy. Thus, the hybrid technique consists of two steps, the first being a modification of the existing numerical procedure in TRAC-BF1/MOD1 and the second being a mass and energy conserving step. These two steps will be discussed separately, after the existing solution procedure is outlined.

2.3.1.1 Original (TRAC-BD1) Numerical Procedure. The two-fluid conservation equations consisting of mass, thermal energy and momentum equations are solved in finite-difference form on a staggered mesh. The independent variables are the total pressure, void fraction, vapor temperature, and liquid temperature and are defined at cell centers (whole number subscript j+1, etc.) and the liquid and vapor velocities are defined on the cell edges (half-integer subscript j+1/2, j-1/2, etc.).

The semi-implicit numerical integration technique uses a mixture of beginning of time step and end of time step values to solve the conservation equations. The mass equations are given by

$$\frac{\alpha_{k,j}^{n+1}\rho_{k,j}^{n+1} - \alpha_{k,j}^{n}\rho_{k,j}^{n}}{\Delta t} - \frac{1}{Vol_j}\left[\chi_{k,j+1/2}^{n} V_{k,j+1/2}^{n+1} A_{j+1/2} + \chi_{k,j-1/2}^{n} V_{k,j-1/2}^{n+1} A_{j-1/2}\right]$$

$$= \Gamma_k^{n+1} \; ; \; k = f, g \tag{2.3-2}$$

where $\alpha_f + \alpha_g = 1$ and

$$\chi_{k,j+1/2}^{n} = \begin{cases} \alpha_{k,j}^{n}\rho_{k,j}^{n}; & V_{k,j+1/2}^{n} \geq 0 \\ \alpha_{k,j+1}^{n}\rho_{k,j+1}^{n}; & V_{k,j+1/2}^{n} < 0 \end{cases} \tag{2.3-3}$$

$$\chi_{k,j-1/2}^{n} = \begin{cases} \alpha_{k,j-1}^{n}\rho_{k,j-1}^{n}; & V_{k,j-1/2}^{n} \geq 0 \\ \alpha_{k,j}^{n}\rho_{k,j}^{n}; & V_{k,j-1/2}^{n} < 0 \end{cases} \tag{2.3-4}$$

where

α	=	void fraction
ρ	=	density
V	=	velocity
A	=	area
Δt	=	time step
Γ	=	mass source per unit volume per unit time
Vol	=	volume of cell
k	=	f for liquid and g for vapor
n	=	beginning of time step
n+1	=	end of time step
i, j+1, j-1	=	cell center

$j\pm1/2$ = cell edge.

The phasic momentum equations are given by

$$\frac{V^{n+1}_{k,j+1/2} - V^{n}_{k,j+1/2}}{\Delta t} + V^{n}_{k,j+1/2} \nabla V^{n}_{k,j+1/2} = - \frac{1}{\bar{\rho}^{n}_{k,j+1/2}} \frac{P^{n+1}_{j+1} - P^{n+1}_{j}}{\Delta X_{j+1/2}}$$

$$+ g \cos\theta - F^{n+1}_{i_{k,j+1/2}} - F^{n+1}_{w_{k,j+1/2}} - F^{n+1}_{vm_{k,j+1/2}} \qquad (2.3\text{-}5)$$

$$\nabla V^{n}_{k,j+1/2} = \begin{cases} \dfrac{V^{n}_{k,j+1/2} - V^{n}_{k,j-1/2}}{\Delta X_{j}}; & V^{n}_{k,j+1/2} \geq 0 \\ \dfrac{V^{n}_{k,j+3/2} - V^{n}_{k,j+1/2}}{\Delta X_{j+1}}; & V^{n}_{k,j+1/2} < 0 \end{cases} \qquad (2.3\text{-}6)$$

where

ρ = average density

Δx = distance

Δt = time step

F_i = interfacial force per unit volume

F_w = wall force per unit volume

F_{vm} = virtual mass force per unit volume.

The energy equations have been omitted here, as they parallel the mass equations. However, all equations for the one-dimensional components are given in full detail as coded in Sections 2.1.7 through 2.1.15 of the models and correlations document associated with this code manual.[2.3-3]

2.3.1.2 Modified Basic Step. The existing semi-implicit numerical algorithm is called the basic step in the Courant violating numerical procedure and is modified to make it stable for time steps exceeding the material Courant limit. The essential modification is to change the velocity divergence term in the momentum equation to make it more implicit, since it is the completely explicit nature of this term that creates the material Courant limitation. This term, as modified by GE, becomes

$$\nabla V^{n}_{k,j+1/2} = \begin{cases} \dfrac{\bar{V}^{n+1}_{k,j+1/2} - V^{n}_{k,j+1/2}}{\Delta X_j}; & V^{n}_{k,j+1/2} \geq 0 \\ \dfrac{V^{n}_{k,j+3/2} - \bar{V}^{n+1}_{k,j+1/2}}{\Delta X_{j+1}}; & V^{n}_{k,j+1/2} < 0 \end{cases} \tag{2.3-7}$$

where the cell edge velocity denoted by the overbar in the velocity difference has been made implicit. This modification is sufficient to allow time steps beyond the material Courant limit. A second modification is made to the flux terms in the mass and energy equations to make them implicit in the "within cell" quantities.

$$X^{n}_{k,j+1/2} = \begin{cases} \alpha^{n+1}_{k,j}\rho^{n+1}_{k,j}; & V^{n}_{k,j+1/2} \geq 0 \\ \alpha^{n}_{k,j+1}\rho^{n}_{k,j+1}; & V^{n}_{k,j+1/2} < 0 \end{cases} \tag{2.3-8}$$

$$X^{n}_{k,j-1/2} = \begin{cases} \alpha^{n}_{k,j-1}\rho^{n}_{k,j-1}; & V^{n}_{k,j-1/2} \geq 0 \\ \alpha^{n+1}_{k,j}\rho^{n+1}_{k,j}; & V^{n}_{k,j-1/2} < 0 \end{cases} \tag{2.3-9}$$

2.3.1.3 **Mass and Energy Stabilizer Step.** The second step in the hybrid Courant violating numerical procedure is the mass and energy conserving step. The mass stabilizer equations are

$$\frac{\alpha\rho^{n+1}_{k,j} - \alpha\rho^{n}_{k,j}}{\Delta t} + \frac{1}{Vol_j}\left[X^{n+1}_{k,j+1/2}V^{n+1}_{k,j+1/2}A_{j+1/2} + X^{n+1}_{k,j-1/2}V^{n+1}_{k,j-1/2}A_{j-1/2}\right] = \Gamma^{n+1}_{k} \tag{2.3-10}$$

where

$$X^{n+1}_{k,j+1/2} = \begin{cases} \alpha\rho^{n+1}_{k,j}; & V^{n+1}_{k,j+1/2} \geq 0 \\ \alpha\rho^{n+1}_{k,j+1}; & V^{n+1}_{k,j+1/2} < 0 \end{cases} \tag{2.3-11}$$

$$X^{n+1}_{k,j-1/2} = \begin{cases} \alpha\rho^{n+1}_{k,j-1}; & V^{n+1}_{k,j-1/2} \geq 0 \\ \alpha\rho^{n+1}_{k,j}; & V^{n+1}_{k,j-1/2} < 0 \end{cases} \tag{2.3-12}$$

and the independent variables are the macroscopic phasic densities which are the product of the phasic void fraction and phasic density. The phasic velocities in the flux terms are taken from the results of the basic step.

If the mass equation for the basic step is subtracted from the mass stabilizer equation, the phasic mass source disappears. The difference equation that results is in terms of beginning and end of time step macroscopic phasic density and the beginning of time step phasic void fraction and phasic density. These equations for each cell form a tridiagonal system of equations in the macroscopic phasic density, which is solved for the new time macroscopic phasic densities. The two phasic energy equations are solved for the macroscopic phasic internal energies $(\alpha_k \rho_k e_k)^{n+1}$ in the same way. The phasic void fraction is obtained by linearizing the phasic macroscopic densities and internal energies in terms of the total pressure and phasic temperature obtained from the basic step and solving for the phasic void fraction. This process does not conserve mass and energy exactly, because the results of the basic step were used to eliminate the phasic mass and energy source terms. If the basic step were solved exactly (i.e., convergence criteria ϵ in basic step = 0 to machine precision), this procedure would conserve mass and energy exactly. The degree of mass and energy conservation therefore depends upon the convergence of the basic step and can be controlled by the user through the convergence criterion for the basic step.

2.3.2 Three-Dimensional Conventional Numerics

The Courant-limit-violating numerics have not yet been implemented in three-dimensional components. The numerical solution still follows the original formulation. However, for three-dimensional flow, the formulation of $\bar{V}\cdot\nabla\bar{V}$ requires some additional notation. The three vector components of $\bar{V}\cdot\nabla\bar{V}$ can be written in cylindrical coordinates as

$$(\bar{V}\cdot\nabla\bar{V})_r = V_r\frac{\partial V_r}{\partial r} + \frac{V_\theta}{r}\frac{\partial V_r}{\partial \theta} - \frac{V_\theta^2}{r} + V_z\frac{\partial V_r}{\partial z} \tag{2.3-13}$$

$$(\bar{V}\cdot\nabla\bar{V})_\theta = V_r\frac{\partial V_\theta}{\partial r} + \frac{V_\theta}{r}\frac{\partial V_\theta}{\partial \theta} + \frac{V_r V_\theta}{r} + V_z\frac{\partial V_\theta}{\partial z} \tag{2.3-14}$$

$$(\bar{V}\cdot\nabla\bar{V})_z = V_r\frac{\partial V_z}{\partial r} + \frac{V_\theta}{r}\frac{\partial V_z}{\partial \theta} + V_z\frac{\partial V_z}{\partial z}\ . \tag{2.3-15}$$

These equations apply for either phase. The finite difference approximation for the z component of $\bar{V}\cdot\nabla\bar{V}$ is given by

$$\left[(\bar{V}\cdot\nabla\bar{V})_z\right]_{i,j,k+1/2} = \frac{(V_r\delta_r V_z)_{i,j,k+1/2}}{\Delta r} + \frac{(V_\theta\delta_\theta V_z)_{i,j,k+1/2}}{r\Delta\theta} + \frac{(V_z\delta_z V_z)_{i,j,k+1/2}}{\Delta z} \tag{2.3-16}$$

where the notation, $(V_r\delta_r V_z)_{i,j,k+1/2}$ implies a donor cell difference in the r

direction about i,j,k+1/2 based on the sign of $V_{r_{i,j,k+1/2}}$. The above donor cell differences are

$$(V_r\delta_r V_z)_{i,j,k+1/2} = \begin{cases} V_{r_{i,j,k+1/2}}\left(V_{z_{i,j,k+1/2}} - V_{z_{i-1,j,k+1/2}}\right) \text{ for } V_{r_{i,j,k+1/2}} \geq 0 \\ V_{r_{i,j,k+1/2}}\left(V_{z_{i+1,j,k+1/2}} - V_{z_{i,j,k+1/2}}\right) \text{ for } V_{r_{i,j,k+1/2}} < 0 \end{cases} \quad (2.3\text{-}17)$$

$$(V_\theta\delta_\theta V_z)_{i,j,k+1/2} = \begin{cases} V_{\theta_{i,j,k+1/2}}\left(V_{z_{i,j,k+1/2}} - V_{z_{i,j-1,k+1/2}}\right) \text{ for } V_{\theta_{i,j,k+1/2}} \geq 0 \\ V_{\theta_{i,j,k+1/2}}\left(V_{z_{i,j+1,k+1/2}} - V_{z_{i,j,k+1/2}}\right) \text{ for } V_{\theta_{k,j,k+1/2}} < 0 \end{cases} \quad (2.3\text{-}18)$$

$$(V_z\delta_z V_z)_{i,j,k+1/2} = \begin{cases} V_{z_{i,j,k+1/2}}\left(V_{z_{i,j,k+1/2}} - V_{z_{i,j,k-1/2}}\right) \text{ for } V_{z_{i,j,k+1/2}} \geq 0 \\ V_{z_{i,j,k+1/2}}\left(V_{z_{i,j,k+3/2}} - V_{z_{i,j,k+1/2}}\right) \text{ for } V_{z_{i,j,k+1/2}} < 0 \end{cases} \quad (2.3\text{-}19)$$

The velocities in TRAC-BF1/MOD1 three-dimensional mesh space are defined as normal to the face. Therefore, the axial velocity on an axial cell face is defined ($V_{z_{i,j,k+1/2}}$) and saved from time step to time step. However, velocities that are not normal to the face must be estimated. For example, $V_{r_{i,j,k+1/2}}$ and $V_{\theta_{i,j,k+1/2}}$ are estimated by the averaging technique

$$V_{r_{i,j,k+1/2}} = \frac{1}{4}\left(V_{r_{i+1/2,j,k}} + V_{r_{i-1/2,j,k}} + V_{r_{i+1/2,j,k+1}} + V_{r_{i-1/2,j,k+1}}\right) . \quad (2.3\text{-}20)$$

For the three-dimensional components, the complete as-coded finite-difference equations are provided in Reference 3, Sections 2.1.16 through 2.1.30.

2.3.3 Solution Method

The overall solution strategy is described first, then details of the solution method are presented.

2.3.3.1 Outer Iteration Strategy. Solution of the thermal-hydraulic equations for all components is controlled by Subroutines TRANS, PREP, OUTER, and POST. Subroutine TRANS controls the overall strategy, whereas the others call each component in turn.

At least four computational passes are made through each component. An initial pass is made to update certain explicit information that must be available before performing the hydrodynamics calculation. This is done by a call to PREP. The heat-transfer coefficients and relative velocities are examples of information calculated on the first pass. The next two or more passes call the basic hydrodynamic routines until a solution is found within

the convergence criterion or the maximum number of iterations is exceeded. This stage of the calculation is done by a call to OUTER, which performs both a forward elimination and a backward substitution pass. The recommended convergence criterion (EPSO) is 10^{-3}, and the maximum outer iteration count (OUTMAX) generally should range between 6 and 10. The order in which OUTER calls the given components is determined by the IORDER array that is set after input by SRTLP.

If the outer iteration process converges, a final pass is made by Subroutine POST to update the wall, slab, or rod heat conduction and to generate the information required to begin the next time step. If the outer iteration fails to converge, the time step size is halved (subject to the constraint that Δt must be greater than or equal to the minimum time step size indicated in the input); then, another attempt to converge the outer iteration cycle begins. After six unsuccessful attempts, the code shuts down after producing a dump and edit.

2.3.3.2 Details of the Solution Method. The solution procedure begins by successive processing of all one-dimensional components in subroutine TF1D, which, in turn, calls TF1E, TF1I, and FF1D. For each such component, processing begins by solution of the vapor and liquid equations of motion in Subsection 2.3.1 at each junction within the components. This yields

$$\tilde{V}_{g,j+1/2},\ \tilde{V}_{\ell,j+1/2},\ DVV_{j+1/2},\ \text{and}\ DVL_{j+1/2}$$

where

$$V^{n+1}_{g,j+1/2} = \tilde{V}_{g,j+1/2} + DVV_{j+1/2}\delta(P_{j+1} - P_j) \tag{2.3-21}$$

$$V^{n+1}_{\ell,j+1/2} = \tilde{V}^{n+1}_{\ell,j+1/2} + DVL_{j+1/2}\delta(P_{j+1} - P_j) \tag{2.3-22}$$

where the notation δF indicates temporal variation in F during a time step. Next, the finite difference forms of the mass and energy equations for each hydrodynamic cell within the component are linearized in terms of δP_j, $\delta\alpha_j$, δT_{vj}, $\delta T_{\ell j}$ and the new time phase velocities

$$V^{n+1}_{g,j+1/2},\ V^{n+1}_{g,j-1/2},\ V^{n+1}_{\ell,j+1/2},\ \text{and}\ V^{n+1}_{\ell,j-1/2}$$

at the cell boundaries. The set of linearized mass and energy equations for the component are next solved by substituting the above values for new time velocities to obtain the a_{ij}'s in the following equations:

$$\delta P_j = a_{1j} + a_{2j}\delta\Delta P_L + a_{3j}\delta\Delta P_R + a_{4j}\delta\Delta P_T \tag{2.3-23}$$

$$\delta\alpha_j = a_{5j} + a_{6j}\delta\Delta P_L + a_{7j}\delta\Delta P_R + a_{8j}\delta\Delta P_T \quad (2.3\text{-}24)$$

$$\delta T_{vj} = a_{9j} + a_{10j}\delta\Delta P_L + a_{11j}\delta\Delta P_R + a_{12j}\delta\Delta P_T \quad (2.3\text{-}25)$$

$$\delta T_{\ell j} = a_{13j} + a_{14j}\delta\Delta P_L + a_{15j}\delta\Delta P_R + a_{16j}\delta\Delta P_T \quad (2.3\text{-}26)$$

where

δP_j = temporal variation in pressure cell j

$\delta\alpha_j$ = temporal variation in void fraction in cell j

δT_{vj} = temporal variation in vapor temperature in cell j

$\delta T_{\ell j}$ = temporal variation in liquid temperature in cell j

$\delta\Delta P_L$ = temporal variation in the pressure difference at the left component junction

$\delta\Delta P_R$ = temporal variation in the pressure difference at the right component junction

$\delta\Delta P_T$ = temporal variation in the pressure difference at the tee component junction.

(See Steps 1 through 5 in Figure 2.3-1). All linear coefficients (a_{ij}, i = 1,16) are stored for later back-substitution.

After the linearized equations in all one-dimensional components have been solved in terms of the junction pressure differences, the following expression can be written at each component-to-component junction

$$\delta\Delta P_i = \delta P_- - \delta P_+ \quad (2.3\text{-}27)$$

where the subscript i indicates the junction number and δP_+ and δP_- are evaluated at the two adjacent cell centers. When δP_+ or δP_- are within one-dimensional components, Equation (2.3-23) is substituted for the appropriate cells into Equation (2.3-27) to eliminate δP_+ and δP_- in favor of junction pressure difference temporal variations, $\delta\Delta P_j$. If there are no three-dimensional components present in the calculation, a closed linear system of equations in the junction pressure difference variations ($\delta\Delta P_j$) is formed by these substitutions together with the boundary conditions. This system [Equation (2.3-28) below, with only the first vector on the R.H.S.] is

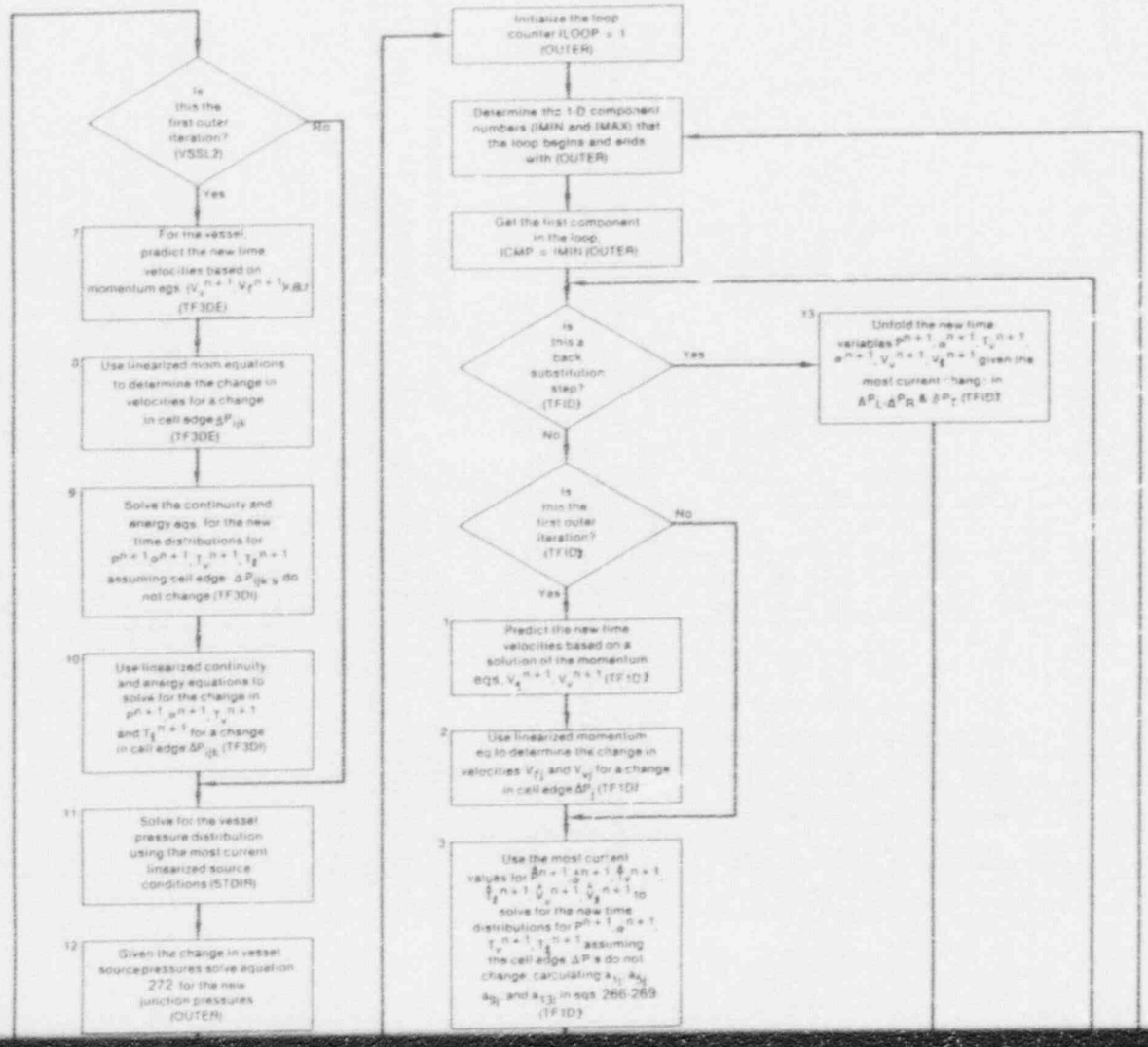
Initialize the loop counter (LOOP = 1 (OUTER)
Determine the 1-D component numbers (IMIN and IMAX) that the loop begins and ends with (OUTER)
Get the first component in the loop, (CMP = IMIN (OUTER)
Is this a back substitution step? (TF1D)
Yes
Unfold the new time variables $P^{n+1}, \alpha^{n+1}, T_v^{n+1}, \alpha^{n+1}, V_v^{n+1}, V_\ell^{n+1}$ given the most current changes in $\Delta P_L, \Delta P_R$ & ΔP_T (TF1D)
No
Is this the first outer iteration? (TF1D)
No
Yes
1 Predict the new time velocities based on a solution of the momentum eqs. V_ℓ^{n+1}, V_v^{n+1} (TF1D)
2 Use linearized momentum eq to determine the change in velocities $V_{\ell j}$ and V_{vj} for a change in cell edge ΔP_j (TF1D)
3 Use the most current values for $\beta^{n+1}, \alpha^{n+1}, \rho_\ell^{n+1}, \rho_v^{n+1}, \hat{V}_\ell^{n+1}, \hat{V}_v^{n+1}, \hat{V}_{vg}^{n+1}$ solve for the new time distributions for $P^{n+1}, \alpha^{n+1}, T_v^{n+1}, T_\ell^{n+1}$ assuming the cell edge ΔP's do not change, calculating a_{1j}, a_{2j}, a_{3j} and a_{13} in eqs. 266-269 (TF1D)
Is (this the first outer iteration? (VSSL2)
No
Yes
7 For the vessel, predict the new time velocities based on momentum eqs. $(V_v^{n+1}, V_\ell^{n+1})$ (TF3DE)
8 Use linearized mom equations to determine the change in velocities for a change in cell edge ΔP_{ijk} (TF3DE)
9 Solve the continuity and energy eqs. for the new time distributions for $P^{n+1}, \alpha^{n+1}, T_v^{n+1}, T_\ell^{n+1}$ assuming cell edge ΔP_{ijk}'s do not change (TF3DI)
10 Use linearized continuity and energy equations to solve for the change in $P^{n+1}, \alpha^{n+1}, T_v^{n+1}$ and T_ℓ^{n+1} for a change in cell edge ΔP_{ijk} (TF3DI)
11 Solve for the vessel pressure distribution using the most current linearized source conditions (STDIR)
12 Given the change in vessel source pressures solve equation 272 for the new junction pressures (OUTER)

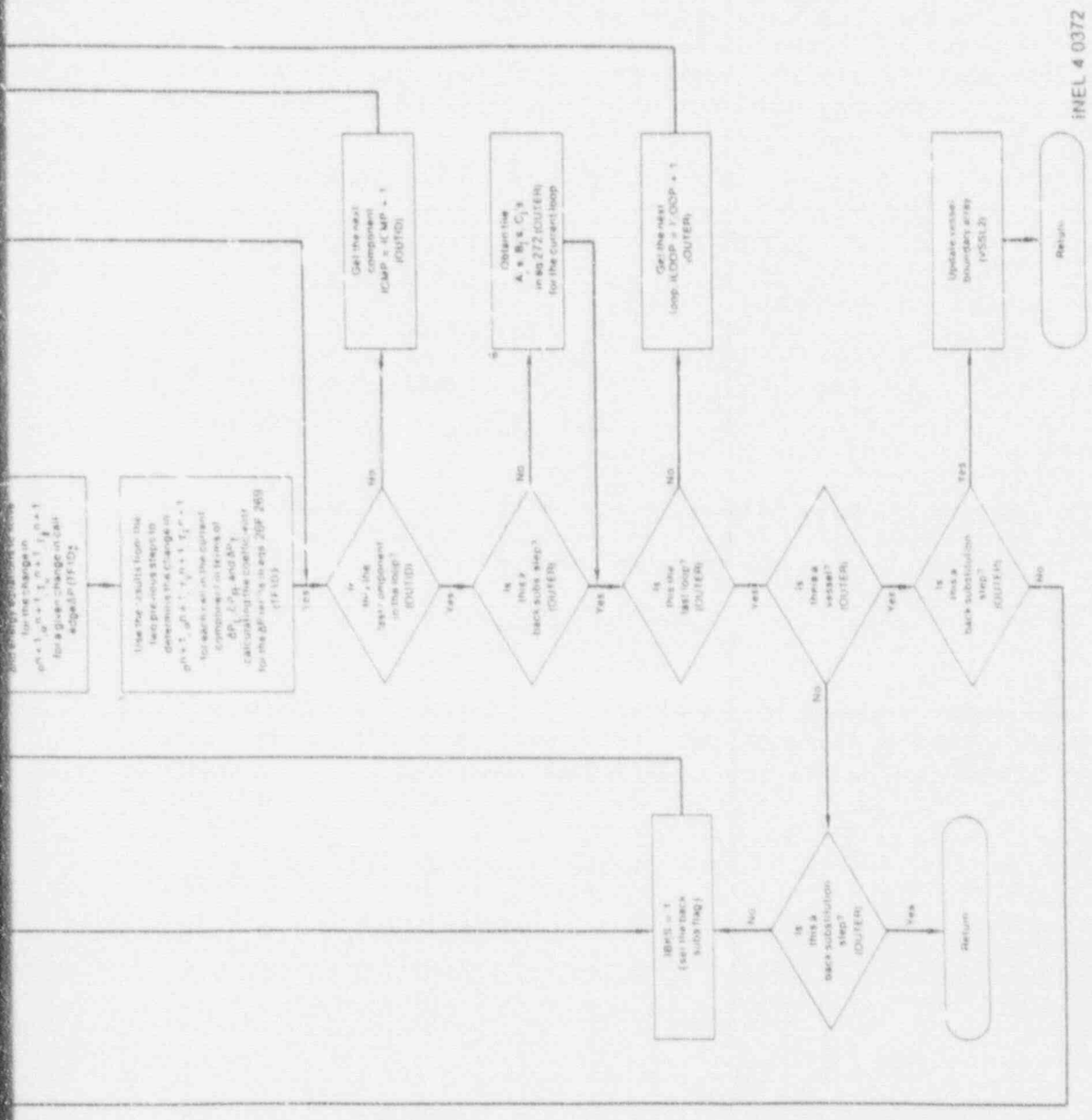

Figure 2.3-1. Logic chart for a single outer interatinn pass routine.

9209220469-01

then solved in OUTER by direct methods (Step 6 in Figure 2.3-1; the B_i's and C_i's are zero in this case). A back-substitution pass through all one-dimensional components then follows, in which the known $\delta\Delta P_i$ terms are used to obtain values for the remaining independent variables (see Step 13 in Figure 2.3-1) as prescribed by Equations (2.3-23) through (2.3-26).

When one or more three-dimensional components are present, the situation is slightly more complicated. For the network illustrated in Figure 2.3-2, a linear set of equations in $\delta\Delta P_i$ results after all possible substitutions are made as described above. The equations have the form

$$\begin{bmatrix} X & X & 0 & 0 & 0 & 0 \\ X & X & X & 0 & X & 0 \\ 0 & X & X & X & X & 0 \\ 0 & 0 & X & X & 0 & 0 \\ 0 & X & X & 0 & X & X \\ 0 & 0 & 0 & 0 & X & X \end{bmatrix} \begin{bmatrix} \delta\Delta P_1 \\ \delta\Delta P_2 \\ \delta\Delta P_3 \\ \delta\Delta P_4 \\ \delta\Delta P_5 \\ \delta\Delta P_6 \end{bmatrix} = \begin{bmatrix} X \\ X \\ X \\ X \\ X \\ X \end{bmatrix} + \begin{bmatrix} X \\ 0 \\ 0 \\ 0 \\ 0 \\ 0 \end{bmatrix} \delta P_{v1} + \begin{bmatrix} 0 \\ 0 \\ 0 \\ X \\ 0 \\ 0 \end{bmatrix} \delta P_{v4} \qquad (2.3\text{-}28)$$

where X indicates nonzero matrix and vector elements and δP_{v1} and δP_{v4} are the temporal pressure variations in the vessel cells adjacent to Junctions 1 and 4, respectively. This system is solved directly to obtain

$$\delta\Delta P_i = A_i + B_i \delta P_{v1} + C_i \delta P_{v4} \text{ for } i = 1,2,\ldots \qquad (2.3\text{-}29)$$

(see Step 6 in Figure 2.3-1). Treating the momentum, mass, and energy equations in the three-dimensional components in a similar manner as described above for one-dimensional components, a system of the following form is obtained:

$$\begin{bmatrix} X & X & \cdots & X \\ X & X & \cdots & \cdot \\ \cdot & & & \cdot \\ \cdot & & & \cdot \\ \cdot & & & \cdot \\ X & \cdots & & X \end{bmatrix} \begin{bmatrix} \delta P_{v1} \\ \cdot \\ \cdot \\ \cdot \\ \cdot \\ \delta P_{vN} \end{bmatrix} = \begin{bmatrix} X \\ X \\ \cdot \\ \cdot \\ \cdot \\ X \end{bmatrix} + \begin{bmatrix} X & X \\ X & X \\ \cdot & \cdot \\ \cdot & \cdot \\ \cdot & \cdot \\ X & X \end{bmatrix} \begin{bmatrix} \delta\Delta P_1 \\ \delta\Delta P_4 \end{bmatrix} \qquad (2.3\text{-}30)$$

where N is the number of cells in the vessel. This system of equations is now closed by substitution of Equation (2.3-29) for the junction pressure difference temporal variations ($\delta\Delta P_1$ and $\delta\Delta P_4$). The system is solved in one of two ways (see Steps 7 through 12 in Figure 2.3-1). If the input variable,

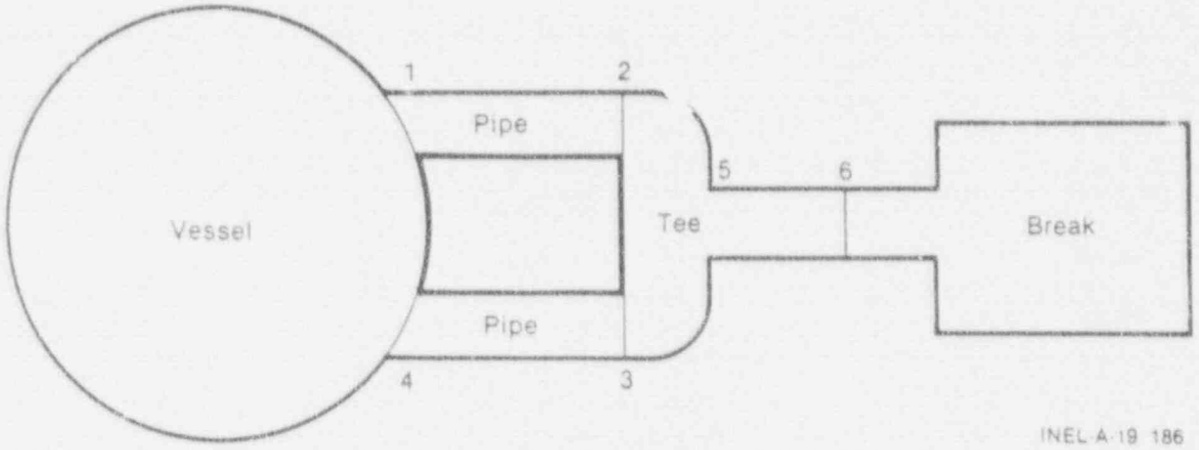

Figure 2.3-2. Component network with one three-dimensional vessel.

IITMAX, is set to zero, the system is solved directly using calls to Subroutines STDIR, SOLVE, and BACIT. If IITMAX >0, an iterative solution procedure is used. This iteration is a combination of a Gauss-Seidel and a coarse-mesh rebalance. The recommended convergence criterion for this iteration (EPSI) is 10^{-5}, and the maximum allowed number of iterations (IITMAX) is 30 to 50. Back-substitution through the one-dimensional components again completes the solution of the full linear system.

A complete pass through the outer iteration logic is illustrated in the logic chart given in Figure 2.3-1. The routine name performing the function described is also given. References are made to the coefficients given in the previous equations.

A single, complete pass through this solution procedure provides the solution for the linearized finite difference equations. Subsequent passes through the procedure for the same time step produce a Newton iteration on the nonlinear difference equations, with quadratic convergence.

2.3.4 Explicit Leak Path Model

The leak path concept is used in TRAC-BF1/MOD1 as a means of transferring mass and energy between components through an explicit flow path separate from the normal semi-implicit junction flow path. The use of such a fully explicit flow is helpful, since it reduces the complexity of the TRAC-BF1/MOD1 network and requires less execution time than the implicit coupling found in the normal TRAC-BF1/MOD1 solution method described in Subsection 2.3.2. The leak path concept is useful in situations where momentum transfer is not important and where flow instabilities due to the explicit nature of the leak path are not likely to occur. These criteria are satisfied for such cases as the small, transverse flow from a channel assembly into the surrounding core

bypass region and for feedwater flow between a FILL and the vessel downcomer.

The leak path concept includes flow between all one-dimensional and three-dimensional components (exclusive of the BREAK component). Each leak path connects two components, one designated the From component and the other designated the To component. These designations refer to a conventional flow direction and do not change if the actual flow direction reverses. Positive leak path flow implies flow from the From component to the To component. All leak path geometric data and connection data are input and stored as part of the From component data base. The geometric data include the leak path flow area, loss coefficient, and elevation difference, while the connection data include the From cell number, the To component number, the To cell number, and the To level number (used only if the To component is a VESSEL). All components except VESSEL and BREAK may be used as From components, and all components except BREAK may be used as To components. A given component may be used as the From component for only one leak path, but no restriction is placed on the number of leaks To a given component or cell within that component.

The concept of a *disconnected* FILL component is also included in this model to facilitate the use of FILL components as the From component of a leak path. A disconnected FILL is specified by an input junction number of zero and is not connected to any other component through a conventional junction. Flow from a disconnected FILL to a component takes place only through a leak path. The use of a disconnected FILL and associated leak path permits a reduction in the number of components in a TRAC-BF1/MOD1 model, since FILL components may be connected directly to a VESSEL cell or 1-D component cell through a leak path without the use of an intervening PIPE or TEE.

Leak path hydraulic data are stored and are available to all components. The donor cell fluid properties for the leak are loaded by Subroutine LEKLOD, which is called for each component during the initial pass phase of the TRAC-BF1/MOD1 calculation. This subroutine performs a search over all leak paths in the leak path array. If a given component connects to a leak path (either To or From) and if the previous time step leak velocity is consistent with the given component being a donor component, then fluid properties from the leak cell of the given component are loaded into the appropriate locations in the leak path array.

2.3.4.1 **Leak Path Velocity Calculation.** The explicit leak path mixture velocities are calculated by Subroutine CLEK. A schematic diagram of a leak path and its associated components is shown in Figure 2.3-3. In this figure,

A = leak path flow area

K = leak path form loss coefficient

V_m = mixture velocity of leak path flow

Q = mixture density

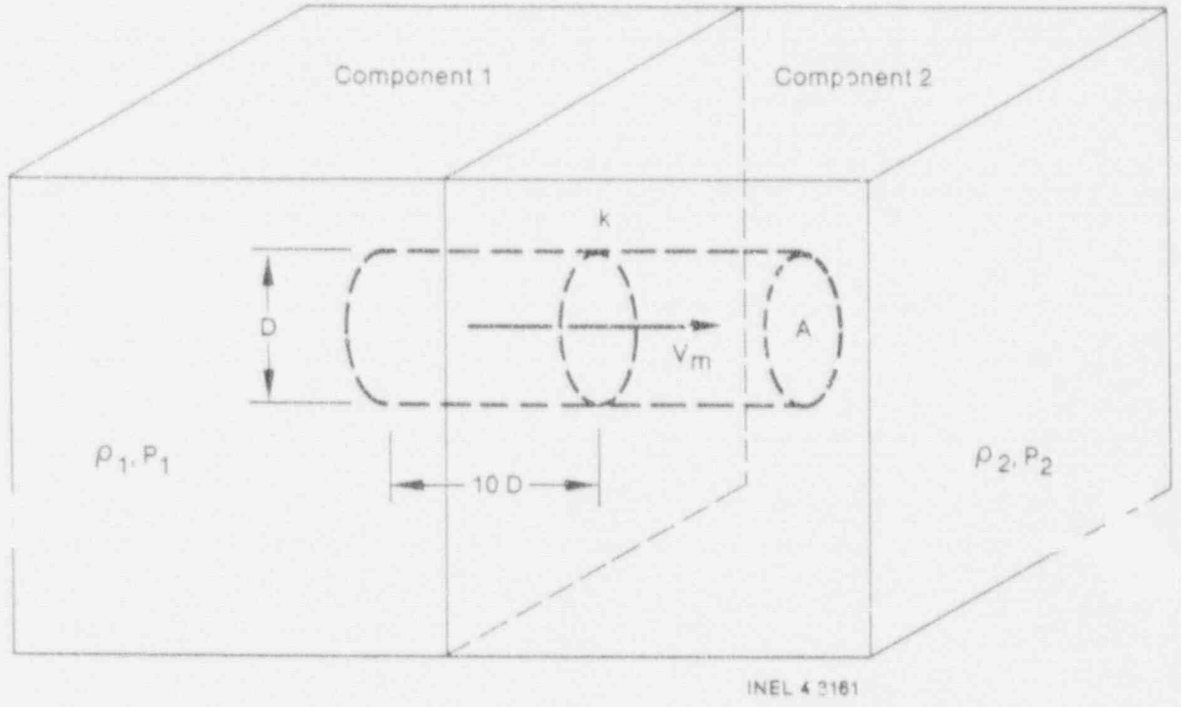

Figure 2.3-3. Leak path model.

P = pressure.

The effective mass m_{eff} of the fluid moving through the leak orifice is calculated by assuming that the moving fluid lies in a cylindrical jet whose length on each side of the orifice is ten times its diameter, or

$$m_{eff} = 10DA(\rho_1 + \rho_2) \tag{2.3-31}$$

where

$$D = \text{(effective orifice diameter)} = (4A/\pi)^{1/2} \tag{2.3-32}$$

The equation of motion for fluid in the leak path is then given by

$$A(P_1 - P_2) = m_{eff}\frac{dV_m}{dt} + \frac{1}{2}Ak\rho|V_m|V_m \tag{2.3-33}$$

where the two right side terms account for inertial and frictional effects, respectively.

Writing Equation (2.3-33) in semi-implicit finite difference form yields

$$\Delta P^n = \frac{m_{eff}\left(V_m^{n+1} - V_m^n\right)}{A\ \Delta t} + \frac{1}{2} k \rho |V_m^n| V_m^{n+1} \qquad (2.3\text{-}34)$$

where ρ is the donor cell fluid density determined by the sign of V_m^n.

Equation (2.3-34) is then readily solved for

V_m^{n+1}

yielding

$$V_m^{n+1} = \frac{\Delta P^n + \frac{m_{eff}}{A\Delta t} V_m^n}{\frac{m_{eff}}{A\Delta t} + \frac{1}{2} k \rho |V_m^n|} \qquad (2.3\text{-}35)$$

The numerator of Equation (2.3-33) determines the sign of V^{n+1} since the denominator of this equation is always positive. Hence, the sign of this numerator is used for determining the donor cell direction for ρ.

The calculated value of V_m^{n+1} is then used for calculating source terms for addition to the From and To component mass and energy equations. For both components, these source terms are of the form

$$S_{\ell m} = \rho_\ell (1 - \alpha) A_{tot} V_m^{n+1} \qquad (2.3\text{-}36)$$

$$S_{vm} = \rho_v \alpha\ A_{tot} V_m^{n+1} \qquad (2.3\text{-}37)$$

for the liquid and vapor mass source terms, and

$$S_{\ell e} = (e_\ell \rho_\ell + P)(1 - \alpha) A_{tot} V_m^{n+1} \qquad (2.3\text{-}38)$$

$$S_{ve} = (e_v \rho_v + P) \alpha\ A_{tot} V_m^{n+1} \qquad (2.3\text{-}39)$$

for the liquid and vapor energy source terms. In these source terms, ρ_ℓ and ρ_v are liquid and vapor densities, e_ℓ and e_v are the donor-celled liquid and vapor specific internal energies, and α is the donor-celled void fraction. These quantities are all donor celled according to the sign of the numerator of Equation (2.3-35). The pressure P used in these source terms is the donor

component pressure.

When the From or To component is a CHAN, A_{TOT} is the total leakage path flow area for all channel assemblies represented by the CHAN component. Since the leak path model assumes homogeneous flow, the leak path velocities for both liquid and vapor phases are the same as the mixture velocity.

If the From component of a leak path is a FILL, the leak path phasic velocities will not be calculated by Subroutine CLEK but will instead be set equal to the FILL phasic velocities, as determined by the normal FILL logic.

Leak path mass, energy, and noncondensable source terms are calculated by existing Subroutine MELK, which is called from the one- and three-dimensional hydrodynamic routines for each component cell connected to a leak path. Subroutine MELK calculates source terms for both To and From cells, with an algebraic sign adjustment to account for direction of leak flow. For example, if the current cell is a From cell for a leak path and if the leak path velocity is positive, then the mass and energy source terms for that cell will be negative. The source terms for the two cells connected by a leak path will be equal in magnitude and opposite in sign, thus assuring conservation of mass and energy. Subroutine MELK is also called during the TRAC-BF1/MOD1 postpass calculation to obtain leak path mass fluxes for use in the system mass balance calculation. Subroutine MBLK accounts for boron transfer through generalized leak paths.

2.3.5 Numerics of Flow Limit Models

The flow limit models are discussed in Subsection 2.1.3. The method for applying flow limit models is presented below.

The choked flow criteria described in Subsection 2.1.3.1 for two-phase, pure vapor, and pure liquid flow have been selected for modeling critical flow in TRAC-BF1/MOD1. These criteria establish the flow limitation to be imposed at user-specified cell boundaries within one-dimensional components. For the user-specified, one-dimensional cell boundary, the TRAC-BF1/MOD1 finite-difference equations are to be solved subject to the constraint

$$\frac{\alpha_g \rho_\ell V_g + \alpha_\ell \rho_g V_\ell}{\alpha_g \rho_\ell + \alpha_\ell \rho_g} \leq a_{HE} \ . \qquad (2.3\text{-}40)$$

The TRAC-BF1/MOD1 solution scheme for one-dimensional components consists of a forward elimination step, where explicit new-time velocities and velocity derivatives with respect to pressure are calculated, and a back-substitution step, where final new-time velocities are calculated after the outer iteration network solution has given a consistent set of boundary conditions between one- and three-dimensional components. Both steps are coded in Subroutines TF1E and CHOKE.

The method chosen to implement the critical flow constraint is consistent with existing TRAC-BF1/MOD1 numerics. Explicit new-time velocities and their derivatives are first calculated as if the flow was not choked. Then, these velocities are used to evaluate the inequality [Equation (2.3-40)]. If the flow is choked, Equation (2.3-40) is solved simultaneously with the assumption

$$s = \frac{(V_g)_{new}}{(V_\ell)_{new}} = \begin{cases} 1.0, \text{ if } 0 \le \alpha < 0.01 \text{ or} \\ \quad \text{if } 0.999999 < \alpha \le 1.0 \text{ or} \\ \quad\quad \text{if } \dfrac{(V_g)_{old}}{(V_\ell)_{old}} \ge 0 \\ \dfrac{(V_g)_{old}}{(V_\ell)_{old}}, \text{ if } 0.01 \le \alpha \le 0.999999 \text{ and} \\ \quad\quad \text{if } \dfrac{(V_g)_{old}}{V_\ell)_{old}} \ge 0 \end{cases} \tag{2.3-41}$$

To obtain the choked flow limited velocities, we have

$$\left.\begin{aligned} V_\ell &= [sign(V_\ell)]a_{HE} \\ V_g &= V_\ell \end{aligned}\right\} \text{ if } 0.0 \le \alpha < 0.01 \tag{2.3-42}$$

$$\left.\begin{aligned} V_\ell &= [sign(V_m)]\frac{\alpha_g\rho_\ell + \alpha_\ell\rho_g}{\alpha_g\rho_\ell s + \alpha_\ell\rho_g}a_{HE} \\ V_g &= sV_\ell \end{aligned}\right\} \text{ if } 0.01 \le \alpha \le 0.999999 \tag{2.3-43}$$

$$\left.\begin{aligned} V_g &= [sign(V_g)]a_{HE} \\ V_\ell &= V_g \end{aligned}\right\} \text{ if } 0.999999 < \alpha \le 1.0\ . \tag{2.3-44}$$

The velocity derivatives with respect to junction pressure difference are then calculated numerically by determining the change in the choked velocity resulting from a small pressure perturbation upstream of the choking point. This ensures compatibility with Equation (2.3-40) in the back-substitution step for sufficiently small pressure changes. The as-coded mathematical description is provided in Reference 3, Section 7.2.

A similar approach is used to implement the CCFL correlations given in Subsection 2.1.3.2. The new-time vapor and liquid velocities are computed from the phasic momentum equations. The computed liquid velocity is then compared with the flooded (maximum) liquid velocity computed by the flooding

correlation using the vapor velocity from the momentum solution

$$V_{\ell,max} = \frac{-[g\sigma(\rho_\ell - \rho_g)]^{1/4}}{m^2\alpha_\ell\sqrt{\rho_\ell}}\left(K^{1/2} - K_g^{1/2}\right)^2 . \qquad (2.3\text{-}45)$$

If the liquid velocity computed from the momentum solution exceeds the maximum liquid velocity computed using Equation (2.3-45), it is set equal to the maximum velocity; otherwise, it is not changed.

$$V_\ell = \begin{cases} V_\ell, & \text{if } V_\ell < V_{\ell,max} \\ V_{\ell,max}, & \text{if } V_\ell \geq V_{\ell,max} \end{cases} . \qquad (2.3\text{-}46)$$

If the liquid velocity is limited (reset to the maximum value), the derivative of the liquid velocity used during the implicit part of the momentum solution will also be altered. The new value of the derivative of the liquid velocity is found by differentiating Equation (2.3-45) with respect to pressure drop across the cell boundary

$$\frac{\partial V_\ell}{\partial(\Delta P)} = \frac{1}{m^2}\left\{\left[\frac{Kg\sigma(\rho_\ell - \rho_g)^{1/4}\alpha_g(\rho_g)^{1/2}}{\alpha_\ell^2\rho_\ell V_g}\right]^{1/2} - \frac{\alpha_g(\rho_g)^{1/2}}{\alpha_\ell(\rho_\ell)^{1/2}}\right\}\frac{\partial V_g}{\partial(\Delta P)} \qquad (2.3\text{-}47)$$

where $\partial V_g/\partial(\Delta P)$ is determined from the momentum equation for the vapor phase.

This procedure is illustrated in Figure 2.3-4. The Kutateladze numbers obtained from the explicit solution of the phasic momentum equations define a point $(K_{g1},K_{\ell 1})$ lying to the left of the correlation line. In this case, the liquid Kutateladze number is altered (decreased in magnitude) holding the vapor Kutateladze constant so that the solution point lies on the correlation line, point $(K_{g1},K'_{\ell 1})$. The liquid velocity is then recomputed using the new solution point [Equation (2.3-45)].

The derivative of the liquid velocity is also recomputed so that the solution point tracks along the correlation line during the implicit portion of the solution procedure. An ambiguity arises whenever the vapor Kutateladze number lies above the countercurrent flow cutoff point, solution point $(K_{g2},K_{\ell 2})$. The correlation states that countercurrent flow cannot exist for the vapor Kutateladze number obtained from the explicit momentum solution. (The liquid velocity must be greater than zero, since no liquid can flow downward.) However, the correlation does not define the solution point in the cocurrent region. For these situations, we assume that the interfacial friction law implied by the flooding correlation depends only on the magnitude of the relative velocity between the phases and not on the signs of the individual phase velocities. We can then extrapolate the flooding correlation

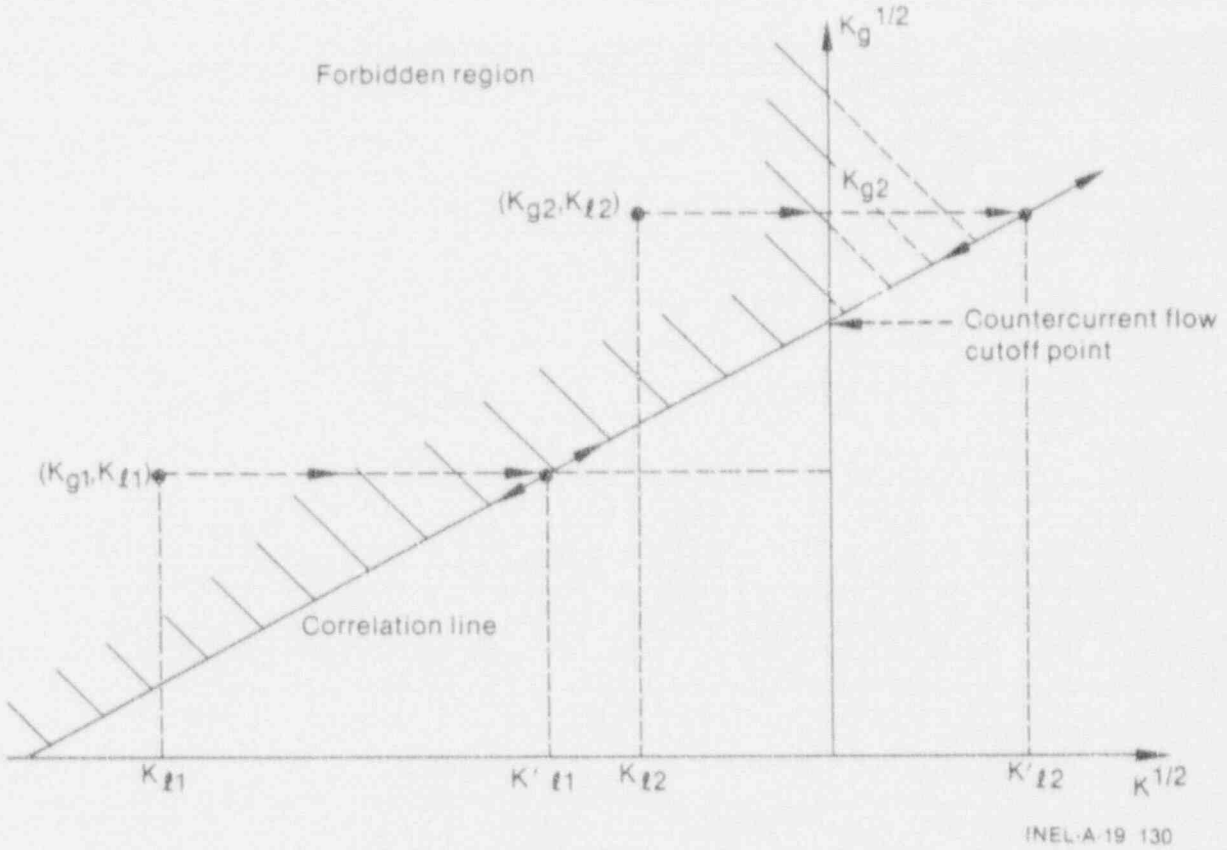

Figure 2.3-4. Flooded flow situation.

into the cocurrent flow region, as indicated in Figure 2.3-4, and proceed as before. The as-coded mathematical description is presented in Volume 3, Section 7.3.

2.3.6 Numerics of Level Tracking Model

As discussed in Subsection 2.1.4, once a two-phase level is determined to exist in a hydrodynamic cell, the above- and below-level void fractions (α^+, α^-, respectively) are defined and stored. When the flux terms for mass and energy are defined for the vertically oriented faces between this cell and its neighboring cells, the donor void fractions are determined as discussed in Subsection 2.3, except that now, whenever a phase velocity is *out* of the cell with the level, α^+ or α^- is used as the donor void fraction in place of the cell average void fraction. Choice of values depends on whether the cell boundary in question is above the level (α^+ being used in this case) or below (α^- being used in this case). The same approach is used for the void fraction dependent flow work terms in the energy equations.

When a two-phase level is determined to exist in a cell, the time (DTLEV) required for the level to cross the cell upper or lower boundary is estimated

from the calculated level velocity, VLEV. If DTLEV exceeds the current time step DELT, no action is taken and the level remains in the cell. If DELT exceeds DTLEV, the level flag (ILEV) is turned off in the current cell and turned on in the cell which the two-phase level is approaching. All level parameters (DZL, VLEV, α^+, and α^-) in this cell are then set based on the previous values in the cell from which the level originates.

When a two-phase level crosses a cell boundary, there is a step change in the void fraction and phase velocities at the boundary. To stabilize the calculations, the level model calculates modified phase velocities to be used in the explicit calculations during the time step after the two-phase level crosses a boundary. The modified velocities are determined from the jump condition

$$VLEV = \frac{J_g^- - J_g^+}{\alpha_j^- - \alpha_j^+} \tag{2.3-48}$$

or

$$VLEV = \frac{J_\ell^- - J_\ell^+}{\alpha_j^+ - \alpha_j^-} \ . \tag{2.3-49}$$

For a rising level that will cross a cell boundary at the next time step, as shown in Figure 2.3-5, the liquid velocity at the boundary after the level crosses can be calculated using Equation (2.3-49). The result is

$$(V_\ell)^n_{j+1/2} = \frac{\left(\alpha_j^+ - \alpha_j^-\right) VLEV_j + \left(1 - \alpha_j^+\right)(V_\ell)^n_j}{\left(1 - \alpha_j^-\right)} \ . \tag{2.3-50}$$

Equation (2.3-48) is used to calculate the vapor velocity at a cell boundary after a falling level crosses it. In this case, $VLEV_j < 0$ in Figure 2.3-5, and the result is

$$(V_g)^n_{j-1/2} = \frac{\alpha_j^-(V_g)^n_j - \left(\alpha_j^- - \alpha_j^+\right) VLEV_j}{\alpha_j^+} \ . \tag{2.3-51}$$

where $\partial V_g/\partial(\Delta P)$ is determined from the momentum equation for the vapor phase.

2.3.7 Water Packing

Significant pressure excursions often are seen in computations with

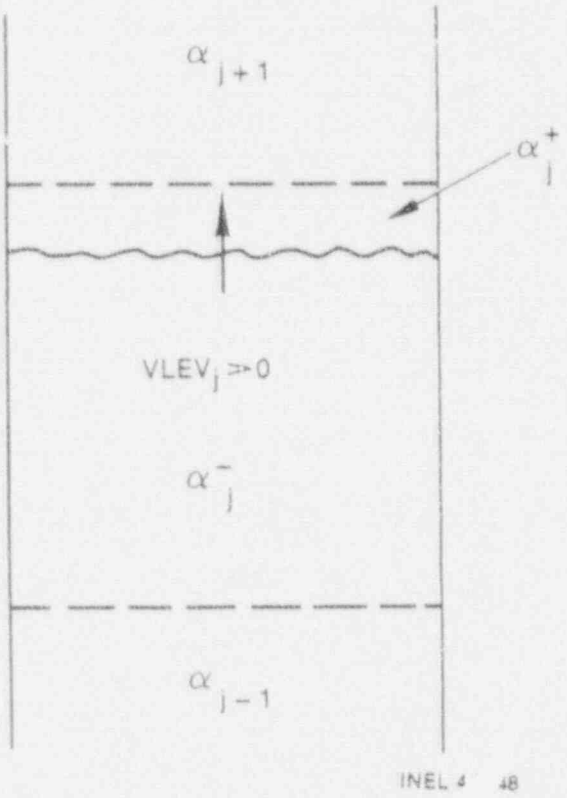

Figure 2.3-5. Rising two-phase level.

finite-difference hydrodynamics codes such as TRAC-BF1/MOD1. Sometimes these excursions reflect real pressure spikes from water hammer effects. However, they may also occur as numerical artifacts due to filling of a hydrodynamic cell with nearly incompressible pure liquid as a result of condensation inside the cell or rapid propagation of a liquid-vapor interface. In such instances, the finite-difference equation of motion for the liquid phase fails to produce a mass flow out of the cell (toward the high void region) that balances the flow into the cell. The result is an abrupt computed increase in cell pressure, which produces the required liquid flow out of the cell.

In TRAC-BF1/MOD1, a method has been implemented for mitigating this "water packing" effect. The method forces a discontinuous change to the liquid velocity profile when large pressure increases or decreases are detected. (Negative pressure spikes may occur when the inverse of the above described situation occurs; i.e., when liquid outflow exceeds inflow. In this instance, the liquid flow mismatch is termed a "stretch.") The as-coded numerical solution for water packing/stretching is provided in Reference 3, Section 2.1.31.2

2.3.8 Numerics of Interfacial Shear

The detailed numerical method for the interfacial shear calculation is described in Reference 3, Section 6.1.11. The information provided therein deals with finite limits on variables, volume averaging for properties, and time-step weighting.

2.3.9 Numerics of Interfacial Heat Transfer

The detailed numerical method for the interfacial heat transfer calculation is described in Reference 3, Section 4.1.11. The information provided therein deals with volume averaging and the treatment of metastable states.

2.3.10 References

2.3-1. J. H. Mahaffy, *A Stability-Enhancing Two-Step Method for One-Dimensional Two-Phase Flow*, NUREG/CR-0971, LA-7951, 1979.

2.3-2. J. G. M. Andersen, K. H. Chu, and J. C. Shaug, *BWR Refill-Reflood Program, Task 4.7 - Model Development. Basic Models for the BWR Version of TRAC*, NUREG/CR-2573, EPRI NP-2375, GEAP-22051, September 1983.

2.3-3. J. A. Borkowski and N. L. Wade, Eds., *TRAC-BF1/MOD1 Models and Correlations*, NUREG/CR-4391, EGG-2680, August 1992.

2.4 REACTOR KINETICS

Power generation in the reactor core during a computer simulation is calculated by Subroutine POWER. Three methods are provided for determining the power. The first method is simply a table lookup of power, using the power-versus-time table supplied as input. Linear interpolation is used to extract values lying between entries in the table. In the second method, the power is determined from the solution of the point reactor kinetics equations and the decay heat equations. In the third, a two-group, one-dimensional, axial diffusion theory solution is performed.

2.4.1 Point Kinetics Equations

The point-reactor kinetics equations include effects that arise from direct fission power and decay of delayed neutron precursors. The decay heat equation describes the effects that arise from the decay of fission products. The point kinetics and decay heat equations are

Point Kinetics Equations

$$\frac{dP}{dt} = \frac{(1 - \beta)}{\Lambda}(R - 1)P + \sum_{i=1}^{n} \lambda_i C_i \qquad (2.4\text{-}1)$$

$$\frac{dC_i}{dt} = -\lambda_i C_i + \frac{\beta_i}{\Lambda} P \text{ for } i = 1,2,\ldots n \qquad (2.4\text{-}2)$$

Decay Heat Equations

$$\frac{dH_{ij}}{dt} = -\lambda^{H}_{ij} H_{ij} + \frac{E_{ij} P_i}{Q} \text{ for } j = 1,2,\ldots m + i = 1,2,3 \qquad (2.4\text{-}3)$$

where

β = total effective delayed neutron fraction

β_i = effective delayed neutron fraction of delayed group i (see Table 2.4-1)

C_i = fission power of delayed neutron group i (W)

E_{ij} = effective energy input to decay group i from fission of isotope i (MeV/fission-s)

H_{ij} = decay power of decay heat group j from fissile isotope i (W)

Table 2.4-1. Delayed neutron constants

Group i	β_i	λ_i
1	2.47 x 10-4	0.0127
2	1.38 x 10-3	0.0327
3	1.22 x 10-3	0.115
4	2.64 x 10-3	0.311
5	8.32 x 10-4	1.40
6	1.69 x 10-4	3.87

Λ = prompt neutron generation time (s)

λ_j = decay constant of delayed neutron group i (see Table 2.4-1) (1/s)

λ^H_{ij} = decay constant for decay heat group j from fissile isotope i (1/s)

m = number of decay heat groups

n = number of delayed neutron groups

n_f = number of fissile isotopes

P = instantaneous total fission power (W)

P_i = instantaneous fission power of isotope i (W)

Q = total energy release per fission (MeV/fission)

R = total reactivity ($).

Equation (2.4-1) describes the time rate of change of the total instantaneous power. The first term on the right side describes the power generated by fissions caused by neutrons generated during the fission process. The second term describes the power generated by fissions caused by neutrons released during the decay of fission products.

Equation (2.4-2) describes the time rate of change of power generated by fissions caused by neutrons emitted by fission products as they decay. The first term on the right describes the decay of these fission products, while the second term describes their production by the fission process.

Equation (2.4-3) describes the time rate of change of another set of fission products that also decay; but, instead of producing neutrons, they

emit beta and gamma rays which, when absorbed by the surrounding material, produce heat. Because this heat only appears after the decay of the fission products, it is called the decay heat. The power determined from Equation (2.4-1) would be the power deposited in the core if there was no decay heat stored in the fission products. Since some of the instantaneous power is stored in the fission products and some of the previously stored energy is released, the effective power becomes the instantaneous power minus the portion of the instantaneous power stored in the fission products plus the portion of the previously stored power that appears at this time due to the decay of the fission products generated previously.

In order to determine the power deposited in the core (P_{eff}), the point-reactor kinetics equations must be solved to obtain the instantaneous power. Once the instantaneous power is determined, the decay heat equations can be solved and P_{eff} computed from

$$P_{eff} = P - \frac{\sum_{i=1}^{N_f} P_i \sum_{j=1}^{m} E_{ij}}{Q\lambda_{ij}^{K}} + \sum_{i=1}^{n_f} \sum_{j=1}^{m} H_{ij} \quad . \tag{2.4-4}$$

The point-reactor kinetics equations [Equations (2.4-2) through (2.4-4)] are solved by numerical integration using a fourth-order Runge-Kutta technique, as modified by Gill.[2.4-1,2] This technique is fast, highly accurate, and has excellent round-off error-limiting characteristics. However, because this is an explicit technique, the maximum time step size is governed by a stability condition

$$\Delta t_{max} = \frac{0.8\Lambda}{\beta \max [R - 1, 1]} \tag{2.4-5}$$

which could limit the problem time step size, Δt_p. To prevent this occurrence in cases where $\Delta t_{max,calc} < \Delta t_p$, the kinetics equations are integrated over K equal subintervals, Δt_{rk}. $\Delta t_{max,calc}$ is given by

$$\Delta t_{max,calc} = Min \left[\frac{0.4\Lambda}{\beta \, Max \, [R, \, |1 - R|]}, \frac{0.002}{\Delta R} \, \Delta t \right] \tag{2.3-6}$$

where

$$K = INT \left(\frac{\Delta t_p}{\Delta t_{max,calc}} \right) + 1 \quad . \tag{2.4-7}$$

However, if $\Delta R < 0.002$, the ΔR is set equal to 0.002 for the evaluation of $\Delta t_{max,calc}$ only. Therefore, Δt_{rk} is given by

$$\Delta t_{rk} = \frac{\Delta t_p}{K} \quad . \tag{2.4-8}$$

In cases where Δt_{max} exceeds Δt_p, only one integration is performed using Δt_p.

2.4.1.1 Calculation of Total Reactivity. In order to solve the point kinetics equations, the total reactivity R must be computed. In TRAC-BF1/MOD1, the total reactivity is the sum of two terms, the user-input control reactivity and the code-calculated feedback reactivity. The control reactivity is computed from a table lookup of user-input values. The control reactivity is intended to model the reactivity associated with control rod motion or any other external changes that might be made to the system during a transient. The feedback reactivity is due to changes in the power caused by changes to the hydraulic state of the reactor during the course of a transient; that is, changes in fuel temperature, moderator temperature, and void fraction. In BWRs, soluble boron may be injected into the reactor in the event that the reactor cannot be shutdown due to a failure of the control rods or their drive mechanisms. The effects of soluble boron are also included in the feedback reactivity.

The feedback reactivity is computed through the use of user-input reactivity coefficients. A rigorous analysis of reactivity feedback and a detailed discussion of the generation of reactivity coefficients and their use in commercial BWRs is rare. The assumption of a uniform reactor core (that is, that the reactor core has uniform properties) is usually made in point-reactor kinetics. For a uniform reactor core with a uniform change in the core property q (e.g., fuel temperature, moderator temperature, void fraction or boron concentration), the reactivity coefficient C_q is

$$C_q = \frac{1}{k}\frac{\partial k}{\partial q} = \frac{\partial}{\partial q} \ln k \tag{2.4-9}$$

where k is the neutron multiplication factor. Conversely, if the reactivity coefficient is known for a given uniform reactor, the feedback reactivity due to a small change δq in q is

$$\frac{\Delta k}{k} = C_q \, \delta q \quad . \tag{2.4-10}$$

In a commercial BWR, neither the reactor core properties nor the property changes during a transient is uniform. The reactivity coefficients obtained with a uniform reactor assumption cannot be expected to predict the feedback reactivity accurately by using Equation (2.4-10), assuming δq is the change in average property q. When the core average properties are used, the reactivity feedback from a localized core disturbance does not depend on the location of the disturbance in the core. This is not true even in a uniform reactor, since the feedback reactivity also depends on the flux level at the location

of the disturbance. For a nonuniform reactor with distributed disturbance, the feedback reactivity depends on the flux distributions and the distribution of the disturbance. During a pressurization transient in a BWR, the higher void collapse occurs near the core center where the flux is higher. Using reactivity coefficients for a uniform reactor in Equation (2.4-10) with q being the average void fraction in the BWR tends to underestimate void reactivity feedback. Furthermore, the disturbance and the flux distribution may be correlated, and this effect is neglected by using the core average property in Equation (2.4-10). The Doppler reactivity feedback is proportional to the change in the square root of the fuel temperature and should be weighted by the product of the epithermal direct and adjoint Fluxes. Since the highest temperature change occurs where the flux is the highest, there is a positive temperature-flux correlation, resulting in an enhancement of the local reactivity feedback.[2.4-3]

2.4.1.2 Spatial Reactivity Effects. To take the effects of spatial variations in the reactor core disturbances into account, TRAC-BF1/MOD1 calculates the reactivity worth from local disturbances, which is then summed up over the entire core. To do this, various assumptions are made to simplify the problem. As might be expected, uncertainties associated with the simplifying assumptions are introduced. The discussion on the TRAC-BF1/MOD1 reactivity feedback model starts from the two-group perturbation theory of reactivity feedback.

In the two-group perturbation theory, the reactivity change due to a small change in core property $\delta q(x)$, which is a function of position in the core, is[2.4-4] ($R = \Delta k/k$)

$$R = \int dV\ \delta q(\vec{x}) \left\{ \left[\nabla\psi_1(\vec{x}) \left(\frac{\partial D_1(\vec{x}|q)}{\partial q} \nabla\phi_1(\vec{x}) \right) + \nabla\psi_2(\vec{x}) \left(\frac{\partial D_2(\vec{x}|q)}{\partial q} \nabla\phi_2(\vec{x}) \right) \right] \right.$$

$$+ \left[\left(\chi_1 \nu_1 \frac{\partial \Sigma_{f1}(\vec{x}|q)}{\partial q} - \frac{\partial \Sigma_1(\vec{x}|q)}{\partial q} - \frac{\partial \Sigma_{1\to 2}(\vec{x}|q)}{\partial q} \right) \psi_1(\vec{x}) \phi_1(\vec{x}) \right]$$

$$+ \left[\chi_1 \nu_2 \frac{\partial \Sigma_{f2}(\vec{x}|q)}{\partial q} \psi_1(\vec{x}) \phi_2(\vec{x}) \right]$$

$$\left. + \left[\left(\frac{\partial \Sigma_{1\to 2}(\vec{x}|q)}{\partial q} + \chi_2 \nu_1 \frac{\partial \Sigma_{f1}(\vec{x}|q)}{\partial q} \right) \psi_2(\vec{x}) \phi_1(\vec{x}) \right] \right.$$

$$+\left[\left(\chi_2\nu_2\frac{\partial\sum_{f2}(\vec{x}|q)}{\partial q}-\frac{\partial\sum_{2}(\vec{x}|q)}{\partial q}\right)\psi_2(\vec{x})\phi_2(\vec{x})\right]\Bigg\}\Big/Q \qquad (2.4\text{-}11)$$

and

$$Q=\int dV\left[\chi_1\nu_1\sum_{f1}(\vec{x})\psi_1(\vec{x})\phi_1(\vec{x})+\chi_2\nu_1\sum_{f1}(\vec{x})\psi_2(\vec{x})\phi_1(\vec{x})\right.$$

$$\left.+\chi_1\nu_2\sum_{f2}(\vec{x})\psi_1(\vec{x})\phi_2(\vec{x})+\chi_2\nu_2\sum_{f2}(\vec{x})\psi_2(\vec{x})\phi_2(\vec{x})\right] \qquad (2.4\text{-}12)$$

where q enters D, $\sum_{f1}$, $\sum_{1}$, $\sum_{1\to2}$, $\sum_{2}$ as a parameter. The symbols in Equations (2.4-9) and (2.4-10) have the usual meanings and are explained in the Nomenclature. For a light water reactor, $\chi_1 >> \chi_2$ and $\sum_{f2} >> \sum_{f1}$, Equation (2.4-12) becomes

$$Q=\varepsilon\nu\int dV\sum_{f2}(\vec{x})\psi_1(\vec{x})\phi_2(\vec{x}) \qquad (2.4\text{-}13)$$

where ε is the fast fission factor and $\nu=\nu_2$. In a commercial BWR, the important reactor core properties that change during a transient are the fuel temperature, moderator temperature, and moderator void, aside from control rod movement and neutron poison injection. The fission cross section is not directly affected by these changes. The change in the summation of f is mainly from neutron spectral shift and the change in neutron distribution and is usually small. In a computer code like TRAC-BF1/MOD1, the fine details in the local variations of the core parameters are not of interest. What is important are the values averaged over a range of several channel widths. In a large reactor, the average fluxes are slowly varying and the gradients of these average fluxes are small except near the core edges. The terms in the first squared bracket are more important near the core edges and are partly taken into account in the modified one-group theory by considering the dependence of the neutron leakage on the core property q. If the flux gradient terms and the change in fission cross section are neglected, Equation (2.4-11) reduces to

$$R = -\frac{1}{Q}\int dV \delta q(\vec{x}) \left[\frac{\partial \sum_1 (\vec{x}|q)}{\partial q} \psi_1(\vec{x})\phi_1(\vec{x}) + \frac{\partial \sum_{1\to 2} (\vec{x}|q)}{\partial q} \psi_2(\vec{x})\phi_1(\vec{x}) \right.$$

$$\left. - \frac{\partial \sum_2 (\vec{x}|q)}{\partial q} \psi_2(\vec{x})\phi_2(\vec{x}) \right] \qquad (2.4\text{-}14)$$

Consider the case when the disturbance is localized to a small volume ΔV at the position x. When the disturbance is in the fuel temperature T_f, the reactivity change is mainly due to the change in the summation over 1 caused by the Doppler broadening of resonance absorption, and

$$R_{Tf} = -\frac{1}{Q} \frac{\partial \sum_1 (\vec{x})}{\partial T_f} \delta T_f \Delta V \psi_1(\vec{x})\phi_1(\vec{x}) \ . \qquad (2.4\text{-}15)$$

When the disturbance is in the moderator temperature, T_M, or the moderator void α, the reactivity change is mainly due to the change in the neutron slowing down cross section caused by the change in the moderator density

$$R_{TM} = \frac{1}{Q} \frac{\partial \sum_{1\to 2} (\vec{x})}{\partial T_f} \delta T_M \Delta V \psi_2(\vec{x})\phi_1(\vec{x}) \qquad (2.4\text{-}16)$$

$$R_{VD} = \frac{1}{Q} \frac{\partial \sum_{1\to 2} (\vec{x})}{\partial \alpha} \delta\alpha \Delta V \psi_2(\vec{x})\phi_1(\vec{x}) \ . \qquad (2.4\text{-}17)$$

When the disturbance is the change in the poison (boron macroscopic density ρ_B), the reactivity change is mainly due to the change in the thermal neutron absorption

$$R_B = \frac{1}{Q} \frac{\partial \sum_2 (\vec{x})}{\partial \rho_B} \delta\rho_B \Delta V \psi_2(\vec{x})\phi_2(\vec{x}) \ . \qquad (2.4\text{-}18)$$

The reactivities R_{Tf}, R_{TM}, R_{VD}, and R_B due to the local disturbances at the position x depends on the values of functions

$$W_{Tf}(\vec{x}) = \psi_1(\vec{x})\phi_1(\vec{x}) \qquad (2.4\text{-}19)$$

and

$$W_{TM}(\vec{x}) = W_{VD}(\vec{x}) = \psi_2(\vec{x})\phi_1(\vec{x}) \tag{2.4-20}$$

$$W_B(\vec{x}) = \psi_2(\vec{x})\phi_2(\vec{x}) \tag{2.4-21}$$

at the position x, respectively. If the function W_{TF} is normalized to the core volume, then

$$R_{TF} = -\frac{N_{TF}}{Q}\frac{\partial\sum_1(\vec{x})}{\partial T_F}\delta T_F W_{TF}(\vec{x}) \tag{2.4-22}$$

where

$$N_{TF} = \int dV\ \psi_1(\vec{x})\phi_1(\vec{x})\ . \tag{2.4-23}$$

The fuel temperature reactivity coefficient can be defined as

$$R_{TF} = -\frac{N_{TF}}{Q}\frac{\partial\sum_1(\vec{x})}{\partial T_F}\ . \tag{2.4-24}$$

The other local reactivity coefficients can be defined similarly. That is, the moderator temperature coefficient is defined as

$$R_{TM} = -\frac{N_{TM}}{Q}\frac{\partial\sum_{1\to2}(\vec{x})}{\partial T_M} \tag{2.4-25}$$

where

$$N_{TM} = \int W_{TF}(\vec{x})\ dV \tag{2.4-26}$$

the moderator void coefficient is defined as

$$R_{VD} = -\frac{N_{VD}}{Q}\frac{\partial\sum_{1\to2}(\vec{x})}{\partial\alpha} \tag{2.4-27}$$

where

$$N_{VD} = \int W_{VD}(\vec{x})\ dV = N_{TM} \tag{2.4-28}$$

and the boron reactivity coefficient is defined as

$$R_B = -\frac{N_B}{Q}\frac{\partial \sum_2 (\vec{x})}{\partial \rho_B} \qquad (2.4\text{-}29)$$

where

$$N_B = \int W_B(\vec{x})\, dV \; . \qquad (2.4\text{-}30)$$

In a large reactor and away from the core edges where the flux gradients are small and the spatial variations in core properties are small, the local reactivity coefficients can be approximately replaced by the reactivity coefficients for a large uniform reactor having the same geometry and having the uniform core properties the same as the properties at x in the nonuniform reactor. For a nonuniform reactor with spatially varying core property changes, the feedback reactivity is then

$$R_{FB} = \int dV \left[R_{Tf}(\vec{x})\delta T_f(\vec{x})W_{Tf}(\vec{x}) + R_{TM}(\vec{x})\delta T_M(\vec{x})W_{TM}(\vec{x}) + R_{VD}(\vec{x})\delta\alpha(\vec{x})W_{VD}(\vec{x})\right.$$

$$\left. + R_B(\vec{x})\delta\rho_B(\vec{x})W_B(\vec{x})\right] . \qquad (2.4\text{-}31)$$

NOTE: The reactivity coefficients are obtained assuming uniform reactor core properties or infinite lattice. Replacing the local reactivity coefficient near the core edges is not valid; however, the values of the weighting functions W_{Tf}, W_{TM}, W_{VD}, and W_B are small at the core edges and the errors introduced are suppressed.

To apply Equation (2.4-31) in reactivity calculations, the statistical weighting functions have to be known. The direct and adjoint flux functions are needed to calculate the statistical weighting functions. They are not available for TRAC-BF1/MOD1 calculations. However, the power distribution P(x) (which assumes uniform fission cross section) is proportional to the thermal flux ϕ_2 (x) and is required in the TRAC-BF1/MOD1 input; therefore,

$$P(\vec{x}) = E\sum_f (\vec{x})\phi_2(\vec{x}) \qquad (2.4\text{-}32)$$

where E is the energy per fission and

$$\phi_2(\vec{x}) = \frac{P(\vec{x})}{E\sum_f (\vec{x})} \; . \qquad (2.4\text{-}33)$$

If the summation over f is uniform, $\phi_2(x)$ is proportional to P(x). Near the core center or away from the core edge, the neutron fluxes are approximately related by[2.4-5]

$$\psi_1 = \phi_1 \tag{2.4-34}$$

$$\phi_1 = \frac{\sum_2 (\vec{x})}{\sum_1 (\vec{x})} \phi_2 \tag{2.4-35}$$

and

$$\psi_2 = \frac{K_\infty}{k_{eff}(1 + L^2B^2)} \psi_1 \ . \tag{2.4-36}$$

For a BWR in power operation, due to a smaller void, Σ_1 is substantially larger near the bottom of the core than at the top of the core. However, to maintain an optimal axial power shape, the control rods are inserted from the bottom. The thermal neutron absorption Σ_2 is larger near the bottom of the core. If the neutron spectrum does not vary substantially through the core, that is

$$\phi_1(\vec{x}) \propto \phi_2(\vec{x}) \tag{2.4-37}$$

then,

$$W_{TF}(\vec{x}) = W_B(\vec{x}) = W_{1M}(\vec{x}) = W_{VD}(\vec{x}) \propto [P(\vec{x})]^2 \ . \tag{2.4-38}$$

NOTE: The weighting functions are normalized. In TRAC-BF1/MOD1, Equation (2.4-38) is assumed for the reactivity weighting functions and Equation (2.4-31) is the basis for feedback reactivity calculations.

2.4.1.3 Reactivity Coefficients in TRAC-BF1/MOD1. For a given fuel temperature change, the Doppler coefficient is needed to calculate the fuel temperature (Doppler) reactivity. The Doppler coefficient is a function of in-channel void, because of the strong influence of in-channel void on the neutron resonance escape probability. In TRAC-BF1/MOD1, a quadratic representation is used for the R_{TF} dependence on moderator void, shown as

$$R_{TF} = a_{TF} + b_{TF}\alpha + c_{TF}\alpha^2 \ . \tag{2.4-39}$$

This allows the influence of moderator void on fuel temperature reactivity feedback to be taken into account.

Since the change in moderator density with temperature is small, the moderator temperature reactivity feedback during a reactor transient starting from a normal BWR power operation is insignificant in comparison to the void reactivity feedback. The moderator temperature reactivity feedback is

important when the moderator void is essentially nonexistent, like when the reactor is at standby condition. Since the moderator temperature reactivity coefficient varies with moderator temperature itself, the moderator temperature coefficient is allowed a quadratic dependence on the moderator temperature T_M,

$$R_{TM} = a_{TM} + b_{TM}T_M + c_{TM}T_M^2 \quad . \tag{2.4-40}$$

The void collapse (or generation) is the dominant reactivity feedback mechanism during a BWR operational transient. Accurate representation of the void reactivity coefficient is essential for good transient reactor power predictions. The void reactivity coefficient has strong dependence on in-channel void; therefore, it is allowed a quadratic dependence on void fraction α in TRAC-BF1/MOD1. That is,

$$R_{VD} = a_{VD} + b_{VD}\alpha + c_{VD}\alpha^2 \quad . \tag{2.4-41}$$

Since the boron concentration is expressed in ppm in TRAC-BF1/MOD1, the boron density to which the thermal neutron absorption by boron is approximately proportional is proportional to the moderator density. The boron reactivity coefficient is therefore moderator density-dependent. The boron reactivity coefficient is allowed quadratic dependence on moderator density

$$R_B = a_B + b_B\rho_M + c_B\rho_M^2 \tag{2.4-42}$$

where ρ_M is the moderator density.

Equations (2.4-39) through (2.4-42) are used in TRAC-BF1/MOD1 to evaluate the Doppler and other reactivity coefficients for a core cell. The values obtained at a given instance may vary from cell to cell, as the fuel temperature, moderator temperature, moderator void, and moderator density vary. Since the same set of the reactivity coefficient equations are used for the entire core, it is implicitly assumed that each core cell contains the same mixture of fuel types at different exposures.

2.4.1.4 Code Implementation. In TRAC-BF1/MOD1, the reactor core is separated into channel regions (in the CHAN component model) and bypass regions (in the VESSEL component model). The fuel temperature reactivity is calculated for each fueled CHAN cell. All other feedback reactivities are calculated for both the CHAN cells and the VESSEL cells. The same reactivity coefficient equations are used for both the channel regions and the bypass regions. The user may scale the feedback reactivities from the bypass regions relative to the feedback reactivities from the channel regions by the input of a scale factor for the bypass regions.

During the transient calculations and after the thermal-hydraulic calculations are completed for the time step, the changes in reactivity

associated with changes in fuel temperature, moderator temperature, void fraction, and boron concentration are computed for each cell in the core region and are summed to compute the changes in the total feedback reactivity during the time step, written as

$$R_{FB}^{n+1} = R_{FB}^{n} + \delta R_{FB}^{n+1} \tag{2.4-43}$$

where

$$\delta R_{FB}^{n+1} = \delta R_{TF}^{n+1} + \delta R_{TM}^{n+1} + \delta R_{VD}^{n+1} + \delta R_{B}^{n+1} \, . \tag{2.4-44}$$

The individual reactivity contributions are computed from

$$\delta R_{TF}^{n+1} = \sum_{i} R_{TF,i}^{n+1} \left[\left(T_{F_i}^{n+1} \right)^{1/2} - \left(T_{F_i}^{n} \right)^{1/2} \right] W_{TF,i} \tag{2.4-45}$$

$$\delta R_{VD}^{n+1} = \sum_{i} R_{VD,i}^{n+1} \left(\alpha_i^{n+1} - \alpha_i^{n} \right) W_{VD,i} \tag{2.4-46}$$

$$\delta R_{TM}^{n+1} = \frac{\sum_{i} W_{TM,i} R_{TM,i}^{n+1} \left[\left(1 - \alpha_i^{n+1} \right) \rho_{\ell}^{n+1} T_{M,i}^{n+1} - \left(1 - \alpha_i^{n} \right) \rho_{\ell}^{n} T_{M,i}^{n} \right]}{\sum_{i} \left(1 - \alpha_i^{n+1} \right) \rho_{\ell}^{n+1} W_{TM,i}} \tag{2.4-47}$$

$$\delta R_{B}^{n+1} = \frac{R_{B,i}^{n+1} W_{B,i} \left[\left(1 - \alpha_{i-1}^{n+1} \right) \rho_{\ell,i}^{n+1} B_i^{n+1} - \left(1 - \alpha_i^{n} \right) \rho_{\ell}^{n} B_i^{n} \right]}{\sum_{i} \left(1 - \alpha_i^{n+1} \right) \rho_{\ell}^{n+1} W_{B,i}} \tag{2.4-48}$$

where i is the cell index, n and n+1 indicate the old- and new-time values, and the summation is over all cells in the reactor core region. The reactivity coefficients are computed using the new time conditions in each cell. Notice that the moderator temperature and boron feedback contributions are normalized by the amount of liquid in the cells. This is because the property is connected with the liquid phase and cannot exist apart from the presence of liquid.

In addition to the feedback reactivity, the four core average properties are also computed and are included in the TRAC-BF1/MOD1 major edits along with

the individual reactivity contributors. They are computed as

$$\bar{T}_f = \sum_i T_{f,i} W_{TF,i} \tag{2.4-49}$$

$$\bar{\alpha} = \sum_i \alpha_i^{n+1} W_{VD,i} \tag{2.4-50}$$

$$\bar{T}_m = \frac{\sum_i T_{M,i}\left(1 - \alpha_i^{n+1}\right)\rho_{\ell,i}^{n+1} W_{TM,i}}{\sum_i \left(1 - \alpha_i^{n+1}\right)\rho_{\ell,i}^{n+1} W_{TM,i}} \tag{2.4-51}$$

and

$$\bar{B} = \frac{\sum_i \left(1 - \alpha_i^{n+1}\right)\rho_{\ell,i}^{n+1} B_i^{n+1} W_{b,i}}{\sum_i \left(1 - \alpha_i^{n+1}\right)\rho_{\ell,i}^{n+1} W_{B,i}} . \tag{2.4-52}$$

As an option, the user is allowed to choose for each feedback reactivity component whether the power-squared weighting is to be applied or not. When the power-squared weighting is not chosen for a given feedback reactivity component, the simple volume average is used.

In addition to the feedback, the explicit reactivity (control rod) insertion is modeled as a user-input reactivity-versus-time table. This reactivity table represents the additional control rod reactivity worth inserted from steady state. At the beginning of the transient, this reactivity value is therefore zero. The control rod reactivity $(R)_{CR}$ inserted in each time step is found from this reactivity table. The total reactivity inserted into each time step is the sum of the feedback reactivity and the control rod reactivity inserted. The neutron multiplication factor at the zero time step is updated as

$$k^{n+1} = k_m + k^n\left(R_{FB}^{n+1} + R_{CR}^{n+1}\right) \tag{2.4-53}$$

where k^{n+1} and k^n are the neutron multiplication factors at the new and old times, respectively. At the beginning of a transient, k = 1 is assumed. The reactivity R at the new time is

$$R = \frac{k^{n+1} - 1}{k^{n+1}} \qquad (2.4\text{-}54)$$

where R is then used in the point kinetics equation integrator.

2.4.2 One-Dimensional Neutron Kinetics

The one-dimensional kinetics model in TRAC-BF1/MOD1 is a two-group formulation based on the Analytic Nodal Method. The advantage of the one-dimensional kinetics option over traditional point kinetics is that the axial flux profile is allowed to change as a function of time in response to changing thermal-hydraulic conditions and/or control system actions. However, considerably more user input is required in order to implement the one-dimensional kinetics model, as compared to the point kinetics model.

2.4.2.1 Derivation of the Analytic Nodal Kinetics Equations. The two-group, one-dimensional, space- and time-dependent neutron diffusion equations can be written in matrix form as

$$\begin{bmatrix} \frac{1}{v_1} & 0 \\ 0 & \frac{1}{v_2} \end{bmatrix} \frac{\partial}{\partial t} \begin{bmatrix} \phi_1 \\ \phi_2 \end{bmatrix} = \frac{\partial}{\partial z} \begin{bmatrix} D_1 & 0 \\ 0 & D_2 \end{bmatrix} \frac{\partial}{\partial z} \begin{bmatrix} \phi_1 \\ \phi_2 \end{bmatrix} - \begin{bmatrix} \Sigma_{a1}+\Sigma_{r1}+D_1B_1^2 & 0 \\ -\Sigma_{r1} & \Sigma_{a2}+D_2B_2^2 \end{bmatrix} \begin{bmatrix} \phi_1 \\ \phi_2 \end{bmatrix}$$

$$+ \frac{1-\beta}{\lambda} \begin{bmatrix} \chi_1 \\ \chi_2 \end{bmatrix} \begin{bmatrix} \nu\Sigma_{f1} & \nu\Sigma_{f2} \end{bmatrix} \begin{bmatrix} \phi_1 \\ \phi_2 \end{bmatrix} + \sum_i^k \begin{bmatrix} \chi_1 \\ \chi_2 \end{bmatrix} \lambda_k C_k \qquad (2.4\text{-}55)$$

where the space- and time-dependence of all parameters except λ, λ_k, and β is implied and

D_1 = the group 1 diffusion coefficient

D_2 = the group 2 diffusion coefficient

Σ_{a1} = the group 1 macroscopic absorption cross section

Σ_{a2} = the group 2 macroscopic absorption cross section

Σ_{r1} = the group 1 macroscopic downscatter cross section

B_1^2 = the group 1 transverse buckling squared

B_2^2 = the group 2 transverse buckling squared

χ_1 = the fraction of fission neutrons released into group 1. (χ_1 is assumed to be a constant equal to 1.0; no distinction is made in this derivation between the prompt and delayed neutron emission spectra.)

χ_2 = the fraction of fission neutrons released into group 2. (χ_2 is assumed to be a constant equal to 0.0)

$\nu\Sigma_{f1}$ = the group 1 macroscopic production cross section

$\nu\Sigma_{f2}$ = the group 2 macroscopic production cross section

ϕ_1 = the group 1 scalar neutron flux

ϕ_2 = the group 2 scalar neutron flux

λ = a constant parameter used to force criticality for a particular set of input diffusion theory parameters

v_1 = the group 1 average neutron velocity

v_2 = the group 2 average neutron velocity

λ_k = the decay constant for delayed neutron precursor k

C_k = the concentration of delayed neutron precursor k

K = the number of delayed neutron precursor groups

β = the total effective delayed neutron fraction.

Equation (2.4-55) may be written in a more compact form

$$[v]^{-1}\frac{\partial}{\partial t}[\phi] = \frac{\partial}{\partial z}[D]\frac{\partial}{\partial z}[\phi] - [\Sigma_t][\phi] + [\chi](1-\beta)\left[\frac{\nu\Sigma_f}{\lambda}\right]^T[\phi]$$

$$+ \sum_1^k [\chi]\lambda_k C_k \qquad (2.4\text{-}56)$$

where all bracketed quantities denote matrices or vectors.

The region of interest (usually the entire reactor and possibly the axial reflectors) is now partitioned into an arbitrary number of subregions, or nodes. Each node, i, extends from interface i to interface i+1 and is of width h_i, where $h_i = z_{i+1} - z_i$. If it is assumed that suitably averaged,

space-independent (within each node) neutron diffusion theory parameters are available for every node, then Equation (2.4-56) may be integrated over a typical node, i, to yield

$$h_i[v_i]^{-1}\frac{\partial}{\partial t}[\bar{\phi}_i] = -[J_{i+1}] + [J_i] - h_i[\Sigma_i][\bar{\phi}_i]$$

$$+ h_i[\chi](1-\beta)\left[\frac{\nu\Sigma_i}{\lambda}\right][\bar{\phi}_i] + \sum_1^K [\chi]\lambda_k\bar{C}_i \qquad (2.4\text{-}57)$$

where

$$\bar{C}_{ki} = \int_{z_i}^{z_{i+1}} C_k\, dz \qquad (2.4\text{-}58)$$

$$[\bar{\phi}_i] = \frac{1}{h_i}\int_{z_i}^{z_{i+1}} [\phi(z)]\, dz \ (\textit{node-average flux vector}) \qquad (2.4\text{-}59)$$

$$[J_i] = [-D_i]\frac{d}{dz}[\phi(z_i)] \ (\textit{net current vector at } z_i) \qquad (2.4\text{-}60)$$

The equation governing delayed neutron precursor k is given by

$$\frac{\partial C_k}{\partial t} = -\lambda_k C_k + \beta_k\left[\frac{\nu\Sigma_f}{\lambda}\right]^T[\phi] \qquad (2.4\text{-}61)$$

where β_k is the partial effective delayed precursor fraction for precursor k and

$$\sum_1^K \beta_k = \beta\ . \qquad (2.4\text{-}62)$$

Integration of Equation (2.4-61) over node i yields

$$\frac{d}{dt}\bar{C}_{ki} = -\lambda_k\bar{C}_{ki} + h_i\beta_k\left[\frac{\nu\Sigma_{fi}}{\lambda}\right]^T[\bar{\phi}_i]\ . \qquad (2.4\text{-}63)$$

Additional relationships between the node-averaged fluxes and the

interface currents are now required in order to allow the solution of the system of Equations (2.4-57) and (2.4-63) to be obtained for the node-average fluxes and the nodal precursor inventories, $C_{k,i}$, as functions of time. The desired relationships may be obtained using the Analytic Nodal Method.[2.4-6,7] This method produces a flux-current relationship for node i of the form

$$[J_{i,+1}] - [J_i] = [CL_i][\bar{\Phi}_{i-1}] + [CC_i][\bar{\Phi}_i] + [CR_i][\bar{\Phi}_{i+1}] \qquad (2.4\text{-}64)$$

where the coupling matrices $[CL_i]$, $[CC_i]$, and $[CR_i]$ are complicated functions of the nodal cross sections and dimensions.

Substituting Equation (2.4-64) into Equation (2.4-57) and rearranging yields

$$-h_i[v_i]^{-1}\frac{d}{dt}[\bar{\Phi}_i] = [CL_i][\bar{\Phi}_{i-1}] + [CC_i][\bar{\Phi}_i] + [CR_i][\bar{\Phi}_{i+1}] + h_i[\Sigma_{f,i}][\bar{\Phi}_i]$$

$$- h_i[\chi](1 - \beta)\left[\frac{\nu\Sigma_{f,i}}{\lambda}\right]^T[\bar{\Phi}_i] - \sum_i^K [\chi]\lambda_k\bar{C}_{k,i} \; . \qquad (2.4\text{-}65)$$

Equations (2.4-63) and (2.4-65) are the basic time-dependent nodal equations of interest. Note that Equation (2.4-65) is nonlinear because quantities proportional to the time derivatives of the fluxes and precursor concentrations appear in the coupling matrices. This is a consequence of the Analytic Nodal formulation.

2.4.2.2 Input Requirements. The full input specifications are provided in Volume 2, Section 3.5.8. The as-coded documentation of how the input is used is provided in detail in Section 9.4.4 of the models and correlations document associated with this code manual.[2.4-8]

Basically, the user must be able to provide 11 level-averaged parameters: two-group diffusion coefficients, two-group absorption cross sections, fast group downscatter cross section, two-group ν (neutrons per fission) times fission cross sections, two-group values for ν alone, and two-group bucklings. These cross sections must be input as a function of the transient thermal-hydraulic state

$$X = C_f(a_1 + a_2\alpha + a_3\alpha^2) + (1 - C_f)(a_4 + a_5\alpha + a_6\alpha^2)$$

$$+ a_7\left[(T_f)^{1/2} - (T_{f0})^{1/2}\right] + a_8(T_m - T_{m0}) + a_9B \qquad (2.4\text{-}66)$$

where

X = specific transfer coefficient

C_f = control fraction

α = radial-averaged void fraction

T_f = radial-averaged fuel temperature (K)

T_m = radial-averaged moderator temperature (K)

B = radial-averaged boron concentration (ppm)

a_i = user-defined coefficients (for i = 1,2,...9)

T_{fo} = user-defined fuel reference temperature (K)

T_{mo} = user-defined moderator reference temperature (K).

Since there are nine unknowns in Equation (2.4-66), the user must generate parameter sets at a minimum of nine thermal-hydraulic states and boron concentration levels. Normally, these sets are generated using a three-dimensional nodal diffusion code. The three-dimensional neutronic data would then be collapsed to a level average by the nodal diffusion code. The level-averaged neutron data may then be curve-fit to Equation (2.4-66).

A problem may arise where the level averaged thermal-hydraulic outputs (temperatures and void fractions) are not the same when calculated by TRAC-BF1/MOD1 as they were when calculated in the nodal diffusion code. This effect is not unexpected, since the thermal-hydraulic models may differ significantly between the two codes. If the thermal-hydraulic state and, consequently, the predicted cross sections differ, the flux profile predicted by TRAC-BF1/MOD1 would appear skewed when compared to that of the nodal code. One way to address this problem is to fit Equation (2.4-66) using level-averaged data obtained from TRAC-BF1/MOD1. Since the one-dimensional axial power shape and cross-section set is known for each case with the nodal code, those data may be used in TRAC-BF1/MOD1 to obtain the corresponding level-averaged thermal-hydraulic state as calculated by TRAC-BF1/MOD1. Using those data in the curve fit should eliminate the problem.

Two neutronic considerations are pertinent to a realistic simulation using the one-dimensional kinetics options:

1. The range of thermal-hydraulic states used to fit Equation (2.4-66) must bracket the range of thermal-hydraulic states encountered under transient conditions. If not, the code will be forced to extrapolate beyond them.

2. Collapsed cross-section sets of this type are dependent on a wide variety of neutronic considerations, such as burnup, reload configuration, rod insertion patterns, and changes in the flux profile in the transverse plane. The above data must be regenerated

when the neutronic state of the core is perturbed to a sufficient extent.

2.4.3 Decay Heat Model

The 1979 ANS standard decay heat model[2.4-9] has been implemented into TRAC. The use of the new (1981) ANS model is motivated primarily by the increased accuracy it provides for decay heat calculations. Rather than the ±20% attainable with the old ANS standard model, the new standard has been shown to be accurate to within <5% (1σ deviation) for typical assumed reactor transient conditions. Options available through use of this model that have been incorporated into the code are:

1. Specification of the nuclides responsible for fission power (^{235}U, ^{238}U, and ^{239}Pu) and their percentage contribution to fission power.

2. Incorporation of the effect of the plant's operating history (up to four years prior to transient) upon decay heat. Alternately, an infinite operation time may be assumed to simplify decay heat initialization and calculation.

3. Incorporation of heavy element decay heat (from ^{239}U and ^{239}Np).

4. Inclusion of the effect of fission product neutron capture.

All of these features are optional. An additional feature of this model is the decoupling of the reactor kinetics from the VESSEL module. This allows use of the CHAN component (with reactor kinetics) without requiring a VESSEL component.

The fissioning of a ^{235}U atom releases a total of about 200 MeV of energy. Some of this energy (~93%) is immediately available as thermal energy, while a small percentage (~7%) resides in the fission products that later decay to release it. The same process applies to the fission of other materials in reactor fuels--^{238}U and ^{239}Pu. As fission occurs, decay-heat-producing fission products accumulate in the fuel and begin to decay, according to specific time constants that apply uniquely to each fission product. The first ANS standard decay heat model considered 11 decay groups and their associated time constants. The new ANS standard[2.4-9] considers 69 separate decay groups--23 each for the fission of ^{235}U, ^{238}U, and ^{239}Pu.

Use of the model requires knowledge of the energy release rate from each fission stored in each of the decay groups. These are given as $E_{i,j}$ in Tables 2.4-2, 2.4-3, and 2.4-4.[2.4-9] Associated with each $E_{i,j}$ in these tables is a decay constant $\lambda^H_{i,j}$. Three sets of parameters are given--one for each of the fissionable isotopes considered in the new standard, ^{235}U, ^{238}U, and ^{239}Pu. These sets of constants are sufficient to determine the decay heat generation rate for a reactor core if the reactor operating history is known (in terms of fission power level and the fraction of fission power provided by each of the

Table 2.4-2. Parameters for ^{235}U thermal fission decay heat.

j	$E_{1,j}$	$\lambda^H_{1,j}$	j	$E_{1,j}$	$\lambda^H_{1,j}$
1	6.5057E-01	2.2138E+01	13	2.5232E-06	1.0010E-05
2	5.1264E-01	5.1587E-01	14	4.9948E-07	2.5438E-06
3	2.4384E-01	1.9594E-01	15	1.8531E-07	6.6461E-07
4	1.3850E-01	1.0314E-01	16	2.6608E-08	1.2290E-07
5	5.5440E-02	3.3656E-02	17	2.2398E-09	2.7213E-08
6	2.2225E-02	1.1681E-02	18	8.1641E-12	4.3714E-09
7	3.3088E-03	3.5870E-03	19	8.7797E-11	7.5780E-10
8	9.3015E-04	1.3930E-03	20	2.5131E-14	2.4786E-10
9	8.0943E-04	6.2630E-04	21	3.2176E-16	2.2384E-13
10	1.9567E-04	1.8906E-04	22	4.5038E-17	2.4600E-14
11	3.2535E-05	5.4988E-05	23	7.4791E-17	1.5699E-14
12	7.5595E-06	2.0958E-05			

Table 2.4-3. Parameters for ^{239}Pu thermal fission decay heat.

j	$E_{1,j}$	$\lambda^H_{1,j}$	j	$E_{1,j}$	$\lambda^H_{1,j}$
1	2.083E-01	1.002E+01	13	1.747E-06	8.319E-06
2	3.853E-01	6.433E-01	14	5.481E-07	2.358E-06
3	2.213E-01	2.186E-01	15	1.671E-07	6.450E-07
4	9.460E-01	1.004E-01	16	2.112E-08	1.278E-07
5	3.531E-02	3.728E-02	17	2.996E-09	2.466E-08
6	2.292E-02	1.435E-02	18	1.107E-11	9.378E-09
7	3.946E-03	4.549E-03	19	5.730E-11	7.450E-10
8	1.317E-03	1.328E-03	20	4.138E-14	2.426E-10
9	7.052E-04	5.356E-04	21	1.088E-15	2.210E-13
10	1.432E-04	1.730E-04	22	2.454E-17	2.640E-14
11	1.765E-05	4.881E-05	23	7.557E-17	1.380E-14
12	7.347E-06	2.006E-05			

Table 2.4-4. Parameters for ^{238}U thermal fission decay heat.

j	$E_{1,j}$	$\lambda^N_{1,j}$	j	$E_{1,j}$	$\lambda^N_{1,j}$
1	1.2311E+00	3.2881E+01	13	1.0075E-06	7.0465E-06
2	1.1486E+00	9.3805E-01	14	4.9894E-07	2.3190E-06
3	7.0701E-01	3.7073E-01	15	1.6352E-07	6.4480E-07
4	2.5209E-01	1.1118E-01	16	2.3355E-08	1.2649E-07
5	7.[illegible]70E-02	3.6143E-02	17	2.8094E-09	2.5548E-08
6	2.[illegible]1E-02	1.3272E-02	18	3.6236E-11	8.4782E-09
7	6.[illegible]2E-03	5.0133E-03	19	6.4577E-11	7.5130E-10
8	1.2322E-03	1.3655E-03	20	4.4963E-14	2.4188E-10
9	6.840[illegible]E-04	5.5158E-04	21	3.6654E-16	2.2738E-13
10	1.6975E-04	1.7873E-04	22	5.6293E-17	9.0536E-14
11	2.4182E-05	4.9032E-05	23	7.1602E-17	5.6098E-15
12	6.6356E-06	1.7058E-05			

fissionable materials under consideration).

Additional corrections to the calculated decay heat may be made by considering the decay heat of ^{239}U and ^{239}Pu, and inclusion of the effect of neutron capture by fission products. These corrections are incorporated as special algorithms (see Reference 2.4-6) and are available in the code as user options.

Since the new ANS standard allows inclusion of the effect of reactor operating history, special considerations apply to initialization of the model. The decay heat power generation at t = 0 (beginning of the transient) must be determined from the reactor operating history.

The input to the model is the duration of constant reactor fission power periods and the fission power provided by all fissile isotopes being considered (^{235}U only, ^{235}U plus ^{239}Pu, or ^{235}U plus ^{239}Pu plus ^{238}U). A typical reactor operation histogram is given in Figure 2.4-1. In the following equations, the nomenclature is based on definitions given for Equations (2.4-1) through (2.4-3).

The decay heat model can be initiated with or without a reactor power history. If no power history is used, an infinite operating time is assumed, which results in an equilibrium decay heat at transient initiation. In this case, the initial decay heat power is derived from

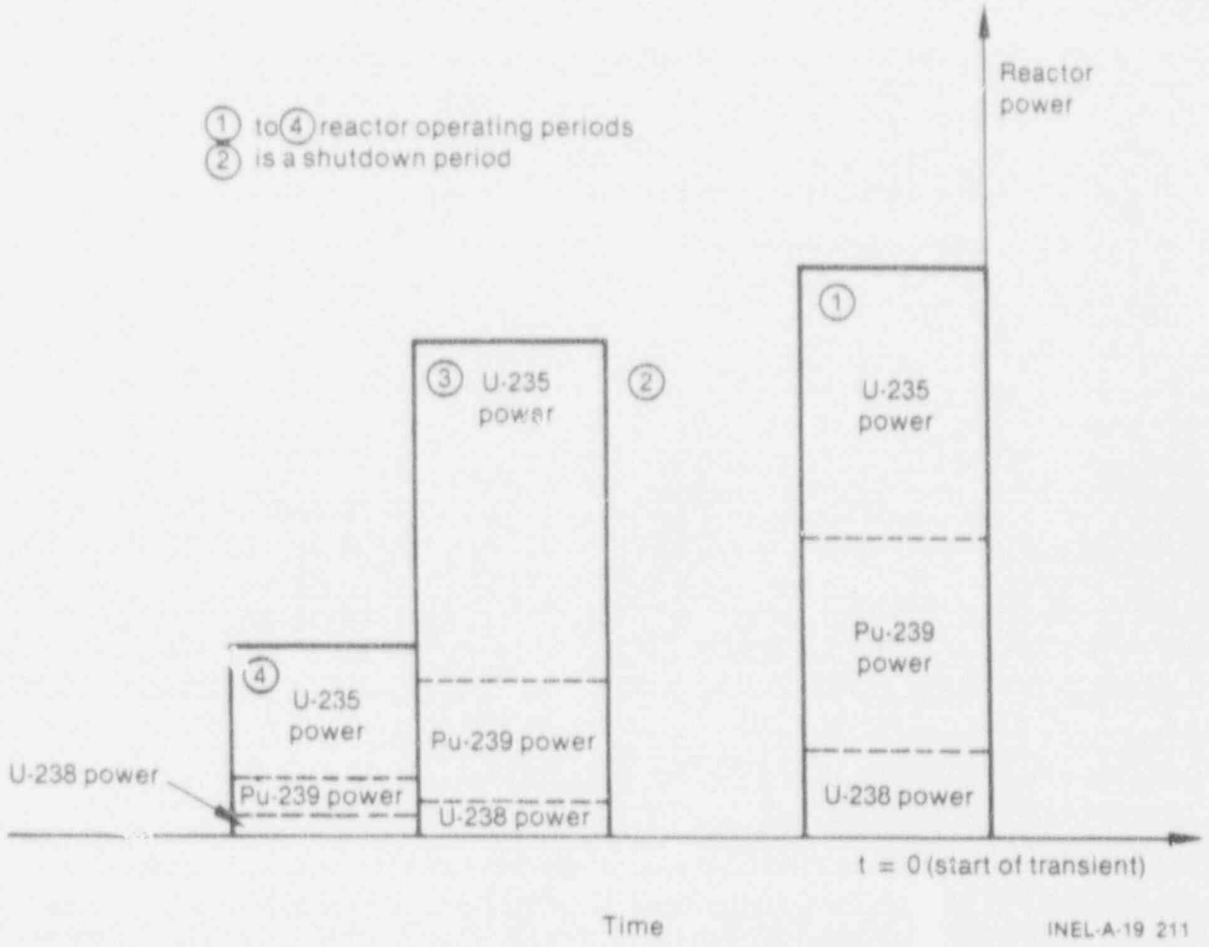

Figure 2.4-1. Typical reactor operating history.

$$\frac{dJ_{ij}}{dt} = 0 = -\lambda^{H}_{ij} H_{ij} + E_{ij}\frac{P_i}{Q} \quad . \tag{2.4-67}$$

In the new ANS standard, j ranges from 1 to 23, while the upper limit on i can be 1, 2, or 3, depending on the number of fissile isotopes being considered, and Q is the total energy per fission. If a reactor power history (consisting of IPOWH operating periods) is input, the decay heat for each decay group is calculated from

$$H_{ij} = \sum_{k=1}^{IPOWH} \frac{E_{ij} P_{ik}}{Q\lambda^{H}_{ij}} \left(1 - e^{-\Delta t_k \lambda^{H}_{ij}}\right) e^{-\lambda^{H}_{ij} \sum_{n=1}^{i} \Delta t_n} \tag{2.4-68}$$

where

Δt_k = duration of operating period k

P_{ik} = power due to isotope i during period k.

The two optional models used with the fission product decay heat, neutron capture, and heavy element decay heat also are initialized differently depending on whether a power history is input. The neutron capture effect is dependent on the burnup ratio of the core and the time elapsed since reactor shutdown. The burnup ratio (ψ) is defined as the total number of fissions (over the core history) divided by the initial number of fissile atoms in the core. The model is recommended only for burnup ratios of <3 fissions per fissile atom and for shutdown times < 10^4 s. In general, it results in <1% increase in decay heat power. If no power history is input, the code assumes a one-year core operation at the input power level and calculates the fissions occurring during that time period at the input power level to derive the burnup ratio of the core. From this burnup ratio, the correction multiplier for the neutron capture effect can be calculated as

$$G^H = 1.-0 + 3.24 \times 10^{-6} \Delta t(1)^{0.4} \psi \tag{2.4-69}$$

where $\Delta t(1)$ is taken to be one year.

If a power history is input, the equation for G^H becomes

$$G^H = 1.0 + \sum_{k=1}^{IPOWH} \left(3.24 \times 10^{-6} + 5.23 \times 10^{-16} \sum_{j=1}^{k} \Delta t_j \right) \Delta t_k^{0.4} \psi_k \tag{2.4-70}$$

where

$$\psi_k = \sum_{i=k+1}^{IPOWH} \frac{\Delta t_k \sum_{\ell=1}^{n_f} P_{k\ell}}{FISSAT\ (3.204 \times 10^{-17})} \tag{2.4-71}$$

and FISSAT is the total number of fissile atoms in the core.

Heavy element decay heat is also initialized differently depending on whether a power history is input. If no power history is input,

$$P_{HE} = P(E_{U239} + E_{N239}) \frac{R_p}{Q} \tag{2.4-72}$$

where E_{U234} and E_{N239} are power fractions due to those isotopes, and R_p is the number of atoms of ^{239}U produced per fission. If a power history table is input, the initialization algorithm becomes

$$P_{HE_{t=0}} = \frac{E_{U239}R_p}{Q}\sum_{i=1}^{IPOWH}\left[\left(1 - e^{-\lambda_{H1}\Delta t_i}\right)e^{\left(-\lambda_{H1}\sum_{j=1}^{i}\Delta t_j\right)}\sum_{k=1}^{n_f}R_{ik}\right]$$

$$+\frac{E_{N239}R_p}{Q}\sum_{i=1}^{IPOWH}\left[\frac{\lambda_{H1}}{\lambda_{H1}-\lambda_{H2}}\left(1 - e^{-\lambda_{H2}\Delta t_i}\right)e^{\left(-\lambda_{H2}\sum_{j=1}^{i}\Delta t_j\right)}\right.$$

$$\left.-\left(\frac{\lambda_{H2}}{\lambda_{H1}-\lambda_{H2}}\right)\left(1 - e^{-\lambda_{H1}\Delta t_i}\right)e^{\left(-\lambda_{H1}\sum_{j=1}^{i}\Delta t_j\right)}\right]\sum_{k=1}^{n_f}P_{ik} \qquad (2.4\text{-}73)$$

and λ_{H1} and λ_{H2} are time constants associated with the decay of ^{239}U and ^{239}Np.

After the transient begins, fission product decay heat is calculated from

$$\frac{dH_{ij}}{dt} = -\lambda_{ij}^{H}H_{ij} + E_{ij}\frac{P_i}{Q} \; . \qquad (2.4\text{-}74)$$

This is solved using a 4th order Runge-Kutta-Gill technique. The neutron capture effect is calculated from

$$G^H = 1.0 + \left[3.24 \times 10^{-6} + 5.23 \times 10^{-10}\Delta t_{tran}\left(\sum_{k=1}^{IPOWH}\Delta t_k\right)^{0.4}\right]\psi \; . \qquad (2.4\text{-}75)$$

Since the transient normally contributes an insignificant change to ψ, this parameter is not updated during the transient.

The heavy element decay heat is changed during the transient according to

$$P_{HE} = \frac{PR_p}{Q}\left\{E_{U239}\left[1 - e^{-\lambda_{H1}\left(\sum_{i=1}^{IPOWH}\Delta t_k + T_{DOWN}\right)}\right]e^{-\lambda_{H1}\Delta t_{tran}}\right.$$

$$- \frac{E_{N239}}{\lambda_{H1} - \lambda_{H2}} \left[1 - e^{-\lambda_{H2}\left(\sum_{i=1}^{IPOWH} \Delta t_k + T_{DOWN} \right)} \right] e^{-\lambda_{H2}\Delta t_{tran}}$$

$$- \lambda_{H2} \left[1 - e^{-\lambda_{H1}\left(\sum_{i=1}^{IPOWH} \Delta t_k + T_{DOWN} \right)} \right] \Bigg\} e^{-\lambda_{H1}\Delta t_{tran}} . \qquad (2.4\text{-}76)$$

If the reactor core is still producing significant fission power, $\Delta t_{tran} = 0$ and two terms in this equation may be omitted.

The total decay heat power, including the user-input arbitrary multiplier, DH, is

$$P_{DH} = D_H \left(G^H \sum_{j=1}^{23} \sum_{k=1}^{n_f} H_{jk} + P_{HE} \right) \qquad (2.4\text{-}77)$$

which is then added to the prompt fission power in place of

$$\sum_{i=1}^{n_f} \sum_{j=1}^{m} H_{ij} \qquad (2.4\text{-}78)$$

in Equation (2.4-4) to give the instantaneous net reactor power.

2.4.4 References

2.4-1. S. Gill, "A Process for the Step-by-Step Equation Integration of Differential Equations in an Automatic Digital Computer Machine," *Proceedings of the Cambridge Philos. Society*, *47*, 1951, pp. 96-108.

2.4-2. R. S. Thompson, "Improving Roundoff in Runge-Kutta Computations with Gill's Method," *Private Communication of the ACM L3*, *12*, December 1970.

2.4-3. J. R. Carew, D. J. Diamond, and M. Todosow, *Spatial Significance of Doppler Reactivity Feedback*, BNL-NUREG-23709, 1979.

2.4-4. J. R. Lamarsh, *Introduction to Nuclear Reactor Theory*, Massachusetts: Addison-Wesley Publishing Co., Inc., 1966, pp. 534-541.

2.4-5. H.-S. Cheng et al., *A Dynamic Analysis of BWR Scram Reactivity Characteristics*, BNL-NUREG-50584, December 1976.

2.4-6. D. W. Nigg, *Two-Dimensional Nodal Neutronic Routines for the TRAC-BD1 Thermal-Hydraulics Program*, EGG-PBS-6372, September 1983.

2.4-7. R. A. Shober et al., "Two Nodal Methods for Solving Time-Dependent Group Diffusion Equations," *Nuclear Science and Engineering*, 64, 1977, pp. 582-592.

2.4-8. J. A. Borkowski and N. L. Wade, Eds., *TRAC-BF1/MOD1 Models and Correlations*, NUREG/CR-4391, EGG-2680, August 1992.

2.4-9. ANS Standards Working Group, "ANS-5.1: Decay Heat Power in Light Water Reactors," ANS, ANSI/ANS-5.1-1979, August 1979.

3. COMPONENT MODELS

Descriptions of the various component models included in TRAC-BF1/MOD1 are given in this section. A physical description of each component is presented with a typical TRAC/BF1/MOD1 noding diagram showing the conventions used to model the component. Mathematical models including finite-difference approximations are given only for those aspects of the component that are not already covered in the basic hydrodynamics and heat-transfer descriptions. User options, restrictions on the use of the component, subroutines used by the component, and input/output information are also given.

3.1 PIPE

The PIPE component models the flow in a one-dimensional duct or pipe. PIPE can be used alone in a problem or it can be used as a connector between components to model a reactor system. The capability is provided to model area changes, wall heat sources, and heat transfer across the inner and outer wall surfaces. A wide selection of pipe materials is available to represent the wall material in the wall conduction calculation.

Figure 3.1-1 shows a typical noding diagram for a pipe containing a Venturi tube and an abrupt area change. The numbers within the pipe indicate cell numbers, and those above indicate cell boundary numbers. The geometry is specified by providing a volume and length for each cell and a flow area and hydraulic diameter at each cell boundary. The junction variables, JUN1 and JUN2, provide reference numbers for connecting a PIPE to other components. The numerical methods used to treat the thermal-hydraulics in PIPE are described in Subsection 2.3.

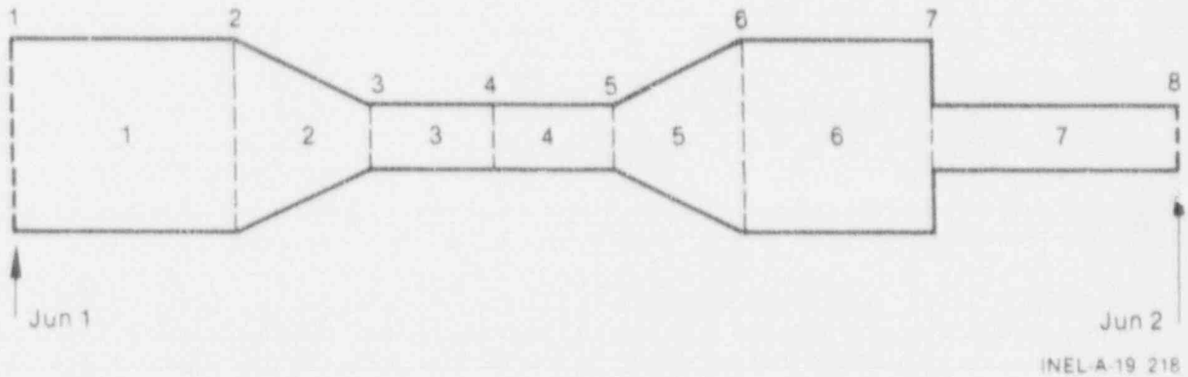

Figure 3.1-1. PIPE noding diagram.

Input options are available to allow for wall heat transfer and to select correlations for CHF. Wall heat transfer can be omitted by setting the number of heat-transfer nodes (NODES) to zero. The CHF calculation can be bypassed by setting the input parameter, ICHF, to a negative value.

Wall friction losses requires a wall roughness input by the user. An abrupt area change can be modeled by input of additional pressure loss factors. Because of backward differencing, a loss factor of 0.5 is inherent in the numerical scheme.

PIPE components may be connected to any other component. However, computational expense increases rapidly with the number of component junctions and the user is cautioned to minimize the number of components used in his model. In addition, one-dimensional cells of grossly different length should not be placed together, as this can cause computational difficulties particularly when area changes also occur.

TRAC-BF1/MOD1 also includes a number of PIPE component options. Generalized heat and mass transfer capabilities allow the user to specify heat and/or mass exchange between any PIPE cell and any other component fluid cell or wall node in the model. The generalized heat transfer option is activated through the IHTS and IWT parameters. The generalized mass transfer option is accessed through the generalized leak path logic described in Subsection 2.3.3. Both options are common to all one- and three-dimensional component models.

Detailed input for the PIPE module, described in Volume 2, is processed by Subroutines FPIPE and REPIP. Subroutine FPIPE reads input data from the input file. Subroutine REPIP reads corresponding data from the restart file. Initialization of remaining variables is performed with Subroutine IPIP. This subroutine establishes the noding for wall heat transfer, sets the remaining fluid properties by calls to THERMO and FPROP, and initializes the boundary data by a call to J1D.

During problem execution, the solution procedure is controlled by Subroutines PIP1, PIP2, and PIP3. At the beginning of each time step, PIP1 calls PRP1D, which in turn calls MPROP, for wall-metal properties, and HTP1P for wall HTCs. During the iterations for a time step, PIP2 calls INNER, which calls JF1D to initiate the hydrodynamic solution. PIP3 updates the wall temperatures, computes new fluid properties (viscosity, heat capacity, and surface tension), and resets the boundary arrays. These functions are executed with a call to PST1D, which subsequently calls THERMO, CYLHT, MIXPRP, and FPROP. If the time step fails to converge, THERMO is called to restore variables to their old values.

Output for a PIPE is managed by Subroutine WPIP. WPIP prints the component number, junction numbers, mass flow rate in and out of the pipe, mass flux in and out of the pipe, pressure, void fraction, liquid and vapor velocities, saturation temperature, liquid and vapor temperatures, liquid and vapor density, cell-to-cell pressure drop, choking, and CCFL counters. If wall heat transfer is included (NODES = 0), information on the heat-transfer

regime, liquid and vapor HTC on inner and outer surfaces, surface heat fluxes to liquid and vapor on the inner wall surface, and heat sources and wall temperatures for each radial node are printed for each axial cell. For an extracted run, the extracted input is written in Subroutine WEPIP.

3.2 BREAK AND FILL

The BREAK and FILL modules are used to impose boundary conditions at any one-dimensional component terminal junction. Consequently, these modules differ from the other component modules in that they do not model any system component per se or perform hydrodynamic or heat-transfer calculations. However, they are treated like any other component with respect to input, initialization, and identification procedures.

The BREAK module implies a pressure boundary condition one cell away from its adjacent component, as shown in Figure 3.2-1. This boundary condition may be constant, user-specified time-dependent or it may be set by the control system or containment models. The BREAK component also supplies the boundary conditions of void fraction and phase temperatures at the terminal junctions of one-dimensional components.

The FILL module imposes a velocity boundary condition one cell away from its adjacent component, as shown in Figure 3.2-2. Like the BREAK module, FILL boundary conditions of velocity, void fraction, and phase temperatures may be constant, user-specified time-dependent, or they may be set by the control system or containment models. In addition, the FILL velocity condition may be specified as a function of adjacent component pressure. (In this case, the pressure functions are imposed in an approximate manner that avoids numerical difficulties caused by instabilities.)

The parameters needed for specifying a FILL or BREAK are described in Volume 2. It is recommended that the cell volume and length in these components be identical to those for the neighboring cell of the adjacent component. The void fraction and fluid temperatures specified in the FILL and BREAK determine the properties of fluid convected into the adjacent component if an inflow condition should occur. (By convention, inflow corresponds to a positive FILL velocity and a negative BREAK velocity.) These components may not be connected directly to the VESSEL component.

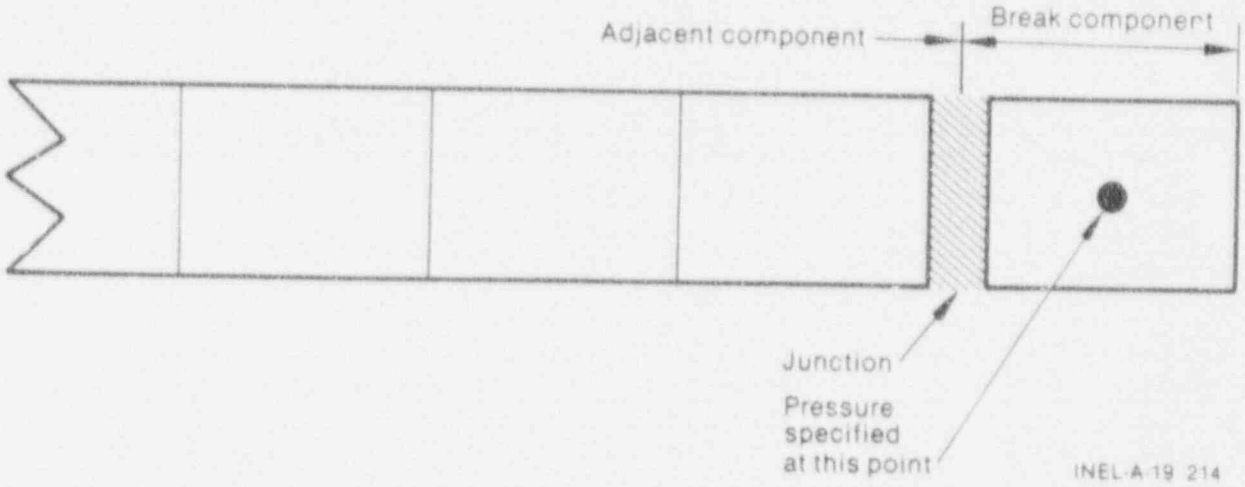

Figure 3.2-1. BREAK noding diagram.

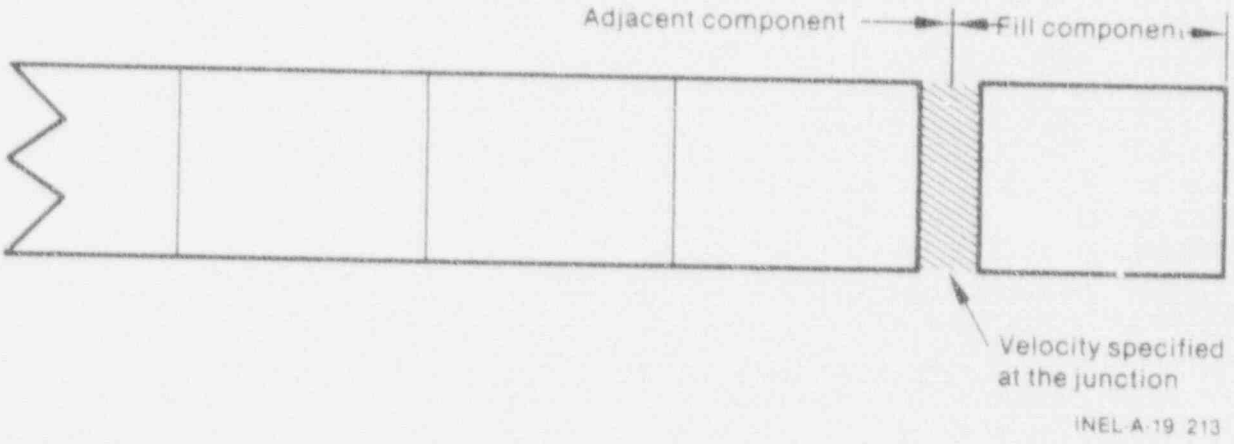

Figure 3.2-2. FILL noding diagram.

3.3 CHAN

The CHAN component has been developed to simulate one or more BWR fuel rod bundles and channel walls. CHAN is a TRAC/BF1/MOD1 PIPE component in which fuel rod heat transfer and channel wall heat transfer models have been added. The CHAN can be used to simulate a single bundle or several bundles in a stand-alone mode in which boundary conditions to the CHAN are supplied by BREAK and FILL components. This capability is quite useful for performing hot bundle analysis or for investigating single bundle experiments. The CHAN component can also be used to simulate rod bundles in a BWR core region.

To model a BWR core, CHAN components would be connected across the usual core region of a VESSEL component. The connections are made with standard VESSEL sources (see VESSEL component description). The three-dimensional hydrodynamics solution in the core region of the VESSEL component would be for the flow in the region outside the BWR channels but inside the core barrel. A typical noding scheme for a BWR vessel is illustrated in Figure 3.3-1. For this nodalization, six CHAN components are used to simulate all fuel bundles in the BWR core region. Within each CHAN component, five rod groups are chosen to model radiation heat transfer. This noding scheme allows for fine nodalization in the radial direction of the core without increasing the number of VESSEL nodes.

The fuel rod and channel wall heat transfer models include a detailed radiation heat transfer (see Subsection 2.2.3), and a bottom-up and top-down quench front (see Subsection 2.2.4) for each rod group as well as for the inside of the channel wall. Heat transfer on the outside of the channel wall is coupled to the VESSEL hydrodynamics solution.

Flow through leakage paths between the fuel bundles and the core bypass region is represented with the generalized mass transfer model. In addition, the CHAN component may transfer heat to any other component in the TRAC/BF1/MOD1 model (except FILL or BREAK components) by use of the generalized heat transfer option.

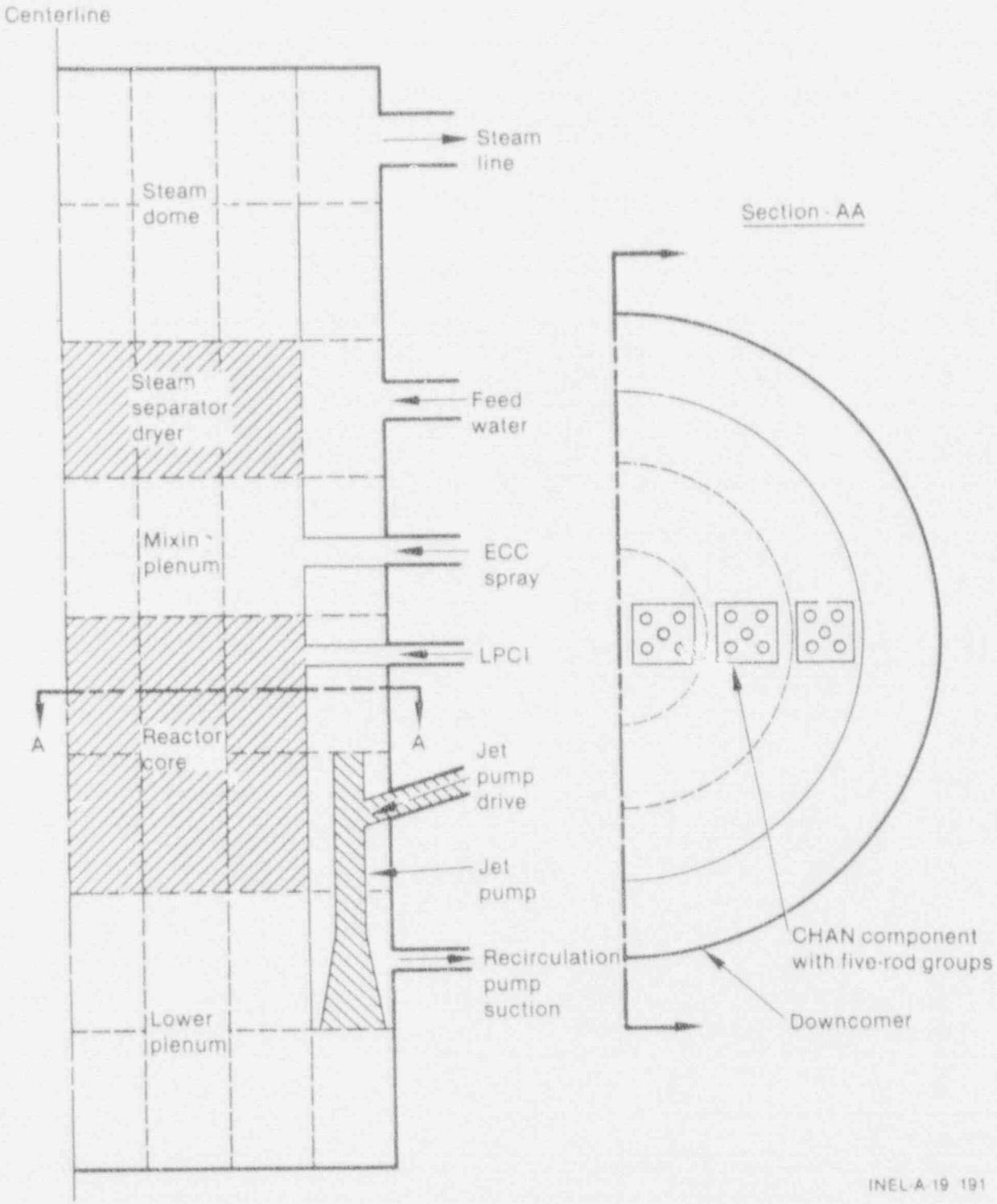

Figure 3.3-1. TRAC-BF1/MOD1 reactor nodalization showing CHAN components.

3.4 PUMP

The PUMP module describes the interaction of the system fluid with a centrifugal pump. The model calculates the pressure differential across the pump and its angular velocity as a function of the fluid flow rate and the fluid properties. The model can treat any centrifugal pump and allows for inclusion of head degradation caused by two-phase effects.

The PUMP model is represented by a one-dimensional component with N cells (N > 1). Figure 3.4-1 shows a typical noding diagram for the PUMP component. The pump momentum is modeled as a source, called SMOM. In older versions, SMOM was required to act between cells 1 and 2. In TRAC-BF1/MOD1, SMOM may act on any interior face. Therefore, it is necessary to construct the cell noding such that the cell numbers increase in the normal flow direction.

The first two criteria precluded the use of a lumped-parameter model. Because the adjacent components are usually described by PIPE modules based on a one-dimensional, two-fluid model, the PUMP is treated likewise. The resulting PUMP module, therefore, combines the PIPE module with pump correlations. The PUMP model is identical to the one-dimensional PIPE model except that the momentum equations at the SMOM face are rewritten as

$$\frac{V_\ell^{n+1} - V_\ell^n}{\Delta t} = \frac{P_1^{n+1} - P_2^{n+1} + \Delta P^n + \left(\frac{\partial \Delta P}{\partial V}\right)^n \left(V_\ell^{n+1} - V_\ell^n\right)}{\rho_m \Delta x} - g \cos\theta \qquad (3.4\text{-}1)$$

and

$$V_g = V_\ell \qquad (3.4\text{-}2)$$

where ΔP is the pressure rise through the pump evaluated from the pump correlation. The steady-state solution of Equation (3.4-1 is

$$\Delta P = P_2 - P_1 + g \cos\theta \qquad (3.4\text{-}3)$$

which is the desired result. Friction does not enter explicitly into the pump motion equation. Therefore, additive friction is not allowed at the SMOM face [FKLOS(2) = 0.0].

It is necessary to evaluate ΔP and its derivative with respect to velocity for a pump cell only once each time step. The source is needed only in Routine TF1E. This evaluation is performed by Subroutine PMPS.

Pump characteristic curves describe the pump head and torque response as a function of fluid volumetric flow rate and pump speed. Homologous curves (one curve segment represents a family of curves) are used for this

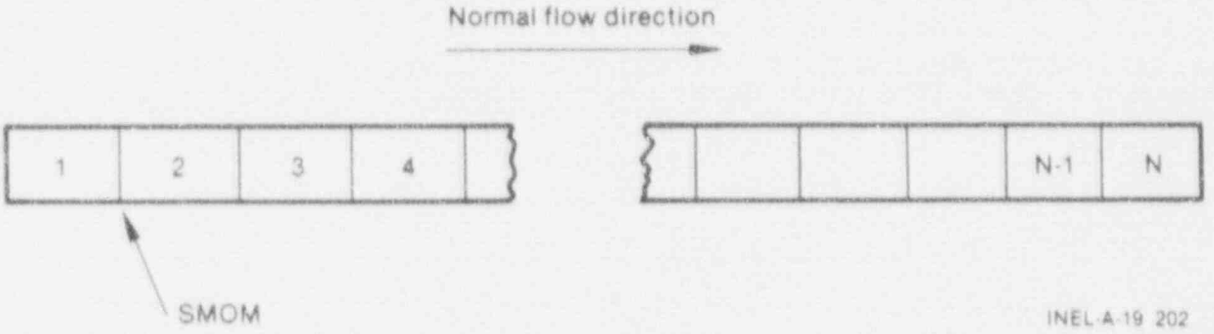

Figure 3.4-1. PUMP noding diagram.

description because of their simplicity. These curves describe, in a compact manner, all operating states of the pump obtained by combining positive or negative impeller velocities with positive or negative flow rates.

To account for two-phase effects on pump performance, the pump curves are divided into two separate regimes. Data indicate that two-phase pump performance in the vapor fraction range of 20 to 80% is degraded significantly in comparison with its performance at vapor fractions outside of this range. One set of curves describes the pump performance for single-phase fluid (void fraction 0.0 or 1.0), and another set describes it for two-phase fluid. The pump head at any vapor fraction is calculated from the relationship

$$H = H_1 - m(\alpha)(H_1 - H_2) \qquad (3.4\text{-}4)$$

where

H = total pump head

H_1 = pump head from the single-phase homologous curves

H_2 = pump head from the fully degraded homologous curves

m = pump degradation multiplier

α = vapor fraction.

The two-phase hydraulic torque is treated similarly. The following definitions are used in the subsequent development.

H = pump head = $\Delta P/\rho$

Q = pump volumetric flow rate

Ω = pump impeller angular velocity

where ΔP is the pump differential pressure and ρ is the pump inlet density. To allow one set of curves to be used for a variety of pumps, the following normalized quantities are used:

$$h = \frac{H}{H_R} \tag{3.4-5}$$

$$q = \frac{Q}{Q_R} \tag{3.4-6}$$

$$w = \frac{\Omega}{\Omega_R} \tag{3.4-7}$$

where the subscript, R, denotes the rated condition. The pump similarity relations[3.4-1] show

$$\frac{h}{w^2} = f\left(\frac{q}{w}\right) . \tag{3.4-8}$$

For small w, this correlation is not satisfactory and the following combination of variables is used

$$\frac{h}{q^2} = f\left(\frac{w}{q}\right) . \tag{3.4-9}$$

The first correlation is used in the range $0 < q/w \leq 1$ and the second is used in the range $0 < w/q \leq 1$. The four resulting curve segments, as well as the curve selection logic used in TRAC-BF1/MOD1, are shown in Table 3.4-1.

The dimensionless hydraulic torque is defined by

$$\beta = \frac{T_{hy}}{T_R} \tag{3.4-10}$$

where T_{hy} is the hydraulic torque and T_R is the rated torque. The single-phase torque, T, is dependent on the fluid density and is calculated from

Table 3.4-1. Definitions of the four curve segments that describe the homologous pump curves.

Curve Segment	q/w	w	q	Correlation
1	≤1	>0		$\frac{h}{w^2} = f\frac{q}{w}$
4	≤1	<0		
3	>1		<0	$\frac{h}{q^2} = f\frac{w}{q}$
2	>1		≥0	

$$T = \beta T_R \left(\frac{\rho}{\rho_R}\right) \tag{3.4-11}$$

where ρ is the pump inlet density and ρ_R is its rated density. The density ratio multiplier is needed to correct for the density difference between the pumped fluid and the rated condition. For two-phase conditions, the impeller torque is calculated from

$$T = T_1 - N(\alpha)(T_1 - T_2) \tag{3.4-12}$$

where T is the total impeller torque, T_1 is the impeller torque from the single-phase homologous curves, T_2 is the impeller torque from the fully degraded homologous curves, and $N(\alpha)$ is the torque degradation multiplier. The homologous, normalized, torque curve segments are correlated in the same manner as the head curve segments shown in Table 3.4-1.

In addition to the homologous head and torque curves, the head and torque degradation multipliers defined in Equations (3.4-4) and (3.4-12) are needed. These functions are usually nonzero only in the vapor-fraction range where the pump head and torque are either partially or fully degraded.

The pump module treats the pump angular velocity as a constant (input) while its motor is energized. After a drive motor trip, the time rate of change for the pump motor assembly is proportional to the sum of the moments acting on it and is calculated from

$$I\frac{d\Omega}{dt} = \sum_i T_i = T_m - (T + T_f + T_B) \tag{3.4-13}$$

where I is the pump motor assembly moment of inertia, T is the impeller

torque, T_f is the torque caused by friction (constant), T_b is the bearing and windage torque, and T_m is the applied motor torque. We assume that T_b is

$$T_b = C \frac{\Omega |\Omega|}{\Omega_R^2} \tag{3.4-14}$$

where C is an input constant and Ω_R is the rated impeller angular velocity. T_f is multiplied by $\Omega/|\Omega|$ so that it also changes sign if the speed reverses. The impeller torque is evaluated using the homologous torque curves and Equation (3.4-12); it is a function of the fluid density and flow rate as well as the pump angular velocity. T_m is defined through the control system. It is initially set to zero and retains that value unless the control system changes it to a nonzero value. For time step (n+1), Equation (3.4-13) is calculated implicitly

$$\Omega^{n+1} = \frac{\Omega^n - \frac{\Delta t}{I}(T - T_m)}{1 + \frac{\Delta t}{I}\left(\frac{T_f}{|\Omega^n|} + C \frac{|\Omega^n|}{\Omega_R^2}\right)} . \tag{3.4-15}$$

The wall heat transfer, wall friction, CHF calculation, and implicit hydrodynamics options are the same for the PUMP module as for the PIPE module. In addition, the following options are specified: pump type, motor action, reverse speed, two-phase, and pump curve. The input variables, IPMPTR and NPMPTX, specify the trip identifier for the pump trip initiation and the number of pairs of points in the pump-speed table (SPTBL), respectively. If IPMPTR = 0, no pump trip action occurs (a constant speed pump).

If the pump motor is energized, its angular velocity is assumed to be the constant value specified. If the motor is not energized, a pump coastdown calculation is performed using the specified initial pump speed.

There are three pump options available (IPMPTY = 1, 2, or 3). For pump Option 1 (IPMPTY = 1), the pump speed variation is specified by input. The pump is energized initially at a constant speed specified by input (OMEGA). The pump motor may be tripped by a TRIP signal. If a pump trip has occurred, the pump speed is taken from a pump speed-versus-time table (array SPTBL). Pump Option 2 (IPMPTY = 2) is similar to Option 1 except a speed table is not input. Instead, the pump speed is calculated from Equation (3.4-15) after a trip has occurred. Pump Option 3 (IPMPTY = 3) allows the pump speed to be calculated by the control system.

If the reverse speed option is specified (IRP = 1), the pump is allowed to rotate in the forward direction only. For this case, if negative rotation is calculated (after trip with pump Option 2), its speed will be set to zero.

If the two-phase option is turned on (IPM = 1), the degraded pump head and torque are calculated from Equations (3.4-4) and (3.4-12). If the

two-phase option is turned off (IPM = 0), only the single-phase head and torque homologous curves are used.

The user may specify pump homologous curves in the input or alternatively use the built-in pump curves. The built-in pump curves are based on the MOD-1 Semiscale system pump.[3.4-2,3,4] The single-phase head (HSP), fully degraded two-phase head (HTP), head degradation multiplier (M), single-phase torque (TSP), fully degraded two-phase torque (TTP), and torque degradation multiplier (N) curves are provided in Figures 3.4-2 through 3.4-7, respectively. Where applicable, the curves are numbered corresponding to the conditions provided in Table 3.4-1. Because these homologous curves are dimensionless, they can describe a variety of pumps by specifying the desired rated density, head, torque, flow, and angular velocities as input.

There are several restrictions and limitations in the current version of the PUMP module. Because there is no pump motor torque-versus-speed model, the pump speed is assumed to be input if the motor is energized. Pump noding is restricted such that the pump momentum source is located between Cells 1 and 2 of the pump model. Finally, the head degradation multiplier, $M(\alpha)$, and the torque degradation multiplier, $N(\alpha)$, are assumed to apply to all operating states of the pump.

The PUMP module input consists of the same geometric and hydrodynamic data and initial conditions required for the PIPE module. In addition, information specific to the pump is required, as described in the input specifications (Volume 2). The speed table (SPTBL) and homologous pump curve arrays must be input in the following order

$$x(1),y(1),x(2),y(2),\ldots,x(n),y(n)$$

Here, x is the independent variable and y is the dependent variable. Furthermore, the independent variables must be input in a monotone increasing order, that is

$$x(n) > x(n-1) > \ldots x(2) > x(1)$$

Linear interpolation is used within the arrays.

3.4.1 References

3.4-1. V. L. Streeter and E. B. Wylie, *Hydraulic Transients*, New York: McGraw-Hill Book Company, Inc., 1967, pp. 151-160.

3.4-2. D. J. Olsen, *Experiment Data Report for Single- and Two-Phase Steady State Tests of the 1-1/2-Loop MOD-1 Semiscale System Pump*, ANCR-1150, May 1974.

3.4-3. G. G. Loomis, *Intact Loop Pump Performance During the Semiscale MOD-1 Isothermal Test Series*, ANCR-1240, October 1975.

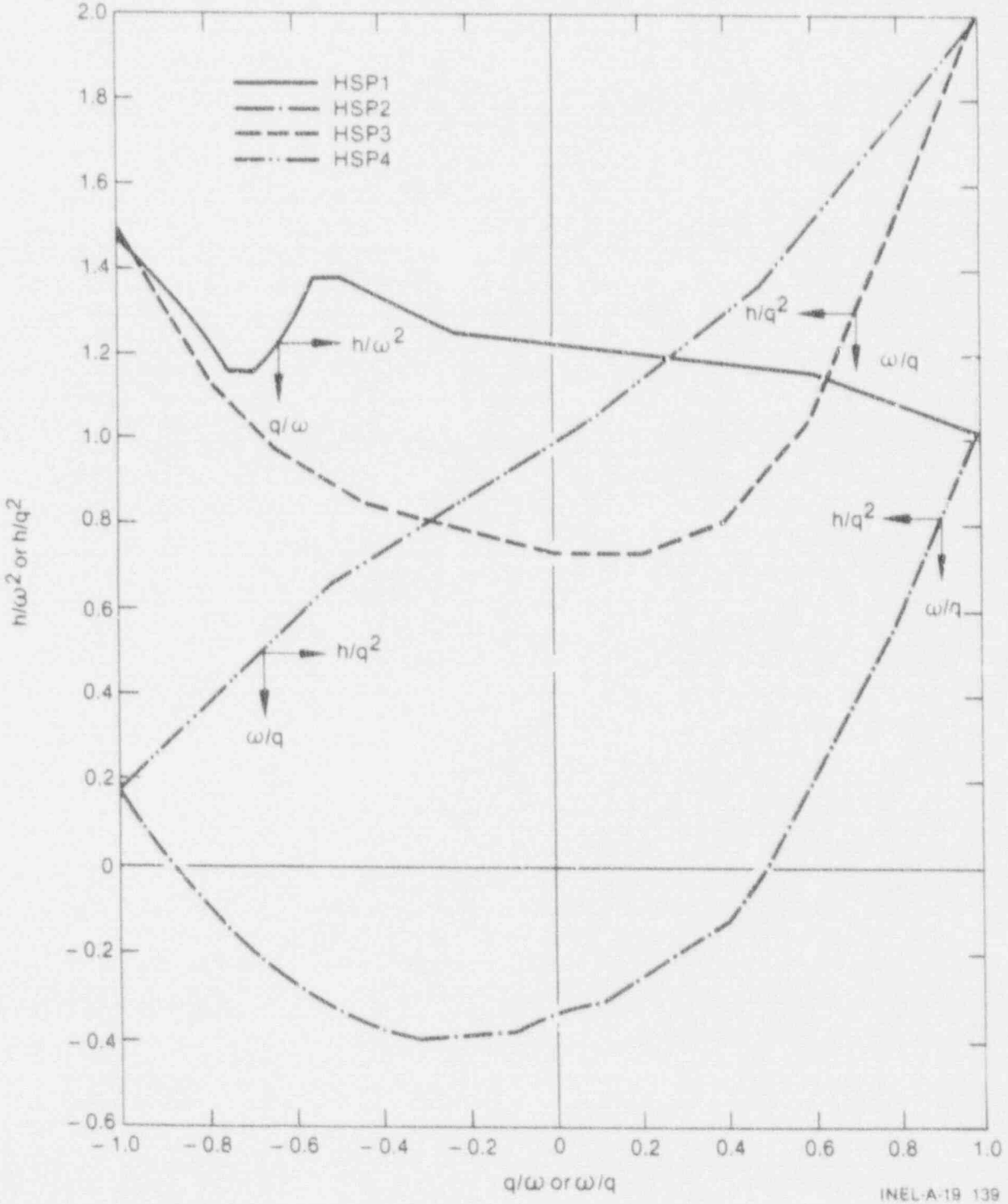

Figure 3.4-2. Single-phase homologous head curves.

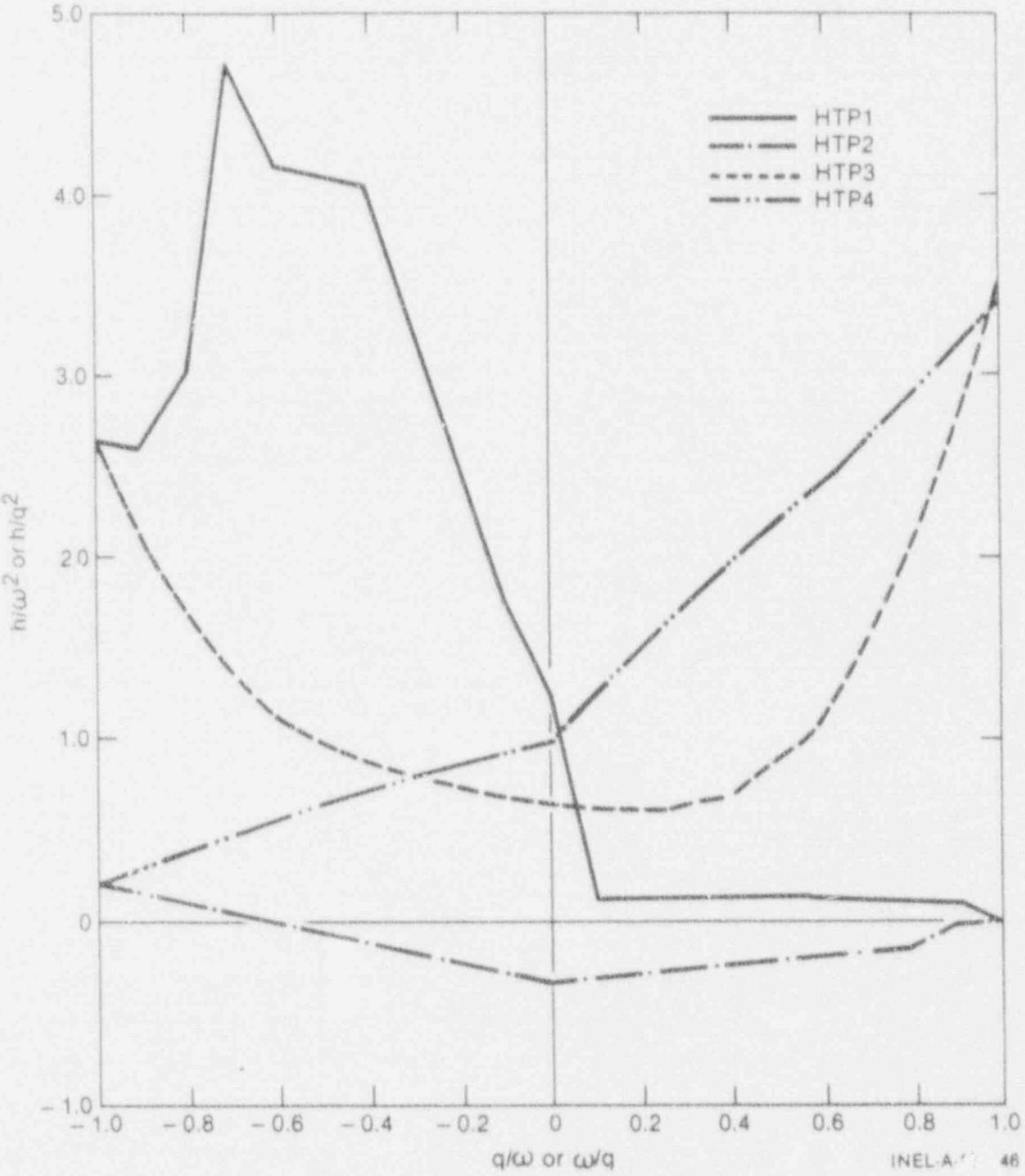

Figure 3.4-3. Fully degraded homologous head curves.

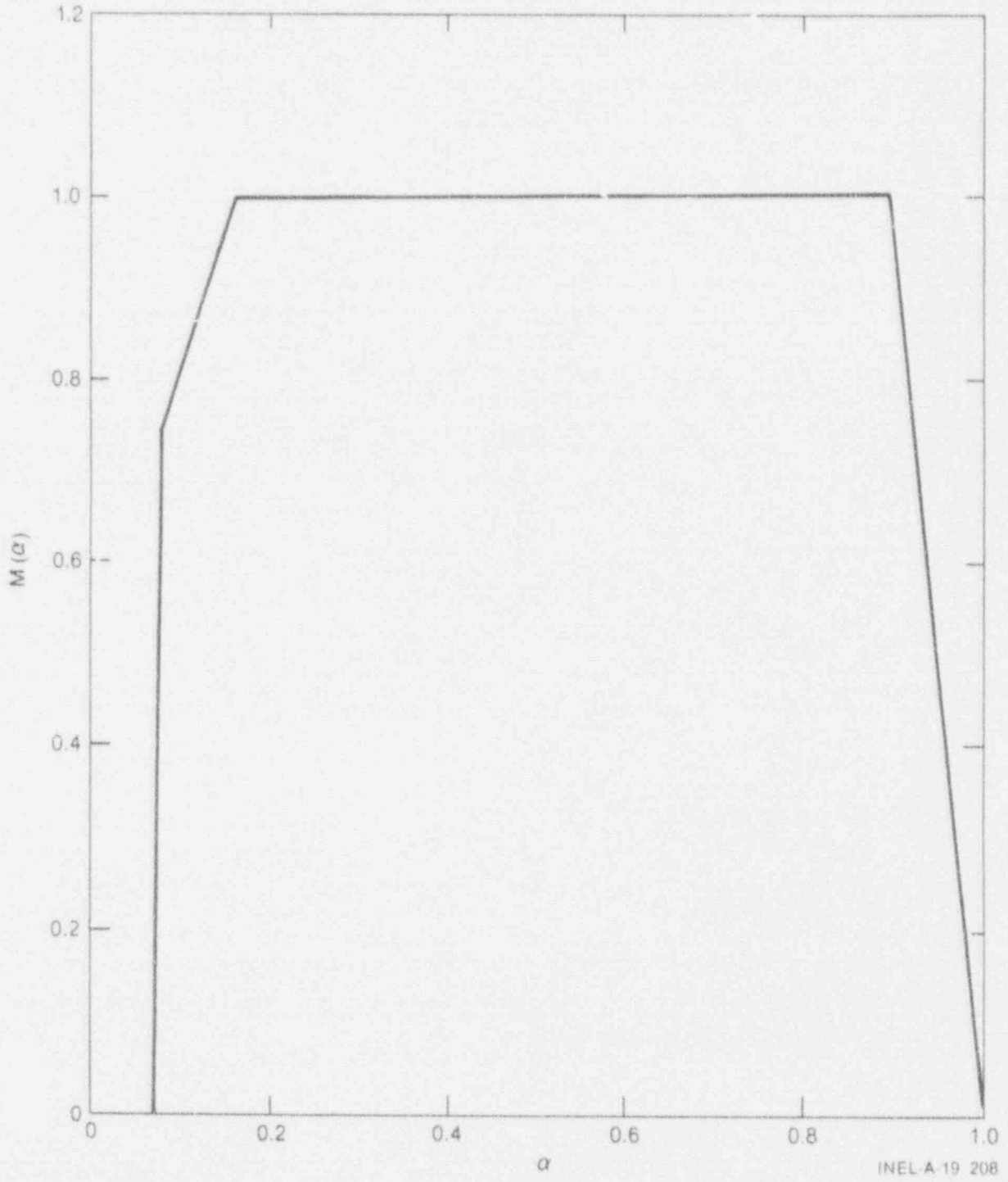

Figure 3.4-4. Head degradation multiplier.

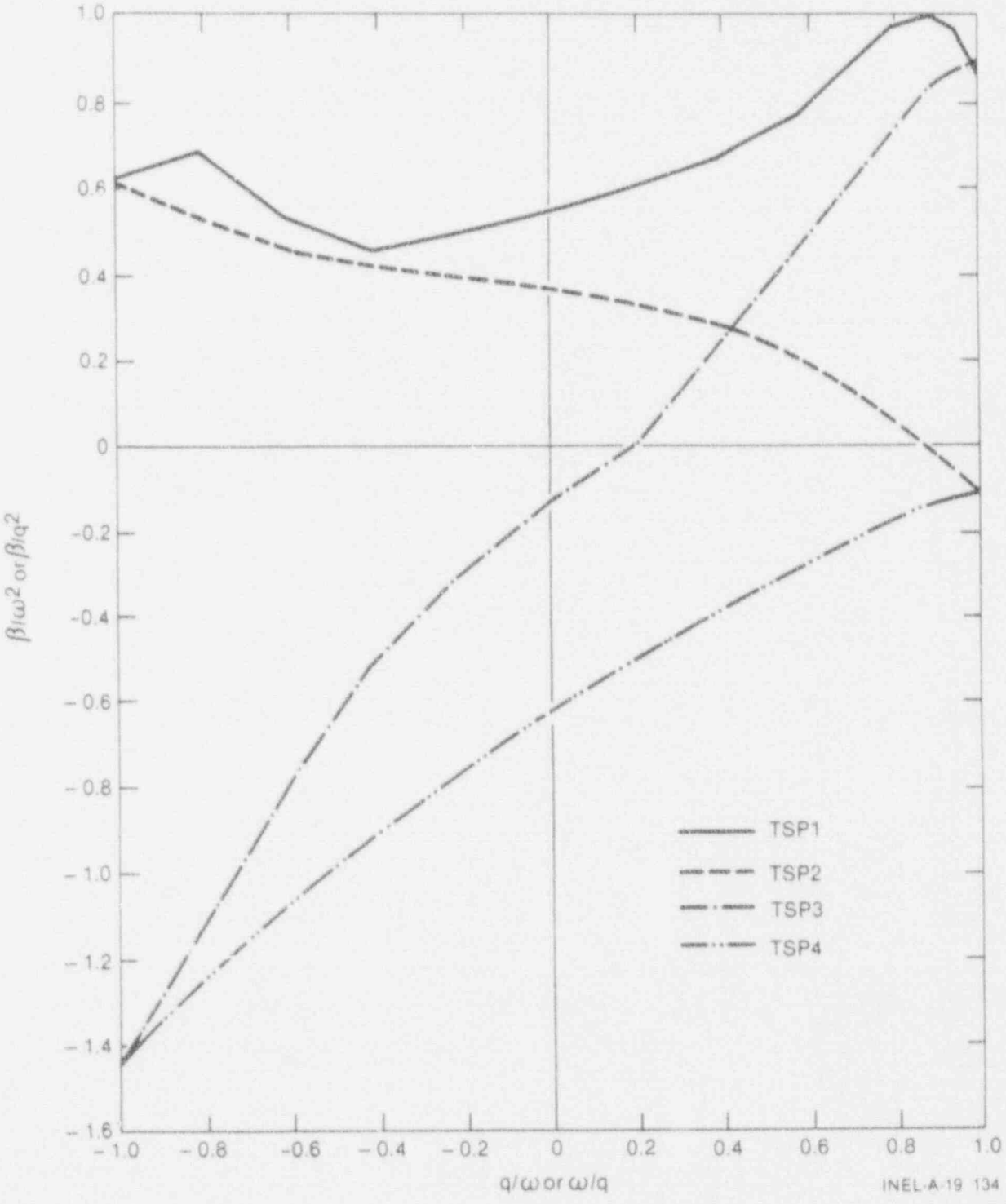

Figure 3.4-5. Single-phase homologous torque curves.

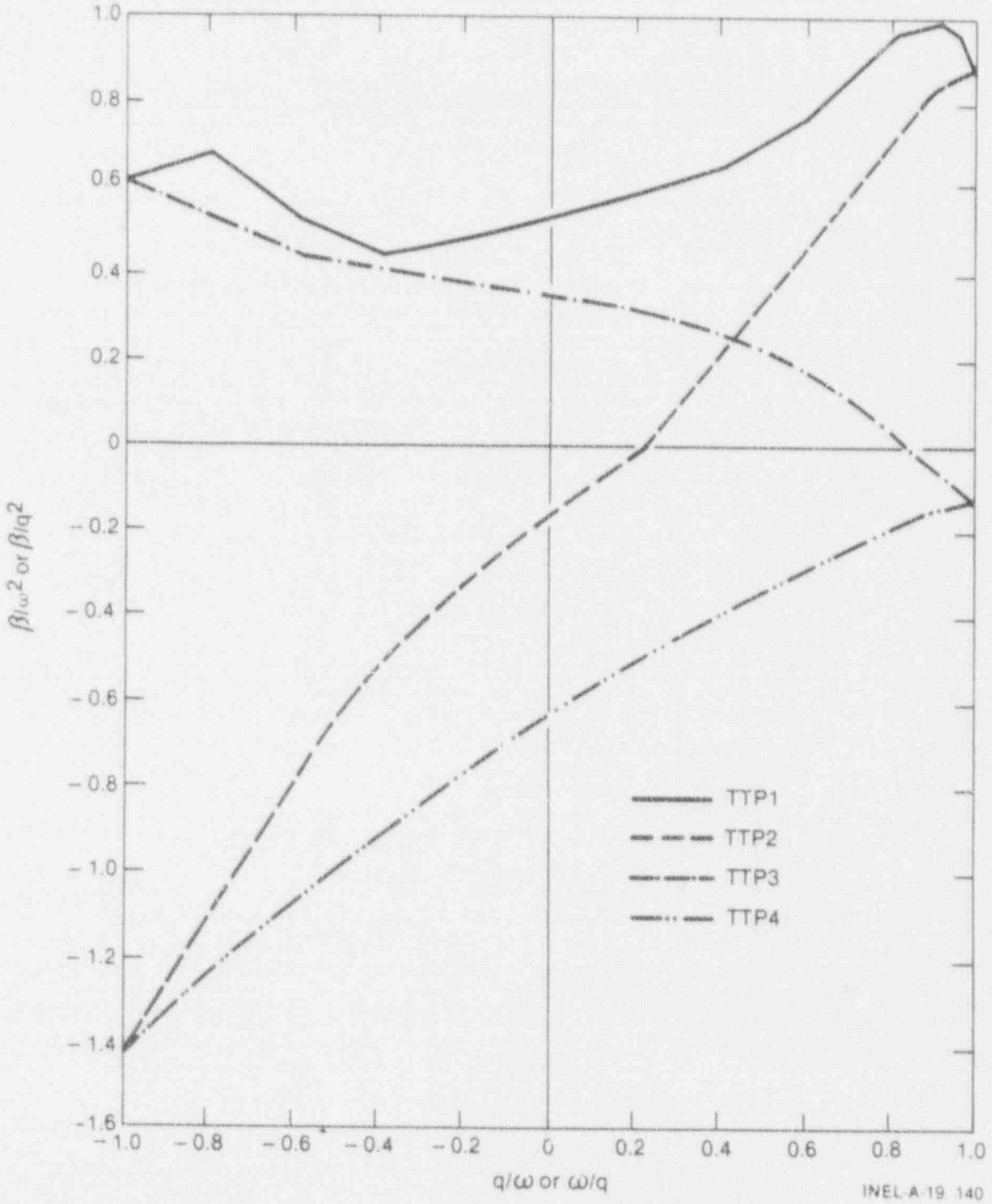

Figure 3.4-6. Fully degraded homologous torque curves.

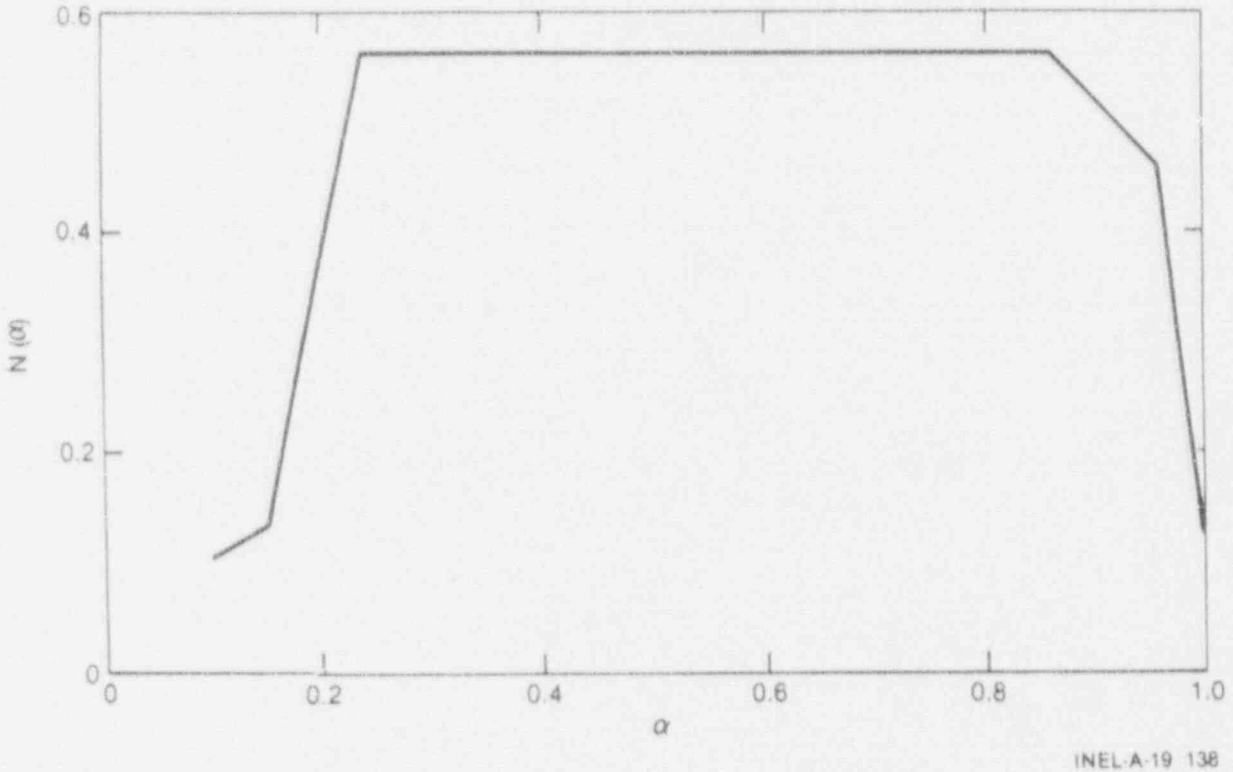

Figure 3.4-7. Torque degradation multiplier.

3.4-4. D. J. Olsen, *Single- and Two-Phase Performance Characteristics of the MOD-1 Semiscale Pump Under Steady State and Transient Fluid Conditions*, ANCR-1165, October 1974.

3.5 TEE

The TEE module models the thermal-hydraulics of three piping branches, two of which lie along a common line. The third enters at some angle from the main axis of the other two (see Figure 3.5-1). In the code, the TEE is treated as two pipes, as indicated in Figure 3.5-1. Beta is defined as the angle from the low-numbered end of PIPE1 to PIPE2. The low-numbered end of PIPE2 always connects to PIPE1. The first pipe extends from Cell 1 to Cell NCELL1 and connects to PIPE2 at Cell JCELL. The second pipe begins at Cell (NCELL1+2) and ends at Cell NCELL2.

The connection is effected through mass, momentum, and energy source terms in PIPE1. PIPE2 sees the connection as boundary conditions from Cell JCELL in PIPE1. The time differencing and iteration procedures are such that conservation of the scalar qualities is preserved (within a convergence tolerance) and the level of implicitness at the connection ensures that no additional stability limitations apply at a TEE. Because the junction between PIPE1 and PIPE2 is always treated partially implicitly, the velocity at that point is always included in the computation of the time step stability limit. Phase separation at the junction is not implemented.

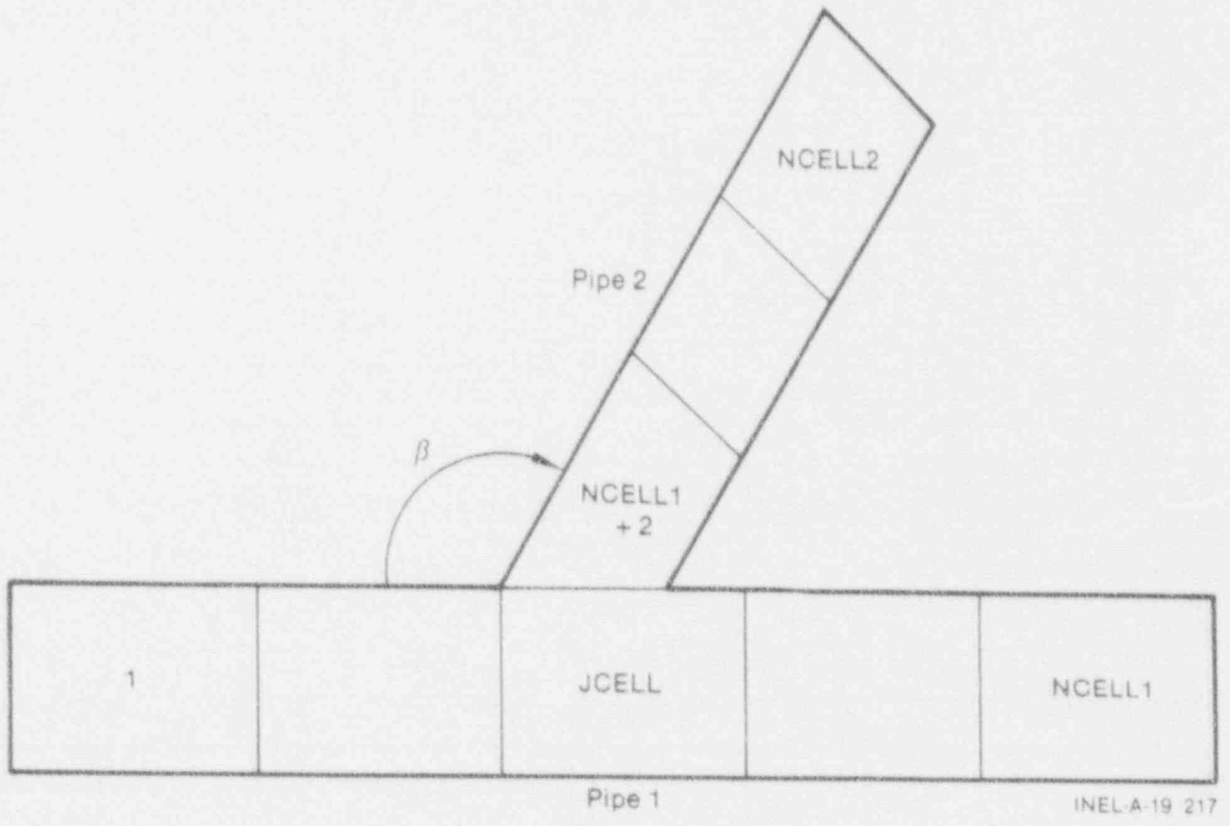

Figure 3.5-1. TEE noding diagram.

The momentum source term at PIPE1 due to PIPE2 is set to zero in the standard TEE component. In most applications of interest, the error incurred by so doing is small. In cases where this is not true, however, the user may use the JETP (jet pump) module in place of the TEE. This module is a special type of TEE in which certain assumptions have been made regarding the normal flow direction and in which the momentum source term in PIPE1 is not neglected (see JETP description).

Because the TEE is modeled as essentially two interconnected pipes, the PIPE model description in Subsection 3.1 should be referenced for additional information on the calculational sequence. The sequence for a TEE includes separate calculations of the primary and secondary sides.

Detailed input specifications for a TEE component are given in Volume 2. Input and output information is very similar to that for a PIPE component except that two pipes are involved in a TEE component.

3.6 JETP

This model is based on the TEE component; however, modifications have been made to include the momentum source term for the junction cell and to correct the momentum equations for smooth and abrupt flow area changes. Further, this model includes an input processor that will initialize a five-cell jet pump model with a minimum number of inputs if the user so designates (see Volume 2).

3.6.1 JETP Momentum Source

The momentum source term to be applied to the momentum equation for primary tube flow (see Figure 3.6-1) is obtained by considering the momentum balance for the noding scheme in Figure 3.6-2 for the different flow configurations that can occur in the jet pump. The momentum source is derived for the liquid phase momentum equations. The results will be applicable to the vapor momentum equation. The steady-state pressure changes due to the meeting of two liquid flows (see Figure 3.6-2) are

for $\cos\phi > 0$, $V_1 > 0$, $V_2 > 0$, $V_3 < 0$

$$\frac{P_1 - P_0}{\langle \rho_\ell \rangle} = 0 \tag{3.6-1}$$

$$\frac{P_2 - P_1}{\langle \rho_\ell \rangle_2} = V_2(V_1 - V_2) + V_3(V_1 + V_3 \cos\phi)\ \frac{\langle (1-\alpha)\rho_\ell \rangle_3 A_3}{\langle (1-\alpha)\rho_\ell \rangle_2 A_2} \tag{3.6-2}$$

for $\cos\phi < 0$, $V_1 < 0$, $V_2 < 0$, $V_3 < 0$

$$\frac{P_2 - P_1}{\langle \rho_\ell \rangle_2} = 0 \tag{3.6-3}$$

$$\frac{P_1 - P_0}{\langle \rho_\ell \rangle_1} = V_1(V_1 - V_2) + V_3(V_2 + V_3 \cos\phi)\ \frac{\langle (1-\alpha)\rho_\ell \rangle_3 A_3}{\langle (1-\alpha)\rho_\ell \rangle_1 A_1}\ . \tag{3.6-4}$$

The momentum equation in the TRAC-BF1/MOD1 solution scheme depends on noding and flow direction. The calculated pressure change for a single-phase steady-state flow without sources, friction loss, and gravity is shown in Table 3.6-1.

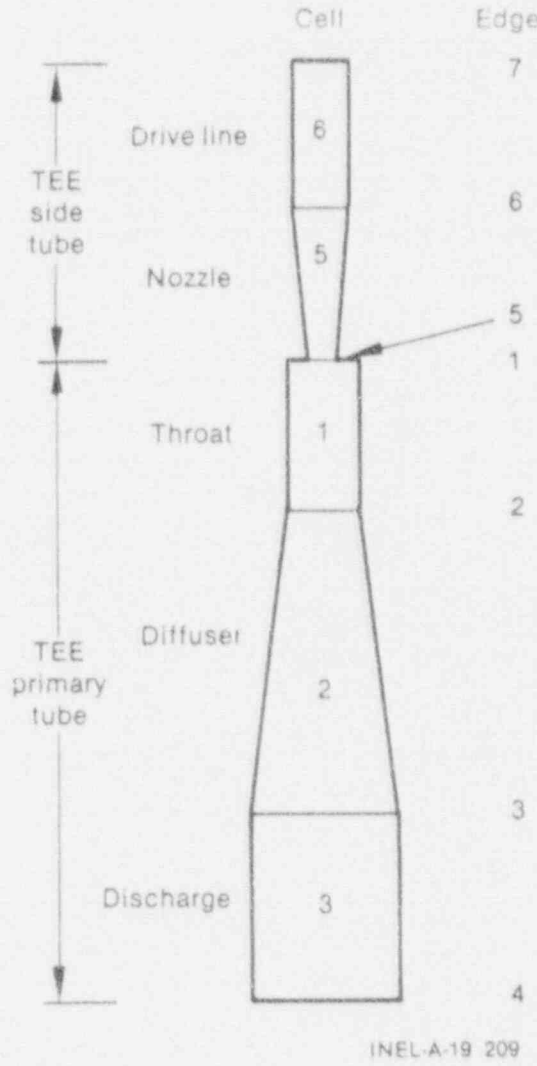

Figure 3.6-1. JETP noding diagram.

Table 3.6-1. Pressure change between Cell 0 and 2 (Figure 3.6-1).

V_1	$(P_1 - P_0)/\langle \varrho_f \rangle_1 =$	V_2	$(P_2 - P_1)/\langle \varrho_f \rangle_2$
≥ 0	0	≥ 0	$V_2(V_1 - V_2)\frac{\Delta x_1 + \Delta x_2}{2\Delta x_1}$
<0	$V_1(V_1 - V_2)\frac{\Delta x_0 + \Delta x_1}{2\,\Delta x_1}$	<0	0

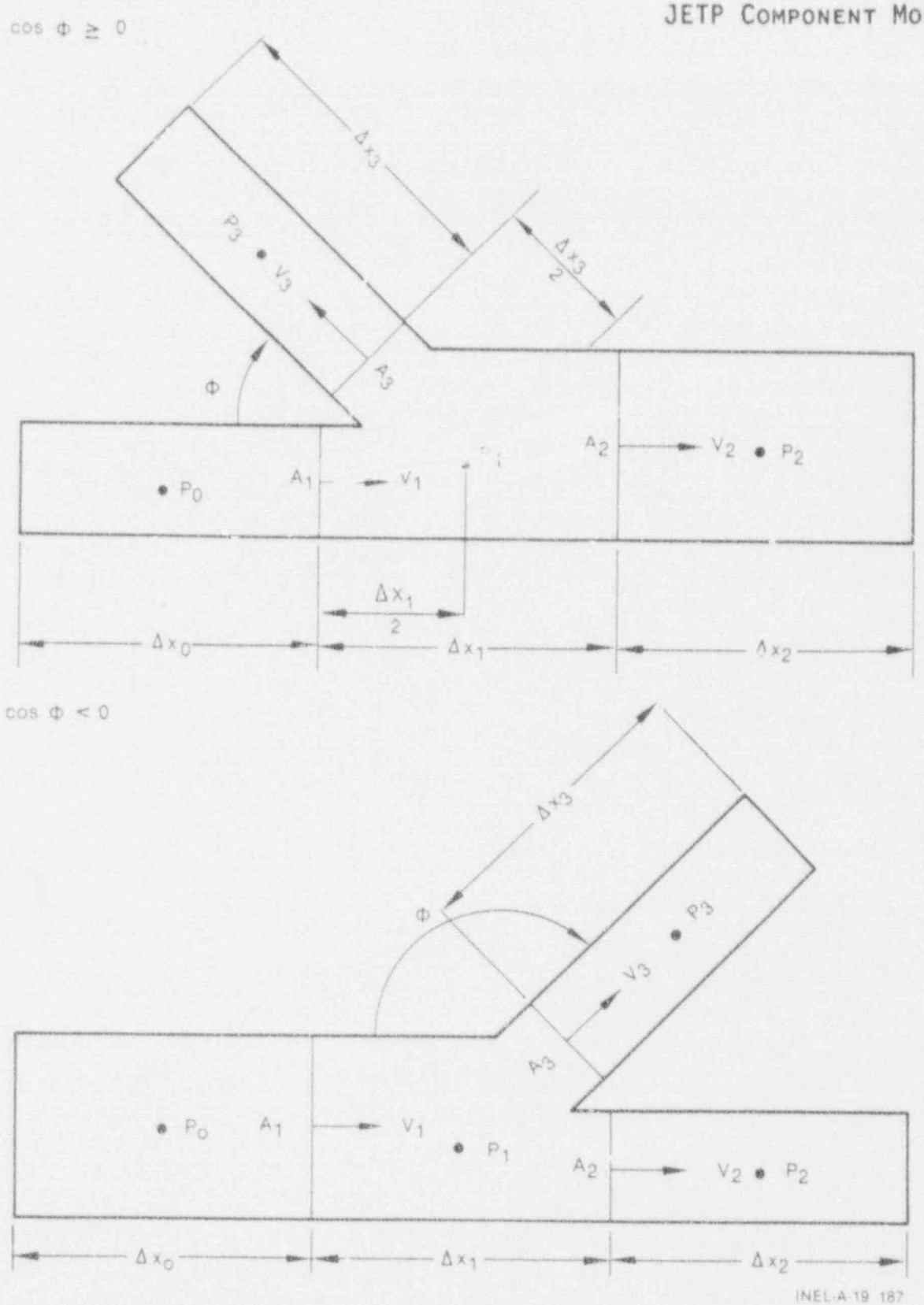

Figure 3.6-2. Noding scheme for TEE component.

Subtracting the pressure drop given in Table 3.6-1 from the total pressure drop (with source) given in Equation (3.6-1) and dividing by the average cell length yields the momentum source term for positive source flow (negative side tube velocity). The momentum source term is listed in Table 3.6-2 for various combinations of positive and negative values of V_1 and V_2. It should be mentioned that Equation (3.6-1) has been used for positive and negative flow direction in the primary tube although the analytical solution is valid for merging flows only.

Table 3.6-2. Momentum source term for TEE component with $V_3 < 0$ (positive source flow).

Cosϕ	V_1	V_2	SSMON =	SSM2 = $V_3(V_1 + V_3\cos\phi)\ \frac{<(1-\alpha)\rho_f>_3 A_3}{<(1-\alpha)\rho_f>_2 A_2}\ \frac{2}{\Delta x_1 + \Delta x_2}$
≥0	≥0	≥0	+0	$+V_2(V_1 - V_2)\ \frac{\Delta x_1 + \Delta x_2}{2\Delta x_1}\ \frac{2}{\Delta x_1 + \Delta x_2}$
	<0	≥0	$-V_1(V_1 - V_2)\ \frac{1}{\Delta x_1}$	$+V_2(V_1 - V_2)\ \frac{\Delta x_1 + \Delta x_2}{2\Delta x_1}\ \frac{2}{\Delta x_1 + \Delta x_2}$
	<0	<0	$-V_1(V_1 - V_2)\ \frac{1}{\Delta x_1}$	$+V_2(V_1 - V_2)\ \frac{2}{\Delta x_1 + \Delta x_2}$
Cosϕ	**V_1**	**V_2**	**SSMON = $V_3(V_2 + V_3\cos\phi)\ \frac{<(1-\alpha)\rho_f>_3 A_3}{<(1-\alpha)\rho_f>_1 A_1}\ \frac{2}{\Delta x_0 + \Delta x_1}$**	**SSM2 =**
<0				
	≥0	≥0	$-V_1(V_1 - V_2)\ \frac{2}{\Delta x_0 + \Delta x_1}$	$-V_2(V_1 - V_2)\ \frac{1}{\Delta x_1}$
	<0	≥0	$+V_1(V_1 - V_2)\ \frac{\Delta x_0 + \Delta x_1}{2\Delta x_1}\ \frac{2}{\Delta x_0 + \Delta x_1}$	$-V_2(V_1 - V_2)\ \frac{1}{\Delta x_1}$
	<0	<0	$+V_1(V_1 - V_2)\ \frac{\Delta x_0 + \Delta x_1}{2\Delta x_1}\ \frac{2}{\Delta x_0 + \Delta x_1}$	+0

In the case of negative source flow (positive side tube velocity), the flow in the primary tube may not be accelerated by the source flow. Therefore, the momentum source term is set to zero. But there is an irreversible loss due to the flow splitting similar to the flow with sudden expansion. For the limiting case with no flow through the side tube, Equation (3.6-1) yields

for $\cos\phi \geq 0$, $V_1 > 0$, $V_2 > 0$, $V_3 = 0$,

$$P_1 - P_0 = 0 \tag{3.6-5}$$

$$\frac{P_2 - P_1}{\langle \rho_\ell \rangle_2} = V_2(V_1 - V_2) \tag{3.4-6}$$

for $\cos\phi < 0$, $V_1 < 0$, $V_2 < 0$, $V_3 = 0$,

$$P_2 - P_1 = 0 \tag{3.6-7}$$

$$\frac{P_1 - P_0}{\langle \rho_\ell \rangle_1} = V_1(V_1 - V_2) \tag{3.4-8}$$

If this equation set is used for all possible steady-state flow conditions with negative source flow ($V_3 \geq 0$) but independent of the side tube connection angle, ϕ, the pressure change across the junction cell would be

for $V_1 > 0$, $V_2 > 0$,

$$P_2 - P_0 = \langle \rho_\ell \rangle_2 V_1(V_1 - V_2) \tag{3.6-9}$$

for $V_1 > 0$, $V_2 < 0$,

$$P_2 - P_0 = 0 \tag{3.6-10}$$

for $V_1 < 0$, $V_2 < 0$,

$$P_2 - P_0 = \langle \rho_\ell \rangle_1 V_1(V_1 - V_2) \tag{3.6-11}$$

This equation set is identical with the backwards differencing equations (Table 3.6-3) for equal length ($\Delta x_o = \Delta x_1 = \Delta x_2$) and is used for negative source flow.

Combining Equation (3.6-9) and Table 3.6-1 as before yields the momentum correction terms for negative source flow listed in Table 3.6-3.

Both the momentum source terms and the momentum correction terms are calculated in Subroutine ETEE, using the new velocities calculated at the previous time step. They are then added to the right side of the momentum equations in the explicit pass in Subroutine TF1E.

Table 3.6-3. Momentum correction term for TEE component with $V_3 > 0$ (negative source flow).

V_1	V_2	SSMON =	S[illegible].2 =
>0	>0	0	$+V_2(V_1 - V_2)\left(1 - \frac{\Delta x_1 + \Delta x_2}{2\Delta x_1}\right)\frac{2}{\Delta x_1 + \Delta x_2}$
>0	<0	0	0
<0	<0	$+V_1(V_1 - V_2)\left(1 - \frac{\Delta x_0 + \Delta x_1}{2\Delta x_1}\right)\frac{2}{\Delta x_0 + \Delta x_1}$	0

Backwards differencing is used for the momentum equation at the first side tube face. Therefore, the solution is independent of the velocities in the primary tube if the source flow is positive (negative side tube velocity). The pressure change between the junction cell and the side tube is zero if the side tube flow area is constant and friction and gravity are neglected. These assumptions agree with those made for the analytical solution of the merging of two liquid flows. The pressure drop between the primary and the side tube for negative source flow due to the velocity change is given

for $\cos\phi \geq 0$, $V_3 > 0$,

$$P_3 - P_1 = \langle\rho_\ell\rangle_3 V_3(-V_2\cos\phi - V_3)\left(-\frac{\Delta x_B + \Delta x_3}{2\Delta x_B}\right) \tag{3.6-12}$$

for $\cos\phi < 0$, $V_3 > 0$,

$$P_3 - P_1 = \langle\rho_\ell\rangle_3 V_3(-V_1\cos\phi - V_3)\left(\frac{\Delta x_B + \Delta x_3}{2\Delta x_B}\right) . \tag{3.6-13}$$

The boundary cell length, Δx_B, is set equal to the side tube cell length, Δx_3 (Subroutine ITEE), to make the pressure drop due to velocity change independent of the junction cell length and hydraulic diameter of the primary tube, as it should be.

3.6.2 Jet Pump Loss Coefficients

The TRAC-BD1/MOD1 jet pump model had a form of the conserving velocity divergence as part of the jet pump specific loss coefficients.[3.6-1] With the implementation of the conserving form of the velocity divergence operator in TRAC-BF1/MOD1, the loss coefficients in the jet pump had to be modified. In addition, new values for the irreversible losses in the jet pump were determined by the General Electric Company.[3.6-2] This section describes the

new form of the irreversible losses in the jet pump. There are several mechanisms for irreversible pressure losses in the jet pump, and they are discussed separately.

3.6.2.1 Diffusor (Expansion) Losses. The irreversible pressure loss coefficient through a diffusor is given by Idelchek[3.6-3] as

$$K_e = C_e \tan\alpha^{1.5} (1 - A*)^2 \qquad (3.6\text{-}14)$$

where

α = diffusor angle

A^* = area ratio of outlet to inlet

C_e = constant.

The recommended value of C_e is 5.5 and is the default value in TRAC-BF1/MOD1. The user may input the value of C_e if he so desires.

This pressure loss coefficient is used at every cell face of the jet pump where the flow areas at the cell centers on either side of the face increase in the direction of flow.

3.6.2.2 Nozzle (Contraction) Losses. The irreversible pressure loss coefficient through a nozzle due to the contraction is given by Idelchek[3.6-3]

$$K_c = C_c \sin\alpha (1 - A*) \qquad (3.6\text{-}15)$$

where

α = contraction angle

A^* = area ratio of outlet to inlet of contraction

C_c = constant.

The recommended value of C_c is 0.38 and is the default value in TRAC-BF1/MOD1. The user has the option to input his own value of C_c. This pressure loss coefficient is used at every face in the jet pump where the flow area at the cell centers on either side of the face decrease in the direction of flow.

3.6.2.3 Inlet Losses. There is an irreversible pressure loss at the jet pump suction inlet due to the contraction of the suction flow from the downcomer to the jet pump. The loss coefficient for this loss has been estimated to be 0.04 from data obtained at the INEL using 1/6 scale jet pumps.[3.6-4] When the flow at the jet pump diffusor outlet reverses, there is a contraction loss from the lower plenum into the jet pump diffusor. The loss coefficient for this loss has been estimated from data to be 0.45. These

values are in the TRAC-BF1/MOD1 code as default values, but the user may change them.

3.6.2.4 Outlet Losses. There is a loss at the diffusor outlet due to the flow expansion from the diffusor outlet into the lower plenum for normal operating conditions in the jet pump. The loss coefficient for this loss is estimated to be 1.0 and is implemented into the TRAC-BF1/MOD1 code at the diffusor outlet for forward flow in the diffusor.

3.6.2.5 Mixing Losses. There are irreversible pressure losses in the mixing region of the jet pump where the high-velocity drive flow mixes with the low-velocity suction flow. These losses have been estimated from the 1/6 scale jet pump data and have been correlated in terms of the drive velocity (V_{DR}), the ratio of suction mass flow rate to drive mass flow rate (M ratio), and the flow regime. The flow regimes are defined for various combinations of positive and negative suction flow, drive flow, discharge flow, and M ratio. The definition of the flow regimes are shown schematically in Figure 3.6-3 and listed in Table 3.6-4. The loss coefficients in the various flow regimes for mixing losses are given in Table 3.6-5.

3.6.2.6 Nozzle Losses. In addition to the pressure losses in the drive nozzles caused by the contraction of the flow, there are additional losses because of the unique geometry of the drive nozzle. These losses have been estimated from the 1/6 scale jet pump data and have been correlated in terms of the M ratio for the various flow regimes. These loss coefficients are listed in Table 3.6-5.

3.6.3 Jet Pump Input Processing

Input for the jet pump component may be either of two types, both described in Volume 2. Type JETP input, read and processed by Subroutines FJTP and FJPC, provides for a five-cell jet pump model (see Figure 3.6-1) with a minimum number of input values. The other type of jet pump input is the standard TEE input, which provides for a jet pump model with five or more cells, and for complete user specification of all cell and cell edge properties. TEE type jet pump input is read and processed by Subroutines FTEE and FJPC.

With Type JETP input, single input values for pressure (P), void fraction (ALP), liquid temperature (TL), vapor temperature (TV), and boron concentration (BORC) are used for all five cells in the jet pump. The following array values are calculated and not read as input. (Subscripts refer to either cells or cell edges, depending upon the given array; see Figure 3.6-1.)

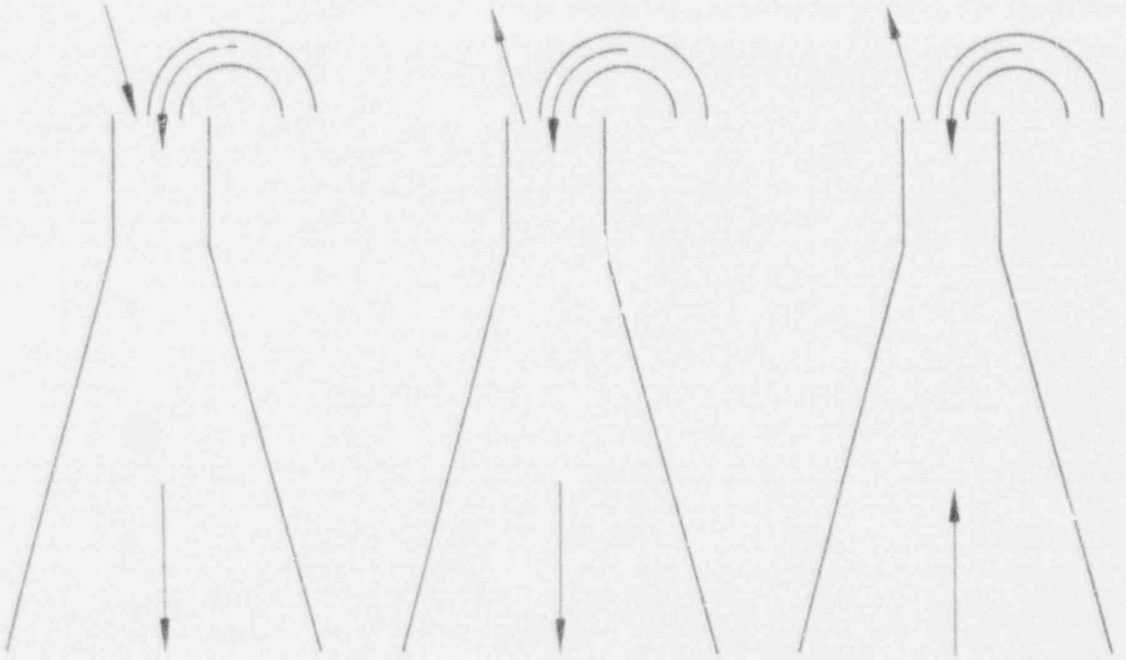

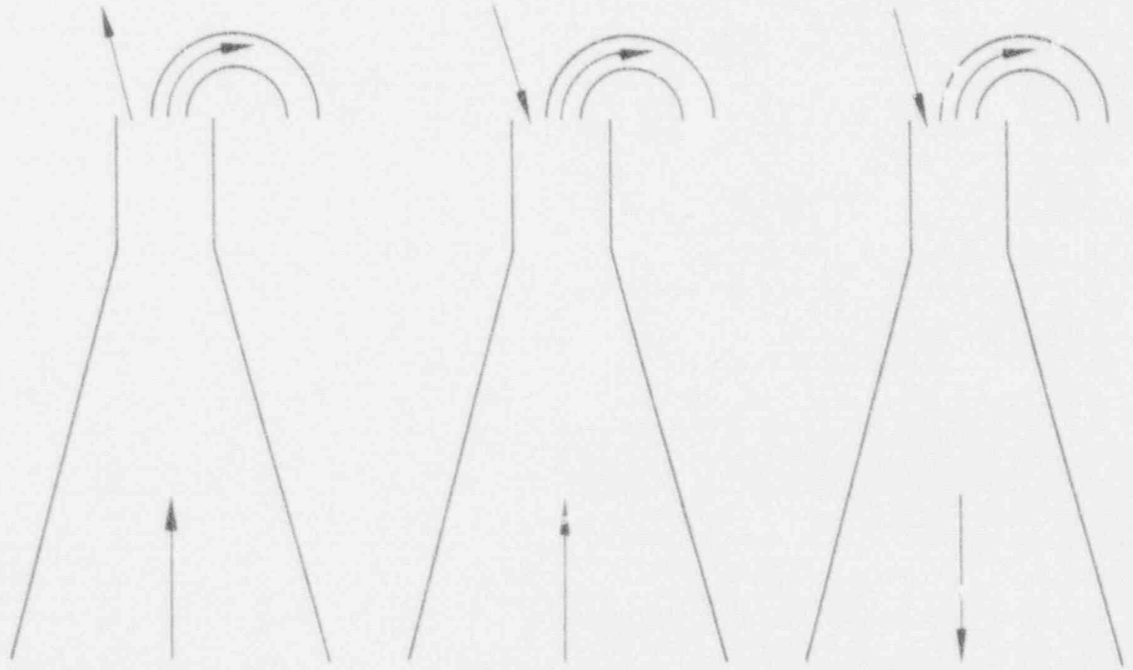

Figure 3.6-3. Jet pump flow regimes.

6 3159

Table 3.6-4. Jet pump flow regimes.

Regime	Drive Flow	Suction Flow	Discharge Flow	M Ratio
1[a]	Positive	Positive	Positive	M > 0
2	Positive	Negative	Positive	0 > M > -1
3	Positive	Negative	Negative	M < -1
4	Negative	Negative	Negative	M > 0
5	Negative	Positive	Negative	0 > M > -1
6	Negative	Positive	Positive	m < -1

a. Flow regime 1 is normal operating regime.

Table 3.6-5. Flow regime dependent loss coefficients.

Regime	Mixing Loss Coefficient	Nozzle Loss Coefficient
1	0	0
2	$-0.134\ M^2V_{DR}^2$	Min [2.5, M(0.08M - 0.06)]
3	$-(0.1 - 0.0333\ M^2V_{DR}^2$	Min [2.5, M(0.08M - 0.06)]
4	0	Max [0.0, 0.48-M (0.33 - 0.055M)]
5	0	Max [0.0, 0.48-M (0.33 - 0.055M)]
6	0	2.55

Su ı flow area:

$$FA_1 \quad FA_2 - FA_5 \tag{3.6-16}$$

Hydraulic diameters

$$HD_j = 2\sqrt{\frac{FA_j}{\pi}} \quad for\ j = 1\ through\ 6 \tag{3.6-17}$$

Vol es:

$$VOL_j = DX_j \frac{FA_j + \sqrt{FA_j\, FA_{j+1}} + FA_{j+1}}{3} \qquad (3.6\text{-}18)$$

Form loss coefficients:

$$FKLOS_j \text{ and } RKLOS_j = 0 \text{ for } j = 3,\ 4,\ 5, \text{ and } 7 \qquad (3.6\text{-}19)$$

Gravity terms:

$$GRAV_j = \begin{cases} -1 \text{ for } j = 1,\ 2,\ 3, \text{ and } 4 \\ +1 \text{ for } j = 5 \end{cases} \qquad (3.6\text{-}20)$$

Choking flags:

$$ICHOKE_j = 0 \text{ for } j = 2,\ 3,\ 4,\ 6, \text{ and } 7 \qquad (3.6\text{-}21)$$

CCFL flags:

$$ICCFL_j = 0 \text{ for } j = 2 \text{ through } 7 \qquad (3.6\text{-}22)$$

Liquid velocities:

$$VLN_j = \begin{cases} \dfrac{VLN_{j+1} FA_{j+1}}{FA_j} \text{ for } j = 2 \text{ and } 5 \\ \dfrac{VLN_2\, FA_2 + VLN_5\, FA_5}{FA_1} \text{ for } j = 1 \end{cases} \qquad (3.6\text{-}23)$$

Vapor velocities:

$$VVN_j = VLN_j \text{ for all } j\,. \qquad (3.6\text{-}24)$$

With either JETP or TEE type input, the user describes the geometry of a single jet pump and supplies input variable NJETP, the number of actual jet pumps lumped together. After all JETP input has been processed, the cell flow areas (FA), volumes (VOL,), and wall areas (WA) are scaled by NJETP.

3.6.4 References

3.6-1. D. D. Taylor et al., *TRAC-BD1/MOD1: An Advanced Best Estimate*

Computer Program for Boiling Water Reactor Transient Analysis, NUREG/CR-3633, EGG-2294, April 1984.

3.6-2. J. G. M. Andersen et al., *BWR Refill-Reflood Program Task 4.7--Model Development TRAC-BWR Component Models*, NUREG/CR-2574, EPRI NP-2376, GEAP-22053, April 1983.

3.6-3. Idelchik, *Handbook of Hydraulic Resistance Coefficient of Local Resistance and Friction*, AEC-TR-6630, 1966.

3.6-4. G. E. Wilson, *INEL One-Sixth Scale Jet Pump Data Analysis*, EGG-CAAD-5357, February 1981.

3.7 VALVE

The VALVE module models the flow in a valve. A valve is modeled as a one-dimensional component with at least two fluid cells, as shown in Figure 3.7-1. The heat-transfer and fluid-dynamics models used in a VALVE calculation are identical to those of a PIPE (see Subsection 3.1).

Modeling valve action is achieved by controlling the flow area and hydraulic diameter between the two fluid cells. The expressions used for this purpose are

flow area = AVLVE x FRACT

and

hydraulic diameter = HVLVE x FRACT

where AVLVE and HVLVE are the fully open valve flow area and hydraulic diameter, respectively. FRACT is the fraction of the valve that is open.

Eight user options are provided for controlling the valve action. Option -1 allows valve area control by a control system. Options 1 to 4 allow trip control, with the valve opening or closing instantly or as a function of time. Option 5 models a check valve; an open or closed condition is determined by a pressure differential between the specified cells and two set points. Option 6 is a motor-operated valve, while Option 7 simulates relief valve multiple set points. The valve option is specified by the value of the input parameter, IVTY. The possible IVTY values and their corresponding options are given in Table 3.7-1. The input parameters needed for the eight VALVE options are given in Volume 2.

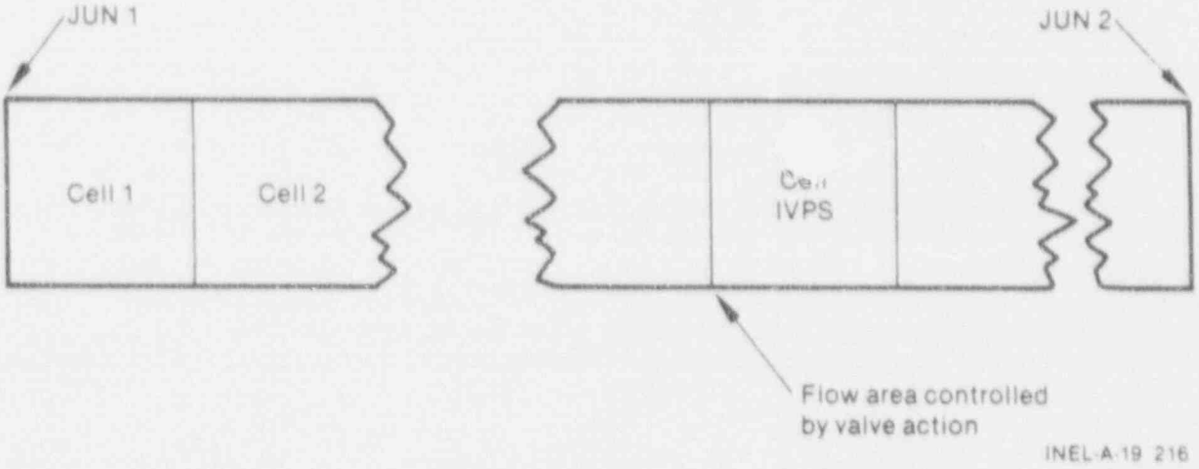

Figure 3.7-1. VALVE noding diagram.

Table 3.7-1. Control options for VALVE.

IVTY	Option
-1	Valve area is controlled by a control system.
1	Valve is normally open and is closed instantly on a trip signal.
2	Valve is normally closed and is opened instantly on a trip signal.
3	Valve is normally open and is closed on a trip signal according to a time-dependent valve table.
4	Valve is normally closed and is opened on a trip signal according to a time-dependent valve table.
5	Check valve is controlled by a static pressure gradient. IVPG is the gradient option. IVPS defines the cell face where the valve orifice is located. If IVPG = 1, DP = P(IVPS - 1) - P(IVPS). If IVPS = 2, DP = P(IVPS) - P*IVPS - 1). If DP + PVC1 $\geq$ 0, valve opens instantly; If DP + PVC2 < 0, valve closes instantly.
6	Power-operated valve that opens or closes on fixed rates based on pressure set points.
7	Relief valve with multiple set points.

3.8 VESSEL

The VESSEL module models a BWR vessel and its associated internals. The component is three-dimensional, using a six-equation, two-fluid model to evaluate the flow through and around all internals of a BWR vessel, including the downcomer, core bypass, and upper and lower plenums. Models incorporated into the VESSEL module are designed mainly for LOCA analysis, but the VESSEL module can be applied to other transient analyses as well. The reactor power is modeled using point-reactor kinetics. Most of the detailed discussion of the fluid-dynamics, heat-transfer, and point-reactor kinetics equations and solution methods for the three-dimensional VESSEL module can be found in Section 2 of this manual. In this section, we discuss the VESSEL geometry and other important considerations.

A three-dimensional, two-fluid, thermal-hydraulic model in cylindrical coordinates describes the vessel flow. A regular cylindrical mesh, with variable mesh spacings in all three directions, encompasses the downcomer, core bypass, and upper and lower plenums of the vessel. The user describes the mesh by specifying the radial, angular, and axial coordinates of the mesh-cell boundaries

$r_i \quad i = 1,...NRSX$

$\theta_j \quad j = 1,...NTSX$

and

$z_k \quad k = 1,...NASX$

where NRSX is the number of rings, NTSX is the number of angular segments, and NASX is the number of axial levels. The point $(r_i,\theta_j,,z_k)$ is a vertex in the coordinate mesh. Mesh cells are constructed and identified by an axial level number and a cell number. For each axial level, the cell number is determined by counting the cells radially outward starting with the first angular segment and the innermost ring of cells, as shown in Figure 3.8-1. Figure 3.8-1 shows the relative face-numbering convention for an individual cell that is used in connecting other components to the vessel.

NOTE: Only three faces must be identified per mesh cell because the other faces will be defined by neighboring cells.

All fluid flow areas (on cell faces) and all fluid volumes are dimensioned so that the internal structure within the vessel can be modeled. Flow areas and fluid volumes are computed based on the geometric mesh spacings and scaled according to factors supplied as input. The scaled volumes and flow area are then used in the fluid-dynamics and heat-transfer calculations. Flow restrictions and the volume occupied by the structure within each mesh cell are modeled through use of these scale factors. For example, the downcomer walls are modeled by setting the appropriate flow area scale factors to zero. A feature is provided to do this automatically in the code if the

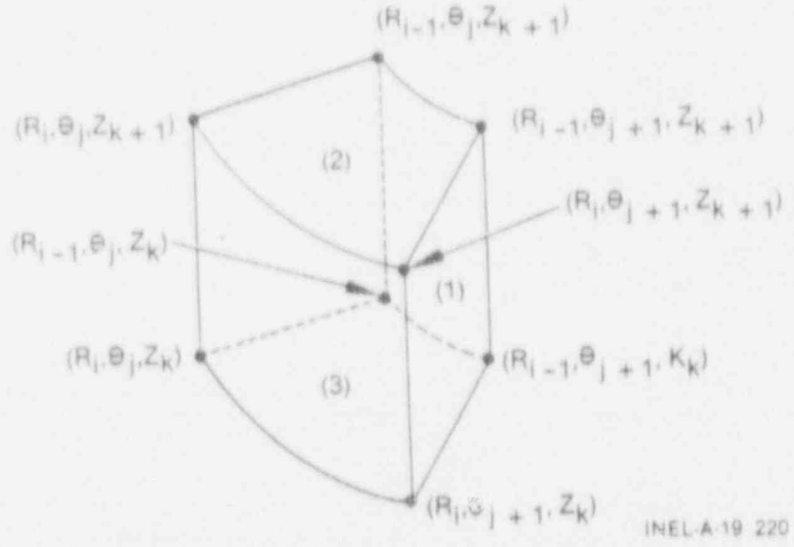

Figure 3.8-1. Boundaries of a three-dimensional mesh cell. The face-numbering convention is also shown. Faces 1, 2, and 3 are in the θ, z, and r directions, respectively.

upper, lower, and radial downcomer position parameters (IDCU, IDCL, and IDCR) are specified, as described in Volume 2. Flow restrictions such as the top and bottom core support plates require scale factors between zero and one. Figure 3.8-2 shows the cell faces scaled to model the downcomer and core support plate flow restrictions.

Plumbing connections from other components to the VESSEL are made on the faces of the mesh cells. Any number of connections may be made to the VESSEL; in fact, any mesh cell in the VESSEL can have one component or more connected to it. Four input parameters are used to describe a connection: ISRL, ISRC, ISRF, and JUNS. The parameter ISRL defines the axial level in which the connection is made; ISRC is the mesh-cell number, as defined above; and ISRF is the face number, as defined in Figure 3.8-1. If ISRF is positive, the connection is made on the face shown in the figure with the direction of positive flow into the cell. If ISRF is negative, the connection is made on the opposite face shown in the figure with the direction of positive flow also into the cell. The parameter, JUNS, is the system junction number used to identify this junction. Figure 3.8-3 shows several VESSEL, PIPE, and JETP connections. Internal and external connections are allowed. The user is cautioned against connecting to the VESSEL any component with a flow area that differs greatly from the flow area of the mesh-cell face to which it is connected because this can cause anomalous pressure gradients. Such a situation can be avoided by proper adjustment of the VESSEL geometry coordinate spacings and/or the use of taper or expansion sections on 1-D components prior to the VESSEL connections.

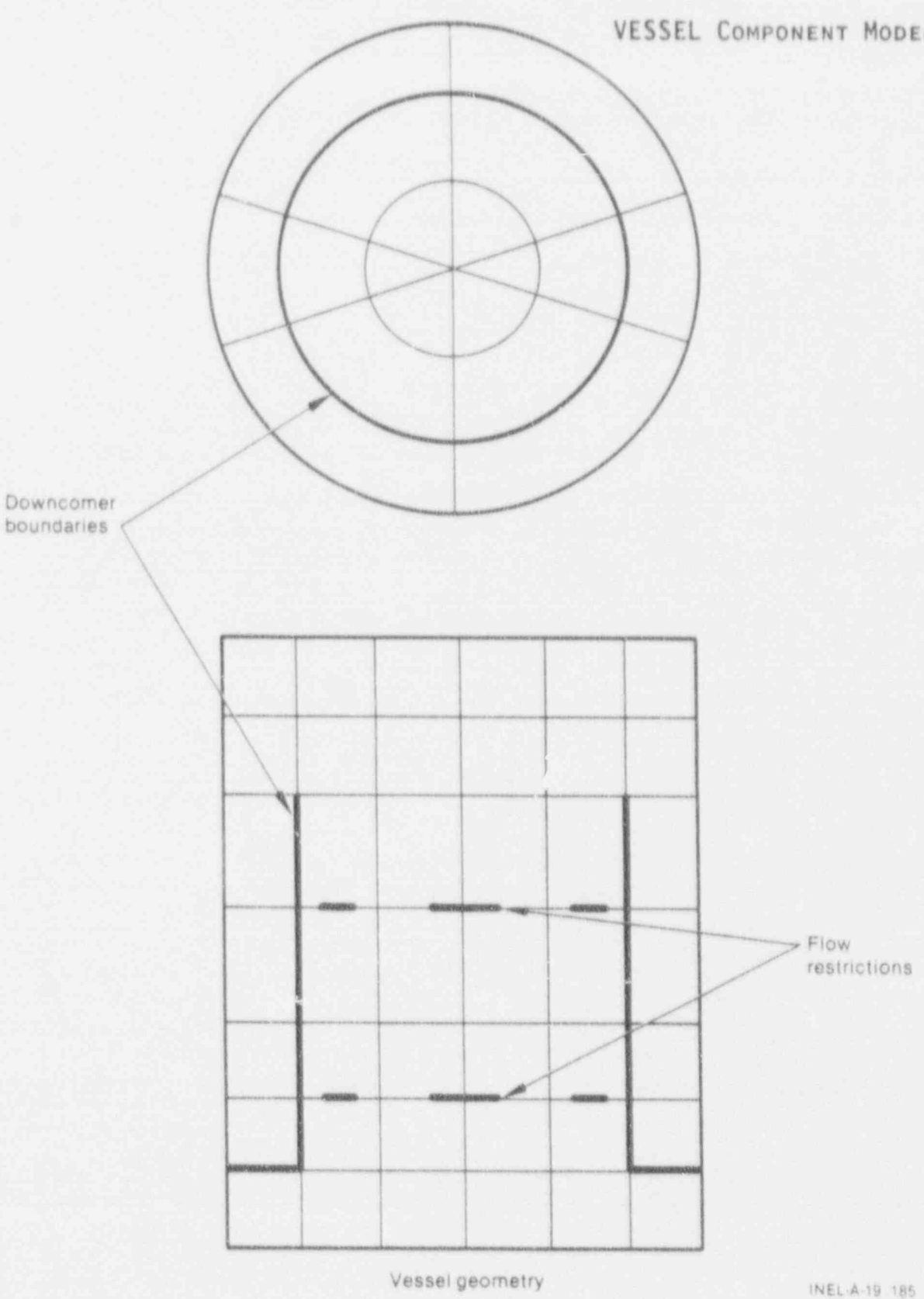

Figure 3.8-2. Flow restrictions and downcomer modeling.

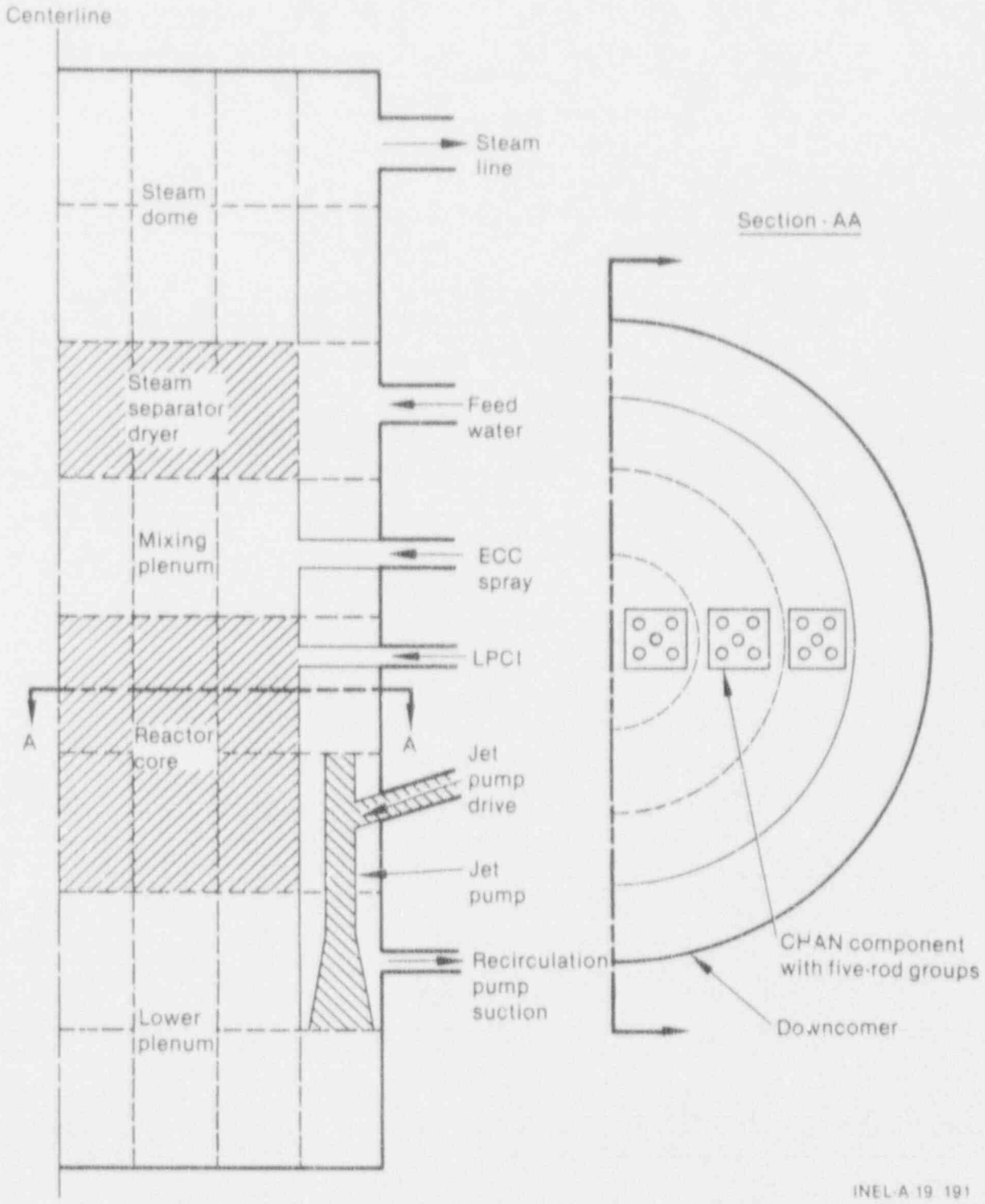

Figure 3.8-3. A typical TRAC-BF1/MOD1 VESSEL nodalization diagram.

The reactor core region in the VESSEL is specified by the upper, lower, and radial core positional parameters (ICRU, ICRL, and ICRR). These parameters define, respectively, the upper, lower, and radial boundaries of the cylindrical core region. The example provided in Figure 3.8-3 shows a possible configuration in which ICRU = 4, ICRL = 2, and ICRR = 3. Each mesh cell stack in the core region contains a CHAN component to simulate the fuel bundles in that core region.

A very important aspect of this three-dimensional VESSEL component is that it results in a multidimensional hydraulic model of regions within a BWR VESSEL in which multidimensional effects may be important. For example, an important aspect of BWR LOCA analysis is the emergency core coolant spray (ECCS) into the upper plenum. The noding diagram in Figure 3.8-3 results in a model in which the radial distribution of ECCS water in the upper plenum is represented by three TRAC-BF1/MOD1 VESSEL radial rings. The solution to the TRAC-BF1/MOD1 conservation equations in that region plus the coupled solutions for the conservation equations in the core bypass, CHANS, separators, and in ECC spray connections will result in a radial distribution of ECC water in the upper plenum. Results to date indicate that the model gives representative ECC water mass and energy distributions within an upper plenum.

A shortcoming of the nodalization in Figure 3.8-3 has been identified and resolved. With the nodalization in Figure 3.8-3, there is insufficient noding in the axial direction to resolve horizontal flow stratification effects in the upper plenum. One solution to this problem is to increase the axial noding in the upper plenum. However, this results in an increase in computer costs for the calculation. Another solution to this problem is to include within the VESSEL hydrodynamics a horizontal flow stratification model. This would have regligible effects on running time.

A horizontal flow stratification model was developed for TRAC-BD1 by J. G. M. Andersen, of the General Electric Co., and has been included into the released version of TRAC-BF1/MOD1. The model consists of adding to the radial and theta momentum equations an additional force term that accounts for the hydrostatic head between two adjacent TRAC-BF1/MOD1 hydrocells that have different water levels. The added force term for the cells in Figure 3.8-4 is

$$P_2 - P_1 = (\rho_\ell - \rho_g) g \Delta z (\alpha_1 - \alpha_2) \ . \qquad (3.8\text{-}1)$$

This force term is assumed to act on the liquid phase only. Thus, tending to enhance horizontal liquid flows from regions of high liquid content to regions of lower liquid content.

Heat slabs of arbitrary masses and volumes can be defined in any mesh cell (including core regions) to model the heat capacity of structures within the VESSEL. An HTC is computed for each slab using the local fluid conditions. The temperature calculation is based on a lumped-parameter model (see Subsection 2.2.1.2).

In addition to the lumped parameter heat model, a double-sided heat slab

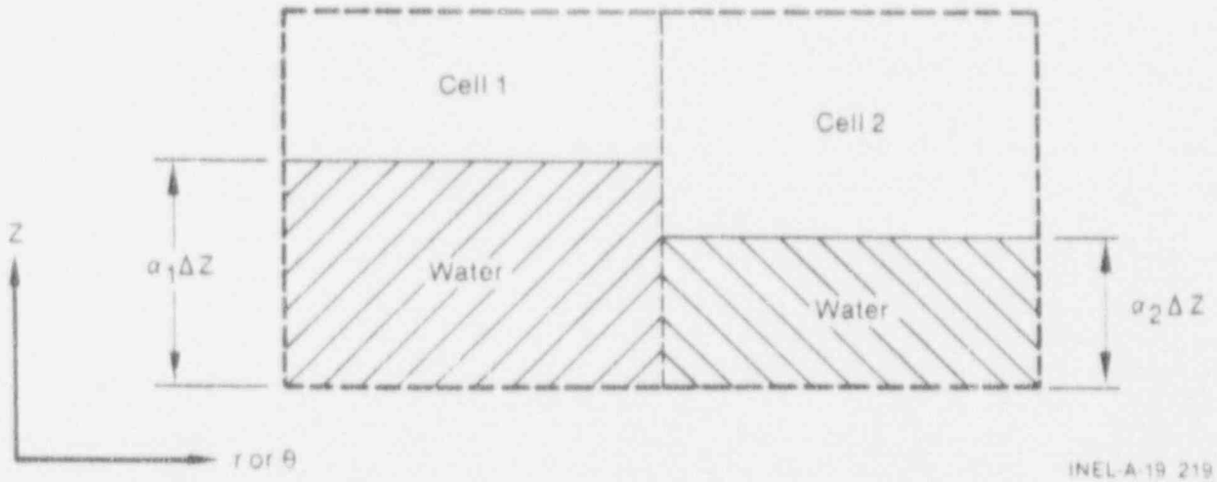

Figure 3.8-4. Representation of hydrostatic head difference in adjacent VESSEL cells.

model has been incorporated into the TRAC-BF1/MOD1 code to permit accurate modeling of heat conduction through cylindrical structures found within a BWR VESSEL. The new double-sided heat slab (double slab) model will allow the user to model heat conduction through a surface separating two different VESSEL radial regions. Double slabs may also be used to model the release of stored energy from the reactor vessel wall. In this case, the outside surface of the double slab will not connect to a VESSEL region but will use boundary conditions specified by the user or by the CONTAINMENT component instead.

A single double-sided heat slab may be associated with each fluid cell on each VESSEL axial level. These double slabs are considered to lie on the outside surface of their associated fluid cell, as shown in Figure 3.8-5. In this figure, the outside surface of the double-sided heat slab associated with fluid Cell 1 is actually in contact with fluid Cell 5. Heat transfer coefficients for both sides of a double-sided heat slab are calculated by Subroutine HTCOR, using the appropriate old-time fluid conditions from the fluid cells on each side of the heat slab. Likewise, the liquid and vapor temperatures from the appropriate fluid cells are used in calculating the heat flux on each surface of the double slab. If the double slab lies on the outside surface of the VESSEL, the external heat transfer coefficients and fluid temperatures are set equal to values supplied by the user or by the CONTAINMENT model. Energy source terms are included in the energy equation for the fluid cells on each side of the double slab to account for energy transfer from the slab.

The heat conduction solution within the double-sided heat slab is performed by Subroutine CYLHT, which is already used for calculation of PIPE wall conduction (see Subsection 2.2.1.1).

The user specifies the inside surface area, thickness, and material type

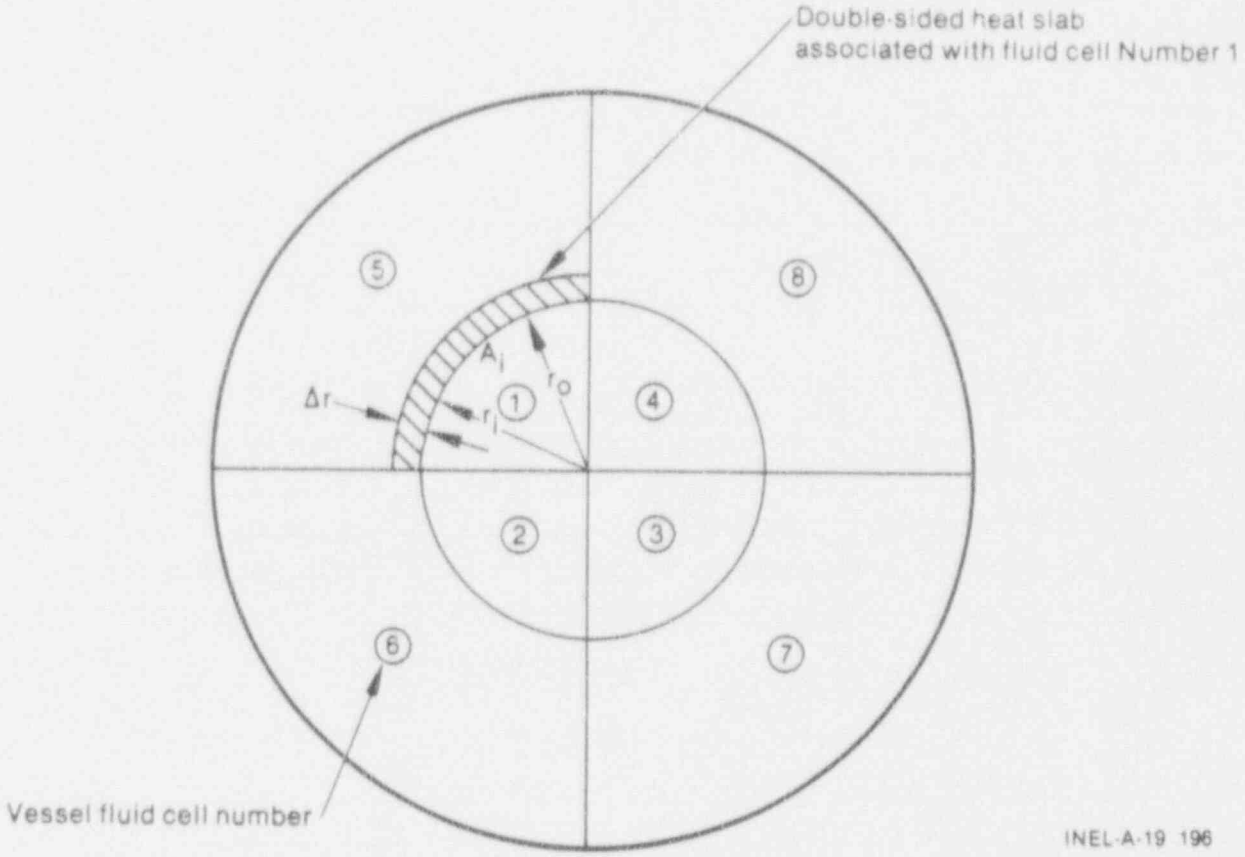

Figure 3.8-5. Sample geometry for double-sided heat slab.

for the double slab associated with each VESSEL cell. If the double slab area for a particular cell is input as zero, no double slab is assumed to exist for that cell. The double slab material properties (density, specific heat, and thermal conductivity) are evaluated separately for each conduction heat transfer node within a double slab, these properties being evaluated at the mean temperature for each node. The number of conduction heat transfer nodes within the double slabs is specified by the user, and the same value is used for all double slabs.

3.9 SEPARATOR-DRYER

TRAC-BF1/MOD1 includes three different options for modeling the function of a BWR steam separator and dryer. The first of these options, the three-dimensional perfect separator, may be used only as part of the VESSEL component, while the second and third options, using the TEE-based separator-dryer component (SEPD), may be used either in conjunction with a VESSEL component or with one-dimensional components.

3.9.1 Three-Dimensional Perfect Separator-Dryer

The function of a BWR separator-dryer may be simulated by setting axial friction factors for the liquid phase and radial friction factors for the vapor phase to very large numbers in the separator region of the VESSEL model. The present separator model provides the user with a convenient means of implementing this separator concept.

Figure 3.9-1 shows the nodalization of a TRAC-BF1/MOD1 VESSEL model. The boundaries of the separator-dryer region are shown by heavy dashed lines. Axial levels ISDL and ISDU denote the lowest and highest boundaries of the separator-dryer, while radial node index ISDR denotes the outer boundary of the separator dryer.

During the velocity calculation in Subroutine TF3E, the separator-dryer model will set axial liquid friction factors equal to CZSDL on all axial faces at level ISDL and with radial indices $\leq$ ISDR. The radial vapor friction factor will be set to CRSDV on radial face ISDR only. CZSDL and CRSDV have default values of 1.0E+26 but may be redefined by the user if desired. With the friction factors set as described above, axial separation of water and steam will occur on every level from ISDL to ISDU inclusive, while radial separation will occur only on radial face ISDR.

The separator-dryer model also sets the axial component of interfacial heat, CFZI, equal to zero on all levels from ISDL to ISDU inclusive in the separator-dryer region. The appropriate pressure drops in the axial and radial directions can be obtained by adjusting the friction loss factors.

3.9.2 TEE-Based Separator-Dryer (SEPD)

The separator/dryer component as implemented in TRAC-BD1/MOD1[3.9-1] consisted of a PIPE component, which represents the separator stand pipe and barrel, and a leak path which transferred the separated liquid and the carryunder vapor to the downcomer. The small time steps necessitated by the use of an explicit leak path were acceptable, since the regular numerics were limited to small time steps by the material Courant limit. With the implementation of the Courant violating numerics in TRAC-BF1/MOD1, the time

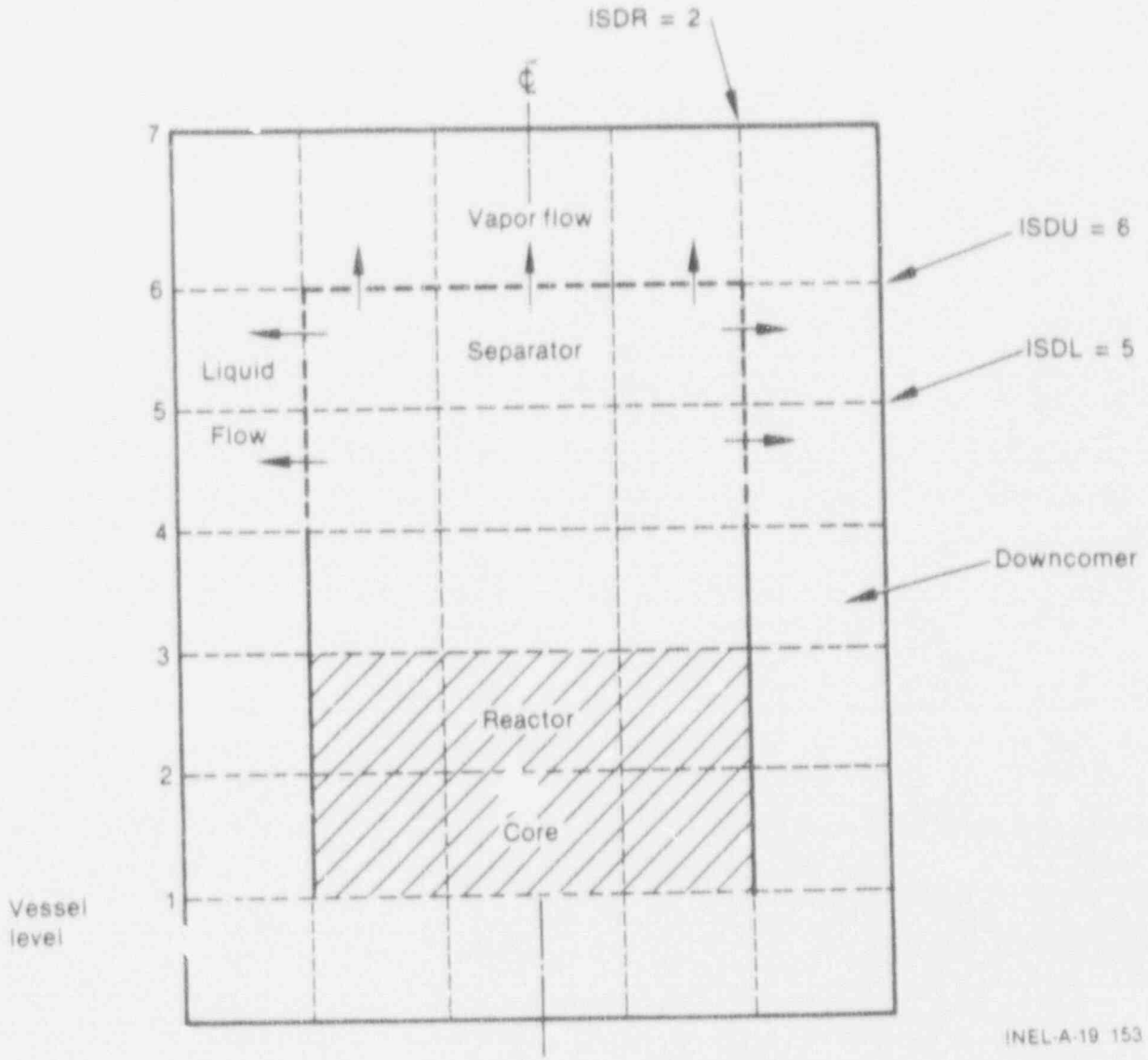

Figure 3.9-1. TRAC-BF1/MOD1 VESSEL model.

step restriction imposed by the leak path in the separator/dryer model became unacceptable and the model was modified to allow larger time steps to be used.

The model used in TRAC-BF1-MOD1 utilizes the TEE component. Both the separator and steam dryer components of a BWR have a single inlet, which accepts two-phase fluid, and two outlets discharging nearly single phase fluid

through each path. The separator accepts moderate-quality two-phase fluid from the mixing plenum and directs high-quality fluid to the steam dryer and low-quality fluid to the downcomer. The steam dryer accepts the high-quality fluid from the separator and removes the residual moisture to provide nearly single-phase steam to the steam dome. The separated liquid is directed back to the liquid pool surrounding the separators.

Each of these components can be represented by a TRAC-BF1/MOD1 TEE component that has three flow paths. The model as developed can be used to represent a separator (or a number of separators), the steam dryer, or both the multiple separators and the steam dryer.

Furthermore, there are two different separator options for determining the liquid carryover and the vapor carryunder qualities--a simple separator option where the user specifies constant carryover and carryunder qualities and a mechanistic separator option in which the carryover and carryunder qualities are computed as functions of the local conditions in the separator. The mechanistic separator methodology and coding implementing the methodology were developed by the General Electric Company (GE).[3.9-2].

The steam dryer also has two options, a prefect separator option in which all liquid is separated regardless of the local conditions and a more mechanistic model in which the dryer efficiency decreases as the vapor velocity increases above a critical dryer inlet velocity. The more mechanistic dryer model was developed by GE[3.9-2] and is adapted from their version of the TRAC-BWR code.

Figure 3.9-2 is a diagram of a combined separator/dryer component. The portion of the primary tube from the inlet to the joining cell represents the separator standpipe and barrel, the joining cell represents the volume between the separator discharge and dryer inlet, and the portion of the primary tube above the joining cell represents the dryer.

The TEE side arm represents the separator shroud. The separated liquid from the dryer flows down along the dryer skirt; this flow path is not explicitly modeled, since it occupies a negligible volume. The separator function occurs across the inlet face of the joining cell where the two-phase mixture leaves the stand pipe and barrel to appear at the inlet to the side arm rather than in the joining cell. The dryer function occurs at the outlet face of the joining cell where the convected void fraction is computed from the dryer efficiency. The phase separation is accomplished by adjusting the void fraction convected across the several faces of the joining cell and by adjusting the flow velocities at the inlet to the TEE side arm. The separator/dryer component thus uses the same methodology as the two-phase level model in which convected void fractions are different than the cell average value. The analogy may be carried further by reference to Figure 3.9-3, in which the phase separation is accomplished by the use of the two-phase level model in the joining cell. The above-level void fraction (void fraction convected across the dryer face) is determined by the dryer efficiency and the below-level void fraction is determined from the vapor carryunder mass flow rate. The phase velocities at the inlet to the TEE side arm are adjusted such

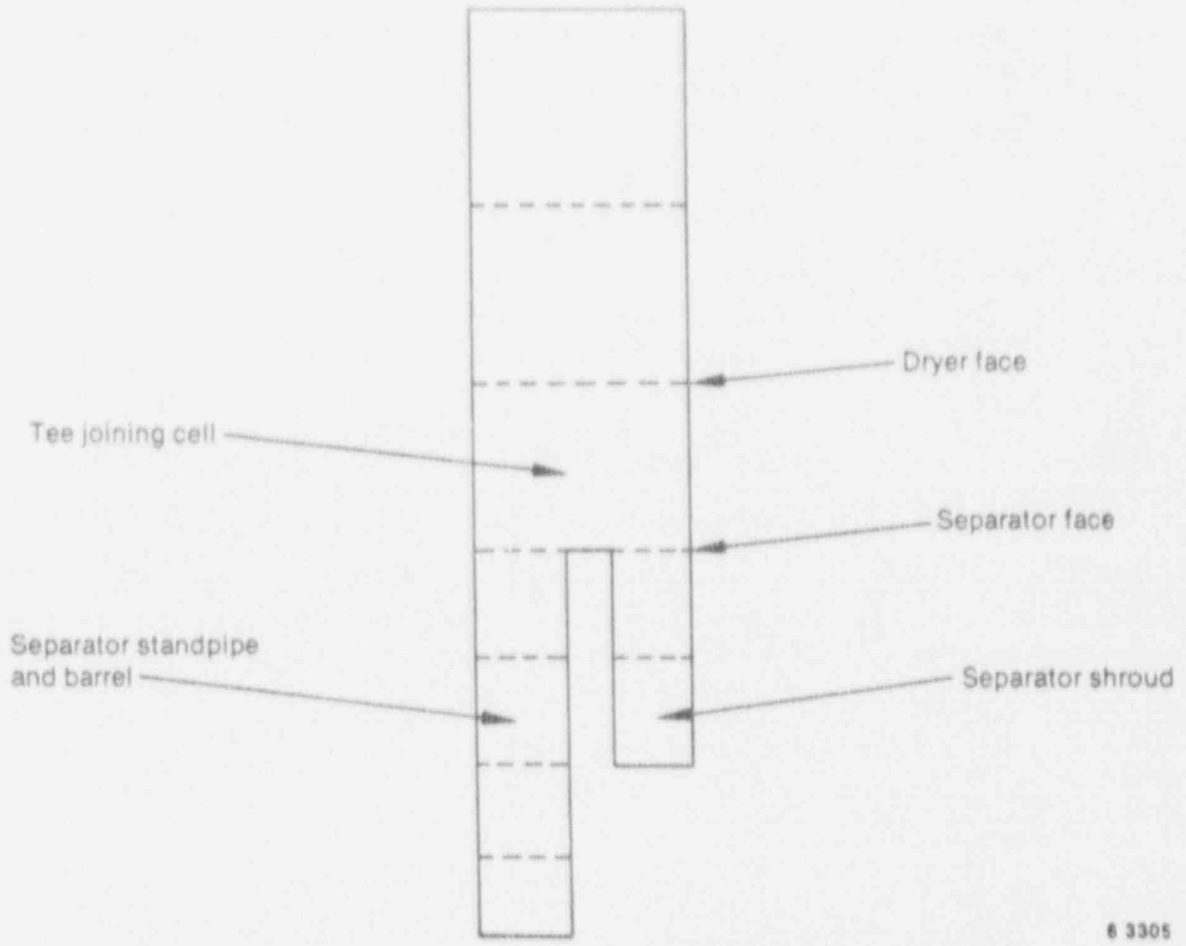

Figure 3.9-2. Diagram of combined separator-dryer.

that the desired cell average void fraction is maintained in the joining cell of the TEE. The side arm velocities are determined by adjusting the loss coefficient at the inlet to the side arm so that the velocity solution is sufficiently implicit to allow large time steps to be taken with the new model.

3.9.2.1 **Model Equations.** The phase separation in the separator/dryer component is accomplished by determining the void fractions convected across the two outlet faces of the joining cell and by adjusting the loss coefficient at the inlet of the TEE side arm.

3.9.2.2 **Dryer Void Fraction.** The void fraction convected across the dryer face is determined by the dryer efficiency. If the simple dryer option is chosen, the dryer efficiency is assumed to be 100%. If the more

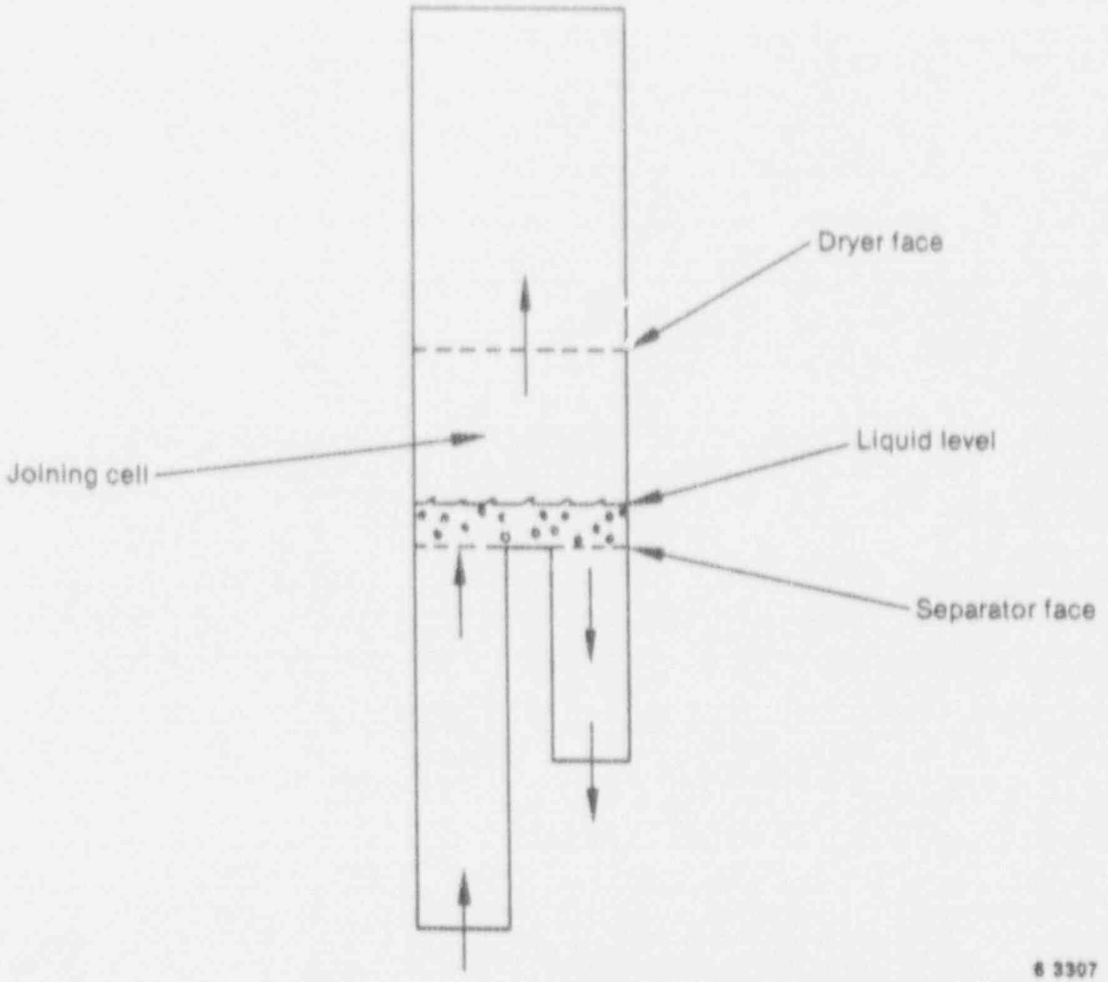

Figure 3.9-3. Separator phase separation.

mechanistic dryer option is chosen, the dryer efficiency is computed from the vapor velocity across the dryer face and the dryer inlet liquid quality.

Once the dryer efficiency has been computed, the void fraction convected across the dryer face is computed. The convected void fraction is 1 for a dryer efficiency of 100% and is the donor void fraction for a dryer efficienry of 0.0%. For dryer efficiencies between 100% and 0%, the convected void fraction is linearly interpolated between the void fractions corresponding to values obtained for efficiencies of 100% and 0%, respectively

This relation is summarized in Equation (3.9-1) as

$$\alpha_b = \eta_b + (1 - \eta_b)\alpha_f \qquad (3.9\text{-}1)$$

where

α_D = convected void fraction at dryer face

η_D = dryer efficiency

α_f = donor void fraction at dryer face.

The dryer efficiency is computed by comparing the dryer inlet liquid quality to a critical dryer inlet liquid quality. The dryer efficiency is 100% if the dryer inlet liquid quality is below the critical dryer inlet liquid quality and is zero if the dryer inlet liquid quality exceeds the critical inlet liquid quality by a user-defined amount, ΔX_d. The dryer efficiency is linearly interpolated between these two extremes based on the dryer inlet liquid quality. The dryer efficiency is given by

$$\eta_D = \begin{cases} 1.0 \text{ for } X_i < X_{i,crit} \\ 1.0 + \dfrac{X_{i,crit} - X_i}{\Delta X_d} \text{ for } X_{i,crit} < X_i < X_{i,crit} + \Delta X_d \\ 0.0 \text{ for } X_i > X_{i,crit} + \Delta X_d \end{cases} \quad (3.9\text{-}2)$$

where

η_D = dryer efficiency

X_i = dryer inlet liquid quality

$X_{i,crit}$ = critical dryer inlet liquid quality, and

ΔX_d = range of dryer inlet liquid quality over which efficiency degrades from 100% to 0%.

The range of dryer inlet liquid quality over which the dryer efficiency degrades is a user-input constant.

The dryer inlet liquid quality is determined from the donor void fraction assuming homogeneous flow at the dryer face and is given by

$$X_i = 1 - \frac{\alpha_f}{\alpha_f + (1 - \alpha_f)\left(\dfrac{\rho_\ell}{\rho_v}\right)} \quad (3.9\text{-}3)$$

where ρ_ℓ and ρ_v are the donor liquid and vapor densities, respectively.

Finally, the critical dryer inlet liquid quality is given as a linear function of the vapor velocity at the dryer face and is given by

$$X_1 = \begin{cases} 1.0 \text{ for } V_{vd} < V_{vd,\ell} \\ 1.0 - \left(\dfrac{V_{vd} - V_{vd,\ell}}{V_{vd,u} - V_{vd,\ell}} \right) \text{ for } V_{vd,\ell} < V_{vd} < V_{vd,u} \\ 0.0 \text{ for } V_{vd,u} < V_{vd} \end{cases} \quad (3.9\text{-}4)$$

where

V_{vd} = vapor velocity at dryer face

$V_{vd,\ell}$ = lower dryer vapor velocity

$V_{vd,u}$ = upper dryer vapor velocity.

The lower dryer vapor velocity is the dryer inlet vapor velocity below which the dryer efficiency is 100% regardless of dryer inlet liquid quality. The upper dryer vapor velocity is the dryer inlet vapor velocity above which the dryer efficiency is less than 100% regardless of dryer inlet liquid quality. The dryer efficiency relationships are summarized in Figure 3.9-4.

3.9.2.3 Separator Void Fraction. The computation of the separator void fraction is much more complicated and is divided into two phases. The first phase of the calculation is the determination of the liquid carryover and vapor carryunder qualities. This calculation is performed once per time step in the prepass phase of the TRAC-BF1/MOD1 numerical integration scheme. If the simple separator option is used, the user-input values of liquid carryunder quality X_{co} and vapor carryunder quality X_{cu} are used. If the mechanistic separator option has been selected by the user, X_{co} and X_{cu} are determined by a call to subroutine SSEPOR, which computes the phasic flow rates of liquid and vapor at the two outlet ports of the separator using the separator geometric data and the local conditions at the separator inlet. (See Reference 3.9-3 for the details of calculation.) The carryover liquid quality X_{co} and the vapor carryunder quality X_{cu} are assumed to remain constant during the iterations used to update the TRAC-BF1/MOD1 hydrodynamic variables.

3.9.2.4 Implicit Portion of Separator Solution. Once the liquid carryover quality X_{co} and the vapor carryunder quality X_{cu} have been determined, the joining cell target void fraction α_j and the vapor carryunder mass flow rate $M_{v,cu}$ are determined. This calculation is performed once per iteration to prevent the overextraction of mass from the joining cell. The joining cell void fraction is determined from the liquid carryover quality assuming homogeneous flow at the exit of the separator and is given by

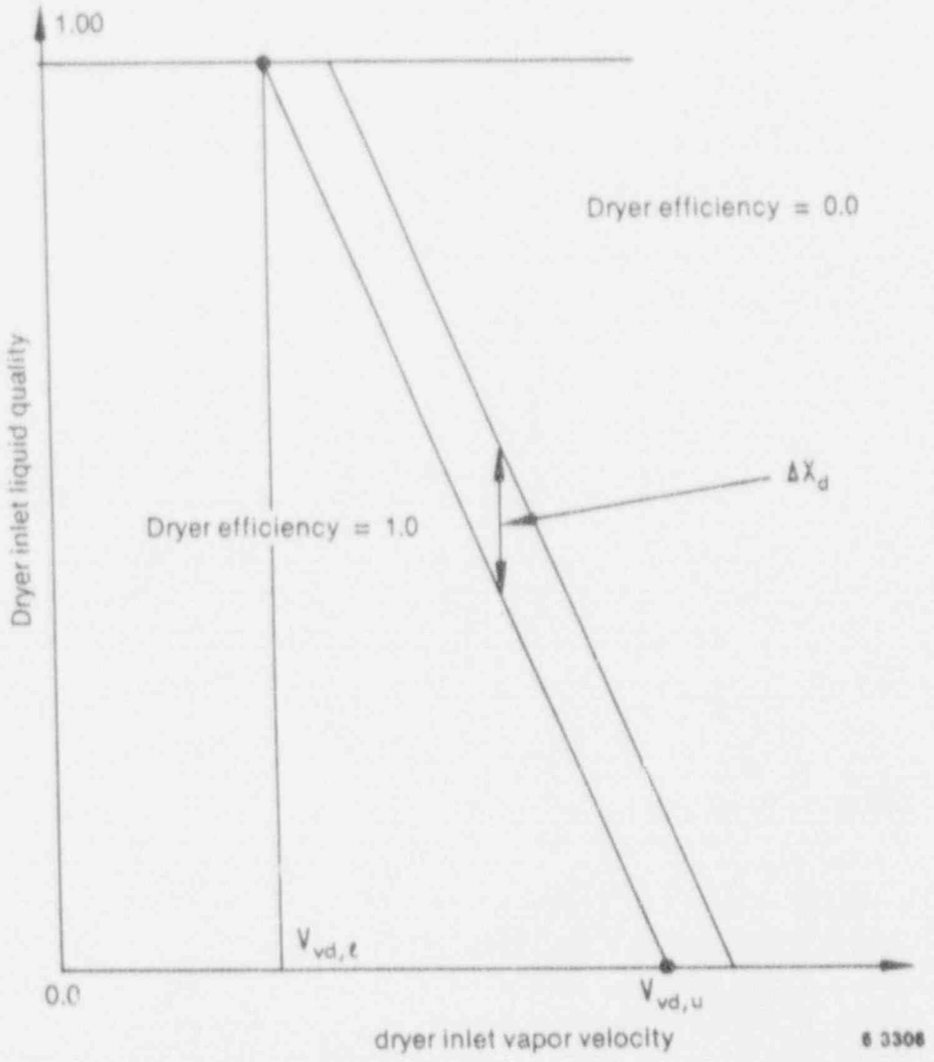

Figure 3.9-4. Dryer efficiency summary.

$$\alpha_o = \frac{1 - X_{co}}{1 - X_{co} + \left(\frac{\rho_v}{\rho_\ell}\right) X_{co}} \qquad (3.9\text{-}5)$$

$$\alpha_o = Min\ [\alpha_o,\ 0.995]\ . \qquad (3.9\text{-}6)$$

The vapor carryunder mass flow rate is computed from a steady-state vapor mass balance on the joining cell and is given by

$$\dot{M}_{v,cu} = \frac{\dot{M}_{v,i} - \left(\frac{1 - X_{co}}{X_{co}}\right)\dot{M}_{\ell,i}}{1 - \left(\frac{1 - X_{cu}}{X_{cu}}\right)\left(\frac{1 - X_{co}}{X_{co}}\right)}$$

where

$\dot{M}_{v,i}$ = vapor mass flow rate into joining cell

$\dot{M}_{\ell,i}$ = liquid mass flow rate into joining cell.

Once the target joining cell void fraction α_o and the vapor carryunder mass flow rate $\dot{M}_{v,cu}$ have been computed, the separator void fraction and side arm fluid velocity can be computed.

The liquid mass flow rate out of the side arm is computed from a steady-state liquid mass balance on the joining cell

$$\dot{M}_{\ell,s} = \dot{M}_{\ell,x} - \Gamma - \dot{M}_{\ell,o} - \frac{F(\alpha_o - \alpha)\rho_\ell}{\Delta t} Vol \qquad (3.9\text{-}8)$$

where

$\dot{M}_{\ell,s}$ = liquid flow rate in side arm

$\dot{M}_{\ell,x}$ = extrapolated liquid inlet mass flow rate

$\dot{M}_{\ell,o}$ = dryer liquid flow rate.

The last term represents the liquid mass flow rate needed to remove the excess liquid in the joining cell and return the joining cell void fraction to the target value during the current time step. The attempt to return the joining cell void fraction to the target value sometimes leads to overextraction of mass from the joining cell. The factor F varies inversely with the number of iterations being used during this time step to attempt to prevent this overextraction and is given by

$$F = \begin{cases} 1.0 \text{ for } OITNO \le 2 \\ 1.0 - 0.25\,(OITNO - 2) \text{ for } 2 < OITNO \le 5 \\ 0.25 \text{ for } 5 < OITNO \end{cases} \tag{3.9-9}$$

where OITNO is the number of iterations. At steady state, when the joining cell void fraction is equal to the desired value, this term is identically zero. The extrapolated liquid mass flow rate is given by

$$\dot{M}^n_{\ell,x} = \dot{M}^n_{\ell,i} + (\dot{M}^n_{\ell,i} - \dot{M}^{n-1}_{\ell,i}) \frac{\Delta t^n}{\Delta t^{n-1}} \tag{3.9-10}$$

where

$\dot{M}^{n-1}_{\ell,i}$ = liquid mass flow rate from previous time step, and

Δt^{n-1} = previous time step size.

The liquid mass flow rate at the dryer face is computed using the current dryer void fraction.

The side arm fluid velocity can now be computed assuming homogeneous flow as

$$V_s = \frac{1}{A}\left(\frac{\dot{M}_{\ell s}}{\rho_\ell} + \frac{\dot{M}_{v,cu}}{\rho_v}\right) \tag{3.9-11}$$

where A is the side arm flow area. The separator void fraction is then computed from

$$\alpha_s = \begin{cases} \alpha & \text{for } V_s < 0.0 \\ \dfrac{\dot{M}_{v,cu}}{\rho_v V_s A} & \text{for } V_s > 0.0 \end{cases} \tag{3.9-12}$$

which means that the actual donor void fraction is used if reverse flow in the side arm is indicated.

3.9.2.5 Separator Velocity Solution. If reverse flow in the side arm is indicated by Equation (3.9-11), the side arm loss coefficient from the previous time step is used. If positive velocity in the side arm is indicated by Equation (3.9-11), then a new side arm loss coefficient is computed.

3.9.2.6 **Side Arm Loss Coefficient.** The side arm loss coefficient needed to balance the imposed pressure gradient is computed from a simplified steady-state momentum equation across the side arm face. This simplified momentum equation includes pressure drop, form losses, and gravity lead across the side arm face and is given by

$$\Delta P = \frac{1}{2} K \rho_m V_s^2 - g \rho_m \Delta X \qquad (3.9\text{-}13)$$

where

ΔP = pressure drop from center of joining cell to center of first side arm cell

K = side arm loss coefficient

ρ_m = average mixture density

g = gravitational constant

ΔX = distance from cell center to cell center.

The gravity head term assumes that the side arm is directed downward, and the input processor flags an error if the user does not specify a vertically directed side arm. This equation is solved for the side arm loss coefficient. The value computed is averaged with the value from the previous time step, and the averaged value is restricted to be within a factor of two of the previous value.

3.9.2.7 **Side Arm Velocity Solution.** The side arm loss coefficient is used in the time-dependent form of the simplified momentum equation to determine the predicted side arm fluid velocity and its derivative with respect to pressure gradient. The predicted fluid velocity is given by

$$V_s^n = \frac{V_s^{n-1} + \Delta t \left(\frac{\Delta P}{\rho_m \Delta X} + g \right)}{1 + \frac{1}{2} \frac{\Delta t}{\Delta X} K \left| V_s^{n-1} \right|} \qquad (3.9\text{-}14)$$

where

V_s^n = predicted side arm velocity

V_s^{n-1} = beginning of time step side arm velocity

and the other terms have been defined previously.

The derivative of the side arm velocity with respect to pressure gradient is given by,

$$\frac{\partial V}{\partial P} = \frac{\Delta t}{\Delta X \rho_m \left(1 + \frac{1}{2}\frac{\Delta t}{\Delta X} K \left|V_s^{n-1}\right|\right)} \qquad (3.9\text{-}15)$$

where $\partial V/\partial P$ is the derivative of the side arm velocity with respect to the pressure gradient. These two values are used in the solution of the continuity and energy equations in place of the regular momentum solution for the first side arm face.

3.9.3 References

3.9-1. D. D. Taylor et al., *TRAC-BD1/MOD1: An Advanced Best Estimate Computer Program for Boiling Water Reactor Transient Analysis, Volume 1: Model Description*, NUREG/CR-3633, EGG-2294, April 1984.

3.9-2. Y. K. Cheung, V. Parameswaran, and J. C. Shaug, *BWR Refill-Reflood Program Task 4.7-Model Development: TRAC-BWR Component Models*, NUREG/CR-2457, GEAP-22052, April 1983.

3.9-3. M. J. Thurgood et al., *COBRA-TRAC-A Thermal-Hydraulics Code for Transient Analysis of Nuclear Reactor Vessels and Primary Coolant Systems, Volume 1*, NUREG/CR-3046, PNL-4385, March 1983.

3.10 CONTAN

The containment (CONTAN) component in TRAC-BF1/MOD1 computes fluid temperature, pressure, and void fraction at the coupling points (BREAK, FILL, and VESSEL components) between the containment and the primary cooling loop (PCL). The containment model is patterned after the lumped parameter containment analysis in CONTEMPT-LT,[3.10-1] where the containment is modeled as a collection of compartments, each of which contains a well-mixed vapor and liquid region. Mass inventories of liquid water, steam, and noncondensable gas (air) and total energy inventories of vapor and liquid are computed as functions of tune. The calculation is performed by explicit integration of a coupled system of ordinary differential equations of the form

$$\dot{\bar{Y}} = \bar{F}(\bar{Y},t) \qquad (3.10\text{-}1)$$

where

$\bar{Y}$ = vector of mass and energy inventories in containment compartments

t = time.

The fluid temperatures and pressures in containment compartments are computed at each time step from the current mass and energy inventories. Mass and energy may enter or leave the containment by the following six paths:

1. PCL BREAK component flows
2. PCL FILL component flows that simulate emergency core cooling systems that draw cooling water from containment pool regions
3. Conduction heat transfer in exterior containment walls and reactor pressure vessel exterior surfaces
4. Liquid sources exterior to the containment that supply makeup water to pool regions and cooling sprays
5. Convective coolers designed to exhaust heat from the containment by use of external cooling fluids
6. Heat sources within the containment itself, such as pump motors.

Within the containment, mass and energy are assumed to be transported by the following processes:

1. Pressure-induced fluid flows through junctions between compartments
2. User-specified forced convective flows between compartments

3. Convective heat transfer between containment fluids and heat structures (thermal masses) inside the containment (walls, metal components, etc.)

4. Finite rate interfacial heat and mass transfer between pool and vapor regions by free convection.

The above processes are represented in separate models that simulate various BWR containment components. These component models are briefly described below.

Compartment. The compartment component simulates a volume or room within the containment. As previously mentioned, a compartment is composed of a vapor and a liquid region, both of which are assumed to be perfectly mixed single-phase regions. Pressure equilibrium, but not temperature equilibrium, is assumed between the two regions; and the vapor region is represented as an isothermal Gibbs-Dalton mixture of noncondensable gas (air) and steam. The pressure of the mixture is the sum of the partial pressures of steam and noncondensable gas. Pressure and temperature in the vapor region are calculated from mass inventories of noncondensable gas and steam, total internal energy, and total vapor region volume.

Heat Structure. The heat structure component simulates heat transfer between a thermal mass and a containment fluid region. The model utilizes the standard TRAC-BF1/MOD1 wall heat transfer correlations to calculate a heat transfer coefficient (h) and uses explicit boundary conditions to calculate the temperature profile in the heat structure at the end of each containment time step. Cylindrical geometry is assumed for the conduction solution in the heat structure. The energy flow rate (U) from the containment region to the heat structure is

$$U = hA(T_f - T_w) \quad . \tag{3.10-2}$$

Cooler. The cooler component simulates the effect of a convective heat source/sink in a containment region. The cooler heat exchange characteristics are specified by the user in either of two forms: (a) The user specifies a constant overall heat transfer coefficient (hA) and a coolant fluid temperature (T_c) that may vary with time. In this case, the energy flow rate from the containment region is calculated from

$$U = (hA)(T_f - T_c) \quad . \tag{3.10-3}$$

(b) the user specifies a cooling rate $\dot{Q}_c$ as a function of time, in which case the energy flow rate from the containment compartment where the cooler is located is simply

$$\dot{U} = \dot{Q}_c \ . \qquad (3.10\text{-}4)$$

By appropriate choices for $T_c(t)$ or $\dot{Q}_c(t)$, the cooler can act as either a heat source or sink.

Passive Flow Junction. The passive junction component simulates pressure-induced convective flow between two compartments. Three types of passive flow junction are allowed:

1. Single-phase gas flow between the vapor regions of two compartments. Flow may occur in either direction, depending on the pressure gradient. This type of junction is intended to simulate an opening or passage connecting two rooms in the containment.

   The mass flow rate is assumed to be the lesser of the two values obtained by assuming (a) steady pipe flow and (b) steady orifice flow through the junction. For steady pipe flow, the mass flow rate is

   $$\dot{M} = \rho A V \qquad (3.10\text{-}5)$$

   where

   ρ = vapor density in donor compartment vapor region

   A = user-supplied junction flow area

   v = junction flow velocity.

   V is computed from the pipe flow equation

   $$P_D - P_R = \frac{1}{2}\frac{FL}{D_H}\rho V^2 \qquad (3.10\text{-}6)$$

   where P_D and P_R are the fluid pressures in donor and receiver compartments, respectively. In the pipe equation, F is computed from the Reynolds number (Re) using the Blasius relation

   $$F = \frac{0.316}{Re^{1/4}} \qquad (3.10\text{-}7)$$

   for turbulent flow, and the Hagen-Poiseuille relation

   $$F = \frac{64}{Re} \qquad (3.10\text{-}8)$$

for laminar flow. The transition Reynolds number is assumed to be 1189. For simple orifice flow, the mass flow rate is

$$\dot{M} = (\rho A V) C_d \qquad (3.10\text{-}9)$$

with all parameters defined as for pipe flow except C_d, which is the orifice discharge coefficient and is assumed to be 0.6. The velocity V is calculated from the Bernoulli equation assuming reservoir-type flow to the orifice

$$P_D = P_R + \rho \frac{V^2}{2} \, . \qquad (3.10\text{-}10)$$

2. Single-phase gas flow in one direction only between the vapor regions of two compartments. This type of junction simulates the pressure relief valve that allows flow in one direction when the pressure difference between compartments reaches a prescribed value. The mass flow rate is computed in the same manner as for Case 1 except that the pressure difference used in the velocity determination is

$$P_D = P_R + \Delta P_{crit}) \qquad (3.10\text{-}11)$$

where ΔP_{crit} is the minimum pressure difference for flow to occur.

3. Single-phase gas flow in one direction only between the vapor region of the donor compartment and the liquid region of the receiver compartment. The flow is computed in the same manner as in Case 2.

The fluid mass flow rates are used to compute the respective rates of change of mass and energy inventories in the donor and receiver compartments.

Forced Flow Junction. The forced flow junction component simulates an active containment system that transports liquid from one compartment to another. The user specifies the volume flow rate [$Q_\ell(t)$] as a function of time and the spray efficiency, if the flow represents a spray cooler. Rates of change of mass and energy inventories in the donor and receiver compartment are computed from the junction mass flows as in the case of the passive flow junction. It should be noted that for all containment flow junctions, the flow work is attributed to the vapor region energy inventories in the donor and receiver compartments, i.e., the liquid is assumed incompressible.

Source/Sink Flow Junction. The source/sink flow junction component simulates an external source of liquid water pumped into the containment. The user specifics the volume flow, rate of liquid [$Q_\ell(t)$] into or out of the containment compartment and, if the junction is a source, the liquid inlet temperature. The mass and energy flow rates into the compartment to which the

junction is attached are computed accordingly.

BREAK, FILL, and VESSEL components may be coupled to the containment at the option of the user. BREAK components so coupled will have fluid conditions (pressure, temperature, and void fractions) corresponding with those at the containment location specified by the user. FILL components drawing liquid from containment sources (such as the pressure suppression pool in the BWR wetwell) will similarly have fluid conditions that are periodically updated by the containment model.

The VESSEL component may be thermally coupled to the containment by the user (see Subsection 3.8). By specifying which containment compartment represents the drywell and the position of the vessel above the drywell floor, the containment module will periodically update the vessel exterior heat transfer coefficients and fluid temperatures that provide the outside boundary condition for the temperature calculation in the vessel wall.

The containment calculation is done in parallel with (and independent of) the PCL and is updated at real time intervals that are specified by the user. Since characteristic physical response times for the containment are generally several orders of magnitude greater than the time step size used for the PCL hydrodynamic calculation, the interval at which the containment calculation is updated may generally be several tens or hundreds of time steps. Therefore, the mass and energy flows between the containment and the PCL are computed at each time step by the PCL component models themselves and integrated over time. These integrated mass and energy flows to/from the containment are then included in the calculation of the rates of change of containment mass and energy inventories during the containment condition update. With the foregoing models, the containment module calculates the function $F[Y(t),t]$ in Equation (3.10-1). From the above descriptions, the form of F is

$$\bar{F}[\bar{Y}(t),t] = \sum_{i=2}^{6} \sum_{j=1}^{N_i} \bar{F}_{ij}[\bar{Y}(t),t] \qquad (3.10\text{-}12)$$

where

N_i = number of containment components of type i used in the containment model

$\bar{F}_{ij}[\bar{Y}(t),t]$ = contribution to Y due to jth component of type i

i = 1,...,6 correspond to COMPARTMENT, HEAT STRUCTURE, COOLER, PASSIVE JUNCTION, FORCED JUNCTION, SOURCE/SINK JUNCTION, components.

The new time inventories at time $(t + \Delta t)$ are computed explicitly as

$$\bar{Y}(t + \Delta t) = \bar{Y}(t) + \bar{F}[\bar{Y}(t), t]\ \Delta t \ . \qquad (3.10\text{-}13)$$

At the end of each time step, the maximum fractional change (FRAC) in mass and energy inventories is computed as

$$FRAC = \max_{\ell} \left| \frac{Y_{\ell}(t + \Delta t) - Y_{\ell}(t)}{Y_{\ell}(t)} \right| \qquad (3.10\text{-}14)$$

where Y_{ℓ} is the ℓth entry in the vector Y.

A maximum time step (τ_{HS}) for stability of the conduction solution for the heat structure temperature profiles is next computer as

$$\tau_{HS} = Min \left[\frac{\left(r_s \Delta r + \frac{\Delta r^2}{4} \right) \rho c}{2 r_s (h_{\ell} + h_v)} \right]_i \quad for\ i = 1, N_{hs} \qquad (3.10\text{-}15)$$

Where

N_{hs} = number of heat structures in TRAC-BF1/MOD1 model

ρ, c = heat structure i material properties

r_s = radius of curvature of heat structure i

Δr = radial node size used in conduction solution for heat structure i.

The time step, Δt, used in the explicit containment integration is controlled on the basis of the current values of FRAC and τ_{HS}. If $\tau_{HS} < \Delta t$ and/or FRAC > 0.05, then the time step is halved and the integration is repeated; if $\tau_{HS} > 2\Delta t$ and FRAC < 0.005, then the time step is doubled. If $0.005 \leq FRAC \leq 0.05$ and $\tau_{HS} > \Delta t$, the time step is not changed and the integration proceeds to the next time step.

A sample containment model is illustrated schematically in Figure 3.10-1. In this model, the VESSEL is thermally coupled to the drywell (Compartment 1). The PCL BREAK component is also located in the drywell, and the drywell is connected to the wetwell with a Type 3 passive flow junction that represents the vents. A Type 2 passive junction represents a vacuum breaker valve between the wetwell and drywell. The walls of the containment are represented by two heat structures. ECC water drawn from the pressure suppression pool is simulated by connecting a FILL to the wetwell (Compartment 2). Finally, a residual heat removal system in the suppression pool is represented by a cooler component.

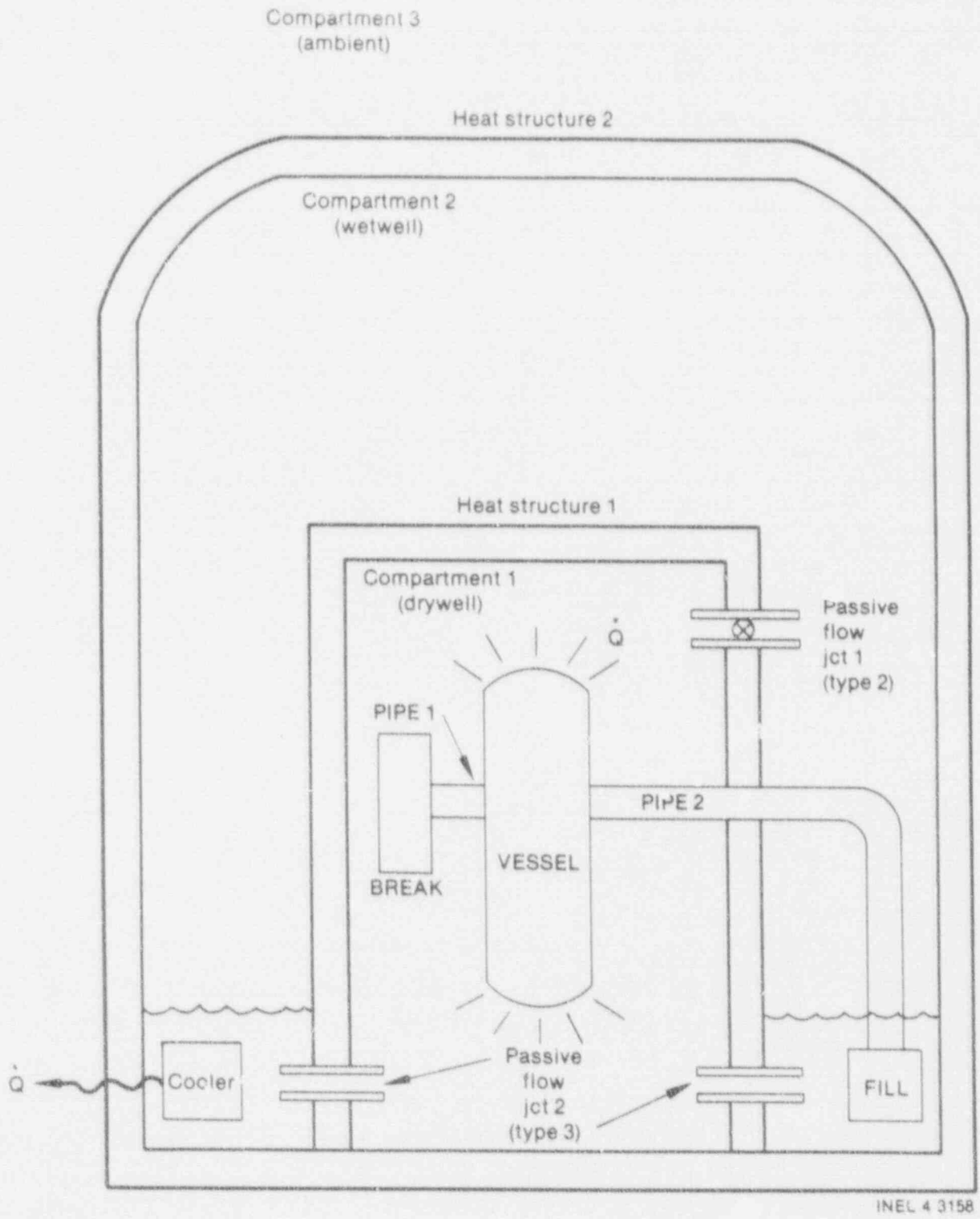

Figure 3.10-1. Sample containment schematic.

It should be noted that the user may assemble any number of each of the six containment components discussed above in any arbitrary fashion and is not limited to a single drywell and wetwell.

3.10.1 Reference

3.10-1. D. W. Hargroves and L. J. Metcalfe, *CONTEMPT-LF/028--A Computer Program for Predicting Containment Pressure-Temperature Response in a Loss-of-Coolant Accident*, NUREG/CR-0255, March 1979.

3.11 CONTROL SYSTEM

The TRAC-BF1/MOD1 control system model is designed to serve two primary purposes. First, it allows the user to model an actual BWR plant control system at any desired level of detail. The accurate modeling of the plant control system can play an important role in the successful analysis of many transients, including ATWS and operational transient analyses. Secondly, the control system may be used to assist in the initialization of any TRAC-BF1/MOD1 plant deck by allowing the user to automatically control the value of certain plant parameters during the initialization process.

In practice, the control system model permits the user to take data from the TRAC-BF1/MOD1 thermal-hydraulic (T/H) data base, perform a wide variety of user-specified operations on these data in an external control system, then use the results of these operations to adjust geometric or dynamic variables in the TRAC-BF1/MOD1 data base. For example, pressure in a BWR main steamline may be used as input to the control system that generates an output signal to adjust the area of the steamline pressure control valve (PCV). A large number of control loops of a similar nature may be utilized to simulate an entire BWR plant control system.

3.11.1 Control Blocks

A TRAC-BF1/MOD1 control system model is built up from basic functional elements called control blocks. Each control block performs a simple operation on input data to generate an output value. A complete list of the types of control blocks and a description of their operations is found in Table 3.11-1. The various control block types require from zero to three input values, and each generates a single output value. Input and output values may be logical (0 or 1) or continuously varying, depending upon the type of control block. Associated with each control block are the following user-specified parameters:

1. A control block number from 1 to 999, uniquely identifying each block. Block numbers need not be consecutive.

2. The type of operation to be performed upon the input data.

3. The constants C1 and C2[a]

---

a. The various control block constants (C1, C2, XMAX, and XMIN) may not be required, depending on the control block type. See Table 3.11-1 for specific requirements.

Table 3.11-1. Description of control block operations.

Type	Block[a] Type	Block[b] Input 1	Block Input 2	Block Input 3	Block Const 1	Block[c] Const 2	Gain[c] Factor	Upper[c] Limit	Lower[d] Limit	Initial Value	Control Block Name	Control Block Mathematical Operation[e]
1	ABSV	X1	N/A	N/A	N/A	N/A	G	XMAX	XMIN	XIV	Absolute Value	XOUT = G*ABS(X1)
2	ACOS	X1	N/A	N/A	N/A	N/A	G	XMAX	XMIN	XIV	Arcosine	XOUT = G*ACOS(X1), XOUT in Radians
3	ADD	X1	X2	N/A	N/A	N/A	G	XMAX	XMIN	XIV	Add	XOUT = G*(X1+X2)
4	AINT[f]	X1	N/A	N/A	N/A	N/A	G	XMAX	XMIN	XIV	Integral value	XOUT = G*FLOAT[IFIX(X1)]
5	AND[f]	L1	L2	N/A	N/A	N/A	N/A	N/A	N/A	LIV	Logical And	LOUT = 1.0 IF[(L1.EQ.1.0).AND. (L2.EQ.1.0)] = 0.0 Otherwise.
6	ASIN	X1	N/A	N/A	N/A	N/A	G	XMAX	XMIN	XIV	Arcosine	XOUT = G*ASIN(X1), XOUT in Radians
7	ATAN	X1	N/A	N/A	N/A	N/A	G	XMAX	XMIN	XIV	Arctangent	XOUT = G*ATAN(X1), XOUT in Radians
8	ATN2	X1	X2	N/A	N/A	N/A	G	XMAX	XMIN	XIV	Arctangent	XOUT = G*ATAN2(X1/X2), XOUT in Radians
9	CONS	N/A	N/A	N/A	C1	N/A	N/A	N/A	N/A	XIV	Constant	XOUT = C1
10	COS	X1	N/A	N/A	N/A	N/A	G	XMAX	XMIN	XIV	Cosine	XOUT = G*COS(X1), X1 in Radians
11	DEAD	X1	N/A	N/A	C1	C2	G	XMAX	XMIN	XIV	Dead Band, Zone, Space	XOUT = G*(X1-C2) IF(X1.GT.C2) = G*(X1-C1) IF(X1.LT.C1) = 0.0 Otherwise.
12	DER	X1	(X2)	N/A	N/A	N/A	G	XMAX	XMIN	XIV	Derivative	XOUT = G*(dX1/dt)
13	DIML	X1	(X2)	(X3)	N/A	N/A	G	XMAX	XMIN	XIV	Double Integrator with XOUT Limited	See Section 1.2.3.6
14	DIV	X1	X2	N/A	N/A	N/A	G	XMAX	XMIN	XIV	Divide	XOUT = G*X1/X2
15	EOR[f]	L1	L2	N/A	N/A	N/A	N/A	N/A	N/A	LIV	Logical Exclusive Or	LOUT = 1.0 IF[(L1 + L2).EQ.1.0] = 0.0 Otherwise.
16	EQUL[f]	L1	L2	N/A	N/A	N/A	N/A	N/A	N/A	LIV	Logical Equivalent	LOUT = 1.0 IF(L1.EQ.L2) = 0.0 Otherwise.
17	EXP	X1	N/A	N/A	N/A	N/A	G	XMAX	XMIN	XIV	Exponential	XOUT = G*EXP(X1)

Table 3.11-1. (continued)

Type	Block[a] Type	Block[b] Input 1	Block Input 2	Block Input 3	Block Const 1	Block[c] Const 2	Gain[c] Factor	Upper[c] Limit	Lower[d] Limit	Initial Value	Control Block Name	Control Block Mathematical Operation[e]
18	FLFP[f]	L1	(L2)	L3	N/A	N/A	N/A	N/A	N/A	L1V	Logical Flip-flop	LOUT = Flip-flop output which changes state whenever L1 changes state (only if L3 = 1.0).
19	GATE[f]	X1	L2	N/A	N/A	N/A	N/A	N/A	N/A	X1V	Gate	XOUT = X1 IF(L2.EQ.1.0) = 0.0 IF(L2.EQ.0.0)
20	GREQ[f]	X1	X2	N/A	N/A	N/A	N/A	N/A	N/A	L1V	Greater than or equal to	LOUT = 1.0 IF(X1.GE.X2) = 0.0 Otherwise.
21	GRTH[f]	X1	X2	N/A	N/A	N/A	N/A	N/A	N/A	L1V	Greater than	LOUT = 1.0 IF(X1.GT.X2) = 0.0 Otherwise
22	INSW[f]	X1	X2	L3	N/A	N/A	N/A	N/A	N/A	X1V	Input Switch	XOUT = X1 IF(L3.EQ.1.0) = X2 IF(L3.EQ.0.0)
23	INT	X1	N/A	N/A	N/A	N/A	G	XMAX	XMIN	X1V	Integrate	See Section 1.2.3.6
24	INTM	X1	L2	L3	N/A	N/A	G	XMAX	XMIN	X1V	Integrate with mode control	See Section 1.2.3.6
25	IOR[f]	L1	L2	N/A	N/A	N/A	N/A	N/A	N/A	L1V	Logical Inclusive Or	LOUT = 0.0 IF[(L1 + L2).EQ.0.0) = 1.0 Otherwise
26	LAG	X1	N/A	N/A	C1	N/A	G	XMAX	XMIN	X1V	First Order Lag	XOUT = G*X1/(1.0 + C1*s), s is Laplace Operator
27	LDLY[f]	L1	(L2)	N/A	C1	(C2)	N/A	N/A	N/A	L1V	Logic Delay	LOUT = 0.0 IF[(L1.EQ.0.0).OR. (TIMET.GT.(C1 + C2))] = 1.0 IF[(L1.EQ.1.0).AND. (TIMET.LE.(C1 + C2))] where (C2) is the TIMET when L1 Switches from 0.0 to 1.0
28	LGPC[f]	L1	(L2)	L3	N/A	N/A	N/A	N/A	N/A	L1V	Logic General Purpose Counter	LOUT = 0.0 IF(L3.EQ.0.0), Reset Mode = Number of times L1 has changed state since enabled (when L3 = 1.0), count mode
29	LISW[f]	L1	L2	L3	N/A	N/A	N/A	N/A	N/A	L1V	Logic Input Switch	LOUT = L1 IF(L3.EQ.1.0) = L2 IF(L3.EQ.0.0)
30	LLAG	X1	(X2)	(X3)	C1	C2	G	XMAX	XMIN	X1V	Lead-lag Transfer Function	XOUT = G*X1*(1.0 + C1*S)/(1.0 + C2*S) ,S is Laplace Transform Operator

Table 3.11-1. (continued)

Type	Block[a] Type	Block[b] Input 1	Block Input 2	Block Input 3	Block Const 1	Block[c] Const 2	Gain[c] Factor	Upper[c] Limit	Lower[d] Limit	Initial Value	Control Block Name	Control Block Mathematical Operation[e]
31	LINT	X1	N/A	N/A	N/A	N/A	G	XMAX	XMIN	XIV	Limited Integrator	XOUT = G* X1*dt + XIV, X1 is set to 0.0 if XOUT is against a limit and the sign of X1 does not change
32	LOGN	X1	N/A	N/A	N/A	N/A	G	XMAX	XMIN	XIV	Natural Logarithm	XOUT = G*ALOG(X1)
33	LSEQ[f]	X1	X2	N/A	N/A	N/A	N/A	N/A	N/A	LIV	Less than or Equal to	LOUT = 1.0 IF(X1.LE.X2) = 0.0 Otherwise.
34	LSTH[f]	X1	X2	N/A	N/A	N/A	N/A	N/A	N/A	LIV	Less than	LOUT = 1.0 IF(X1.LT.X2) = 0.0 Otherwise.
35	MAXS	X1	X2	N/A	N/A	N/A	N/A	N/A	N/A	XIV	Maximum of 2 signals	XOUT = AMAX1(X1,X2)
36	MAXT	X1	N/A	N/A	N/A	N/A	N/A	N/A	N/A	XIV	Maximum during transient	XOUT = AMAX1(X1,XOUT)
37	MINS	X1	X2	N/A	N/A	N/A	N/A	N/A	N/A	XIV	Minimum of 2 signals	XOUT = AMIN1(X1,X2)
38	MINT	X1	N/A	N/A	N/A	N/A	N/A	N/A	N/A	XIV	Minimum during transient	XOUT = AMIN1(X1,XOUT)
39	MULT	X1	X2	N/A	N/A	N/A	N/A	G	XMAX	XIV	Multiply	XOUT = G*X1*X2
40	NAND[f]	L1	L2	N/A	N/A	N/A	N/A	N/A	N/A	LIV	Logical "Not And"	LOUT = 0.0 IF[(L1 + L2).EQ.2.0] = 1.0 Otherwise.
41	NEQ[f]	L1	L2	N/A	N/A	N/A	N/A	N/A	N/A	LIV	Logical "Not Equal"	LOUT = 1.0 IF(L1.NE.L2) = 0.0 Otherwise.
42	NOR[f]	L1	L2	N/A	N/A	N/A	N/A	N/A	N/A	LIV	Logical "Not Inclusive Or"	LOUT = 1.0 IF[(L1 + L2).EQ.0.0] = 0.0 Otherwise.
43	NOT[f]	L1	N/A	N/A	N/A	N/A	N/A	N/A	N/A	LIV	Logical "Not" or Negation	LOUT = 1.0 IF(L1.EQ.0.0) = 0.0 IF(L1.EQ.1.0)
44	PDIF	X1	X2	N/A	N/A	N/A	G	XMAX	XMIN	XIV	Positive Difference	XOUT = G*(X1 - X2) IF(X1.GT.X2) = 0.0 Otherwise.

Table 3.11-1. (continued)

Type	Block[a] Type	Block[b] Input 1	Block Input 2	Block Input 3	Block Const 1	Block[c] Const 2	Gain[c] Factor	Upper[c] Limit	Lower[d] Limit	Initial Value	Control Block Name	Control Block Mathematical Operation[e]
45	QUAN[f]	X1	N/A	N/A	N/A	N/A	G	XMAX	XMIN	XIV	Quantizer	XOUT = G*FLOAT[IFIX(Z1+0.5)] IF(X1.GE.0.0) = G*FLOAT[IFIX(X1 - 0.5)] IF(X1.LT.0.0)
46	RAMP	N/A	N/A	N/A	C1	N/A	G	XMAX	XMIN	XIV	Ramp	XOUT = G*TIMET-C1) IF(TIMET GT.C1) = 0.0 Otherwise.
47	RAND[f]	N/A	N/A	N/A	C1	N/A	G	XMAX	XMIN	XIV	Random Number Generator	XOUT = G*RANF(DUMY) IF(TIMET.GE.C1) = 0.0 Otherwise.
48	SIGN	X1	X2	N/A	N/A	N/A	N/A	N/A	N/A	XIV	Sign Function	XOUT = $_{\pm}$X1$_{\pm}$ IF(X2.GE.0.0) = $_{\pm}$X1$_{\pm}$ IF(X2.LT.0.0)
49	SIN	X1	N/A	N/A	N/A	N/A	N/A	XMAX	XMIN	XIV	Sine	XOUT = G*SIN(X1), X1 in Radians
50	SINV	X1	N/A	N/A	N/A	N/A	G	XMAX	XMIN	XIV	Sign Inversion	XOUT = -G*X1
51	SOTF	X1	(X2)	(X3)	C1	C2	G	XMAX	XMIN	XIV	Second Order Transfer Function	XOUT = G*X1/(1.0 + C1*s + C2*s**2), s is Laplace Transform Operator
52	SQRT	X1	N/A	N/A	N/A	N/A	G	XMAX	XMIN	XIV	Square Root	XOUT = G*SQRT(X1)
53	STEP	N/A	N/A	N/A	C1	N/A	G	XMAX	XMIN	XIV	Step	XOUT = G IF(TIMET.GE.C1) = 0.0 Otherwise.
54	SUBT	X1	X2	N/A	N/A	N/A	G	XMAX	XMIN	XIV	Subtract	XOUT = G*(X1 - X2)
55	TAN	X1	N/A	N/A	N/A	N/A	G	XMAX	XMIN	XIV	Tangent	XOUT = G*TAN(X1), X1 in Radians
56	TIME	N/A	N/A	N/A	N/A	N/A	N/A	N/A	N/A	XIV	Time	XOUT = TIMET
57	TRIP[f]	L1	N/A	N/A	N/A	N/A	N/A	N/A	N/A	LIV	Trip Status	LOUT = L1 = 1.0 if Trip + Delay time has elapsed = L1 = 0.0 Otherwise.
58	VLIM	X1	X2	X3	N/A	N/A	G	N/A	N/A	XIV	Variable Limiter	XOUT = X2 IF[(G*X1).GT.X2], at upper limit = X3 IF[(G*X1).LT.X3], at lower limit = G*X1 Otherwise, between limits

Table 3.11-1. (continued)

Type	Block[a] Type	Block[b] Input 1	Block Input 2	Block Input 3	Block Const 1	Block[c] Const 2	Gain[c] Factor	Upper[c] Limit	Lower[d] Limit	Initial Value	Control Block Name	Control Block Mathematical Operation[e]
59	WSUM	X1	X2	N/A	C1	C2	G	XMAX	XMIN	XIV	Weighted Summer	XOUT = G*(C1*X1 + C2*X2)
60	XPO	X1	X2	N/A	N/A	N/A	G	XMAX	XMIN	XIV	Exponentiate	XOUT = G*(X1**X2)
61	ZOH[f]	X1	L2	N/A	N/A	N/A	N/A	N/A	N/A	XIV	Zero Order Hold	XOUT = X1 IF(L2.EQ.1.0) = XOUT Otherwise.
100	DLAY	X1	n	N/A	C1	N/A	G	XMAX	XMIN	XIV	Time Delay	XOUT = XIV IF(TIMET.LE.C1) = G*X1(TIMET-C1) Otherwise Where n is number of delay table time intervals.
101	FNG1	X1	n	N/A	N/A	N/A	G	XMAX	XMIN	XIV	Function of one independent variable	XOUT = G*f_n(X1); where n is function table number.

a. An "X" parameter indicates a continuous variable; and "L" parameter indicates a logical (or discrete) parameter having a value of 0.0 or 1.0 only.

b. Variables enclosed in ( ) are not input variables but are used internally by the control block for data storage.

c. If G, XMAX, and XMIN are required for a control block, a constant gain factor and constant upper and lower limits will be applied at the values given. Default values for the limits are +1.0E+50 and -1.0E+50. If XOUT-GT-XMAX, XOUT is set equal to XMAX. If XOUT-LT-XMIN, XOUT is set equal to XMIN.

d. An initial value (XIV or LIV) is loaded into a control block output (XOUT or LOUT) at TIMET = 0.0 s.

e. XOUT appearing on the right-hand side of a defining equation indicates a previous time step value.

f. These blocks may not be included in a control system implicit loop.

4. The gain factor G.

5. The maximum and minimum limits XMAX and XMIN.

6. The initial value (XIV or LIV) of the block output.

7. An optional 10-character name.

A control block may be represented schematically by a control block diagram, as shown in Figure 3.11-1.

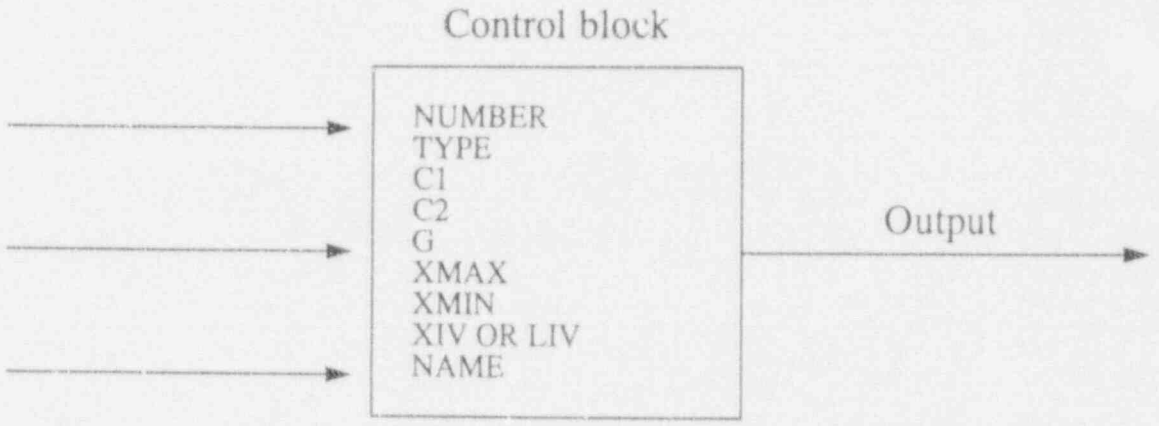

Figure 3.11-1. Schematic control block diagram.

The input values to control blocks may be obtained from the TRAC-BF1/MOD1 thermal-hydraulic data base (pressure, liquid level, and flow rate) or from the output of other control blocks. Thus, an extensive network of control blocks can be assembled to perform very complex operations. Control block outputs may be used as input values for other control blocks, or may be used to control (redefine) the values of variables in the TRAC-BF1/MOD1 component data base (VALVE areas, PUMP torques, and FILL velocities). Table 3.11-2 contains a list of variables from the TRAC-BF1/MOD1 data base that may be used as control block inputs or may be adjusted by control block outputs.

Figure 3.11-2 illustrates a system comprised of seven control blocks, representing a basic BWR pressure control system, designed to control the steam line inlet pressure by varying the pressure control valve area. This system obtains one of its inputs (steam line pressure) from the TRAC-BF1/MOD1 component data base and uses one of its outputs (new valve area) to alter the VALVE component data base. The remaining inputs and outputs are internal to the control system simulation.

Table 3.11-2. Control system input/output variables.

Variable Symbolic Name	Description	Input Components (Variable may be input to control system from these components)	Output Components (Variable may be adjusted by control system output for these components)	Comments
TIME	Reactor Time (s)	TIME	None	
POWR	Total Reactor Power (W)	NEUTRON KINETICS	NEUTRON KINETICS	
TRIP	Trip Condition	TRIP	TRIP	Input variable IOCMP is Trip Number
ALFA	Vapor Fraction	CHAN, FILL, PIPE, PUMP, TEE, VALVE, VESSEL	FILL	
PRES	Pressure (Pa)	BREAK, CHAN, PIPE, PUMP, TEE, VALVE, VESSEL	BREAK	
TLIQ	Liquid Temperature (K)	CHAN, FILL, PIPE, PUMP, TEE, VALVE, VESSEL	FILL	
TVAP	Vapor Temperature (K)	CHAN, FILL, PIPE, PUMP, TEE, VALVE, VESSEL	FILL	
MDOT	Mass Flow Rate (kg/s)	CHAN, FILL, PIPE, PUMP, TEE, VALVE	FILL	For MDOT and ENTH: IOCEL=1 gives inlet quantity
ENTH	Mixture Enthalpy (J/kg)	CHAN, PIPE, PUMP, TEE, VALVE	None	IOCEL=2 gives outlet quantity IOCEL=3 gives TEE side arm quantity
TORQ	Torque (N-M)	PUMP, TURB	PUMP	Value is dimensionless (fraction of rated torque) for PUMP
OMEG	Angular Speed (rad/s)	PUMP, TURB	None	
AREA	Valve Area (fraction of fully open area)	VALVE	VALVE, TEE	Controls area of face NCELL1 in TEE used as feedwater heater.
LLEV	Downcomer Liquid Level (m)	VESSEL, PIPE, TEE	None	IOCEL is VESSEL Theta Zone Number. Measured from bottom end of component for PIPE and TEE.
RHOC	Control Rod Reactivity (ak/k)	KINETICS	None	

Table 3.11-2. (continued)

Variable Symbolic Name	Description	Input Components (Variable may be input to control system from these components)	Output Components (Variable may be adjusted by control system output for these components)	Comments
RHOA	Additive Control Reactivity (ak/k)	None	KINETICS	
BORC	Core Average Boron Concentration (ppm)	KINETICS	NONE	
CROD	Control rod group position	KINETICS	KINETICS	IOCEL is control rod group number

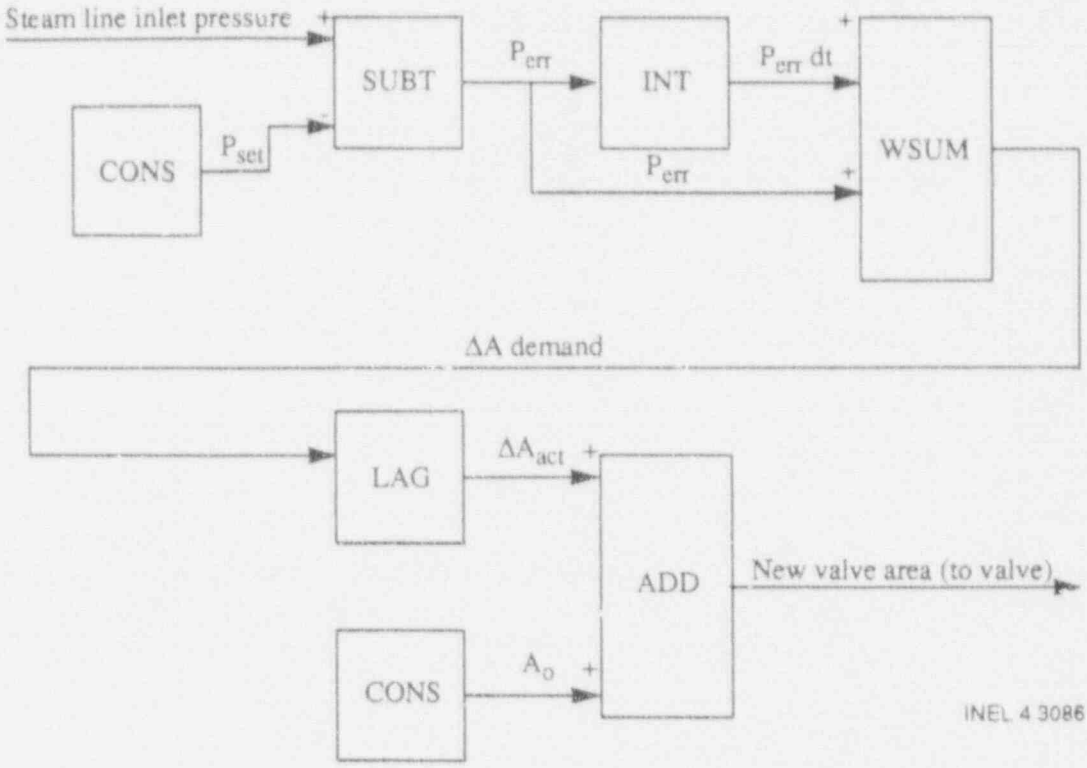

Figure 3.11-2. Simplified BWR pressure control system.

3.11.2 Control System Computational Sequence

The control system calculation is managed by subroutine CONSYS, which is called during the post-pass phase of the TRAC-BF1/MOD1 computational cycle. In its normal mode of operation, CONSYS begins the computation of each control block by obtaining the specified inputs for the control block. The symbolic locations of the inputs required for each control block are user-supplied. If the designated input is from another control block, the stored output from that control block is loaded into the input array for the current control block. If the requested input is from the TRAC-BF1/MOD1 thermal-hydraulic data base, the data base for the required TRAC-BF1/MOD1 component is moved into the TRAC-BF1/MOD1 BLANK COMMON storage array and the desired parameter value is located and loaded into the control input array.

The computational cycle continues with the execution of the control block operation by subroutine CONBLK. The newly updated control block output is then stored for use by other control blocks. If the output value is to be used to control a variable in the TRAC-BF1/MOD1 component data, the data base for that component is altered accordingly, so that the altered value will be used during the next thermal-hydraulic time step.

For this computational scheme to be both stable and accurate, it is

important that the control blocks be executed in an implicit sequence. The definition of an "implicit sequence" depends on whether a control block is a state variable block (involves an integration with respect to time) or an algebraic variable block (involves no integration with respect to time). State variable block types are DINL, INT, INTM, LAG, LINT, LLAG, and SOTF, as indicated in Table 3.11-1 and defined in Section 3.11.5, while all other block types are algebraic. State variable blocks are assumed to be integrating input (derivative) values generated during the previous control system calculation; hence, the output values from these blocks are not considered to be at the current time step level (current with the thermal-hydraulic state of the TRAC-BF1/MOD1 system) until their integration has been performed. State variable blocks must be executed *before* their input blocks are executed to assure that the inputs to the state blocks have not been changed during the current time step (have the same value they had at the start of the current time step).

Algebraic variable blocks, on the other hand, use current time step outputs from the thermal-hydraulic data base and from other control blocks to calculate new derivative inputs for use by state variable blocks in the next time step. Hence, algebraic blocks must be executed *after* their input blocks have been executed. This assures that all of their inputs from other algebraic blocks are at the advanced time step level.

3.11.3 Automatic Sorting of Control Blocks

An automatic sorting algorithm is used to determine an implicit control block execution sequence, based on the criteria described above. Control blocks may be input in any order and with any unique control block numbers between 1 and 999 that the user may choose. Control system initialization routines will then sort the blocks into an optimal execution order and renumber the control blocks based on their sequence of execution. The user-assigned control block numbers are retained for graphing and editing purposes but are not used as part of the internal control system calculation.

The automatic sorting algorithm proceeds in the following manner:

1. State variable blocks are located in the control system input deck, and these blocks are placed at the top of the sequence list, making certain that blocks appear above their input in this list.

2. Algebraic variable blocks are then added to the sequence list below the state variable blocks. Algebraic blocks are added to the list only when all of their input blocks are already on the list; hence, several passes through the control system input deck are required to completely sort all of the algebraic blocks.

3. In the event that all of the algebraic blocks cannot be sorted, the existence of an "implicit loop" is noted. An example of an implicit loop is shown in Figure 3.11-3, which represents the equation Z = Y

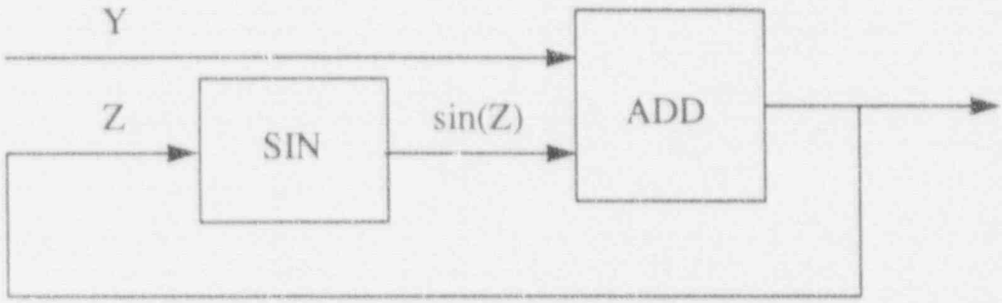

Figure 3.11-3. Implicit loop example.

+ sin(Z). Neither the SIN block nor the ADD block can be sorted, because each requires input from the other. Implicit loops are executed as a unit and are placed as a unit in the sequence list, so that blocks supplying inputs to the loop lie above the loop and blocks requiring input from the loop lie below the loop.

Since the user can input both steady-state and transient blocks together but only one type is used, the above procedure only applies to the type being used; i.e., execution order sequence numbers are not calculated for transient blocks if the steady state flag is set to one. Resorting is done on restart in case the user has changed his steady-state and transient flags.

3.11.4 Control System Implicit Loops

A control system simulation may occasionally involve the use of control system implicit loops, as illustrated in Figure 3.11-3. As mentioned above, such loops are given special treatment in the control system sorting scheme and solution scheme. Since such a loop cannot be sorted into an implicit execution order so that inputs are always calculated before they are used, a method of simultaneously solving for all of the outputs in an implicit control block loop must be used. The simultaneous solution used in TRAC-BF1/MOD1 is performed in the following manner.

$x_1, \ldots x_M$ are block outputs in an implicit loop containing M control blocks. We are seeking a solution for the new time output of the ith control block of the form

$$x_i^{n+1} = x_i\left(x_1^{n+1}, \ldots x_M^{n+1}\right) . \qquad (3.11\text{-}1)$$

This solution may be written in linearized form as

$$x_i^{n+1} = x_i\left(x_1^n, \ldots x_M^n\right) + \sum_{j=1}^{M} \frac{dx_i}{dx_j}\left(x_j^{n+1} - x_j^n\right) . \qquad (3.11\text{-}2)$$

Equation (13.11-2) yields a set of simultaneous equations that may be solved by matrix inversion to yield an exact solution for x_i^{n+1}, i = 1,...M, if the control block functions are all linear. For nonlinear block functions, Equation set (13.11-2) may be solved in the following iterative form:

$$x_i^{n+1} = x_i\left(x_1^{n+1}, \ldots x_M^{n+1}\right) + \sum_{j=1}^{M} \frac{dx_i}{dx_j}\left(x_j^{n+1} - x_j^n\right) . \qquad (3.11\text{-}3)$$

where new and old iterative values are as indicated. The iterative value of the derivative in Equation (13.11-3) is given by

$$\frac{dx_i}{dx_j} = \frac{dx_i}{dx_j}\left(x_1^{n+1}, \ldots x_M^{n+1}\right) \qquad (3.11\text{-}4)$$

and is calculated during each iteration by subroutine CONBLK, along with the first term on the right-hand side of Equation set (13.11-3), which represents the block outputs evaluated with previous iterate inputs.

The TRAC-BF1/MOD1 matrix inversion subroutines SGNDE and SGNSL are used to solve Equation set (13.11-3) for x_i^{n+1}, i=1,...M, during each iteration.

For the first iteration, $x_j^{n+1} = x_j^n$ is used as the previous iterate value, while, for succeeding iterations, previous iterate values are calculated as a weighted average of current iterate and previous iterate values, or

$$x_i^{n+1} = WX_i^{n+1}\big|_{new} + (1 - W)\, x_i^{n+1}\big|_{old} . \qquad (3.11\text{-}5)$$

The value indicated as 'old' is calculated at the end of each iteration and represents the value that will be used as the previous iterate value in the next iteration. A value of 0.4 for the weighting factor W has been found to yield the most rapid convergence in a variety of test cases, and this fixed value is used in this model. Iterations continue until fractional changes between successive iterate output values are less than 1.E-6 for all control blocks in the implicit loop. If convergence has not been obtained in a maximum of 20 iterations, a warning message is printed, and the nonconverged solution is treated as though it were converged.

Only algebraic variable blocks will be found in implicit loops, and only those whose derivatives of output value with respect to input value are well

defined are allowed to be included in implicit loops. If the sorting algorithm encounters a logical or discontinuous-type control block (for example XOR or RAND blocks) in an implicit loop, it issues a warning message, then removes the loop from implicit status. The blocks in this loop will be executed explicitly, meaning that a simultaneous solution will not be performed and some control blocks in the loop will be executed before their input blocks are executed, leading to potential instability. Those block types that may not be included in an implicit loop are indicated by a superscript f on Table 3.11-1.

While the TRAC-BF1/MOD1 control system model does provide a means of treating implicit loops in a control system model, it is recommended that implicit loops be avoided if at all possible, since the iterative solution method used to solve these loops can be excessively expensive in terms of computer time if the loops contain many control blocks. Implicit loops are broken by the presence of a state variable block in the loop; hence, many implicit loops can be eliminated by the addition of a LAG block in the loop.

3.11.5 Integration of State Variable Control Blocks

The state variable control block types are DINL, INT, INTM, LAG, LINT, LLAG, and STOF. The method of integration with respect to time used in all of these blocks is trapezoidal integration, that is, the input (derivative) value to be integrated is taken to be the simple average of the previous time step input and current completed time step input. This method requires that previous time step input values be saved but permits greater numerical accuracy at large time steps than rectangular integration, which uses only current completed time level inputs.

A pass is taken through the control system calculation at time zero (before the TRAC-BF1/MOD1 thermal-hydraulic equations have been advanced) to load initial input values for use as old time inputs by the state variable blocks in the next pass through the control system. The user-supplied initial control block output values are used for determining these initial inputs and for initializing the output values of state variable blocks.

The computational method used for each of the state variable block types is illustrated in the following section. In each case, Y is the block output value, X1 is the block input value, X2 is the intermediate integral value for double integrations, dt is the control system time step size, and G is the control block gain.

DINL (double integrator with output limiting)

$$X2^{n+1} = X2^{n} + 0.5\left(X1^{n} + X1^{n+1}\right) G\, dt \qquad (3.11\text{-}6)$$

$$Y^{n+1} = Y^n + 0.5(X2^n + X2^{n+1})\,dt \qquad (3.11\text{-}7)$$

Equations (3.11-6) and (3.11-7) are evaluated in sequence. $X2^n = 0$ at time zero. If $y^{n+1} >$ XMAX or $y^{n+1} <$ XMIN, then the output of the block supplying input XI is set to zero if its output sign is such as to hold the DINL output locked at its limit.

INT (simple integrator)

$$Y^{n+1} = Y^n + 0.5(X1^n + X1^{n+1})\,G\,dt \qquad (3.11\text{-}8)$$

INTM (integrator with mode control)

If (L2 + L3) = 0 (reset mode),

$$Y^{n+1} = XIV\ . \qquad (3.11\text{-}9)$$

If (L2 + K3) = 2 (integrate mode),

$$Y^{n+1} = Y^n + 0.5(X1^n + X1^{n+1})\,G\,dt \qquad (3.11\text{-}10)$$

If (L2 + L3) = 1 (hold mode),

$$Y^{n+1} = Y^n\ . \qquad (3.11\text{-}11)$$

L2 and L3 are logic input variables (1 or 0) to block inputs 2 and 3.

LAG (first order lag)

$$Y^{n+1} = Y^n + \frac{0.5\left[G\left(X1^n + X1^{n+1}\right) - \left(Y^n + Y^{n+1}\right)\right]dt}{C1} \qquad (3.11\text{-}12)$$

C1 is the lag time constant. This equation is rearranged algebraically and solved for Y^{n+1}.

LINT (limited integrator)

$$Y^{n+1} = Y^n + 0.5(X1^n + X1^{n+1})\,G\,dt \qquad (3.11\text{-}13)$$

If $y^{n+1} >$ XMAX or $y^{n+1} <$ XMIN, then the output of the block supplying input XI is set to zero if its output sign is such as to hold the LINT output locked at its limit.

LLAG (lead-lag transfer function)

$$X2^n = \frac{(GX1^n - X2^n)}{C2} \tag{3.11-14}$$

$$X2^{n+1} = \frac{(GX1^{n+1} - X2^{n+1})}{C2} \tag{3.11-15}$$

$$X2^{n+1} = X2^n + 0.5\,(X2^n + X2^{n+1})\,dt \tag{3.11-16}$$

$$Y^{n+1} = X2^{n+1} + C1\,X2^{n+1} \tag{3.11-17}$$

X2 is the intermediate state derivative, and C1 and C2 are the lead and lag time constants. Equation (3.11-12) is evaluated, then Equations (3.11-13) and (3.11-14) are solved simultaneously. Equation (3.11-14) is finally solved to obtain a value for Y^{n+1}. $X2^n$ is initialized to the same value as $X1^n$.

SOTF (second order transfer function)

$$X2^n = \frac{(GX1^n - Y^n - C1X2^n)}{C2} \tag{3.11-18}$$

$$X2^{n+1} = \frac{(GX1^{n+1} - Y^{n+1} - C1X2^{n+1})}{C2} \tag{3.11-19}$$

$$X2^{n+1} = X2^n + 0.5\,(X2^n + X2^{n+1})\,dt \tag{3.11-20}$$

$$Y^{n+1} = Y^n + 0.5\,(X2^n + X2^{n+1})\,dt \tag{3.11-21}$$

C1 and C2 are the transform coefficients in the Laplace transform

$$Y = \frac{X1}{1.0 + C1S + C2S^2} \tag{3.11-22}$$

where S is the Laplace transform operator. The above equations are solved simultaneously for Y^{n+1}. $X2^n$ is initialized to the same value as $X1^n$.

3.11.6 Control System Time Step Control

The TRAC-BF1/MOD1 control system calculation may be executed with a smaller time step size than the thermal-hydraulic calculation. This feature allows the control system model to be calculated accurately, independent of the TRAC-BF1/MOD1 thermal-hydraulic time step size. Selection of the maximum allowable control system time step size is based on the following criteria:

1. **Accuracy in the calculation of state variable control blocks.** This criterion is satisfied by limiting the control system time step size to 1/2 of the shortest time constant occurring in any of the state variable control blocks.

2. **Detection and resolution of discontinuous transient events.** This criterion is satisfied by limiting the control system time step size to 1/10 of the shortest delay time occurring in any LDLY control block.

Control system stability is not a consideration in the selection of time step size, since the control system solution scheme is fully implicit.

If the control system time step logic determines that the maximum allowable control system time step size is greater than or equal to the thermal-hydraulic time step size, then the thermal-hydraulic time step size will be used for the control system time step size. If the maximum allowable control system time step size is less than the thermal-hydraulic time step size, then the thermal-hydraulic time step size will be divided into the smallest number of equal intervals such that the interval size is less than or equal to the maximum control system time step size. This interval is then used as the control system time step size. In this manner, the control system calculation may be taken in several steps while it catches up with the thermal-hydraulic calculation. At the end of this series of steps the control system calculation will be at the same time level as the thermal-hydraulic calculation. If the control system maximum time step size changes during this series of steps, the remaining time to complete the series is again divided into equal intervals, each of which is less than or equal to the new maximum control system time step size.

To further enhance the ability of TRAC-BF1/MOD1 to resolve discontinuous transient events, the trip logic will anticipate the activation of certain trips and will adjust the thermal-hydraulic time step size so that these trips will be activated exactly at the end of a time step. This will help eliminate the problem of stepping far past a trip activation time in a single time step, as might happen when a Courant limit violating numerical scheme is used. This anticipation of trip activation will take place for all trips set and activated by time and for other trips that are set by a thermal-hydraulic condition and then activated after a time delay, provided the trip setting and activation do not take place during the same time step. If the thermal-hydraulic time step size is adjusted in anticipation of a trip activation, the control system time step size will be adjusted accordingly.

3.12 TURB

The turbine model in TRAC-BD1/MOD1 was designed to provide a basic capability to model BWR main steam turbines together with those used for driving feedwater pumps as part of the balance-of-plant package. The original generic model[3.12-1] was based on a simple thermodynamic description of flow through a turbine with user-specified performance parameters, such as rated mass flow, thermodynamic stage efficiency. The conservation equations for mass, momentum, and energy in this model were solved fully explicitly. This approach was satisfactory for calculations with time step sizes on the order of 0.1 s or less.

TRAC-BF1/MOD1 incorporates stability-enhancing two-step numerics, permitting the use of large computational time steps under slowly varying conditions. The use of such large time steps necessitated the elimination of explicit numerical integration in the turbine model in order to guarantee computational stability. The modifications required to achieve this elimination and to solve the fluid dynamic equations for the turbine using the normal semi-implicit scheme are described below.

3.12.1 Physical Model of Turbine

The turbine is modeled as a one-dimensional branching flow component or tee. The principal branch represents the turbine inlet and outlet, and the turbine nozzles, rotor blades, stator blades and internal flow passages (hereafter referred to as turbine internals). The secondary branch, or side arm, represents either a liquid drain or a steam tap for driving a feedwater heater. Consistent with the modeling philosophy used to develop the original model in TRAC-BD1/MOD1,[3.12-1] the flow through the turbine internals is not treated in detail from first principles. Instead, the processes of momentum and energy exchange are lumped into source terms in the one-dimensional conservation equations. The idealized physical model is illustrated schematically in Figure 3.12-1. The assumed characteristics of this model are summarized below.

The two-phase inlet flow enters from the left and is homogenized in Region A prior to entry into the turbine internals (Region B). Heat exchange with the walls may occur in Region A, but all fluid dynamic processes associated with the internals are lumped into Region B. In this region, the fluid state is changed and momentum and energy are extracted by the turbine rotor. The net effect is that (a) the fluid pressure drops; (b) the total energy flow rate of the working fluid drops by an amount equal to the mechanical power output of the turbine rotor; (c) a saturated mixture is achieved, corresponding to the steam partial pressure in Region C; and (d) the velocity of the fluid changes due to density and/or flow area changes between entry to and exit from Region B. The flow area at the entrance to Region B is assumed equal to that at the inlet to Region A and the flow area at the exit from Region B is assumed equal to that at the exit from Region C.

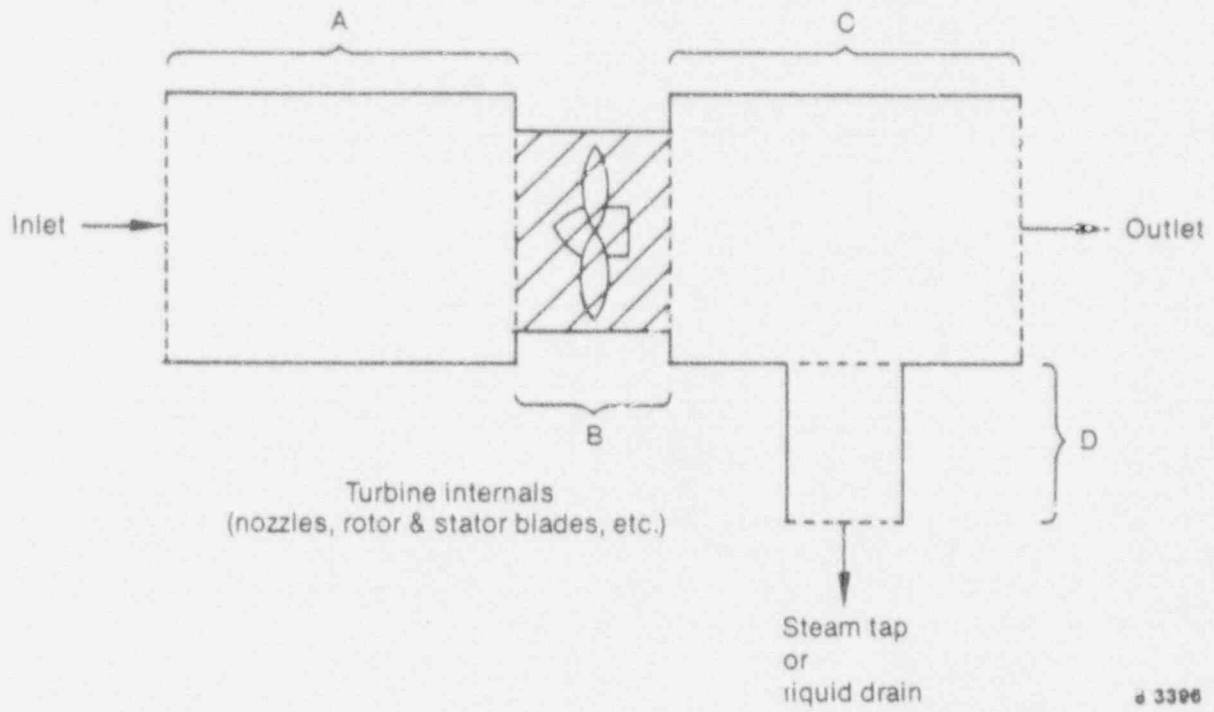

Figure 3.12-1. Idealized turbine model.

The flows through Regions A and C are determined by the pressure gradient, the inertia of the fluid, and the wall friction losses (including form loss factors at the turbine entrance and exit). The flow through Region B is determined by the pressure gradient, the fluid inertia, and an effective form loss factor chosen to give the correct steady-state mass flow rate through the first turbine stage.[3.12-2]

The flow through Region D depends on whether the side arm represents a steam tap or a liquid drain. If it is a steam tap, the flow is determined in the same manner as for Regions A and C. If it is a liquid drain, it is determined from the user-input liquid separation efficiency (SEPEF). In this case, the vapor velocity is set to zero and the liquid velocity is set to the value required to extract (SEPEF) times (the total liquid mass in Region C) in a single computational time step.

Region B is assumed to have zero volume. Thus, the mass flow rate into the region is identically equal to the flow rate out, and the only effect of the region is to change the state of the working fluid and to transfer energy from the fluid to the turbine rotor.

3.12.2 Numerical Model

The conservation equations for momentum, mass, and energy used in TRAC-BF1/MOD1 are given in Section 2.1.1 [Equations (2.1-1) through (2.1-8)]. The semi-implicit finite-difference form of these equations used in the TRAC-BF1/MOD1 numerical scheme are given in Section 2.3.1 [Equations (2.3-15) through (2.3-22)]. The original turbine model has been reformulated as a standard TEE and thus makes use of the above semi-implicit formulation of the fluid dynamic equations. The necessary modifications to the numerical model for the TEE component to achieve this objective are explained with the aide of Figure 3.12-2.

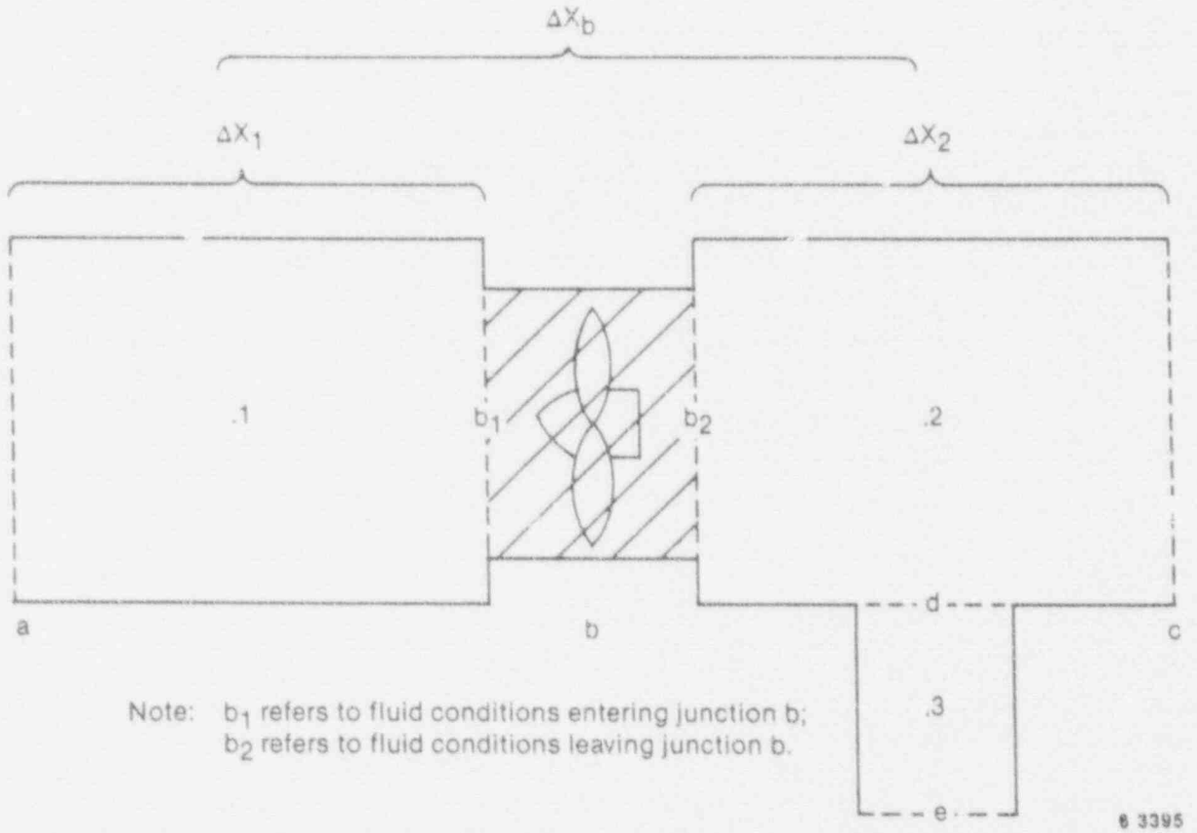

Figure 3.12-2. Schematic of numerical model for turbine.

The turbine TEE consists of two cells in the primary tube and N cells in the side arm, where N is specified by the user. Since all side arm cells except the first are treated exactly like a normal TEE component, only the first cell is indicated in Figure 3.12-2. The lumped effects of the turbine internals are felt at Junction b (hereafter referred to as the turbine membrane). As explained previously, the working fluid enters Junction b at the conditions prevailing at the center of Cell 1 and leaves as a saturated

mixture at the pressure of Cell 2. The turbine membrane is assumed to possess zero volume, so the mass flow rate into Junction b is identically equal to the mass flow rate out of the junction.

The normal flow conditions for the turbine are into Cell 1 at Junction a, from Cell 1 to Cell 2 at Junction b, out of Cell 2 at Junction c and d, and toward the exit of the side arm at all other side arm junctions. The modifications explained below are applicable only for the case of normal flow and positive pressure gradient at Junction b (i.e., $p_2 < p_1$). For other flow conditions the described modifications do not apply and the fluid equations are solved by the unmodified TRAC-BF1/MOD1 semi-implicit scheme.

3.12.3 Momentum Equation

The normal TRAC-BF1/MOD1 momentum equations are written as velocity equations for the liquid and vapor phases. Solution of the linearized equations yields expressions for the explicit new time junction phase velocities, $\tilde{V}_g^{n+1}$ and $\tilde{V}_\ell^{n+1}$, assuming no change in the pressure drop across the junction and implicit correction term, $\frac{\partial V_g^{n+1}}{\partial(\Delta P)}$ and $\frac{\partial V_p^{n+1}}{\partial(\Delta P)}$ for each phase velocity due to variation in the junction pressure drop during the time step. There is no change to the normal TRAC-BF1/MOD1 scheme for obtaining these terms at Junctions a and e.

The momentum (or velocity) equation used at Junction b is obtained by assuming the flow is homogeneous, and the total pressure drop between Cells I and 2 is lumped in a single form loss term characterized by the coefficient f_{turb}. Thus, the momentum equation solved at b is

$$\frac{\partial V_m}{\partial t} + V_m \frac{\partial V_m}{\partial X} = \frac{1}{P_m}\frac{\partial P}{\partial X} - \frac{f_{turb} V_m^2}{\Delta X_b} \quad . \tag{3.3-1}$$

The form loss coefficient is obtained as follows. First, the steady- state turbine nozzle velocity[3.12-1] is computed.

$$V_{NOZ} = \left(\frac{2\gamma}{\gamma - 1} \frac{P_1}{\rho_1} r_{b_1}^{2/\gamma} - r_{b_1}^{\gamma+1/\gamma} \right)^{1/2} . \qquad (3.12\text{-}2)$$

Next, the mass flow rate corresponding to this nozzle velocity is used to obtain the steady mixture velocity at b:

$$V_{m,b} = \frac{FA_{NOZ}}{FA_b} V_{NOZ} . \qquad (3.12\text{-}3)$$

Finally, f_{turb} is determined by substituting the velocity obtained from Equation (3.12-3) into the finite-difference approximation of the steady-state form of Equation (3.12-1)

$$f_{turb} = - \frac{V_{m,b_1}^n \left(V_{m,b_1}^n - V_{m,a}^n \right) \frac{\Delta X_b}{\Delta X_1} + \frac{1}{\rho_{m,1}^n} \left(P_2^n - P_1^n \right)}{\left(V_{m,b_1}^n \right)^2} . \qquad (3.12\text{-}4)$$

(To prevent numerical instabilities, a lower limit of 0.001 is placed on the numerical value of f_{turb}. With f_{turb} determined from the above explicit expression, the transient, semi-implicit, finite-difference approximation to Equation (3.12-1) becomes

$$\frac{V_{m,b_1}^{n+1} - V_{m,b_1}^n}{\Delta t} + V_{m,b}^n \left(\frac{V_{m,b_1}^n - V_{m,a}^n}{\Delta X_1} \right) = - \frac{1}{\rho_{m,1}^n} \left(\frac{P_2^{n+1} - P_1^{n+1}}{\Delta X_b} \right) - f_{turb} V_{m,b_1}^n V_{m,b_1}^{n+1} . \qquad (3.12\text{-}5)$$

Linearizing the pressure term in the above equation yields the following explicit values for $\tilde{V}_{m,b}^{n+1}$ and $\frac{\partial V_m^{n+1}}{\partial \Delta P}$:

$$\bar{V}_{m,b}^{n+1} = \frac{-\frac{\Delta t}{\rho_1}\frac{P_2^n - P_1^N}{\Delta X_b} + V_{m,b_1}^n - V_{m,b_1}^n\left[V_{m,b_1}^n\left(\frac{V_{m,b_1}^n - V_{m,a}^n}{\Delta X}\right)\Delta T\right]}{1.0 + \frac{V_{m,b_1}^n f_{turb}\Delta t}{\Delta X_b}} \qquad (3.12\text{-}6)$$

$$\frac{\partial V_{m,b_1}^{n+1}}{\partial \Delta P_b} = \frac{\frac{\Delta t}{\rho_1 \Delta X_b}}{1.0 \frac{V_{m,b_1}^n f_{turb}\Delta t}{\Delta X_b}} . \qquad (3.12\text{-}7)$$

Due to the assumption of homogeneous flow, $\bar{V}_{g,b_1}^{n+1}$ and $\bar{V}_{\ell,b_1}^{n+1}$ are set equal to $\bar{V}_{m,b_1}^{n+1}$; and $\frac{\partial V_{g,b_1}^{n+1}}{\partial \Delta P}$ and $\frac{\partial V_{\ell,b_1}^{n+1}}{\partial \Delta P}$ are set equal to $\frac{\partial V_{m,b_1}^{n+1}}{\partial \Delta P}$.

At Junction c, the only modification to the momentum equation is in the spatial acceleration terms. Since the phase velocities that are stored in the data base for Junction b are the phase velocities entering the turbine membrane (V_b), the spatial gradient terms in the momentum equations at Junction c must be altered to reflect the velocity differences between the exit of the turbine membrane and turbine exit. Thus, the spatial terms used in the vapor and liquid momentum solutions at Junction c are of the form

$$\frac{V_{p,c}^n\left(V_{p,c}^n - V_{m,b_2}^n\right)}{\Delta X_2}$$

where

$$V_{m,b_2}^n = V_{m,b_1}^n\left(\frac{FA_1}{FA_3}\right)\left(\frac{\rho_{m,b_1}^n}{\rho_{m,b_2}^n}\right) \qquad (3.12\text{-}8)$$

ρ_{m,b_1}^n = mixture density at entrance to turbine membrane cell (centered value in Cell 1)

ρ^n_{m,b_2} = mixture density at exit of turbine membrane.

The momentum equation at Junction d is treated differently depending on whether the side arm represents a steam tap for feedwater heaters or a liquid separator drain. In the former case, the only modification to the normal TRAC-BF1/MOD1 momentum solution occurs when the control system is used to regulate the mass flow rate out the side arm. For this case, the side arm loss coefficients FKLOS and RKLOS are set each time step by the control system and are not directly controlled by the user.

In the case of the side arm representing a liquid separator drain, the momentum equations at Junction d are replaced with "pseudo momentum equations" designed to pull liquid only out of Cell 2 in a manner that approximates the effect of the true separation process. With the separator efficiency (SEPEF) set by the user, the explicit new time liquid velocity is defined as

$$\tilde{V}^{n+1}_{\ell,d} = SEPEF \left(\frac{1 - \alpha^n_2}{FA_d \Delta t} \right) . \qquad (3.12\text{-}9)$$

As previously discussed, this velocity is such that all the liquid present in Cell 2 at the end of the previous time step would leave through the side arm during the current time step if $V^{n+1}_{\ell,d}$ is not implicitly changed during the time step.

The implicit correction term $\frac{\partial V^{n+1}_{\ell,d}}{\partial(\Delta P_d)}$ is obtained by defining a "pseudo loss coefficient," f_{side}, as follows:

$$\Delta P_d = f_{side}\, \rho_\ell V^n_{\ell,d} . \qquad (3.12\text{-}10)$$

This expression is differentiated with respect to (ΔP_d) to obtain the following value for the implicit term:

$$\frac{\partial V^{n+1}_{\ell,d}}{\partial(\Delta P_d)} = \frac{1}{2} \frac{\tilde{V}^{n+1}_{\ell,d}}{P^n_3 - P^n_2} . \qquad (3.12\text{-}11)$$

When $(P_3^n - P_2^n) < 0$, both the explicit and implicit terms are set to zero. Also, to avoid numerical instability during startup, the maximum explicit velocity is limited to 50 m/s. The vapor velocity and its implicit correction term are both set to zero for the liquid separator option.

The above approach to computing the separator liquid velocity is not mathematically rigorous. The implicit correction term should clearly be tied

to the change in the void fraction in Cell 2 and not to the pressure drop. However, the present approach is much simpler and has produced satisfactory results in test calculations to date.

3.12.4 Continuity Equation

The continuity equations for vapor and liquid mass are solved by the unmodified TRAC-BF1/MOD1 scheme in all cells of the turbine except Cell 2. For normal flow, the effect on the working fluid of passing through the turbine membrane is to lower the mixture enthalpy and pressure and change the mixture quality. This change in the mixture quality, together with the change in the specific internal energy of the steam and liquid after passing through Junction b, must be reflected in the continuity (and energy) equations for Cell 2.

The state of the mixture leaving Junction b is computed by assuming that the turbine membrane extracts adiabatically an amount of energy given by:

$$w_{turb} = \eta \Delta h_{ideal} \qquad (3.12\text{-}12)$$

where

Δh_{ideal} = ideal enthalpy change of working fluid assuming an isentropic ideal gas expansion from pressure P_1 to pressure P_2.

Both η and Δh_{ideal} are computed explicitly, as described in Reference 3.12-2. Applying the 1st law, the enthalpy of the mixture on exit from Junction b is computed from the equation:

$$\frac{1}{2} V^2_{m,b_1} + h_{b_1} = \frac{1}{2} V^2_{m,b_2} + h_{b_2} + w_{turb} \,. \qquad (3.12\text{-}13)$$

Assuming that the working fluid leaves Junction b as a saturated mixture of vapor and liquid at pressure P_2, Equation (3.12-13) leads to the following expression to compute the homogeneous exit quality, x_{b2}, leaving Junction b:

$$x_{b_2} = \frac{x_{b_1} h^n_{g,b_1} + \left(1 - x_{b_1}\right) h^n_{\ell,b_1} + \left(\frac{V^n_{m,b_1}}{2}\right)^2 - w_{turb} - h^n_{\ell,b_2} + \left(\frac{V^n_{\ell,c}}{2}\right)^2}{h^n_{g,b_2} - h^n_{\ell,b_2}} \,. \qquad (3.12\text{-}14)$$

With X_{b2}, the explicit estimate for the homogeneous velocity at the turbine membrane exit may be computed from mass continuity as follows:

$$\tilde{V}^{n+1}_{m,b_2} = \frac{\rho^{n}_{m,b_1}}{\rho^{n}_{m,b_2}} \frac{FA_{b_1}}{FA_{b_2}} \tilde{V}^{n+1}_{m,b_1} \quad . \tag{3.12-15}$$

The implicit correction term is then

$$\frac{\partial \tilde{V}^{n+1}_{m,b_2}}{\partial(\Delta P_b)} = \frac{\rho^{n}_{m,b_1}}{\rho^{n}_{m,b_2}} \frac{FA_{b_1}}{FA_{b_2}} \frac{\partial \tilde{V}^{n+1}_{m,b_1}}{\partial(\Delta P_{b_1})} \quad . \tag{3.12-16}$$

The explicit estimates for the integrated mass flux terms for vapor and liquid entering Cell 2 from Cell 1 are now computed from the corresponding terms representing mass flux out of Cell 1 together with the above value for x_{b2} as follows:

$$\tilde{M}^{n+1}_{g,b_2} = \tilde{M}^{n+1}_{g,b_1} + \tilde{M}^{n+1}_{\ell,b_1} x_{b_2} \tag{3.12-17}$$

$$\tilde{M}^{n+1}_{\ell,b_2} = \tilde{M}^{n+1}_{g,b_1} + \tilde{M}^{n+1}_{\ell,b_1} - \tilde{M}^{n+1}_{g,b_2} \quad . \tag{3.12-18}$$

The terms $\tilde{M}_{g,b}$ and $\tilde{M}_{\ell,b}$ are computed by the normal TRAC-BF1/MOD1 numerical scheme. The implicit corrections to the integrated mass flux terms are also obtained from the corresponding terms computed for the mass flows out of Cell 1. Thus,

$$\frac{\partial M^{n+1}_{g,b_2}}{\partial(\Delta P_b)} = \alpha_{b_2} \rho_{g,b_2} FA_{b_1} \frac{\rho_{m,b_2}}{\rho_{m,b_1}} \frac{\partial V^{n+1}_{m,b_1}}{\partial(\Delta P_b)} (\Delta t) \tag{3.12-19}$$

$$\frac{\partial M^{n+1}_{\ell,b_2}}{\partial(\Delta P_b)} = (1 - \alpha_{b_2}) \rho_{\ell,b_2} FA_{b_1} \frac{\rho_{m,b_2}}{\rho_{m,b_1}} \frac{\partial V^{n+1}_{m,b_1}}{\partial(\Delta P_b)} (\Delta t) . \tag{3.12-20}$$

By formulating the mass flux terms and the implicit corrections in the above fashion, mass is identically conserved across Junction b.

3.12.5 Energy Equation

The energy equation has been modified from the normal scheme only in Cells 1 and 2 of the turbine. The modification for Cell 1 reflects the effect

of frictional dissipation. At this point, it is noted that the energy equations used in the TRAC-BF1/MOD1 thermal-hydraulic solution[3.12-1] are thermal energy equations. They were obtained from the total energy (1st law) equations by subtracting out the volume integrals of the product of the respective phase volumetric fluxes ($FA \cdot V_p$) with their corresponding momentum equations. However, implicit in the form of the resulting energy equations is the assumption that frictional dissipation is zero. For most flow situations modeled with TRAC-BF1/MOD1, the dissipation terms are small and can be neglected. To account for the possibility of a large frictional (or form) loss through the turbine entrance (Junction a), the effect of dissipation has been added to the thermal energy equation for Cell 1.

By performing the above-mentioned operations on the one-dimensional momentum and energy equations, the following terms are added to the thermal energy equations:

$\alpha_p \rho_p V_p^3 [d(FA)/dx]\, dx$ is added to the left-hand side of the mixture energy equation (see Section 2.1.1) and $V_p(FA)f_p\, dx$ is added to the right-hand side of the vapor energy equation (see Section 2.1.1). In the mixture energy equation, both the vapor and liquid dissipation terms ($p = g$ and ℓ) are added, while in the vapor energy equation, only the vapor terms are used ($p = g$). (Note that the above form of the dissipation terms neglects the effect of dissipation due to the interfacial shear.)

In the turbine energy equation modifications for Cell 1, the area change term above is neglected. The second term is evaluated assuming that all terms under the integral (3.12-11) are constant and equal to the values at Junction a. f_p is simply the total wall friction term in the momentum equation for Junction a and is a linear combination of V_g^2 and V_ℓ^2. Thus, the dissipation term for Cell 1 is approximated as

$$V_p(FA)f_p\, dx = V_p\left(A_p V_g^2 + B_p V_\ell^2\right) \tag{3.12-21}$$

and the term on the right-hand side is written semi-implicitly as

$$V_p\left(A_p V_g^2 + B_p V_\ell^2\right) = V_p^{n+1} A_p^n (V_g^n)^2 + B_p^n (V_\ell^n)^2 . \tag{3.12-22}$$

The coefficients A_p and B_p are simply products and quotients of volume fractions, phasic densities, and friction factors and are evaluated explicitly, as indicated. The fact that V_p^{n+1} appears in the above expression requires additions to both the explicit residual in the energy equation for Cell 1 and the implicit derivative of the residual with respect to the pressure drop across Junction a. These additions are, respectively

$$(DISS)_g^{n+1} = \bar{V}_{g,a}^{n+1} FA_a \alpha_{DC,a} \rho_{g,a} DX_a \alpha_{DC,a} WFV_a (V_{g,a}^n)^2 + (1 - \alpha_{DC,a}) WFL_a (V_{\ell,a}^n)^2 \frac{\rho_{\ell,a}}{\rho_{g,a}}$$

(3.12-23)

$$(DISS)_\ell^{n+1} = \bar{V}_{\ell,a}^{n+1} FA_a (1 - \alpha_{DC,a}) \rho_{\ell,a} DX_a \alpha_{DC,a} WFV_a (V_{g,a}^n)^2 \frac{\rho_{g,a}}{\rho_{\ell,a}} + (1 - \alpha_{DC,a}) WFL_a (V_{\ell,a}^n)^2$$

(3.12-24)

$$\frac{\partial (DISS)_g^{n+1}}{\partial (\Delta P_a)} = \frac{\partial V_{g,a}^{n+1}}{\partial (\Delta P_a)} \frac{(DISS)_g^{n+1}}{\bar{V}_{g,a}^{n+1}}$$

(3.12-25)

$$\frac{\partial (DISS)_p^{n+1}}{\partial (\Delta P_a)} = \frac{\partial V_{\ell,a}^{n+1}}{\partial (\Delta P_a)} \frac{(DISS)_g^{n+1}}{\bar{V}_{g,a}^{n+1}} .$$

(3.12-26)

The effects of friction in the turbine internals are presumably accounted for in the turbine stage efficiency η and the pressure drop, and thus the addition of dissipation to the thermal energy equation is performed only in Cell 1 to reflect the effect of wall friction and form loss at the turbine entrance.

The energy equation for Cell 2 must be modified to reflect the altered specific enthalpies and phasic mass flows at the exit of the turbine membrane. This is done by altering the energy flux terms due to vapor and liquid flow into the cell at b_2 in the same manner as was done for the mass flux terms. Thus,

$$E_{p,b_2} = M_{p,b_2} e_{p,b_2} .$$

(3.12-27)

In addition to the above correction, the dilatation terms $[P_k^{n+1} \nabla_k (\alpha^n V_g^{n+1})$ and $P^{n+1} \nabla_k (\alpha^n V_g^{n+1} + (1 - \alpha^n) V_\ell^{n+1})]$ must be altered to reflect the change in void fraction, mixture velocity, and flow area as the working fluid crosses the turbine membrane. The modified terms for the vapor and mixture energy equations for Cell 2 are, respectively,

$$P_2^{n+1}\left(\frac{\alpha_{b_2}^{n} V_{g,b_2}^{n+1} - \alpha_2^{n} V_{g,c}^{n+1}}{\Delta x_2}\right)$$

and

$$P_2^{n+1}\left(\frac{\alpha_{b_2}^{n} V_{g,b_2}^{n+1} + (1 - \alpha_{b_2}^{n}) V_{\ell,b_2}^{n+1} - \alpha_2^{n} V_{g,c}^{n+1} + (1 - \alpha_2^{n}) V_{\ell,c}^{n+1}}{\Delta x_2}\right) .$$

(Again, note that junction properties such as velocity and flow area that are stored in the data base for Junction b are those appropriate at the upstream side of the turbine membrane, b_1, in Figure 3.12-2.)

3.12.6 Critical Flow

The criterion for critical or choked flow at the turbine membrane is the same as was used in the previous model.[3.12-1] When the pressure ratio P_2/P_1 exceeds the critical value, the explicit new time velocity is computed as follows:

$$\tilde{V}_{NOZ}^{n+1} = \left(\frac{2\gamma}{\gamma - 1}\,\frac{P_1^{n}}{\rho_{m,1}^{n}}\, r_{crit}^{2/\gamma} - r_{crit}^{\gamma+1/\gamma}\right)^{1/2} . \qquad (3.12\text{-}28)$$

The implicit correction to the choked velocity arises due to changes in the upstream pressure (P_1) only. However, since the TRAC-BF1/MOD1 network solution is based on pressure differences across junctions rather than cell pressures, it is assumed that

$$\frac{\partial V_{NOZ}^{n+1}}{\partial(\Delta P_b)} = \frac{\gamma}{\gamma - 1}\,\frac{1}{\rho_{m,1}^{n}}\, r_{crit}^{2/\gamma} - r_{crit}^{\gamma+1/\gamma}\left(\tilde{V}_{NOZ}^{n+1}\right)^{-1} . \qquad (3.12\text{-}29)$$

Choking at all turbine junctions other than b is treated by the normal critical flow model in TRAC-BD1,[3.12-1] with the single exception of Junction d when the side arm is treated as a liquid separator drain. In this case, a critical flow model is clearly not applicable.

3.12.7 References

3.12-1 D. D. Taylor et al., *TRAC-BD1/MOD1: An Advanced Best Estimate*

Computer Program for Boiling Water Reactor Transient Analysis, Volume 1, NUREG/CR-3633, EGG-2994, April 1984.

3.12-2. M. M. Giles, *TRAC-BD1 Turbine Model*, EGG-CBB-6029, September 1982.

3.13 HEATR

The HEATR component in TRAC-BF1/MOD1 provides the capability of modeling typical feedwater heaters (FWH) found in BWR steam supply systems. This permits greater detail in modeling the balance-of-plant components that may play important roles in operational transient simulations. The component may also be used to simulate the main steam condenser.

The HEATR is based on the TEE component and includes changes to the TRAC-BF1/MOD1 heat transfer correlation package and special treatment of the momentum and mass flow in the primary tube. A typical HEATR component is shown in Figure 3.13-1. Included in the figure is a PIPE component that represents the heat transfer tubes within the heater. The combination of the HEATR and PIPE represents a typical tube-in-shell heat exchanger, with attached drain-cooler region. The steam enters the shell (Cell 1), condenses, enters the drain cooler (Cell 2) as single-phase liquid (normally), undergoes further cooling and, finally, exits the HEATR. The side arm is included and attached to the steam shell cell, since high-pressure saturated liquid (from turbine separators or higher-pressure feedwater heaters) is frequently input to the heater shells in a separate flow path. Typical shell void fractions

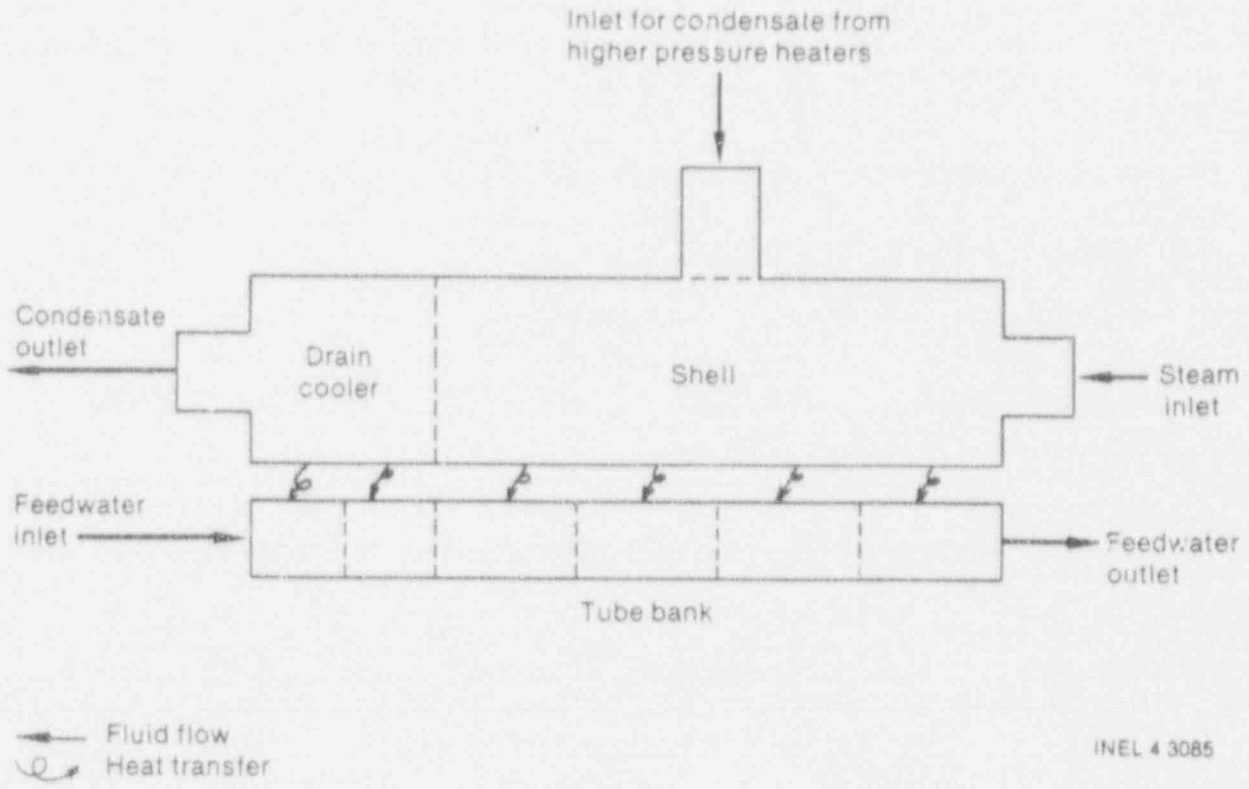

Figure 3.13-1. TRAC-BF1/MOD1 model of feedwater heater using a HEATR component (modified TEE) and PIPE component for the tube bank.

are about 0.5, while the drain cooler normally receives only liquid from the cell. The determination of the donor-celled void fraction from the shell to the drain cooler requires both extra user input and code hydrodynamic calculation changes. The user must specify the drain cooler inlet height and a table of shell liquid level versus void fraction. The donor-celled void fraction (α_{DC}) is

$$\alpha_{DC} = \begin{cases} 0.0 \text{ if liquid level} \geq \text{D.C. height} \\ 1.0 \text{ if liquid level} \leq \text{D.C. height} - 0.05\ m \\ 20.0 \times (\text{D.C. height} - \text{liquid level}) \text{ otherwise} \end{cases} \quad (3.13\text{-}1)$$

This provides a gradual change of α_{DC} as the drain cooler inlet is uncovered by a dropping shell liquid level.

Another change to the hydrodynamic equations was forced by the normally high inlet steam velocities found in the main condenser. Momentum flux was eliminated at the drain cooler inlet interface. This was done to prevent V - ∇V induced pressurization of the first cell in the drain cooler.

Correlations appropriate to flow condensation on horizontal and vertical tube banks[3.13-1] have been introduced. In addition, a correlation for single-phase (liquid) convection across tube banks[3.13-2] has been implemented in order to better describe the behavior in the liquid-filled regions of the FWH. These correlations are presently available in the code for HEATRs only--the previous models for convection and condensation are still used for other components. The correlations used are:

For condensing flow on horizontal tube banks,

$$h_v = X_f \frac{k_\ell}{D_t} Re_\ell^{1/2} \left(1 + \frac{0.276}{X_f^4 Fr H_f} \right)^{1/4} . \quad (3.13\text{-}2)$$

For condensing flow on vertical tube banks,

$$h_v = X_f \frac{k_\ell Re_\ell^{1/2}}{D_t} + 0.943 \left[\frac{h_{fg} k_\ell^3 \rho_\ell^2 g}{\mu_\ell D_B (T_s - T_w)} \right]^{1/4} . \quad (3.13\text{-}3)$$

For liquid crossflow across tube banks,

$$h_\ell = 0.36 \frac{k_\ell}{D_t} \left(\frac{D_h \rho_\ell V_\ell}{\mu_\ell} \right)^{0.55} \left(\frac{C_{p_\ell} \mu_\ell}{k_\ell} \right)^{1/3} . \quad (3.13\text{-}4)$$

X_f, H_f, R_f, Re_ℓ (liquid film Reynolds number) and Fr (Froude number) are dimensionless parameters defined as

$$X_t = 0.9\left(1 + \frac{1}{R_t + H_t}\right) \tag{3.13-5}$$

$$H_t = \frac{k_\ell (T_s - T_w)}{\mu_\ell h_{fg}} \tag{3.13-6}$$

$$R_t = \left(\frac{\rho_\ell \mu_\ell}{\rho_g \mu_g}\right)^{1/2} \tag{3.13-7}$$

$$Re_\ell = \frac{\rho_\ell V_g D_t}{\mu_\ell} \tag{3.13-8}$$

$$Fr = \frac{V_g^2}{gD_t} \, . \tag{3.13-9}$$

The TRAC-BF1/MOD1 method for handling condensation requires that all the energy be taken out of the liquid phase; condensation then occurs due to interfacial heat transfer. This being the case, the liquid and vapor coefficients must be adjusted accordingly

$$h_\ell = FRACL\ H_\ell + (1 - FRACL)\ h_g \left(\frac{T_s - T_w}{T_L - T_w}\right) \tag{3.13-10}$$

$$h_g = 0.0 \tag{3.13-11}$$

where h_ℓ and h_g are the heat transfer coefficients returned by HTCOR. FRACL is the fraction of the heat transfer tubes that are covered by liquid. This is determined by user input of two tables, shell liquid level versus shell void fraction and FRACL versus liquid level.

When the HEATR is used to model a main turbine condenser, some special modeling features are used. The cooling water in the tubes is normally not part of the reactor fluid loop. Code changes to permit such a disconnected loop have been made, and now model configurations shown in Figure 3.13-2 are

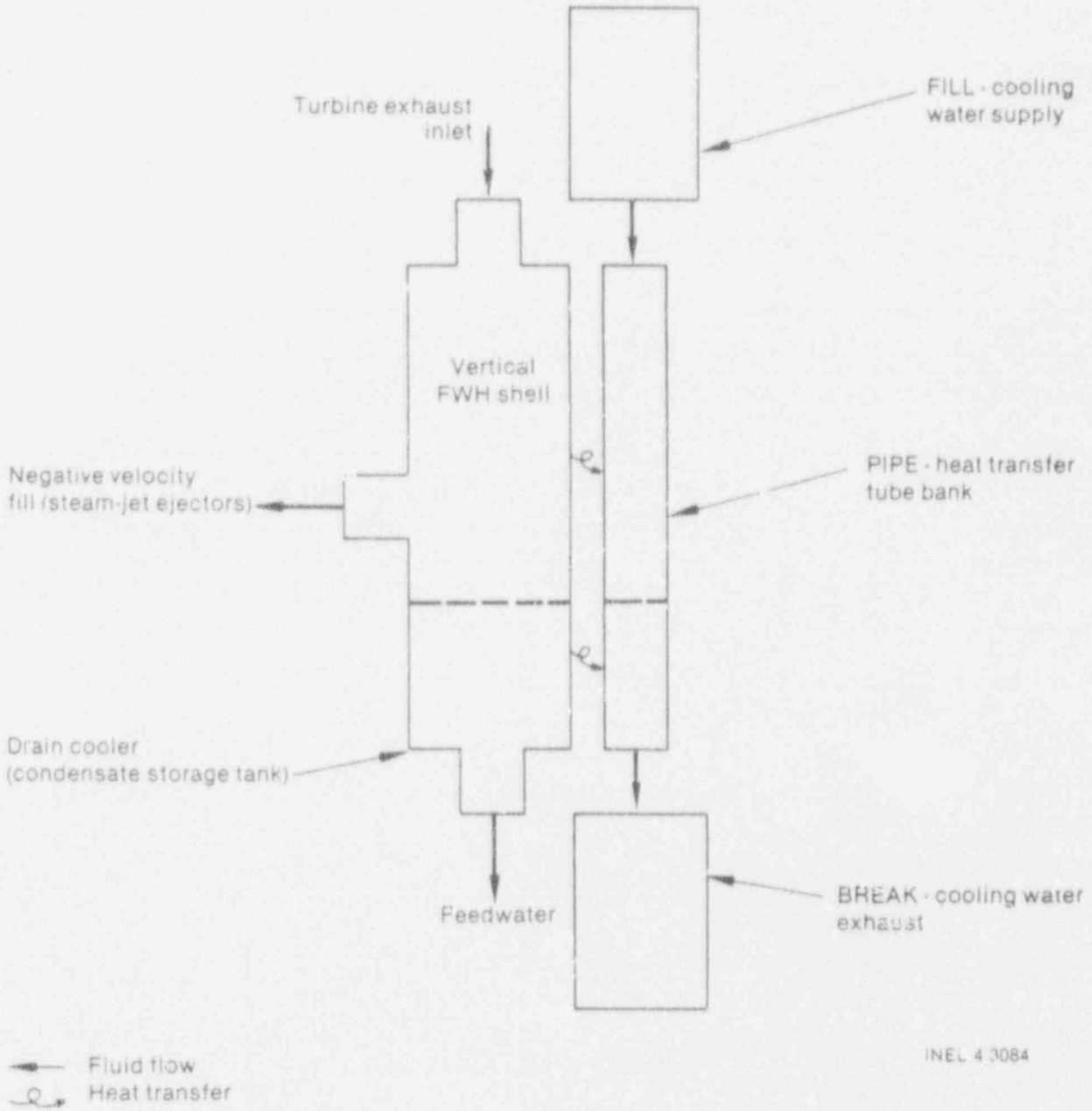

Figure 3.13-2. Arrangement for main steam condenser model.

permissible. In this case, the HEATR side arm may be connected to a small negative FILL to model the steam-jet ejectors used to prevent buildup of noncondensable in the condenser shell. When the HEATR is used to model a condenser, the drain cooler may be assumed to represent the condensate storage tank.

Condensers are usually controlled (by way of a valve on the drain cooler outlet) to maintain a specified water level in the shell. The HEATR has a built-in controller that can adjust the flow area at the third interface (first interface internal to the drain cooler). This requires at least two cells in the drain cooler (with the controlled area between them). The control input is LIQLEV in Cell 1 of the heater component. The output is AREA of Face 3 in the HEATR. Refer to the control system description for information needed to model such a control system. Some special features of TEEs that are used as HEATRs are

1. Side arm input is simplified--the pipe arrays do not have to be input for the side arm

2. Heat transfer from the walls of the shell is not presently modeled (NODES = 0)

3. The shell must consist of only one cell, but the drain cooler may contain as many cells as required. The side-arm always connects to the first cell (shell).

4. The heat transfer PIPE may contain as many cells as needed. U-tubes may be represented by appropriate assignment of the KRVC array.

5. Internal flow area may be controlled as described above.

3.13.1 References

3.13-1. T. Fujii, H. Vehara, and C. Kurato, "Laminar Filmwise Condensation of Flowing Vapour on a Horizontal Cylinder," *International Journal of Heat and Mass Transactions*, *15*, 1972, pp. 235-246.

3.13-2. D. Q. Kern, *Process Heat Transfer*, New York: McGraw-Hill Book Company, Inc., 1950.

4. CONCLUDING REMARKS

TRAC-BF1/MOD1 is a best-estimate computer code for the analysis of various transients in BWR systems and related experimental facilities. It provides a consistent and unified means to analyze system behavior following a large- or small-break LOCA, from the blowdown phase, through the core heatup, reflood, and quench, and finally through the refill phase of the accident. It also provides a basic capability for the analysis of operational transients, up to and including ATWS, for which a point reactor kinetics model is adequate.

The present volume describes the equations and mathematical models that collectively provide the theoretical basis of TRAC-BF1/MOD1. The most basic part of these equations describes a fully nonhomogeneous, nonequilibrium, two-fluid, thermal-hydraulic model of two-phase flow in all parts of a BWR system, including a three-dimensional treatment of flow in the vessel. The basic equations are complemented with flow regime-dependent constitutive relations for transfer of mass, energy, and momentum through the interface between the fluid phases and in contact with the walls. There are also special models for nonhomogeneous, thermal equilibrium critical two-phase flow and countercurrent flow limiting processes in particular BWR geometries.

Other important parts of the formulations include (a) detailed modeling of BWR fuel bundle heat transfer, including heat conduction in fuel, cladding, and the gap between them, as well as heat removal through thermal radiation and convection in various forms, including all phases of heat transfer along the boiling curve, and (b) appropriate modeling of processes in particular BWR hardware components, such as jet pumps, fuel channels, steam separators, and dryers.

In the TRAC-BD1/MOD1 release, the following features were incorporated:

- Balance of plant component models, such as turbines, feedwater heaters, and steam condensers in generic form
- A simple lumped-parameter containment model
- A comprehensive control system model
- Reactivity feedback model, including the effect of soluble boron
- Boron transport model
- Noncondensable gas transport model, including the effects of noncondensable gas on heat transfer
- Mechanistic separator dryer model
- Two-phase level tracking model

Concluding Remarks

- Generalized component-to-component heat and mass transfer models
- Moving mesh quench front tracking model for fuel rods and for inside and outside surfaces of fuel channel walls
- Improved constitutive relations for heat, mass, and momentum transfer between the fluid phases and between the fluid phases and structure.

With the release of TRAC-BF1, the numerical models were upgraded to include:

- Material Courant-limit-violating numerical solution for all one-dimensional hydraulic components
- One-dimensional neutron kinetics model
- Improved interfacial heat transfer
- Improved interfacial shear model
- A condensation model for stratified vertical flow
- Implicit steam separator/dryer model
- Implicit turbine model
- Improved control system logic and solution method.

The TRAC-BF1/MOD1 code is described by three documents: *TRAC-BF1/MOD1: An Advanced Best-Estimate Computer Program for Boiling Water Reactor Accident Analysis, Volumes 1 and 2, and TRAC-BF1/MOD1 Models and Correlations. Volume 1: Model Description* describes the thermal-hydraulic models, numerical methods, and component models available. *Volume 2: User's Guide* describes the input and output of the TRAC-BF1/MOD1 code and provides guidelines for use of the code modeling of BWR systems. *TRAC-BF1/MOD1 Models and Correlations* is designed for those users wishing a detailed mathematical description of each of the models and correlations available in TRAC-BF1/MOD1. This document reflects the as-coded configuration of the descriptive information provided in Volume 1.

APPENDIX A

THERMODYNAMIC PROPERTIES

APPENDIX A

THERMODYNAMIC PROPERTIES

The thermodynamic properties subroutines used in TRAC-BF1/MOD1 are based on polynomial fits to steam table data for water and ideal gas behavior for the noncondensable gas component. The thermodynamic property routines are used by all TRAC-BF1/MOD1 component modules. Tables A-1 through A-8 list the values of the constants.

Subroutine THERMO supplies thermodynamic properties for TRAC-BF1/MOD1. The input variables are the total pressure, the partial pressure of the noncondensable gas component, and the liquid and gas-phase temperatures. The output variables include the saturation temperature corresponding to total pressure; the saturation temperature corresponding to the partial pressure of steam; the specific internal energies of liquid, gas, and noncondensable; the saturated liquid and steam enthalpies corresponding to the partial pressure of steam; the liquid, gas, and noncondensable densities; the derivatives of saturation temperatures and enthalpies with respect to pressure; and, finally, the partial derivatives of liquid, steam, and noncondensable internal energies and densities with respect to pressure (at constant temperature) and with respect to temperature (at constant pressure).

The range of validity for the thermodynamic properties supplied by THERMO is

$273.15\ K \leq T_\ell \leq 713.94\ K$;

$273.15\ K \leq T_v < 3000.0\ K$; and

$1.0\ Pa \leq p \leq 450.0\ E5\ Pa$.

If THERMO is provided with data outside these ranges, it adjusts the data to the corresponding limit and issues a warning message.

A-1 SATURATION PROPERTIES

A-1.1 Relationship between Saturation Pressure and Temperature

The saturation line that lies between the triple point (273.15 K) and the critical point (647.3 K) is divided into two regions of temperature and pressure, and a separate correlation is used in each region.

A-1.1.1 First Region of Temperature and Pressure. The first region of temperature is defined by

Table A-1. Miscellaneous constants.

Constant	Value	Constant	Value
A_{11}	1.00008875 E-3	C_{19}	Not used
A_{12}	7.691625 E2	C_{20}	9.056466 E4
A_{13}	1.300115 E-3	C_{21}	370.4251
A_{14}	1. E-5	C_{22}	1004.832
C_1	- 2263.0	C_{23}	$C_{16} \cdot C_4$
C_2	0.434	C_{24}	4186.8
C_3	- 6.064	C_{25}	287.03
C_4	$C_{12}/(C_{16} - 1)$	C_{26}	$C_{24}\ (C_5 - C_{29})$
C_5	273.15	C_{27}	$C_{26} + C_{10}$
C_6	$C_{27} - C_{12} \cdot C_5$	C_{28}	$(C_{12} - C_{25})/C_{12}$
C_7	C_{24}	C_{29}	273.15
C_8	$- 0.61132 + C_7(C_5 - C_{29})$	C_{30}	1.0
C_9	990.0	C_{31}	450.0 E5
C_{10}	$h_{fg}(C_5)$	C_{32}	C_5
C_{11}	1. E5	C_{33}	713.94026
C_{12}	461.49	C_{34}	C_5
C_{13}	0.0228	C_{35}	3000.0
C_{14}	0.65141	C_{36}	610.8
C_{15}	0.0	C_{37}	221.2 E5
C_{16}	1.3	C_{38}	647.3
C_{17}	$C_{22} - C_{}$	C_{39}	139.6997 E5
C_{18}	C_{22}/C_{17}	C_{40}	609.625

Table A-2. Constants for steam internal energy function.[a]

Region	Maximum Pressure (Pa)	Ave	Bve	Cve	Dve
1	20 E5	2.49497 E6	2.08558 E-1	-1.35539 E-7	2.852268 E-14
2	50 E5	2.56003 E6	3.10861 E-2	-6.89888 E-9	4.32037 E-16
3	100 E5	2.59155 E6	8.77499 E-3	-1.794999 E-9	4.29999 E-17
4	150 E5	2.66060 E6	-1.3545 E-2	6.425 E-10	-4.21 E-17
5	200 E5	3.82016 E6	-2.30199 E-1	1.40689 E-8	-3.1786 E-16
6	220 E5	-1.21034 E8	1.80188 E1	-8.74424 E-7	1.40911 E-14
7	250 E5	2.20 E6	0.	0.	0.
8	300 E5	2.20 E6	0.	0.	0.
9	350 E5	2.20 E6	0.	0.	0.
10	400 E5	2.20 E6	0.	0.	0.
11	450 E5	2.20 E6	0.	0.	0.

a. Constants in TRAC-BF1/MOD1 have 14 significant figures.

Table A-3. Constants for gamma function.[a]

Region	Maximum Pressure (Pa)	Avg	Bvg	Cvg	Dvg
1	20 E5	1.06668	2.83108 E-8	-2.1151 E-14	4.7404 E-21
2	50 E5	1.07354	2.651805 E-9	-6.3461 E-16	3.9824 E-23
3	100 E5	1.077773	-2.43 E-11	-7.19799 E-17	4.87999 E-25
4	150 E5	1.085113	-1.9307 E-9	8.91 E-17	-3.896 E-24
5	200 E5	1.16398	-1.63385 E-8	9.5856 E-16	-2.1194 E-23
6	220 E5	3.88988	-3.85959 E-7	1.74763 E-14	-2.6377 E-22
7	250 E5	2.71687	-2.28327 E-7	1.04173 E-14	-1.58428 E-22
8	300 E5	3.97498	-3.06571 E-7	1.063789 E-14	-1.22579 E-22
9	350 E5	1.29469	-2.48349 E-8	7.8979 E-16	-8.079 E-24
10	400 E5	1.05905	-2.46159 E-9	8.8399 E-17	-8.0799 E-25
11	450 E5	1.143019	-7.709599 E-9	1.933599 E-16	-1.46399 E-24

a. Constants in TRAC-BF1/MOD1 have 14 significant figures.

Table A-4. Constants for steam heat capacity function.[a]

Region	Maximum Temperature (K)	Acp	Bcp	Ccp	Dcp
1	323.15	-7.9678 E[illegible]	2.81876 E1	-1.01806 E-1	1.2499 E-4
2	373.15	-9.70826 E2	2.8325 E1	-9.76562 E-2	1.16 E-4
3	423.15	-1.66497 E3	3.315936 E1	-1.0861179 E-1	1.2399 E-4
4	473.15	-6.142048 E3	6.363098 E1	-1.77623 E-1	1.7599 E-4
5	523.15	-8.228995 E4	5.377395 E2	-1.16125	8.5599 E-4
6	573.15	-6.5842 E5	3.79343 E3	-7.29249	4.704 E-3
7	623.15	3.45616 E5	-2.2129 E2	-2.4524	3.14799 E-3
8	647.3	1.979837 E6	-1.478255 E4	3.16564 E1	-2.08433 E-2
9	673.3	-9.62493 E7	4.363367 E5	-6.58876 E2	3.31461 E-1
10	723.3	-1.10749 E7	4.80737 E4	-6.9212 E1	3.30917 E-2

a. Constants in TRAC-BF1/MOD1 have 14 significant figures.

Table A-5. Constants for liquid internal energy function.[a]

Region	Maximum Temperature (K)	Afe	Bfe	Cfe	Dfe
1	423.15	-1.14367 E6	4.1868 E3	0	0
2	473.15	8.09575 E6	-5.70088 E4	1.34436 E2	-9.78797 E-2
3	523.15	-1.93739 E6	9.74928 E3	-1.32995 E1	1.08799 E-2
4	573.15	-5.32458 E6	2.91794 E4	-5.04522 E1	3.456 E-2
5	623.15	-6.35835 E7	3.2873 E5	-5.63712 E2	3.276 E-1
6	645.15	-6.62391 E9	3.16056 E7	-5.02637 E4	2.665 E1
7	673.15	-5.4759 E9	2.46356 E7	-3.6931 E4	1.84547 E1
8	713.94	-7 15364 E7	3.05608 E5	-4.24245 E2	1.97199 E-1

a. Constants in TRAC-BF1/MOD1 have 14 significant figures.

Table A-6. Miscellaneous liquid property constants.[a]

Constant	Value
C_{k0}	-8.329 E-4
C_{k2}	-2.2458 E-17
C_{k4}	-1.4504 D-16
a_ℓ	7.146

a. Constants in TRAC-BF1/MOD1 have 14 significant figures.

Table A-7. Constants in liquid specific volume function.[a]

Region	Maximum Temperature (K)	Avo	Bvo	Cvo	Dvo
1	373.15	1.705767 E-3	-6.03208 E-6	1.5944 E-8	-1.2149 E-11
2	473.15	5.21459 E-4	3.518922 E-6	-9.73048 E-9	1.085668 E-11
3	573.15	-1.493186 E-2	9.793156 E-5	-2.01728 E-7	1.40804 E-10
4	603.15	-4.93342 E-1	2.59285 E-3	-4.53871 E-6	2.65379 E-9
5	613.15	-3.45589	1.735179 E-2	-2.90474 E-5	1.62202 E-8
6	623.15	-1.19525 E1	5.89049 E-2	-9.67866 E-5	5.30292 E-8
7	633.15	-3.74466 E1	1.81734 E-1	-2.940499 E-4	1.5863 E-7
8	643.15	-3.97132 E2	1.88015	-2.96739 E-3	1.561217 E-6
9	653.15	-2.31427 E3	1.07102 E1	-1.65217 E-2	8.49552 E-6
10	663.15	2.048156 E3	-9.345278	1.4212 E-2	-7.2037 E-6
11	673.15	-7.38647 E1	3.31449 E-1	-4.96087 E-4	2.477179 E-7
12	713.94	-2.189132 E1	9.67584 E-2	-1.14289 E-4	7.05672 E-8

a. Constants in TRAC-BF1/MOD1 have 14 significant figures.

Table A-8. Constants in liquid specific volume correction factor.[a]

Region	Maximum Temperature (K)	Afn	Bfn	Cfn	Dfn
1	373.15	-4.24863 E9	3.75167 E7	-1.00649 E5	8.75072 E1
2	473.15	-2.79363 E8	5.566317 E6	-1.49217 E4	1.0834095 E1
3	573.15	-1.17912 E8	4.38322 E6	-1.208837 E4	8.60345
4	603.15	-4.54151 E9	2.73686 E7	-5.18947 E4	3.15812 E1
5	613.15	-4.01043 E10	2.029257 E8	-3.40759 E5	1.900066 E2
6	623.15	-6.01738 E10	2.99849 E8	-4.96759 E5	2.73686 E2
7	633.15	2.05788 E10	-8.95038 E7	1.282278 E5	-6.072229 E1
8	643.15	8.379355 E10	-3.899718 E8	6.050262 E5	-3.129196 E2
9	653.15	9.240237 E10	-4.267492 E8	6.569561 E5	-3.371112 E2
10	663.15	-2.75477 E10	1.2580004 E8	-1.914749 E5	9.713614 E1
11	673.15	6.860819 E8	-3.063602 E6	4.561362 E3	-2.264207
12	713.94	4.34584 E7	-1.83799 E5	2.59716 E2	-1.224404 E-1

a. Constants in TRAC-BF1/MOD1 have 14 significant figures.

$273.15\ K \leq T_s \leq 370.4251\ K$

$1\ Pa < p_s < 90564.66\ Pa.$

In this region, thermodynamic relations are used to define the saturation properties. The enthalpy of vaporization, $h_{\ell v}$, is represented as a linear function of temperature

$$h_{\ell v} = 3180619.59 - 2470.2120\ T_s \ . \tag{A-1}$$

The Clausius-Clapeyron equation, which assumes that steam is an ideal gas and neglects liquid volume compared to steam volume, can be written as

$$\frac{dp_s}{dT_s} = \frac{h_{\ell v} p_s}{R_v T_s^2} \tag{A-2}$$

where R_v is the gas constant for steam. Substituting for $h_{\ell v}$ and integrating, using the boundary condition $p_s = 24821$ Pa at $T_s = 338$ K, gives

$$p_s = 24821 \left(\frac{T_s}{338} \right)^{-5.3512} \exp \left[\frac{20.387\ (T_s - 338)}{T_s} \right] . \tag{A-3}$$

To compute the saturation temperature for a given pressure, this equation must be solved iteratively. To simplify the solution and avoid iteration, an approximate solution is used that gives the value of saturation temperature to within a fraction of a percent error. First, an approximate value of saturation temperature is determined from

$$T_{s,ap} = \frac{2263}{6.064 - 0.434 \ln \left(\frac{p_s}{100000} \right)} \tag{A-4}$$

which gives the saturation temperature within a few degrees of its correct value. This value is corrected by integrating the Clausius-Clapeyron equation, assuming constant $h_{\ell v}$ between $T_{s,ap}$ and T_s, which gives

$$T_s = \frac{T_{s,ap}}{1 - \left[\frac{R_v T_{s,ap}}{h_{\ell v}(T_{s,ap})} \right] \ln \left[\frac{p_s}{p_{s,a}(T_{s,ap})} \right]} \tag{A-5}$$

where $h_{\ell v}(T_{s,ap})$ and $p_s(T_{s,ap})$ are calculated using the equations above at $T_{s,ap}$. The derivative along the saturation line is also needed and is given by

$$\frac{\partial T_s}{\partial p_s} = \frac{R_v T_s^2}{p_s h_{\ell v}(T_s)} \quad . \tag{A-6}$$

A-1.1.2 Second Region of Temperature and Pressure. The second region of temperature is given by

$T_s \geq 370.4251$ K

$p_s \geq 9.056466$ E4 Pa.

In this range of temperature and pressure, a simpler functional form is used and is written

$$p_s = \frac{1}{A_{14}} \left(\frac{T_s - C_3}{C_1} \right)^{\frac{1}{C_2}} \tag{A-7}$$

$$T_s = C_1 (A_{14} p_s)^{C_2} + C_3 \tag{A-8}$$

$$\frac{dT_s}{dp_s} = \frac{C_2 (T_s - C_3)}{p_s} \quad . \tag{A-9}$$

Los Alamos National Laboratory has since modified the high-pressure range calculation. Those modifications have not as yet been incorporated into TRAC-BF1/MOD1.

A-1.2 Internal Energy of Saturated Steam

There are 12 pressure ranges in which the saturated vapor internal energy and the derivatives of the saturation enthalpy with respect to pressure and temperature are evaluated. The lowest pressure range uses one functional form, while the 11 highest pressure ranges use another functional form with different sets of constants. The two functional forms are given, along with the sets of constants and pressure ranges.

A-1.2.1 Lowest Pressure Range. The lowest pressure range is given by $p_v < 5.0$ E5 Pa, where p_v is the partial pressure of steam. In this pressure range, the internal energy is given by
and

$$e_{vs} = h_{vs} - \frac{p_v}{\rho_{vs}} = h_{vs} - R_v T_s \tag{A-10}$$

and

$$\frac{de_{vs}}{dp_v} = \frac{dh_{vs}}{dp_v} - R_v \frac{dT_s}{dp_v} \ . \tag{A-11}$$

The quantities have been determined by fitting the saturated vapor enthalpy and its derivative with respect to pressure as

$$h_{vs} = C_8 + C_7[T_s(p_v) - C_5] + h_{\ell v}[T_s(p_v)] \tag{A-12}$$

$$\frac{dh_{vs}}{dp_v} = C_7 - 2470.212 \frac{dT_s}{dp_v} \ . \tag{A-13}$$

Other quantities that will be needed later are γ_{vs}, the ratio of vapor specific heats along the saturation line, and its derivative along the saturation line with respect to pressure. These quantities are given by

$$\gamma_{vs} = \frac{h_{vs}}{e_{vs}} \tag{A-14}$$

$$\frac{d\gamma_{vs}}{dp_v} = \frac{dh_{vs}}{dp_v} - \frac{\gamma_{vs}}{e_{vs}} \frac{de_{vs}}{dp_v} \ . \tag{A-15}$$

A-1.2.2 Higher-Pressure Ranges. In the high-pressure ranges, the quantities of interest are determined from polynomials. These polynomials have different coefficients for the different pressure ranges. The pressures ranges and coefficients are given in Tables A-2 and A-3. The functions for pressure range j are

$$e_{vs}(j) = Ave(j) + p_v\{Bve(j) + p_v[Cve(j) + p_v Dve(j)]\} \tag{A-16}$$

$$\frac{de_{vs}(j)}{dp_v} = Bve(j) + p_v[2.0\ Cve(j) + p_v 3.0\ Dve(j)] \tag{A-17}$$

$$\gamma_{vs}(j) = Avg(j) + p_v(Bvg(j) + p_v[Cvg(j) + p_v Dvg(j)]) \quad \text{(A-18)}$$

$$\frac{d\gamma_{vs}(j)}{dp_v} = Bvg(j) + p_v[2.0\ Cvg(j) + p_v 3.0\ Dvg(j)] \quad \text{(A-19)}$$

$$h_{vs}(j) = e_{vs}(j)\gamma_{vs}(j) \quad \text{(A-20)}$$

$$\frac{dh_{vs}(j)}{dp_v} = \gamma_{vs}(j)\frac{de_{vs}(j)}{dp_v} + e_{vs}(j)\frac{d\gamma_{vs}(j)}{dp_v} \ . \quad \text{(A-21)}$$

A-1.3 Heat Capacity of Saturated Steam at Constant Pressure

Although the heat capacity of steam is not an output variable of the THERMO subroutine, it is used in subsequent calculations. The temperature is divided into 10 regions, with the heat capacity and its derivative with respect to pressure being determined from the same polynomial function in each temperature range with different coefficients. The polynomial function is given by

$$Cps(j) = Acp(j) + T_s(Bcp(j) + T_s[Ccp(j) + T_s Dcp(j)]) \quad \text{(A-22)}$$

$$\frac{dCps(j)}{dp_v} = (Bcp(j) + T_s[2.0\ Ccp(j) + 3.0\ T_s Dcp(j)])\frac{dT_s}{dp_v} \ . \quad \text{(A-23)}$$

A-2 LIQUID PROPERTIES

A-2.1 Liquid Internal Energy

The liquid internal energy is computed by adding a correction term to the internal energy at saturation (corresponding to saturation pressure at the liquid temperature), that is

$$e_\ell(T_\ell,p) = e_\ell(T_\ell,PSL) + ELP \qquad (A\text{-}24)$$

where PSL is the saturation pressure corresponding to T_ℓ and

$$ELP = (p - PSL)\left(\frac{\partial e_\ell}{\partial p}\right)_{T_\ell} \qquad (A\text{-}25)$$

where the derivative of liquid internal energy with respect to pressure at constant temperature is given by

$$\left(\frac{\partial e_\ell}{\partial p}\right)_{T_\ell} = C_{ko}\left[1 - \exp\,(C_{k4}PSL)\right] + C_{k2}PSL^2 \,. \qquad (A\text{-}26)$$

The derivative of the liquid internal energy is calculated from

$$\left(\frac{\partial e_\ell}{\partial T_\ell}\right)_p = \frac{\partial}{\partial T_\ell} e_\ell(T_\ell,PSL)_p + ERT \qquad (A\text{-}27)$$

where

$$ERT = \frac{\partial}{\partial T_\ell}(ELP)_p$$

$$= \left\{C_{ko}\left[1 - (C_{k4}p + C_{k4}PSL)\exp\,(C_{k4}PSL) - 1\right] + C_{k2}\left[2p\,PSL - 3PSL^2\right]\right\}\frac{dPSL}{dT_\ell} \,. \qquad (A\text{-}28)$$

The liquid internal energy at saturation is computed from a third-order polynomial in each of eight temperature ranges. The polynomial coefficients are different in each temperature range. The temperature ranges and the coefficients for each range are given in Table A-5. The polynomial function is given by

$$e_\ell(T_\ell,PSL) = A\ell e(j) + T_\ell(B\ell e(j) + T_\ell[C\ell e(j) + T_\ell D\ell e(j)]) \qquad (A\text{-}29)$$

for each temperature range j.

A-2.2 Liquid Density

The liquid density is computed in two steps. The density is computed from the primary liquid density function to which a residual void correction is applied.

A-2.2.1 Primary Liquid Density Correlation. The primary liquid density is computed from a correlation for the liquid specific volume as a function of liquid temperature, to which a pressure-dependent correction factor is applied, and is

$$\rho_\ell(T_\ell,p) = \frac{1}{v_\ell(T_\ell)\left[1 - \dfrac{\ln\left(1 + \dfrac{p}{F(T_\ell)}\right)}{a_\ell}\right]} \qquad \text{(A-30)}$$

where

$$v_\ell(T_\ell) = Avo + T_\ell[Bvo + T_\ell(Cvo + T_\ell Dvo)] \qquad \text{(A-31)}$$

and

$$F(T_\ell) = Afn + T_\ell[Bfn + T_\ell(Cfn + T_\ell Dfn)] \; . \qquad \text{(A-32)}$$

The temperature range is broken up into 12 temperature regions, and the polynomial coefficients are different in each region. The temperature regions and the coefficients for each region are listed in Tables A-7 and A-8.

The derivatives of the liquid density with respect to pressure and temperature are found by differentiation of the liquid density function.

A-2.2.2 Residual Void Correction. After evaluation of the functions described above, the liquid density and its derivatives are modified to reflect a residual void fraction. In the following, the unmodified values computed by the formulas described above are denoted by a tilde ($\tilde{}$). There are two pressure ranges for the residual void correction.

A-2.2.2.1 High-Pressure Residual Void Correction--The high-pressure range for the residual void correction is given by

P > 4. E5 Pa.

In the high-pressure region, the corrected liquid density and its derivatives are given by

$$\rho_\ell(T_\ell,p) = \left(1 - \frac{1000}{p}\right) \tilde{\rho}_\ell(T_\ell,p) \tag{A-33}$$

$$\left[\frac{\partial \rho_\ell(T_\ell,p)}{\partial T_\ell}\right]_p = \left(1 - \frac{1000}{p}\right)\left[\frac{\partial \tilde{\rho}_\ell(T_\ell,p)}{\partial T_\ell}\right]_p \tag{A-34}$$

$$\left[\frac{\partial \rho_\ell(T_\ell,p)}{\partial p}\right]_{T_\ell} = \left(1 - \frac{1000}{p}\right)\left[\frac{\partial \tilde{\rho}_\ell(T_\ell,p)}{\partial p}\right]_T + \frac{1000\ \tilde{\rho}_\ell(T_\ell,p)}{p^2} \; . \tag{A-35}$$

A-2.2.2.2 Low-Pressure Residual Void Correction--The low-pressure region for the residual void correction is given by

$P < 4.0$ E5 Pa.

In this region of pressure, the corrected liquid density and its derivatives are given by

$$Alf = 6.25\ E\text{-}9\ p + 0.005 \tag{A-36}$$

$$\rho_\ell(T_\ell,p) = Alf\ \tilde{\rho}_\ell(T_\ell,p) \tag{A-37}$$

$$\left[\frac{\partial \rho_\ell(T_\ell,p)}{\partial p}\right]_{T_\ell} = (1 - Alf)\left[\frac{\partial \tilde{\rho}_\ell(T_\ell,p)}{\partial p}\right]_{T_\ell} + 6.25\ E\text{-}9\ \tilde{\rho}_\ell \tag{A-38}$$

$$\left[\frac{\partial \rho_\ell(T_\ell,p)}{\partial T_\ell}\right]_p = (1 - Alf)\left[\frac{\partial \tilde{\rho}_\ell(T_\ell,p)}{\partial T_\ell}\right]_p \; . \tag{A-39}$$

A-3 VAPOR PROPERTIES

There are two vapor species in TRAC-BF1/MOD1, steam and noncondensable gas. Correlations are provided for the properties of each of these species.

A-3.1 Steam Properties

Steam properties are computed from different correlating functions, depending upon whether the steam is superheated or subcooled.

A-3.1.1 Superheated Steam ($T_v > T_s(p_v)$). Superheated steam is defined as steam whose temperature is greater than the saturation temperature based on the partial pressure of steam.

A-3.1.1.1 Internal Energy of Superheated Steam--The internal energy of steam is computed by integrating the enthalpy from the saturated state to the temperature of interest along a line of constant pressure to give

$$e_v(T_{v,p}) = e_v[T_s(p_v), p_v] + A_{12}\left\{[T_v - T_s(p_v)] + (T_v^2 - \beta)^{1/2} - \frac{T_s(p_v)}{A_{11}C_{ps} - 1}\right\} \qquad \text{(A-40)}$$

and

$$\beta = T_s^2(p_v)\left[1 - \frac{1}{(A_{11}C_{ps} - 1)^2}\right] \qquad \text{(A-41)}$$

where β is the isobaric thermal expansion coefficient.

The saturated vapor enthalpy function was described in Section A-1.2, and the other constants are listed in Table A-1.

The derivative of vapor internal energy with respect to temperature at constant pressure is given by

$$\left(\frac{\partial e_v}{\partial T_v}\right)_{p_v} = \frac{C_4}{1 - \frac{\beta}{\kappa^2}} \qquad \text{(A-42)}$$

and

$$\kappa = A_{13}(e_v - e_{vs}) + T_s\left(1 + \frac{1}{A_{11}C_{ps} - 1}\right) \qquad \text{(A-43)}$$

where κ is the isothermal compressibility.

The derivative of vapor internal energy with respect to pressure at constant temperature is given by

$$\left(\frac{\partial e_v}{\partial p}\right)_{T_v} = -1/2\left(\frac{\partial e_v}{\partial T_v}\right)_p\left[\left(1-\frac{\beta}{\kappa^2}\right)\kappa_p' + \frac{1}{\kappa}\frac{d\beta}{dp}\right] \tag{A-44}$$

$$\kappa_p' = \left(\frac{\partial \kappa}{\partial p_v}\right)_{T_v} - A_{13}\left(\frac{\partial e_v}{\partial p_v}\right)_{T_v}$$

$$= -A_{13}\left(\frac{de_{vs}}{dp_v}\right) + \left(1+\frac{1}{A_{11}C_{ps}-1}\right)\left(\frac{dT_s}{dp_v}\right) - \frac{A_{11}T_s}{(A_{11}C_{ps}-1)^2}\left(\frac{dC_{ps}}{dp_v}\right) \tag{A-45}$$

$$\frac{d\beta}{d\kappa} = \frac{2}{T_s}\left[\beta\frac{dT_s}{dp_v} + A_{11}\frac{dC_{ps}}{dp_v}\left(\frac{T_s}{A_{11}C_{ps}-1}\right)^3\right]. \tag{A-46}$$

A-3.1.1.2 Density of Superheated Steam. The density of superheated steam is given by

$$\rho_v(T_v,p) = \frac{p_v}{(\gamma_{vs}-1)e_{vs}+0.3D_e} \tag{A-47}$$

and

$$D_e = A_{12}\left[T_v - T_s + \left(T_v^2-\beta\right)^{1/2} - \frac{t_s}{A_{11}C_{ps}-1}\right]. \tag{A-48}$$

The derivative of steam density with respect to temperature at constant pressure is given by

$$\left(\frac{\partial \rho_v}{\partial T_v}\right)_p = \frac{-0.3\ \rho_v(T_v,p_v)}{(\gamma_{vs}-1)e_{vs}+0.3D_e}\left(\frac{\partial e_v}{\partial T_v}\right)_p. \tag{A-49}$$

The derivative of steam density with respect to pressure at constant temperature is given by

$$\left(\frac{\partial \rho_v}{\partial p_v}\right)_{T_v} = \frac{1 - \rho_v(T_v,p_v)\left[e_{vs}\frac{\partial \gamma_{vs}}{\partial p_v} + (\gamma_{vs} - 1.3)\frac{\partial e_{vs}}{\partial p_v}\right]}{(\gamma_{vs} - 1)e_{vs} + 0.3\ D_e}$$

$$- \frac{0.3\ \rho_v(T_v,p_v)}{(\gamma_{vs} - 1)e_{vs} + 0.3\ D_e}\left(\frac{\partial e_v}{\partial p_v}\right)_{T_v} . \qquad \text{(A-50)}$$

A-3.1.2 Subcooled Steam [$T_v < T_s(p_v)$]. Subcooled steam is defined as steam whose temperature is less than the saturation temperature based on the partial pressure of steam.

A-3.1.2.1 Internal Energy of Subcooled Steam--The internal energy of steam is computed by integrating the internal energy from the saturated state to the temperature of interest along a line of constant pressure, assuming that the heat capacity at constant volume remains constant at its value on the saturation line. This gives

$$e_v(T_v,p) = e_v[T_s(p_v),p_v] + [T_v - T_s(p_v)]\frac{C_{ps}[T_s(p_v)]}{C_{16}} \qquad \text{(A-51)}$$

$$\left[\frac{\partial e_v(T_v,p_v)}{\partial T_v}\right]_{p_v} = \frac{C_{ps}[T_s(p_v)]}{C_{16}} \qquad \text{(A-52)}$$

$$\left(\frac{\partial e_v(T_v,p_v)}{\partial p_v}\right)_{T_v} = \left\{\frac{\partial e_v[T_s(p_v),p_v]}{\partial p_v}\right\}_{T_v} + \left\{\frac{\partial C_{ps}[T_s(p_v),p_v]}{\partial p_v}\right\}_{T_v}\left[\frac{T_v - T_s(p_v)}{C_{16}}\right]$$

$$- \frac{C_{ps}[T_s(p_v),p_v]}{C_{16}}\left[\frac{\partial T_s(p_v)}{\partial p_v}\right] \qquad \text{(A-53)}$$

where the derivatives and heat capacity of saturated steam were described in Section A-1.

A-3.1.2.2 Density of Subcooled Steam--The density of subcooled steam is computed using the same correlating functions as for superheated steam (as described in Section A-3.1.1.2) except that the correlating parameter, D_e, is given by

$$D_e = \frac{C_{ps}[T_s(p_v), p_v]}{C_{16}}[T_v - T_s(p_v)] \quad . \tag{A-54}$$

A-3.1.3 Steam Density Corrections. There are two separate corrections applied to the steam density as computed from the formulation described in the previous sections. If the computed density is negative, then the steam density and its derivatives with respect to pressure and temperature are recomputed assuming that steam is a perfect gas. These relations are

$$\rho_v(T_v, p) = \frac{p_v}{C_{12} T_v} \tag{A-55}$$

$$\left(\frac{\partial \rho_v}{\partial T_v}\right)_{p_v} = \frac{-\rho_v(T_v, p)}{T_v} \tag{A-56}$$

$$\left(\frac{\partial \rho_v}{\partial p}\right)_{T_v} = \frac{\rho_v(T_v, p)}{p_v} \quad . \tag{A-57}$$

The second correction is used whenever the computed steam density is greater than the computed liquid density. In this case, the vapor density and its derivatives with respect to pressure and temperature are set approximately equal to their corresponding liquid properties. Thus,

if $\rho_v(T_v, p_v) \geq 0.999\ \rho_\ell(T_\ell, p)$, then

$$\rho_v(T_v, p_v) = 0.999\ \rho_\ell(T_\ell, p) \tag{A-58}$$

$$\left[\frac{\partial \rho_v(T_v, p_v)}{\partial p_v}\right]_{T_v} = 0.999 \left[\frac{\partial \rho_\ell(T_\ell, p)}{\partial p_v}\right]_{T_\ell} \tag{A-59}$$

$$\left[\frac{\partial \rho_v(T_v,p_v)}{\partial T_v}\right]_{p_v} = 0.999\left[\frac{\partial \rho_\ell(T_\ell,p)}{\partial T_\ell}\right]_{p_v} . \qquad \text{(A-60)}$$

A-3.2 Noncondensable Gas Properties

The density and internal energy of the noncondensable gas are computed from the perfect gas law and are given by

$$e_a(T_v,\rho_a) = C_{17}T_v \qquad \text{(A-61)}$$

$$\left[\frac{\partial e_a(T_v,\rho_a)}{\partial T_v}\right]_p = C_{17} \qquad \text{(A-62)}$$

$$\left[\frac{\partial e_a(T_v,\rho_a)}{\partial \rho_a}\right]_{T_v} = 0 \qquad \text{(A-63)}$$

$$\left[\frac{\partial \rho_a(T_v,\rho_a)}{\partial \rho_a}\right]_{T_v} = \frac{1}{C_{25}T_v} \qquad \text{(A-64)}$$

$$\left[\frac{\partial \rho_a(T_v,\rho_a)}{\partial T_v}\right]_{\rho_a} = -C_{25}\rho_a(T_v,\rho_a)\left[\frac{\partial \rho_a(T_v,\rho_a)}{\partial \rho_a}\right]_{T_v} \qquad \text{(A-65)}$$

$$\rho_a = (T_v,\rho_a) = \rho_a\left[\frac{\partial \rho_a(T_v,\rho_a)}{\partial \rho_a}\right]_{T_v} . \qquad \text{(A-66)}$$

A-3.3 Properties of Water Mixtures

The internal energy of a mixture of steam and noncondensable gas is given by the density-weighted average of the internal energies of the two species

$$e_m(T_{v,p}) = \frac{\rho_v(T_v,p_v)e_v(T_v,p_v) + \rho_a(T_v,p_a)e_a(T_v,p_a)}{\rho_v(T_v,p_v) + \rho_a(T_v,p_a)} \quad . \tag{A-67}$$

The density of a mixture of steam and noncondensable gas is the sum of the densities of the two species.

APPENDIX B

MATERIAL PROPERTIES

APPENDIX B

MATERIAL PROPERTIES

An extensive library of temperature-dependent material properties is incorporated in the TRAC-BF1/MOD1 code. The entire library is accessible by the CHAN fuel rod components, while component walls and VESSEL double-sided heat slabs have access to structural material property sets only. There are 10 sets of materials properties that comprise the library, each set supplying values for thermal conductivity, specific heat, density, and spectral emissivity for use in heat transfer calculations. The first five sets contain properties for nuclear-heated or electrically heated fuel rod simulation. Included are nuclear fuels, zircaloy cladding, fuel-cladding gap gases, electrical heater rod filaments, and electrical heater rod insulating material. The last five sets are for structural materials, including stainless steels, carbon steel, and Inconel. The material indices used in the library are:

1. mixed-oxide fuel
2. zircaloy
3. gas gases
4. boron nitride insulation
5. constantan/nichrome heater
6. stainless steel, Type 304
7. stainless steel, Type 316
8. stainless steel, Type 347
9. carbon steel, Type A508
10. Inconel, Type 718.

In addition to the library of built-in material properties, the code provides for user-supplied tables of materials properties.

Figure B-1 illustrates the calling tree for obtaining the property values. Subroutines MFROD and MPROP are simple processors for calculating the average temperature and calling the appropriate subroutine based on the user-supplied material index. Subroutine FROD controls the fuel-cladding gap conductance and fuel rod thermal conduction calculations. Gap gas properties are calculated only when the dynamic fuel-cladding gap heat transfer coefficient option is used.

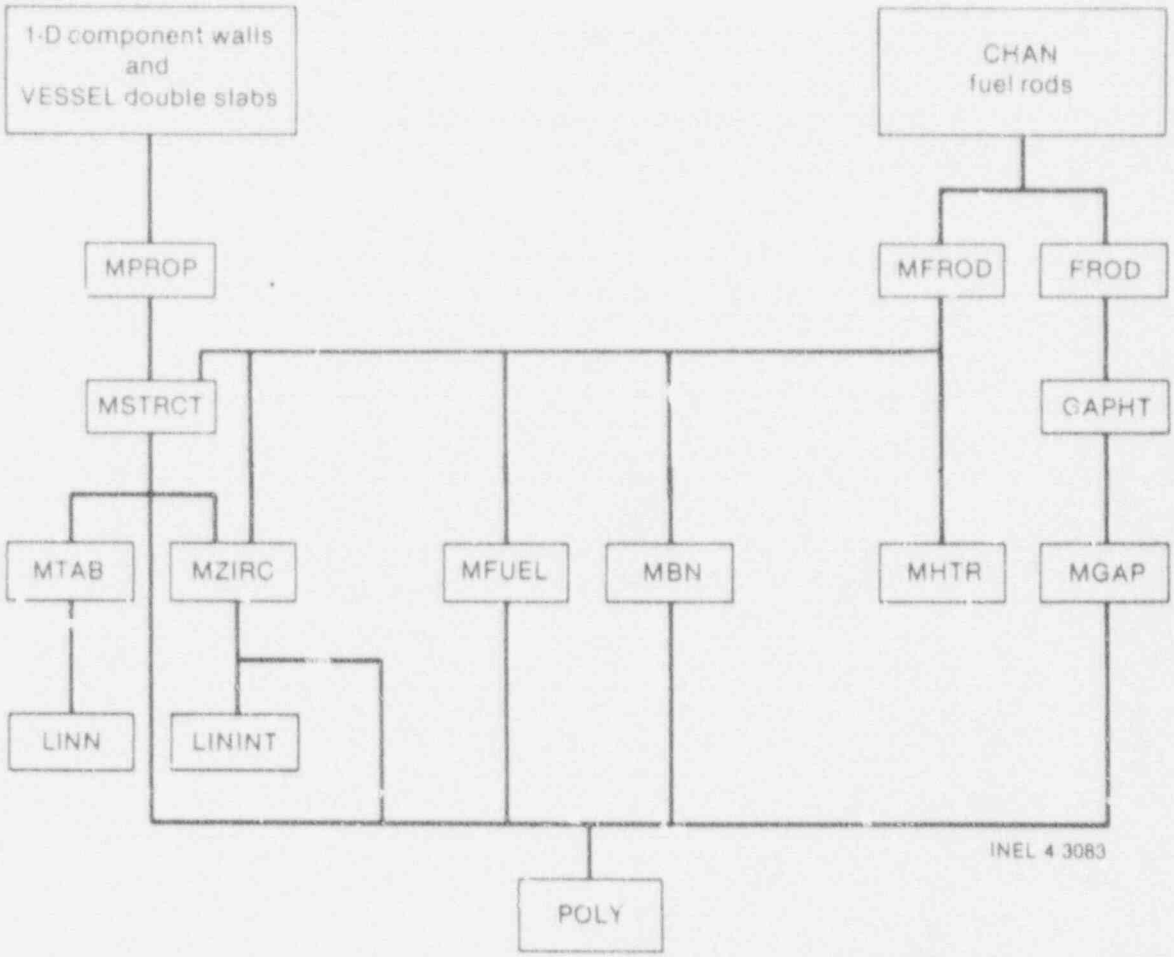

Figure B-1. Material properties code organization.

Density variation with thermal expansion is currently suppressed, because it is inconsistent with the fixed-node conduction solution. When node spacing changes are implemented, the expansion calculation may be activated.

B-1. NUCLEAR FUEL (UO_2-PuO_2) PROPERTIES

Subroutine MFUEL calculates the properties for mixed-oxide nuclear fuels. Values obtained are influenced by three user-supplied input variables: fraction of theoretical density, fraction of plutonium oxide in the fuel, and fuel burnup. Property changes upon melting are not included in this code version.

B-1.1 Density

A constant value is used;

$$\rho = f_{TD}\left[\left(1 - f_{PuO_2}\right)\rho_{UO_2} + f_{PuO_2}\rho_{PuO_2}\right] \qquad \text{(B-1)}$$

where

fTD = fraction of theoretical fuel density

f_{PuO_2} = weight fraction of PuO_2 in fuel

ρ_{UO_2} = 1.097 E4

ρ_{PuO_2} = 1.146 E4.

B-1.2 Specific Heat

The mixed-oxide fuel specific heat correlations ar taken from the MATPRO report[B-1]

$$c_p = 15.496\,\frac{b_1 b_4^2 \exp\left(\frac{b_4}{T}\right)}{\left[T^2 \exp\left(\frac{b_4}{T}\right) - 1\right]^2} + 2b_2T + \frac{b_3 b_5}{b_6 T^2}\exp\left(\frac{-b_5}{b_6 T}\right) \qquad \text{(B-2)}$$

where

c_p = specific heat capacity (J/kg·K)

T = fuel temperature (K)

and

b_1 = 19.145 for UO_2; 19.53 for UO_2-PuO_2

b_2 = 7.8473 E-4 for UO_2; 9.25 E-4 for UO_2-PuO_2

b_3 = 5.6437 E6 for UO_2; 6.02 E6 for UO_2-PuO_2

b_4 = 535.285 for UO_2; 539.0 for UO_2-PuO_2

b_5 = 37694.6 for UO_2; 40100.0 for UO_2-PuO_2

b_6 = 1.987 for UO_2; 1.987 for UO_2-PuO_2.

B-1.3 Thermal Conductivity

The mixed-oxide fuel thermal conductivity correlations are taken from the MATPRO report[B-1] and include porosity and density correction factors.

For $T_c \leq T_1$,

$$k = \left[c \left(\frac{c_1}{c_2 + T_c} \right) + c_3 \exp\left(c_4 T_c\right) \right] \tag{B-3}$$

For $T_c > T_1$,

$$k = c\, c_5 + c_3 \exp\left(c_4 T_c\right) \tag{B-4}$$

where

T_c = temperature (°C)

f_{TD} = fraction of theoretical density

$$c = 100.0 \left[\frac{1 - \beta(1 - f_{TD})}{1 - 0.05\beta} \right] \tag{B-5}$$

$$\beta = c_6 + c_7 T_c \tag{B-6}$$

and

c_1 = 40.4 for UO_2; 33.5 for UO_2-PuO_2

c_2 = 464.0 for UO_2; 375.0 for UO_2-PuO_2

c_3 = 1.216 E-4 for UO_2; 1.54 E-4 for UO_2-PuO_2

c_4 = 1.867 E-3 for UO_2; 1.71 E-3 for UO_2-PuO_2

c_5 = 0.0191 for UO_2; 0.0171 for UO_2-PuO_2

c_6 = 2.58 for UO_2; 1.43 for UO_2-PuO_2

c_7 = -5.8 E-4 for UO_2; 0.0 for UO_2-PuO_2

T_1 = 1650.0 for UO_2; 1550.0 for UO_2-PuO_2.

B-1.4 Spectral Emissivity

The mixed-oxide spectral emissivity is calculated as a function of temperature based on MATPRO correlations. The values for UO_2 fuel and UO_2-PuO_2 fuel are assumed to be equivalent.

For $T \leq 1000°C$,

$$\epsilon = 0.8707 \tag{B-7}$$

For $1000 < T \leq 2050°C$,

$$\epsilon = 1.311 - 4.404\ E\text{-}4\ T \tag{B-8}$$

For $T > 2050°C$,

$$\epsilon = 0.4083\ . \tag{B-9}$$

B-2. ZIRCALOY CLADDING PROPERTIES

Subroutine MZIRC calculates the properties for zircaloy and oxidized zircaloy cladding. The values obtained are for zircaloy-4. Zircaloy-2 properties are assumed to be identical. The equations used are based on the correlations in the MATPRO report.[B-1]

B-2.1 Density

A constant value is used;

$$\rho = 6551.4\ . \tag{B-10}$$

B-2.2 Specific Heat

Since zircaloy undergoes a phase change (alpha to beta) from 1090 to 1248 K, with a resultant sharp spike in the specific heat value during the transition, the specific heat is calculated by linear interpolation. Table B-1 provides the values of specific heat versus temperature that are used for $T \leq 1248$ K.

For $T > 1248$ K, $C_p = 356$ J/kg·K.

Table B-1. Specific heat versus temperature for $T \leq 1248$ K.

T (K)	C_p (J/kg·K)
300	281
400	302
640	381
1090	375
1093	502
1113	590
1133	615
1153	719
1173	816
1193	770
1213	619
1233	469
1248	356

B-2.3 Thermal Conductivity

Four-term polynomials are used to calculate the zircaloy and oxidized zircaloy thermal conductivities. Kelvin temperature is the independent variable, and the polynomial constants are

a_0 = 7.51 for Zr; 1.96 for ZrO_2

a_1 = 2.09 E-2 for Zr; -2.41 E-4 for ZrO_2

a_2 = -1.45 E-5 for Zr; 6.43 E-7 for ZrO_2

a_3 = 7.67 E-9 for Zr; 1.95 E-10 for ZrO_2.

The form of the polynomial used in this section and the subsequent materials properties sections is

$$Y = a_0 + a_1 x + a_2 x^2 + \ldots + a_m x^m . \qquad \text{(B-11)}$$

B-2.4 Spectral Emissivity

The emissivity of zircaloy is temperature-dependent, and the emissivity of zircaloy oxide is temperature- and time-dependent. For simplicity, a constant value of $\varepsilon = 0.75$ is currently used.

B-3. FUEL-CLADDING GAP GAS PROPERTIES

Subroutine MGAP calculates values for the gap gas mixture thermal conductivity used in predicting gap heat-transfer coefficients. The method is taken from MATPRO[B-1] and is based on calculating mixture values for a possible seven constituent gases

$$k_{gap} = \sum_{i=1}^{n} \left(\frac{k_i x_i}{x_i + \sum_{\substack{j=1 \\ j \neq 1}}^{n} \Psi_{ij} x_j} \right) \tag{B-12}$$

where

k_{gap} = gap mixture thermal conductivity (W/m·K)

$$\Psi_{ij} = \Phi_{ij} \left[1 + 2.41 \frac{(M_i - M_j)(M_i - 0.142\, M_j)}{(M_i + M_j)^2} \right] \tag{B-13}$$

$$\Phi_{ij} = \frac{\left[1 + \left(\frac{k_i}{k_j} \right)^{1/2} \left(\frac{M_i}{M_j} \right)^{1/4} \right]^2}{2^{3/2} \left(1 + \frac{M_i}{M_j} \right)^{1/2}} \tag{B-14}$$

k_i = constituent gas thermal conductivity (W/m·K)

M_i = constituent gas molecular weight

x_i = constituent gas mole fraction.

The seven constituent gases considered are helium, argon, xenon, krypton, hydrogen, air/nitrogen, and water/vapor. Except for water/vapor, their thermal conductivities are defined as

$$k = aT^b \tag{B-15}$$

where

T = temperature (K)

a = 3.36 E-3 for He; 3.421 E-4 for Ar; 4.0288 E-5 for Xe; 4.726 E-5 for Kr; 1.6355 E-4 for H; and 2.091 E-4 for air/N

b = 0.668 for He; 0.701 for Ar; 0.872 for Xe; 0.923 for Kr; 0.8213 for H; and 0.846 for air/N.

For water/vapor, the correlation is

$$k = (2.2428\ E\text{-}7 + 5.0534\ E\text{-}10\ T - 1.853\ E\text{-}14\ T^2)\frac{p_g}{T} + \frac{1.0086\ p_g^2}{T^2(T - 273)^{4.2}}$$

$$+ 1.76\ E\text{-}4 + 3.261\ E\text{-}5\ T + 3.209\ E\text{-}8\ T^2 - 7.733\ E\text{-}12\ T^3 \qquad \text{(B-16)}$$

where p is the gap gas pressure (N/m^2).

When the gap dimension shrinks to the order of the gas mean free path, a correction factor is applied to the light gas thermal conductivities to account for the change in energy exchange between gas and surface. Once again utilizing the MATPRO recommendations,[B-1] the correction factor for hydrogen and helium is

$$k = \frac{k_i}{1 + fk_i} \qquad \text{(B-17)}$$

where

$$f = \frac{0.2103\sqrt{T_g}}{p_g\lambda} \qquad \text{(B-18)}$$

T_g = average gap gas temperature (K)

λ = characteristic fuel RMS roughness (4.389 E-6 m).

B-4. ELECTRICAL FUEL ROD INSULATOR (BN) PROPERTIES

Subroutine MBN calculates values for boron nitride insulators used in electrically heated nuclear fuel rod simulators. Magnesium oxide insulators are assumed to have roughly equivalent values.

B-4.1 Density

A constant value of 2002 kg/m^3 from Reference B-2 is used.

B-4.2 Specific Heat

A four-term polynomial is used to calculate the specific heat. The independent variable is temperature (°F), and the constants are modifications of those reported in Reference B-3; a_0 = 760.59; a_1 = 1.7955; a_2 = -8.6704 E-4; and a_3 = 1.5896 E-7.

B-4.3 Thermal Conductivity

The boron nitride thermal conductivity[B-4] is calculated based on a conversion to SI units of a curve fit

$$k = 25.27 - 1.365\ E\text{-}3\ T_f \qquad \text{(B-19)}$$

where

k = thermal conductivity (W/m·K)

T_f = temperature (°F).

B-4.4 Spectral Emissivity

A constant value of unity is used for the boron nitride spectral emissivity.

B-5. ELECTRICAL FUEL ROD HEATER COIL (CONSTANTAN) PROPERTIES

Subroutine MHTR calculates property values for constantan heater coils as used in electrically heated nuclear fuel rod simulators. Nichrome coils, used in some installations in place of constantan, are assumed to have similar properties. The correlations used are from Reference B-4.

B-5.1 Density

A constant value of 8393.4 kg/m^3 is used.

B-5.2 Specific Heat

$$c_p = 110\ T^{0.2075} \qquad \text{(B-20)}$$

where

c_p = specific heat (J/kg·K)

T_f = temperature (°F).

B-5.3 Thermal Conductivity

$$k = 29.18 + 2.683\ E\text{-}3\ (T_f - 100) \qquad \text{(B-21)}$$

where

k = thermal conductivity (W/m·K)

T_f = temperature (°F).

B-5.4 Spectral Emissivity

A constant value of unity is used.

B-6. STRUCTURAL MATERIAL PROPERTIES

Subroutine MSTRCT supplies property values for five types of structural materials normally used in light water power reactor plants: stainless steel, Type 304; stainless steel, Type 316; stainless steel, Type 347; carbon steel, Type A508; and Inconel, Type 718. A tabulation of the correlations used and a list of associated references are given in Table B-2.

B-7. USER-SUPPLIED MATERIAL PROPERTIES

At the option of the user, Subroutine MTAB gets property values from the user-supplied material property table, using straight-line interpolation.

Table B-2. Structural materials properties.

Material	Property	Independent Variable	Constants in Polynomial Fit[a] a_0	a_1	a_2	a_3	a_4	a_5	a_6	a_7	Reference
SS 304	ϱ	T	7984.0	-2.651×10^{-1}	-1.158×10^{-4}						B-5
	c_p	T_f	426.17	0.43816	-6.3759×10^{-4}	4.4803×10^{-7}	-1.0729×10^{-10}				
	k	T	8.116	1.618×10^{-2}							
	ϵ	—	0.84								
SS 316	ϱ	T	8084.0	-4.209×10^{-1}	-3.894×10^{-5}						B-5
	c_p	T_f	426.17	0.43816	-6.3759×10^{-4}	4.4803×10^{-7}	-1.0729×10^{-10}				
	k	T	9.248	1.571×10^{-2}							
	ϵ	—	0.84								
SS 347	ϱ	T	7913.0								B-4
	c_p	(T_f-240)	502.416	0.0984							
	k	T_f	14.1926	7.269×10^{-3}							
	ϵ	—	0.84								
A 508	ϱ	T_f	7859.82	-2.6428×10^{-2}	-4.5471×10^{-4}	3.311×10^{-7}					B-6
	c_p	T_f	400.48	0.4582	6.5532×10^{-4}	5.3607×10^{-7}					
	k	T_f	66.1558	-1.4386×10^{-2}	-2.6987×10^{-4}	1.8306×10^{-6}	-6.0673×10^{-9}	1.0524×10^{-11}	-9.1603×10^{-15}	3.1597×10^{-18}	
	ϵ	—	0.84								
In-718	ϱ	T_f	8233.4	-1.8351×10^{-1}	-9.8415×10^{-6}	-6.5343×10^{-9}					B-6
	c_p	T_f	418.18	0.1204							
	k	T_f	10.8046	8.829×10^{-3}							
	ϵ	—	0.84								

a. ϱ = density (kg/m^3); c_p = specific heat (J/kg·K), k = thermal conductivity (W/m·K), ϵ = spectral emissivity, T = temperature (K), T_f = temperature (°F), and $y = a_0 + a_1x + a_2x^2 + \ldots a_mx^m$

B-8. REFERENCES

B-1. J. K. Hohorst, Ed., *SCDAP/RELAP5/MOD2 Code Manual, Volume 4: MATPRO--A Library of Materials Properties for Light-Water-Reactor Accident Analysis*, NUREG/CR-5273, EGG-2555, February 1990.

B-2. Y. S. Touloukian, Ed., *Thermophysical Properties of High Temperature Solid Materials*, New York: MacMillan Co., 1967.

B-3. Electric Power Research Institute, *A Prediction of the Semiscale Blowdown Heat Transfer Test S-02-8 (NRC Standard Problem Five)*, EPRI NP-212, October 1976.

B-4. W. L. Kirchner, *Reflood Heat Transfer in a Light Water Reactor, Volumes I and II*, NUREG-0106, August 1976.

B-5. Argonne National Laboratory, *Properties for LMFBR Safety Analysis*, ANL-CEN-RSM-76-1, 1976.

B-6. J. C. Spanner, Ed., *Nuclear Systems Materials Handbook--Volume 1, Design Data*, TID-26666, 1976.

NRC FORM 335 (2-89) NRCM 1102 3201, 3202

U.S. NUCLEAR REGULATORY COMMISSION

BIBLIOGRAPHIC DATA SHEET

(See instructions on the reverse)

1. REPORT NUMBER (Assigned by NRC, Add Vol., Supp., Rev., and Addendum Numbers, if any.)
NUREG/CR-4356
EGG-2626
Vol. 1

2. TITLE AND SUBTITLE
TRAC-BF1/MOD1: An Advanced Best-Estimate Computer Program for BWR Accident Analysis

Model Description

3. DATE REPORT PUBLISHED
MONTH: August
YEAR: 1992

4. FIN OR GRANT NUMBER
L2031

5. AUTHOR(S)
Edited by J. A. Borkowski and N. L. Wade

Contributing Authors
M. M. Giles, S. Z. Rouhani, R. W. Shumway,
G. L. Singer, D. D. Taylor, W. L. Weaver

6. TYPE OF REPORT
Technical

7. PERIOD COVERED *(Inclusive Dates)*

8. PERFORMING ORGANIZATION — NAME AND ADDRESS *(If NRC, provide Division, Office or Region, U.S. Nuclear Regulatory Commission, and mailing address; if contractor, provide name and mailing address.)*

Idaho National Engineering laboratory
EG&G Idaho, Inc.
Idaho Falls, ID 83415

9. SPONSORING ORGANIZATION — NAME AND ADDRESS *(If NRC, type "Same as above"; if contractor, provide NRC Division, Office or Region, U.S. Nuclear Regulatory Commission, and mailing address.)*

Division of Systems Research
Office of Nuclear Regulatory Research
U.S. Nuclear Regulatory Commission
Washington, D.C. 20555

10. SUPPLEMENTARY NOTES

13. ABSTRACT (200 words or less)

The TRAC-BWR code development program at the Idaho National Engineering Laboratory has developed versions of the Transient Reactor Analysis Code (TRAC) for the U.S. Nuclear Regulatory Commission and the public. The TRAC-BF1/MOD1 version of the computer code provides a best-estimate analysis capability for analyzing the full range of postulated accidents in boiling water reactor (BWR) systems and related facilities. This version provides a consistent and unified analysis capability for analyzing all areas of a large- or small-break loss-of-coolant accident (LOCA), beginning with the blowdown phase and continuing through heatup, reflood with quenching, and, finally, the refill phase of tne accident. Also provided is a basic capability for the analysis of operational transients up to and including anticipated transients without scram (ATWS). The TRAC-BF1/MOD1 version produces results consistent with previous versions. Assessment calculations using the two TRAC-BF1 versions show overall improvements in agreement with data and computation times as compared to earlier versions of the TRAC-BWR series of computer codes.

12. KEY WORDS/DESCRIPTORS *(List words or phrases that will assist researchers in locating the report.)*

TRAC, BWR safety analysis

13. AVAILABILITY STATEMENT
Unlimited

14. SECURITY CLASSIFICATION
(This Page) Unclassified
(This Report) Unclassified

15. NUMBER OF PAGES

16. PRICE

NRC FORM 335 (2-89)